ISBN 978-82-471-9807-0 (printed ver.)
ISBN 978-82-471-9371-6 (electronic ver.)
ISSN 1503-8181 (printed ver.)
ISSN 2703-8084 (electronic ver.)

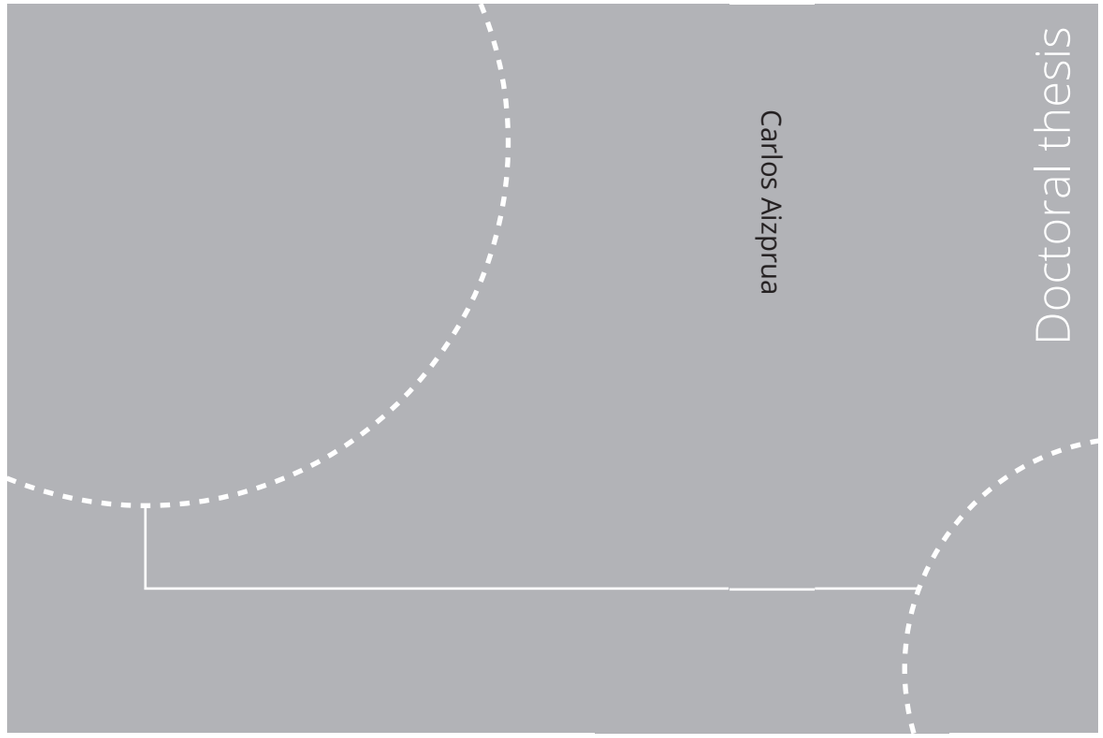

NTNU
Norwegian University of
Science and Technology

Doctoral theses at NTNU, 2021:11

Carlos Aizprua

Forearc crustal structure and controlling factors on basin formation across the southernmost Northern Andes

Geophysical and Geological Investigations

Doctoral theses at NTNU, 2021:11

NTNU

NTNU
Norwegian University of
Science and Technology
Thesis for the degree of
Philosophiae Doctor
Faculty of Engineering
Department of Geoscience and Petroleum

NTNU
Norwegian University of
Science and Technology

Carlos Aizprua

Forearc crustal structure and controlling factors on basin formation across the southernmost Northern Andes

Geophysical and Geological Investigations

Thesis for the degree of Philosophiae Doctor

Trondheim, January 2021

Norwegian University of Science and Technology
Faculty of Engineering
Department of Geoscience and Petroleum

NTNU
Norwegian University of
Science and Technology

NTNU
Norwegian University of Science and Technology

Thesis for the degree of Philosophiae Doctor

Faculty of Engineering
Department of Geoscience and Petroleum

ISBN 978-82-471-9807-0 (printed ver.)
ISBN 978-82-471-9371-6 (electronic ver.)
ISSN 1503-8181 (printed ver.)
ISSN 2703-8084 (electronic ver.)

Doctoral theses at NTNU, 2021:11

Printed by Skipnes Kommunikasjon AS

Carlos A. Aizprua Luna

Forearc crustal structure and controlling factors on basin formation across the southernmost Northern Andes

Geophysical and Geological Investigations

Thesis in cotutelle for the degree of Philosophiae Doctor

Trondheim, January 2021

Norwegian University of Science and Technology
Faculty of Engineering Science and Technology
Department of Geoscience and Petroleum

Université de Lille
École Doctorale Sciences de la Matière, du Rayonnement et de l'Environnement
Spécialité : Sciences de la terre et de l'univers
Laboratoire d'Océanologie et de Géosciences

NTNU
Norwegian University of Science and Technology

Université de Lille

… to my beloved wife, and my two children Mateo and Luna Sofia

Foreword

This research work and its results are part of the requirements for pursuing the degree of Philosophiae Doctor. Work carried out under a cotutelle agreement between the Norwegian University of Science and Technology (NTNU) in Norway and the University of Lille in France.

The origin of this work date back to 2014 when the University of Lille and the Ecuadorian national oil and gas company Petroamazonas established a joint industry-academy project to re-evaluate the region's hydrocarbon potential, focusing on reservoir presence and quality. At the same time, I was looking for a theme to start my research work at the Department of Geosciences and Petroleum (IGP) of the Norwegian University of Science and Technology (NTNU) in Norway. Thanks to the freedom provided by NTNU to choose the topic and Galo Montenegro's recommendation, a former professor in Ecuador, I got involved in the study. My academic supervisor at NTNU was Ståle E. Johansen and Jean-Yves Reynaud and Cesar Witt as supervisor and co-supervisor respectively from the University of Lille.

This research's initial focus was towards using a stratigraphic forward modelling approach to study sediment dispersion in the basin. However, several questions arose regarding the region's tectonic model and how this may have impacted basin segmentation and sediment deposition. Indeed, it pushed back to rethink the research questions and instead oriented it towards building a robust tectonic and stratigraphic framework. Following a drastic and ambitious change in the research topic, this study's time frame was prolonged considerably. Nevertheless, thanks to that decision, I consider we have moved a step further on our understanding of the region. I hope this encourages others to continue further this work and challenge it as new data become available.

Acknowledgements

I would like to express my gratitude to the people that accompanied me through this exciting academic challenge that I have completed. To Ståle E. Johansen, my academic supervisor at NTNU, who allowed me to plan very ambitious and challenging tasks. I must admit in retrospect, I took a high risk in setting such goals. However, Ståle's supports gave me the strength to conclude this work.

To Marco Brønner for his guidance and encouragement to apply non-seismic methods, such as gravity and magnetics, in my research work. Thanks for his patience as I was relatively unfamiliar with this old but quite relevant field of geophysics. A crucial part of this research work, bringing new insights into the region's underlying crustal structure.

To Galo Montenegro, a former professor at the "Escuela Superior Politécnica del Litoral (ESPOL)" in Ecuador, for his recommendation to Petroamzonas EP to incorporated me as part of the regional study on forearc basins along the SW Coast of Ecuador. For accompanying to the field along the Santa Elena Peninsula in Ecuador and Tumbes in Peru. Inspired by his Scout's leadership skills, Galo is "always ready" to help his peers and students both academically and personally.

To Cesar Witt, the responsible for dragging me into one of the most challenging geological puzzles that I have faced so far. I truly appreciate his great humour and willingness for technical discussions. I must say that Cesar is also responsible for my obsession with Peruvian ceviche. The time spend in Zorritos, Peru doing geological fieldwork was usually rewarded by a great Ceviche along the beach. Undoubtedly, Cesar is a great supervisor and critical support for achieving this goal.

To Jean-Yves Reynaud, for his great enthusiasm when discussing sedimentology and stratigraphic aspects to such a significant detail level. I must admit that sometimes I was lost in the details; his passion for the subject is unique. His

phrase of “I am just playing the devil’s advocate role” is inspiring to always look for antimodels or think outside the box.

To Runa Nielsen and Anna Trassaert, the responsible ones to set-up the cotutelle agreement between NTNU and Lille. I truly appreciate all your time to make this agreement happened despite the inconvenience on the way.

To Terje Solbakk and Dicky Harishidayat, former PhD colleagues at NTNU, for their great humour and support during my stay at the NTNU campus.

To the undergraduate students from ESPOL: Carolina Rivas, Alejandra Vera, Cristina Lopez, and Geovanny Benavides, that accompanied me and help me collecting field data for my work. I have great memories of this group and their enthusiasm for the field of geology.

Finally, this work would not have been possible to achieve without my wife's love and support. She was the central pillar for embarking on this adventure and being able to complete it. Thanks for the countless times that you took the role of a father to our son Mateo and now our daughter Luna. It has not been easy for all of us, but now it is over!

Trondheim, January 2021

Carlos Aizprua Luna

Abstract

The southernmost region of the Northern Andes was subject to the collision and accretion of the Caribbean Large Igneous Province (CLIP) during Late Cretaceous. A process that led to the entrapment of an oceanic crustal sliver, so-called “North Andean Sliver (NAS)”, conforming the underlying forearc basement. This study investigates the remnants of such collisional process throughout an integrated analysis of gravity, magnetic, seismic, and considerations from this and previous studies at the surface. The crustal model resulting from this work point towards evidence of a split paleo-island arc accreted almost undeformed to the continental margin and the residuum of a partial melting event. Furthermore, interpretation of the subsurface and 2D crustal forward model across the NAS's southernmost boundary to the margin account for a tear fault system, very likely responsible for the east-north-eastward migration of the NAS.

The trailing edge of the accreted sliver and its interaction with the continental margin indicate the development of a localized outer wedge (Santa Elena High), which may be in close relationship to a process of oblique subduction at a triple plate junction. The resulting configuration led to the development of two types of basins genetically related 1) a forearc s.s. depocenter controlled by the development of an outer forearc high, and 2) a transform boundary basin that records the periods of transtension and tectonic escape, both developed at least since the Oligocene.

The results presented in this research work provide new insights into our understanding of early forearc configuration and further basin development following the accretion of oceanic terranes.

Keywords: Northern Andes, outer forearc high, transform fault boundary, split arc

Résumé

La région la plus méridionale des Andes du Nord a été sujette à la collision et à l'accrétion des terrains océaniques de la plaque Caraïbe au cours du Crétacé supérieur. Ces processus a conduit au piégeage d'un fragment de la croûte océanique, le soi-disant Bloc Nord-Andin, entre une fosse nouvellement formée et la marge sud-américaine. Cette étude examine les rémanents du processus collisionnel à l'aide d'une analyse intégrée de la gravité, du magnétisme, de la sismique et des observations à la surface.

Le modèle crustal résultant de ce travail suggère l'existence d'un arc insulaire bissecté par un bassin marginal, ces deux éléments transférés (presque sans déformation) à la marge continentale lors du processus d'accrétion. L'analyse des anomalies magnétiques et gravimétriques met en évidence l'existence d'un coin mantellique serpentinisé très probablement lié à l'arc magmatique formé entre l'Eocène moyen et le Miocène inferieur.

Le bord sud du bloc accrété et son interaction avec la marge continentale sont étudiés ici avec plus de détail, indiquant que le développement local du haut structural externe (outer wedge) de Santa Elena peut être en relation étroite avec un processus de subduction oblique le long d'une jonction triple des plaques. La configuration qui en a résulté a conduit au développement de deux types de bassins génétiquement liés 1) série d'avant-bras s.s. contrôlé par le développement d'un avant-bras externe haut, et 2) un bassin limite de transformation qui enregistre les périodes de transtension et d'échappement tectonique.

Contents

Chapter 1

Introduction

Active margins and the development of forearc basins are regarded as complex entities with a low preservation potential of the underlying tectonic processes impairing or making ambiguous their geodynamic reconstructions. However, remnants from such tectonic processes may be exposed at the surface or buried by sediments in the subsurface. Thus, an interdisciplinary and multiscale approach is required to reveal the nature and role of the underlying tectonic elements to propose robust models. The models proposed are based on these premises, involving geophysical and geological studies at surface and subsurface levels, aiming to obtain a refined and integrated view of the Northern Andes' southernmost region (SW Ecuador – NW Peru).

This study aims to come forward on our understanding of forearc basin development following the collision, accretion, and entrapment of allochthonous oceanic terranes, at the southernmost Northern Andes. The geological record supporting such tectonic events, in Western Ecuador, have been commonly analysed through aids of geochemical, stratigraphic, and paleomagnetic data at surface. Access to existing subsurface and gravity and magnetic data has been limited up to recent times. This work has benefited from being linked to a joint industry-university project that allowed to access unpublished data. With recent seismicity and tomographic studies along the margin, this work presents a holistic and updated view of the crustal structure of an accreted oceanic terrane. Its alleged role in the development of the forearc region in Western Ecuador, since its emplacement. A particular focus is placed on the preservation potential of the elements from an ancient arc-continent collision

event preceding the development of the coastal forearc basins in Western Ecuador. Throughout the study of the main sedimentary depocenters, which record the continuum and varying processes occurring at the collision front, this work provides further knowledge of the tectonostratigraphic development of the forearc region under an inferred ancient triple plate junction geodynamic framework.

The building blocks of this research work can be grouped in two main components: 1) a series of field campaigns to assess the different sedimentary and tectonic processes associated with Cenozoic deposits, and 2) the analysis of subsurface data based on petroleum 2D/3D seismic and well data, and gravity/aeromagnetic data. The first component was carried out primarily in conjunction with the University of Lille, with a strong focus on the depositional age and provenance analysis of samples obtained on the field along the NW coast of Peru and Ecuador's SW coast. Moreover, the second one was carried out in Norway, at the Norwegian University of Science and Technology, which is the bulk of this research work.

1.1 Thesis Objective

This work aims to get a more comprehensive understanding of the processes linking geodynamics, topographic changes, and basin evolution at the southernmost Northern Andes forearc region. This is achieved based upon the integration of gravity, aeromagnetic, petroleum wells and seismic data, together with a source-to-sink approach involving new field surveys and radiometric dating in the onshore part.

It has a twofold objective: 1) define and propose a crustal model of the forearc region by incorporating previous results from crustal rock exposures along the Western Cordillera and Coastal regions of Ecuador, with recently acquired gravity and aeromagnetic data, and 2) study the role of the accreted terranes on strain partitioning of the forearc region as a plausible primary controlling factor on basin configuration and sediment dispersal possibly since its early emplacement.

Both objectives are linked together to improve our understanding of the link between the remnants of an ancient oceanic terrane and the development of forearc depocenters, possibly since its emplacement. This link is crucial for the ultimate objective of proposing a tectonostratigraphic model constrained to the results derived from the crustal model proposed in this work. This research project does not just bring new insights and knowledge on the Cenozoic development of forearc basins at the Northern Andes' southernmost region. However, it aims to further our understanding on the role and interaction that allochthonous terranes have on the initial and subsequent configuration of forearc basins, an aspect that may be common among Mesozoic systems along the Eastern Pacific. It aims to improve our knowledge of strain-partitioning from oblique subduction along active margins, in the presence of accreted forearc slivers. By studying conjointly, the development of forearc basins, and their interactions with accreted forearc slivers, we may shade light into continental growth and seismicity processes.

1.2 Motivation

It is prevalent to see different approaches link to a specific discipline when investigating forearc regions. Without crossing boundaries and integrating the results from different methods, the uncertainties may increase in our interpretations and lead to not-so-supported models. We should also consider that a pre-conceived model based on former experiences may restrict the progress in science, and therefore we need to challenge their validity constantly. This work has considered previously proposed models to identify their similarities, gaps, and strengths to build on the current research study. Through a multidisciplinary approach of geophysical and geological methods, both at surface and subsurface levels, I have tried to challenge previous models to check their validity and consistency. The current work intends to present a unified model that has been in a constant iteration based on the up-to-date knowledge of forearc basins from a global basis and the recent results from numerical models regarding the accretion of oceanic plateaus. Indeed, this was the central gap

or bottleneck that I found through this work, presenting a constrained tectonostratigraphic model of the southernmost Northern Andes, which unified all the identified tectonic elements concentrated in such a small and complex area. Therefore, an understanding of the crustal structure of Western Ecuador as a starting point is undoubtedly one of the significant milestones within this work. The constant zoom in and zoom out applied within this study allowed to challenge previous and models derived from this study. As an underlying controlling factor on the development of forearc basins in the region, connecting the crustal structure was an important step that challenges previous models and opens up specific geodynamic considerations regarding active margins developed onto ancient accreted oceanic terranes.

1.3 Organization of the thesis

The thesis and results are presented based on a holistic approach given the different scales of observations, which run from the interpretation of gravity and aeromagnetic data down to rock samples analysis. The results are documented by a compilation of three peer-reviewed publications and one draft in preparation for submission.

A comprehensive review regarding the different aspects and controlling factors along convergent margins and the generation of forearc basins is presented in chapter 2. For instance, the up-to-date known mechanisms for ophiolite emplacement and their preservation potential are considered in this chapter. Furthermore, given the relevance of gravity and magnetic data to reveal buried magmatic processes, a compilation of publicly available studies across different accreted and buried ophiolites is presented. This chapter emphasises the role of trapped oceanic slivers along active margins, as a primer on the structuration of forearc basins.

Former models describing the geodynamic aspects of Western Ecuador are not extensively summarized in a dedicated chapter. These are repetitively mentioned within the geological settings of each of the subsequent chapters. Instead, I emphasise the similarities and differences among available studies, within each of the subsequent

chapters. However, the reader is encouraged to look for details of each of the models by referring to the cited references.

In chapter 3, an integrated and novel study of western Ecuador's crustal structure through the aid of unpublished gravity, aeromagnetic, and seismic data is presented. This work put in context all former observations made on the surface, along the Western Cordillera and Coastal region, with the different geophysical anomalies analysed in this work to build and proposed a crustal model of Western Ecuador.

In chapter 4, the Cenozoic evolution of the SW Ecuador is presented based on an integrated view of different tectonic elements, their possible origin, and their interplay with localized but genetically sedimentary basins.

Subsequent chapters 5 & 6 take onboard the key outcomes obtained from the more regional work presented in previous chapters, to study the tectonostratigraphic aspects of the Progreso and Gulf of Guayaquil-Tumbes basins.

The main conclusions of this Ph.D. work and different perspectives are summarised in chapter 7.

Chapter 2

Tectonics and sedimentation along active continental margins

Active continental margins are the most dynamic regions tectonically speaking, where the primary process of rock recycling and continental crust generation occurs. These margins are characterized by the subduction of oceanic lithosphere beneath the continental lithosphere, with or without a volcanic arc built directly on the adjacent continent and connected directly to the hinterland (Frisch *et al.*, 2011). The plate boundary, represented by the trench, conforms to a broad zone of hundreds to thousands of kilometres in length (Figure 2.1). Landwards from the trench, the magmatic arc (when present) is located at a distance that is dependent on the angle of subduction, and the area in between the arc and the trench is denominated the forearc region. The sedimentary basins that develop across this region (s.s. forearc basins) are highly dependent on the volcanism developed landwards and the tectonic processes at the trench. Thus, it sounds imperative to consider all the different processes and their interplay across this region, both in space and through time searching for evidence or remnants in the geological record. This chapter provides an abridged overview of the main processes, highlighting their importance on margin configuration, their reconnaissance through the use of geological and geophysical tools, and their possible role through time.

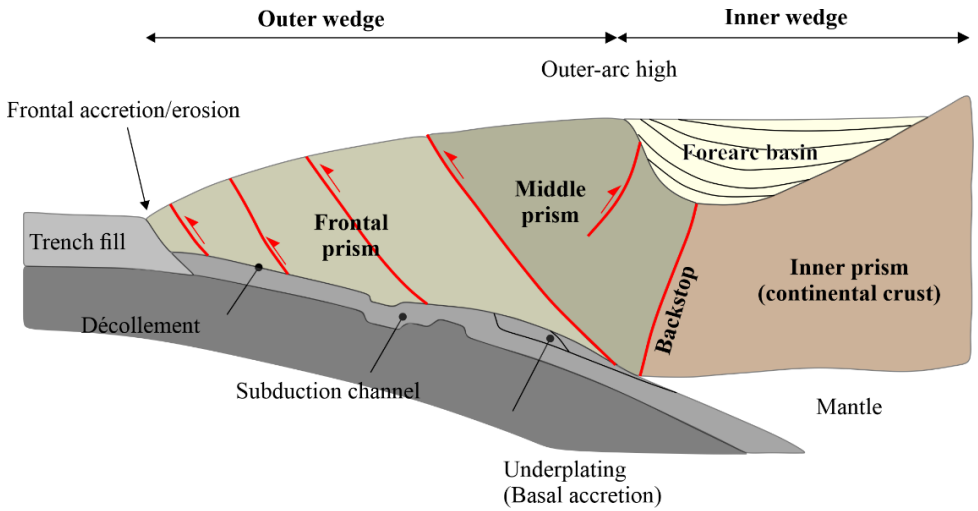

Figure 2.1: Terms related to forearc basins and the plate subduction zone (modified after Noda, 2016).

2.1 Subduction initiation

Before we focus our view on the different tectonic processes involved in the margin configuration, I would like to highlight the different subduction initiation processes. It is recognized that the reconstruction of a subduction initiation process remains enigmatic and controversial for advancing in our understanding of plate tectonics. The ephemeral nature of a subduction initiation process and the constraints imposed by buried evidence in forearc regions impair the access to tectonic, magmatic, and sedimentary responses to subduction initiation processes (Stern *et al.*, 2012). Furthermore, significant parts of the forearc may be lost by tectonic erosion (Scholl and von Huene, 2009; Draut and Clift, 2013); nevertheless, the preserved parts may contain a record of the processes that accompanied subduction initiation of a particular convergent margin. On land, ophiolites may provide access to the forearc composition and magmatic stratigraphy and subsequently understand the subduction initiation process. There are two recognized mechanisms in the literature: spontaneous and induced nucleation of subduction zones (Stern, 2004). However, I will also refer to a particular case of induced nucleation (plume-induced), which may be highly relevant in the southernmost Northern Andes domain.

2.1.1 Induced nucleation of subduction

The existing plate motion causes compression and lithospheric rupture at the boundary between two converging plates forming a subduction zone. Figure 2.2 shows two ways where a continuous plate convergence may yield a new subduction zone. The “transference” way is of particular interest in this work, as it is related to the presence or arrival of a buoyant crustal block at the subduction zone, a topic discussed in chapter 3 for the study area.

2.1.2 Spontaneous nucleation of subduction

Spontaneous subduction occurs when dense and old oceanic lithosphere sinks into the underlying asthenosphere, developing a down-dip sense of motion. A lithospheric weakness is required to overcome the lithospheric strength allowing the collapse (Figure 2.2) (Stern, 2004).

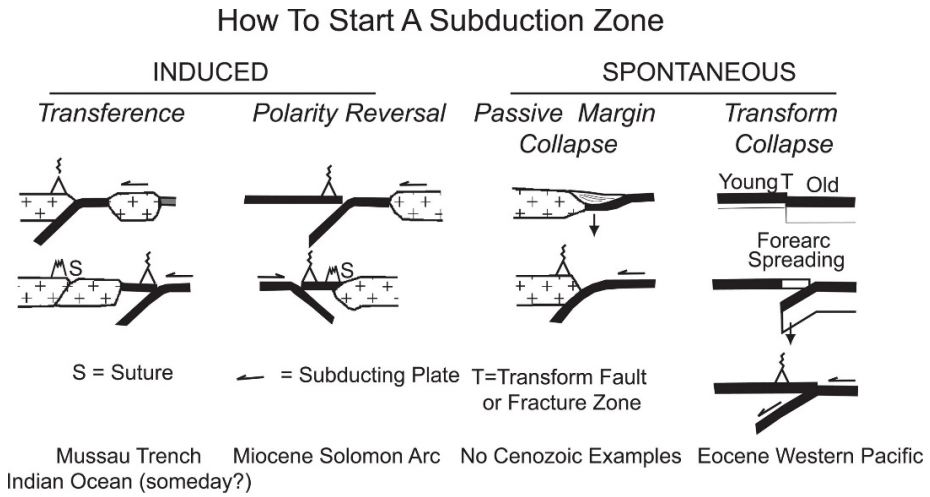

Figure 2.2: Sketches of the two main classes of subduction initiation processes (Stern, 2004).

2.1.3 Plume-induced subduction initiation

The Interaction of a large plume head with dense oceanic lithosphere could weaken the lithosphere by developing transform faults or subduction zones (Whattam and Stern, 2015). Indeed, thermo-mechanical numerical models investigate the lithosphere's interaction with a buoyant mantle plume, demonstrating that a mantle

plume can break the lithosphere and initiate self-sustaining subduction (Ueda *et al.*, 2008; Burov and Cloetingh, 2010). Based on trace element chemistry from most of the 100 Ma and younger units exposed along the southern margin of the Caribbean Plate and NW South America, Whattam and Stern (2015) suggest that there is a continuous evolution from plume magmatism into subduction-related magmatism with time, supporting the plume-induced subduction initiation process (Figure 2.3). The crustal rocks along the Western Cordillera and Coastal region in Ecuador relate to a sliver of the Caribbean Large Igneous Province (CLIP) accreted to the Northern Andes relevance of studying the remnant of such processes to constrain the pre-accretion geometry of the margin better. A combined geological and geophysical view of a remnant of a sliver from the CLIP is presented in chapter 3.

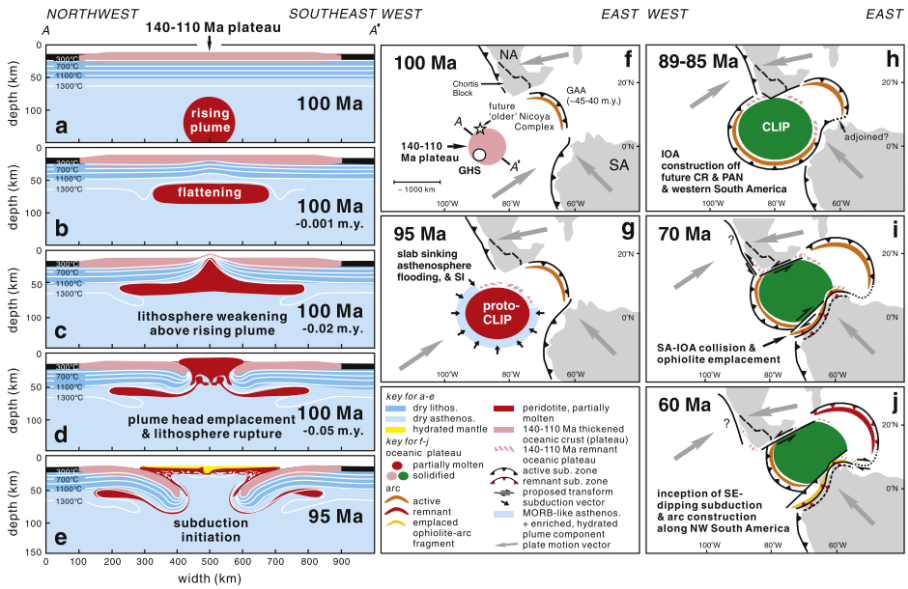

Figure 2.3: (a-e) thermo-mechanical models of Plume induced subduction initiation based on Ueda *et al.* (2008). (f-j) 100-60 Plume induced subduction initiation to volcanic arc generation tectonic reconstruction (further details in Whattam and Stern (2015)).

2.2 Ophiolites and mechanisms for their emplacement

Our understanding of ophiolite emplacement or obduction has been primarily based on the North American Cordillera (Kearey *et al.*, 2009). Their incorporation into land constitutes a fundamental aspect of continental growth and a problem on plate tectonics, as dense oceanic crust becomes emplaced over less dense material of continental margins (Wakabayashi and Dilek, 2003).

Ophiolites are recognized as fossil fragments of upper mantle and oceanic crust exposed on land usually incorporated into the continental margin during continent-continent and arc-continent collisions (Kearey *et al.*, 2009; Dilek and Furnes, 2011). They are mostly found along sutures zones in both collisional-type and accretionary-type orogenic belts. The association of deep-sea sediments, basalts, gabbro, and ultramafic rocks suggests that they originated as oceanic lithosphere and subsequently thrust up into their continental setting by obduction. However, it has been noticed in the past that ophiolites may represent fragments of crust and mantle formed by spreading at a ridge beneath an ancient ocean (Mason, 1985). Several examples suggest that ophiolites may have originated near their emplacement site through the development of Large Igneous Provinces (LIP) (Whattam and Stern, 2015), based on geochemical signatures and the short time between crystallization, collision, and accretion. Ophiolites constitute rock fragments that provide insight into ocean floor construction and continental growth, constituting key petro-tectonic elements for geodynamic reconstructions. Furthermore, their emplacement and nature are expected to vary depending on the age, thickness, and thermal state of oceanic crust, the nature and geometry of the plate boundaries involved (Wakabayashi and Dilek, 2003).

A thorough review of the genesis and tectonics of ophiolites is given by Dilek and Furnes (2011). These authors present a new classification that incorporates the diversity in their structural architecture and geochemical signatures. A particular type of ophiolites that have a mid-ocean-ridge basalt (MORB) composition is subduction-unrelated ophiolites such as the case of the Northern Andean Sliver, where geochemical analysis of surface exposures indicates a MORB signature.

Wakabayashi and Dilek (2003) distinguish four types of ophiolites based on their emplacement mechanism and the nature of the underlying tectonic basement. However, only the first two are discussed in this chapter, given their abundance and importance for the present study: 1) Tethyan; and 2) Cordilleran (Figure 2.4).

Tethyan-type ophiolites structurally overlie passive continental margins, microcontinental fragments, or island arcs. The extrusive section of most of these ophiolites does not have volcaniclastic rocks typical of a volcanic arc. However, many of these ophiolites display geochemical characteristics of subduction zone environments in their upper-crustal part.

Cordilleran-type overlies subduction-accretion complexes instead. The volcaniclastic and intermediate silicic volcanic rocks that are generally associated with island arc development are widespread in the extrusive sections of Cordilleran ophiolites (Wakabayashi and Dilek, 2003). Upper-crustal rock units in Cordilleran ophiolites display island arc tholeiite to calc-alkaline chemical affinities indicating a subduction zone origin. The existence of volcaniclastic rocks is indicative of volcanic arc edifices construction during the evolution of these ophiolites. This last aspect, considered in this work, is further discussed in Chapter 3.

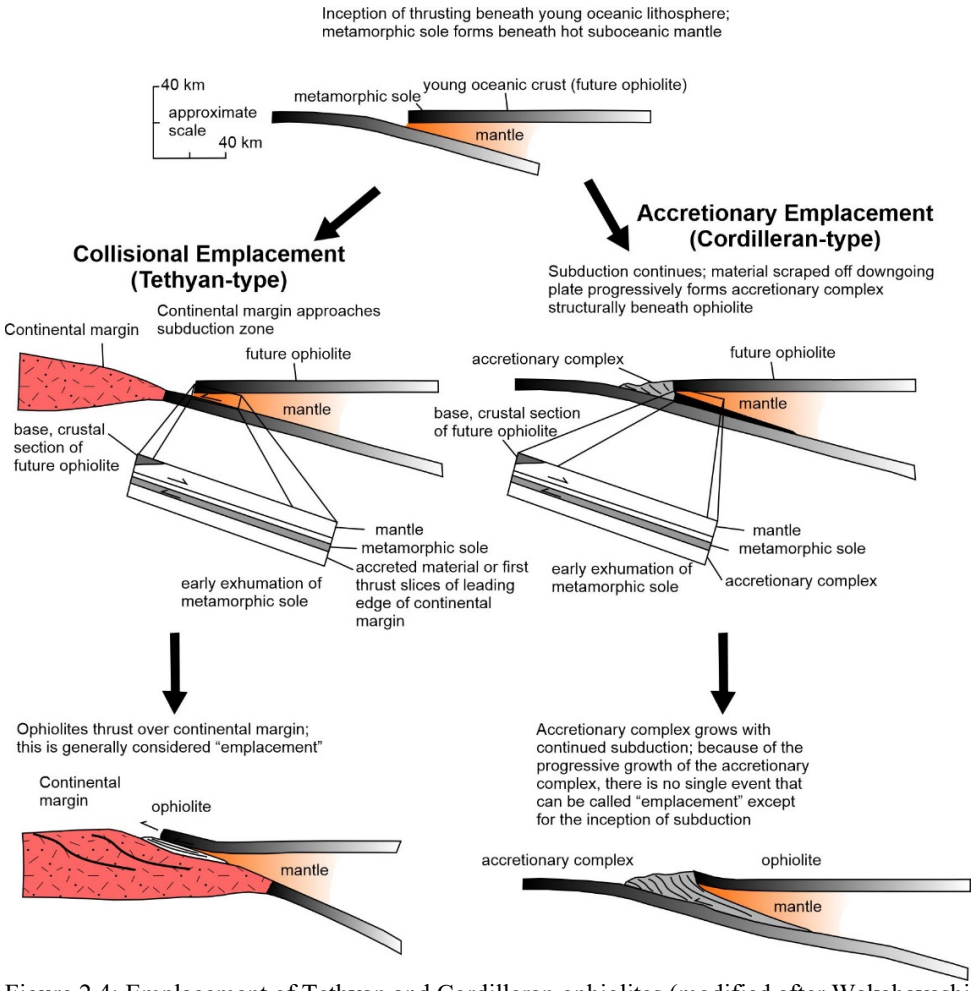

Figure 2.4: Emplacement of Tethyan and Cordilleran ophiolites (modified after Wakabayashi and Dilek, 2003).

Many ophiolite complexes are structurally underlain by fault-bounded sheets of highly strained high-grade metamorphic rocks, called metamorphic soles (Figure 2.4). Metamorphic soles constitute witnesses of the earliest stages of obduction in intra-oceanic settings preceding final emplacement onto continental margin, which is a constraint when building any initial geodynamic stage at convergent plate margins (Wakabayashi and Dilek, 2003; Agard *et al.*, 2012).

As shown in Figure 2.5, major and voluminous magmatic pulses occurred in the Mesozoic at a hemispheric scale (Stern *et al.*, 2012), located along the Caribbean region and Western Pacific (Figure 2.6), and therefore their importance of study to better understand continental growth processes.

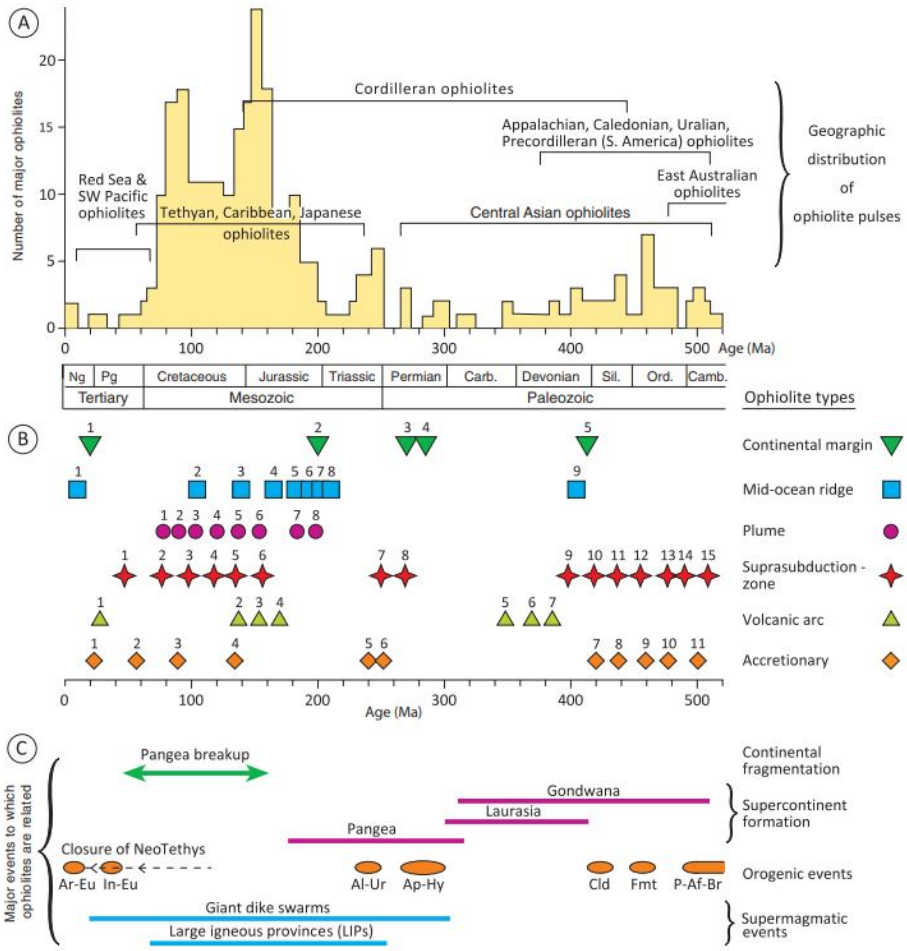

Figure 2.5: Ophiolite pulses and the distribution of major orogenic belts with ophiolite occurrences during the Phanerozoic (Dilek and Furnes, 2011).

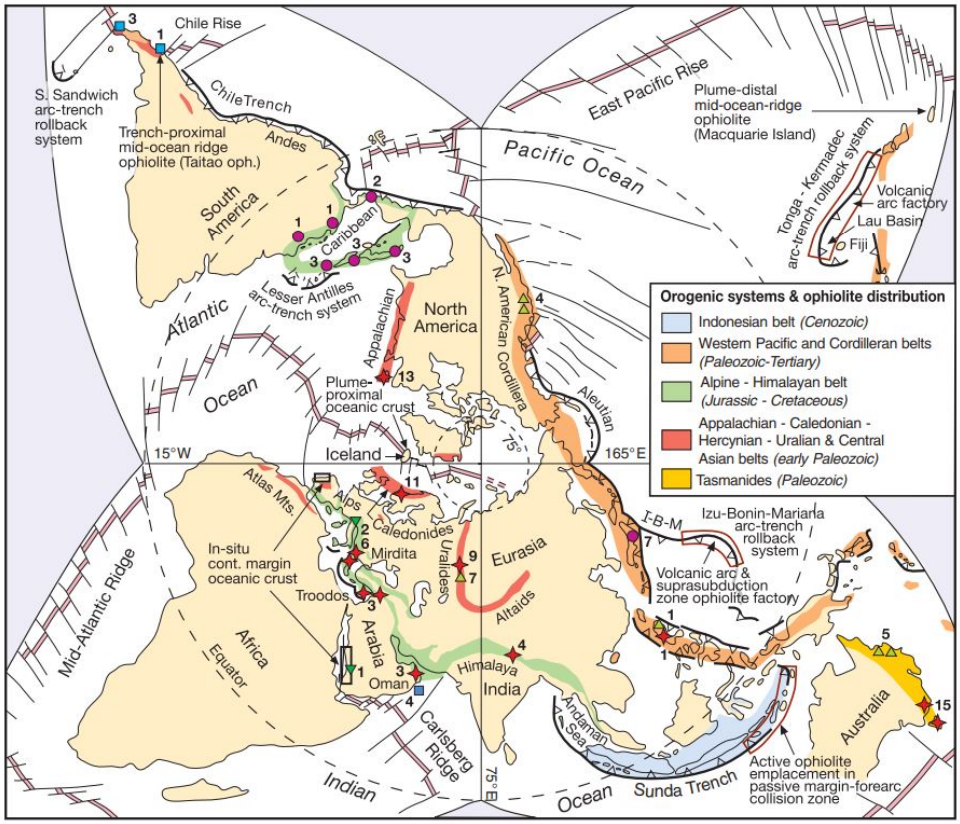

Figure 2.6: Global distribution of major Phanerozoic orogenic belts and ophiolites age clusters on a north polar projection (Dilek and Furnes, 2011).

2.3 Accretionary vs. erosional regimes

Subduction zones as shown in Figure 2.7 can be erosive or accretionary. It has been recognized that the sediments attached to the subducting oceanic plate may underthrust the overriding plate, a process called sediment subduction, and that material from the upper plate can be removed or scraped-off and subducted by a process of subduction erosion (Von Huene and Scholl, 1991).

The notions of sediment subduction arise from unbalanced volumes in regional sediment budgets and the absence of accretionary wedges along some convergent margins. The input material attached to the oceanic crust is primarily composed of

clay, far-travelled terrigenous detritus, and the carbonate and siliceous material supplied by planktonic and benthic organisms. These deposits typically reach only 200-400 m thick, and in the presence of large drainage systems derived from the continent to the ocean, the thickness can be greater than 500m. Such deposits, often transported by some turbidity currents may be concentrated along the trench axis forming a wedge-shaped body that may be added to the upper plate by processes of frontal accretion and basal underplating (Figure 2.8) (Scholl *et al.*, 1980).

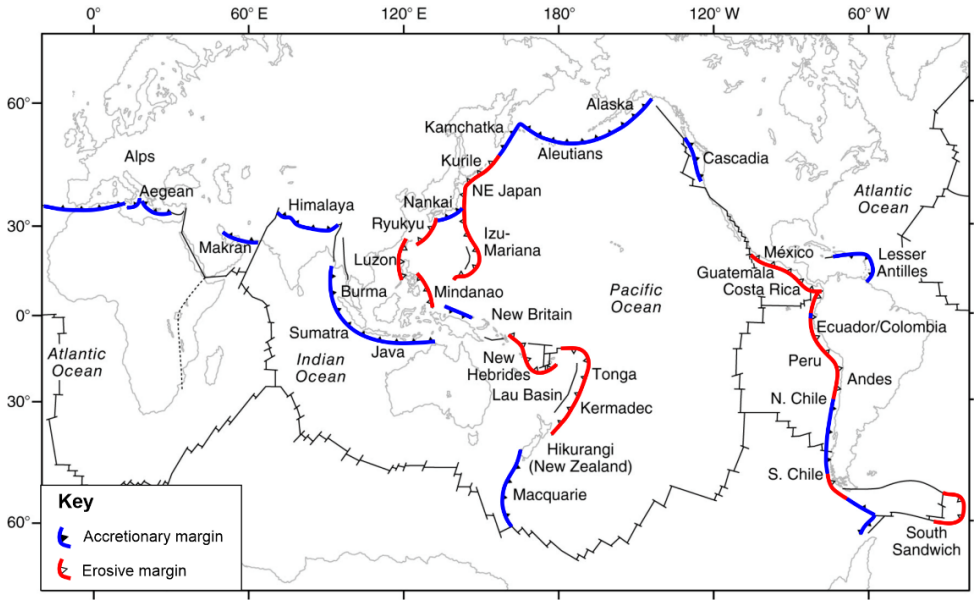

Figure 2.7: The location of convergent plate margins (modified after Kearey *et al.*, 2009).

A region of well-lithified rocks seaward of the volcanic arc, known as the margin mechanical backstop, is characterized by a greater shear strength than the sediments lying trenchward (Byrne *et al.*, 1993; Kopp and Kukowski, 2003). It plays an essential role in the overall growth of forearcs (Byrne *et al.*, 1993). Indeed, numerical and analogue modelling shows that a reasonable contrast in mechanical properties with the sediments trenchward, may result in the development of an outer forearc high, which may bound a relatively undeformed forearc basin landward.

Analogue or numerical modelling has led to a better understanding of the evolutionary processes taking place during an arc-continent collision (see next sections).

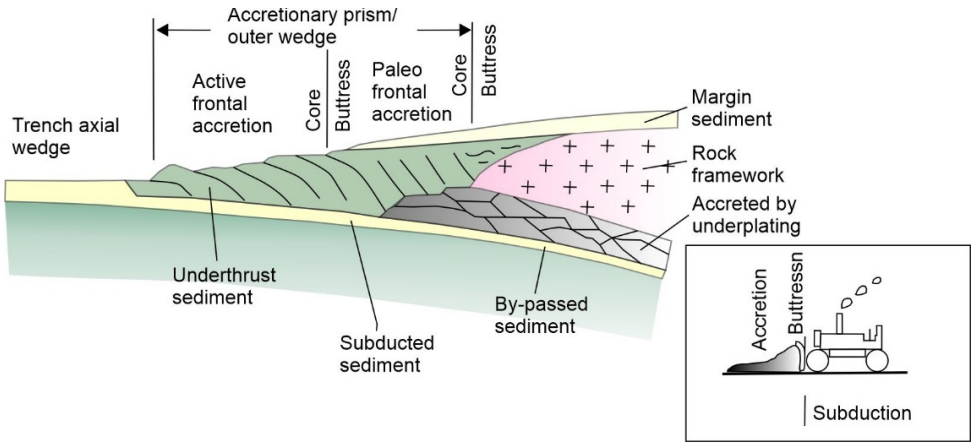

Figure 2.8: Diagram of an accretionary prism/outer wedge and the processes of frontal accretion and underplating that contribute to its volumetric growth (modified after Von Huene and Scholl, 1991).

2.4 Arc-continent collision: insights from analogue and numerical modelling

The natural examples of arc-continent collisions available in the literature show very different geometries and complexities that appear to depend on several first-order parameters, such as the age of the oceanic crust, and the pre-existing structure of the margin and the arc (Brown *et al.*, 2011). Through the aid of geophysical and geological tools (discussed in the last section of this chapter), we may get insights into some of these parameters. Especially for ancient systems, which have undergone post-collision deformation or erosion, leaving us with partial evidence of the original arc-continent collision (Brown *et al.*, 2011). To better understand the evolutionary processes taking place during an arc-continent collision, the use of analogue modelling (Figure 2.9) or numerical techniques provide insights into the geodynamic

evolution of such process. Bellow, I present a non-extensive summary of these techniques and their main conclusions.

2.4.1 Physical modelling of arc-continent collisions

The partial insight given by the geological data on the lithospheric processes involved in arc-continent collisions is limited, requiring to invoke physical or numerical techniques to understand better the evolution of the plausible processes in nature (Boutelier and Chemenda, 2011).

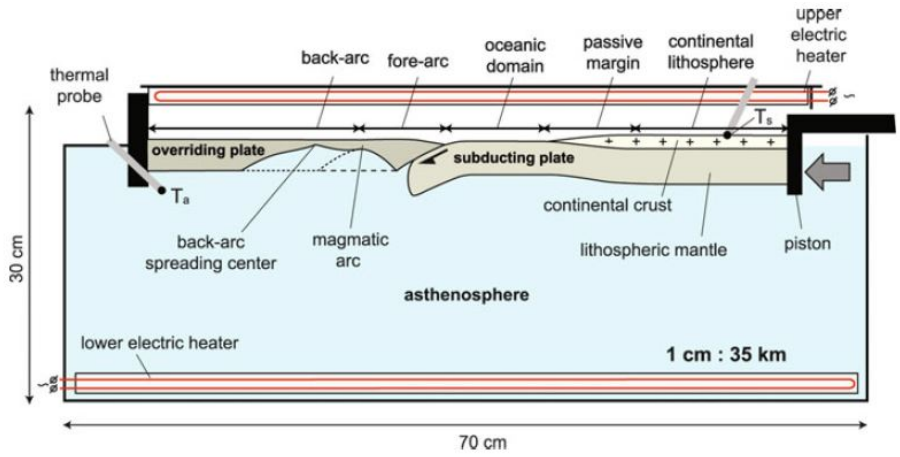

Figure 2.9: Analogue experimental setup (details are provided in Boutelier and Chemenda (2011)).

2.4.1.1 Oceanic subduction

To better illustrate the effects of the bending strength of the subducting lithosphere and the force due to its negative buoyancy on the distribution of stresses along the interplate zone, two regimes of oceanic subduction are identified, which are associated with the compressive or tensile regimes in the arc/back-arc areas.

Under a compressive regime, the subducting lithosphere resists to bending during subduction causing a compressive non-hydrostatic normal stress whose magnitude increases with depth along the interplate zone (Figure 2.10). In the tensile regime, the density of the subducted lithosphere is significantly larger than that of the

surrounding mantle, creating a negative buoyancy that generates a downward pull force, which results in a tensile non-hydrostatic normal stress on the interplate zone. However, when the length of the subducted slab reaches a certain critical value, the slab pull force becomes sufficient to cause slab break-off, after which oceanic subduction switches to the compression regime (Boutelier and Chemenda, 2011). Several numerical models of slab breakoff have shown that the age influences the depth and the implemented rheology in the subducting plate, as a result there is a broad range of depths between 80-510km, requiring 1 to 50 Ma (Fernández-García *et al.*, 2019).

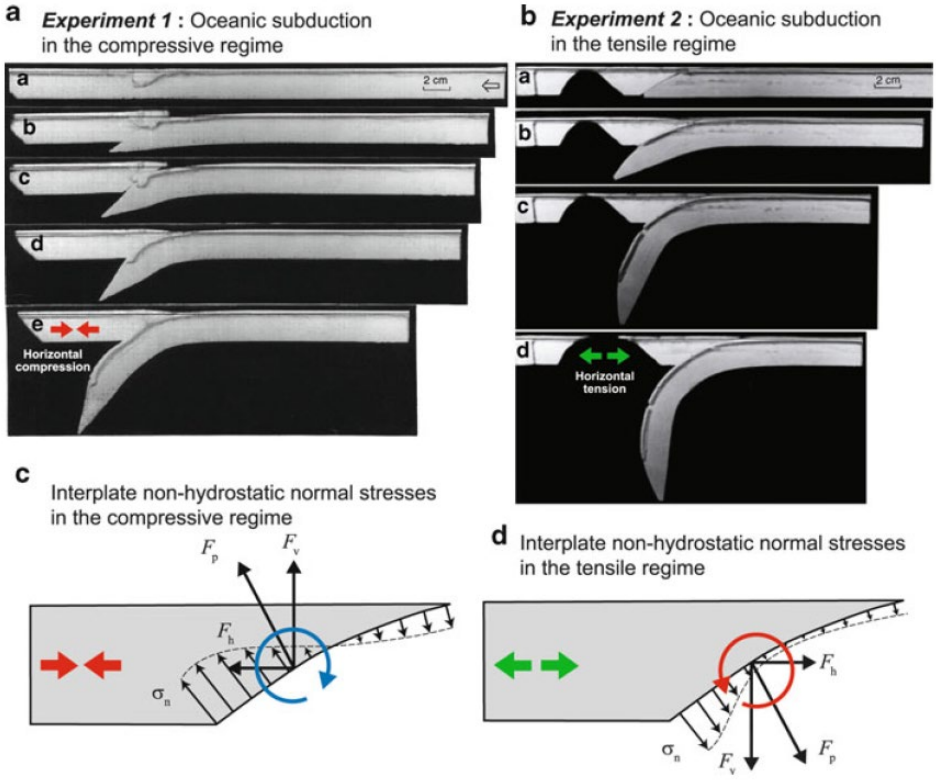

Figure 2.10: Mechanical experiments of oceanic subduction in the compressive (a,c) and extensive (b,d) regimes ((Shemenda, 1993))

2.4.1.2 Continental subduction

Due to the high buoyancy of the subducting continental crust, continental subduction is primarily associated with two principal regimes (Figure 2.11), a high and low compressional regime, characterized by high and low pressure between the overriding and subducting plates respectively (Chemenda *et al.*, 1996). As for oceanic subduction, the regime of continental subduction is mainly controlled by the slab-pull force due to the negative buoyancy of the subducted lithospheric mantle and the bending strength of the lower plate (Boutelier and Chemenda, 2011).

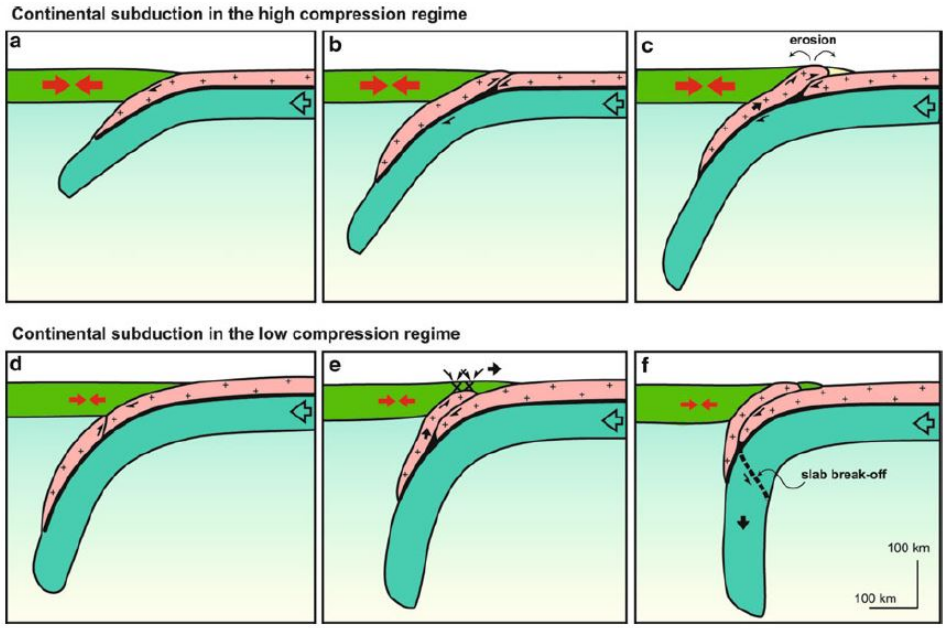

Figure 2.11: Two principal regimes of continental subduction obtained in purely mechanical experiments (Boutelier and Chemenda, 2011).

2.4.2 Numerical models

I have placed an interest in the collision and accretion of oceanic plateaus and their role in continental growth. The numerical models presented by Vogt and Gerya (2014) resulted in oceanic plateau either being lost by subduction (>40 Ma oceanic lithosphere) or accreted onto continental margins (younger oceanic lithosphere). This

study identifies one mode of complete plateau subduction and three modes of terrane accretion, they include: 1) frontal plateau accretion, 2) basal plateau accretion, and 3) underplating plateaus. Although, complete plateau subduction is the dominant process, the other three accretionary modes show that following a collision process the time to re-establish a stable subduction varies depending on the accretion mode. The basal plateau accretion shows an outward migration of the subduction zone, with the incoming oceanic crust underthrusting the fractured terrane, forming a new subduction zone behind the accreted terrane. This result is of crucial importance in this work as it may partly explain the local development of some structural highs following the re-establishment of the new subduction zone (Figure 2.12), an aspect discussed further in Chapter 4.

The oceanic plateau – trench collision appears to strongly influence the shape of the trench surrounding the plateau, causing a reduction on the trench retreat in the case of a plateau with high density, and a trench advance in the case of lower density plateaus (Mason *et al.*, 2010).

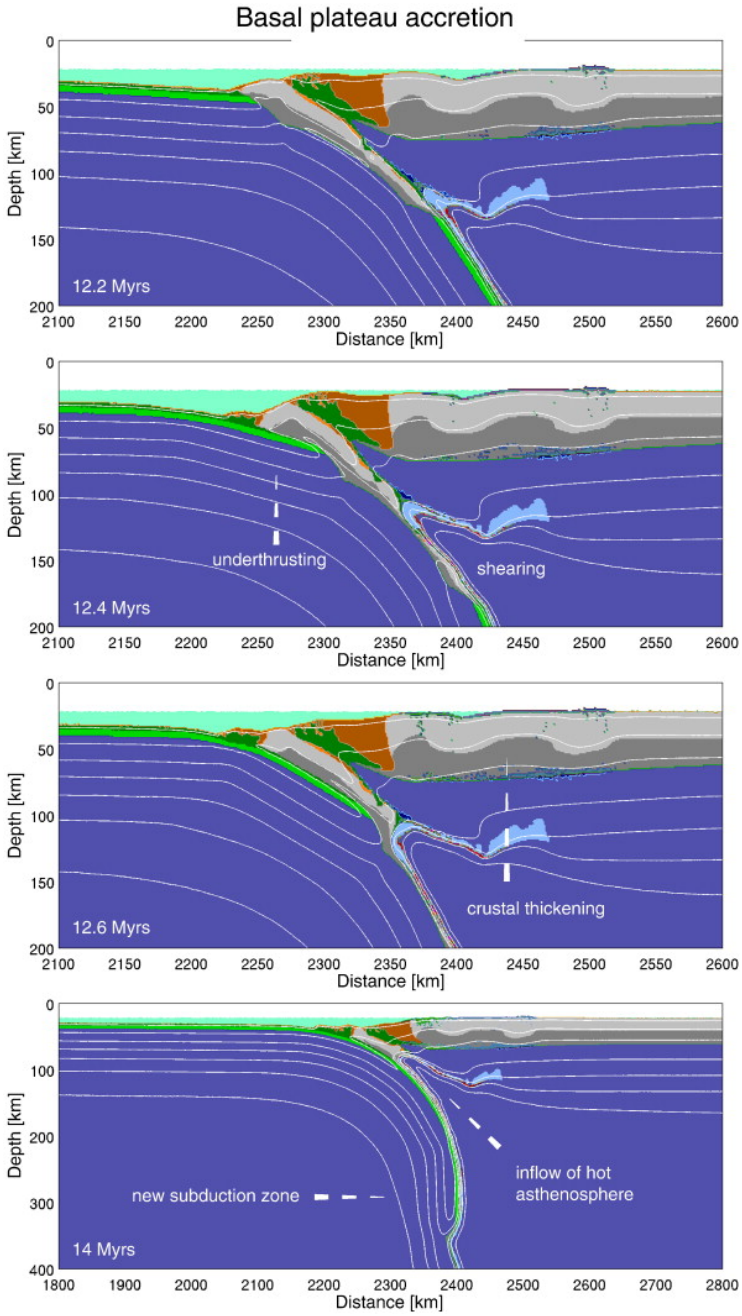

Figure 2.12: Basal plateau accretion mode. Crustal material of the oceanic plateau is scraped off the downgoing slab and accreted onto the continental margin. Strong deformation leads to slab detachment and the outward migration of the subduction zone. Oceanic crust underthrusts the accreted terrane and forms a new subduction zone (subduction zone jump) (Vogt and Gerya, 2014).

2.5 Gravity and magnetic responses of trapped oceanic terranes

The contrasting magnetic and gravity signatures over buried crustal terranes may provide insights into different tectonic processes, such as previously unrecognized sutures or the nature of an underlying block. Figure 2.13 shows the case of an unrecognized oceanic crustal block in Victoria Land in Antarctica (Ferraccioli *et al.*, 2002), where the use of gravity and magnetic aid to distinguished a terrane of oceanic affinity previously not considered. Incorporation of gravity and magnetic signatures may have substantial implications on previous proposed tectonic models, given the new constraints derived from their interpretation.

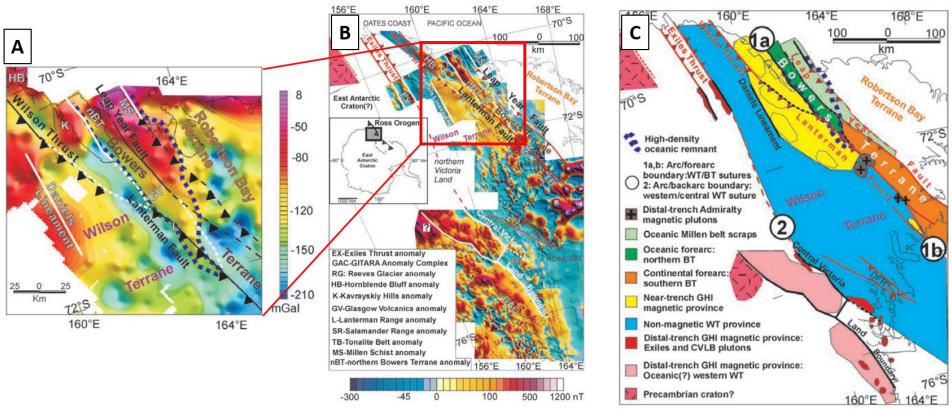

Figure 2.13: a) Bouguer gravity map highlighting in dotted blue line the edges of a previous unidentified high density oceanic body in the Bowers terrane, b) magnetic anomalies over early Paleozoic Victoria Land terranes, c) Crustal interpretation from gravity and magnetic anomalies (Ferraccioli *et al.*, 2002).

An additional process related to subduction is the presence of a hydrated forearc mantle, which may significantly affect the magnetization of the rocks. Blakely *et al.* (2005) identified an apparent spatial disparity between the gravity and magnetic anomalies across the Oregon forearc (Figure 2.14), which is consistent with the presence of a hydrated mantle wedge observed on seismic reflection data. Same authors suggest that a magnetic mantle may be a common forearc setting and thus magnetic anomalies may be useful in mapping hydrated mantle in convergent

margins. This is a key observation that its consider in chapter 3, to analyse the gravity and magnetic anomalies and propose a crustal interpretation.

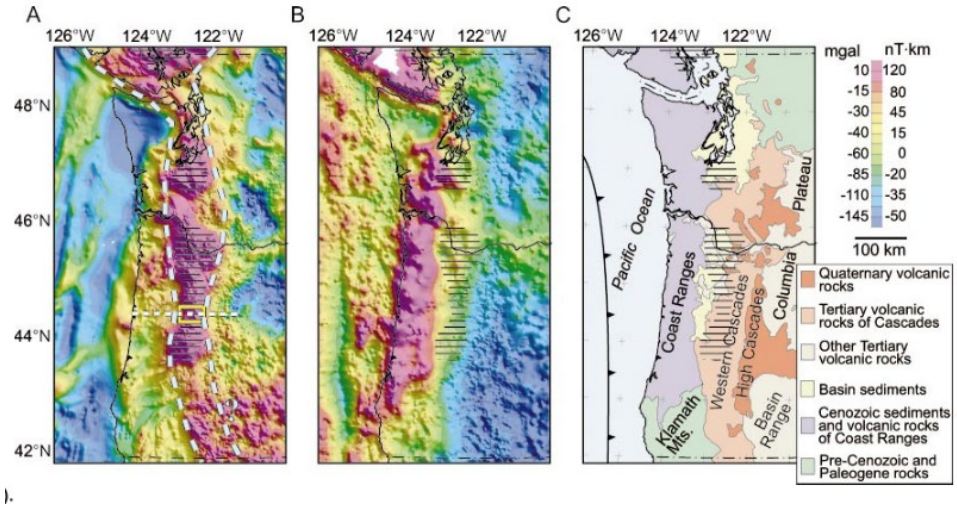

Figure 2.14: a) Aeromagnetic anomalies, b) Bouguer gravity anomalies onshore, free-air anomalies offshore, c) Geology of the Cascadia, black horizontal line pattern shows the location of magnetic anomalies of highest amplitudes Blakely *et al.* (2005).

2.6 Forearc basins

The different processes occurring at the trench that lead to the accretion or erosion of the outer wedge will govern the style of the forearc (Noda, 2016), and thus the depositional environments across the basin. Noda (2016) provides a forearc basin classification, which links to the development of the outer-arc high and the processes occurring at the plate boundary (Figure 2.15). However, the consideration of the mechanical properties and geometry of the backstop may also play an essential role in the forearc basin (Byrne *et al.*, 1993). This las point is especially relevant in this research work, as the nature of the backstop is related to a sliver from the Caribbean Large Igenous Province plateau, aspects cover in chapter 4, 5 and 6. Furthermore, the strain partitioning imposed under oblique subduction may as well be a fundamental factor on the mechanism of sedimentary basin formation at the forearc, by creating localized depressions with higher subsidence rates (Noda, 2013).

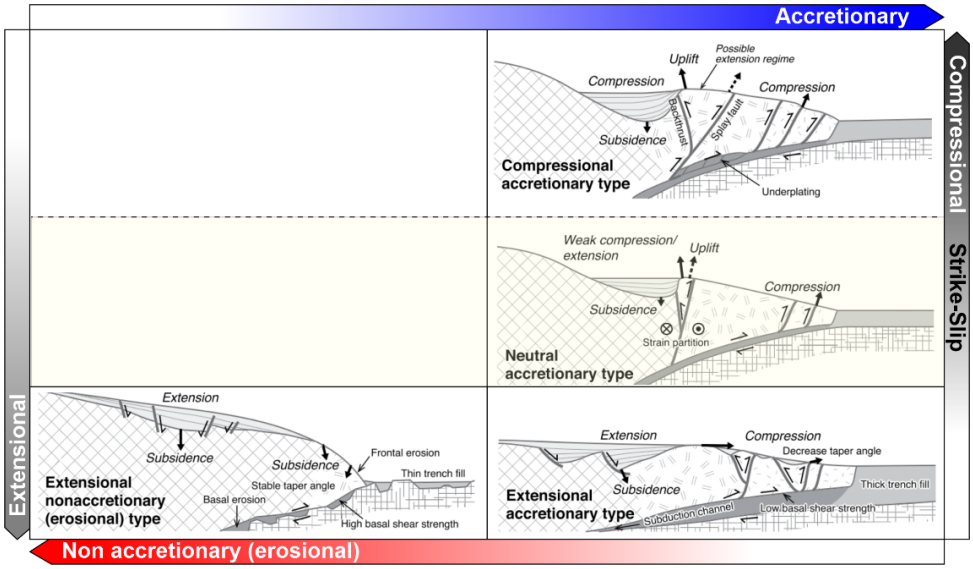

Figure 2.15: Classification of forearc basin (modified after Noda, 2016).

Summary

This summary of the different processes and tectonic elements involved in active margins provides an idea of the different consideration that should be taken, at different scales of observation, when assessing a forearc basin. The variation in processes both in time and space, together with the poor preservation in the geological record of some of these processes may impair our understanding and models. Hence, it is critical to use different tools in an integrated approach. The subsequent chapters address many of these tectonic processes and the integrated approach for their assessment.

Chapter 3

Crustal structure of western Ecuador

The content of this chapter is published in: ***Aizprua, C****., Witt, C., Brøner, M., Johansen, S.E., Barba, D., and Hernandez, M.J., (2020). Forearc Crustal Structure of Ecuador Revealed by Gravity and Aeromagnetic Anomalies and Their Geodynamic Implications, Lithosphere, 2020(1), pp. 1-23.*

Along the Western Cordillera of Ecuador, fault-bounded ophiolites derived from the Late Cretaceous Caribbean Large Igneous Province (CLIP) have provided key petro-tectonic indicators that outline the nature and the mechanism of continental growth in this region. However, most of the forearc basement across Western Ecuador is buried under sediments impairing its crustal structure understanding. Here we propose a first crustal model throughout the spectral analysis of gravity and aeromagnetic data, constrained by observations made both at the surface and subsurface. Three main geophysical domains, within the North Andean Sliver in Western Ecuador, have been defined based on spectral analysis and augmented by 2D forward models. An outer domain, characterized by magnetic anomalies associated with mafic rocks, coincides with evidence of a split intraoceanic arc system. An inner domain governed by long-wavelength mid to deep crust – sourced gravity and magnetic anomalies possibly evidencing the root of a paleo-island arc and the residuum of a partial melting event with subsequently associated serpentinization, the latest possibly associated to an obduction process during the middle Eocene – Oligocene. In addition, our model supports the presence of a lithospheric vertical tear

fault, herein the southern suture domain, inherited from an oblique arc-continent interaction. Our interpretation also brings new insights and constraints on the early geodynamic evolution of the Ecuadorian forearc and provides evidence on the structural style and preservation potential of the forearc basement, most likely the roots of a mature island arc built within an oceanic plateau.

3.1 INTRODUCTION

Major continental growth took place along the NW corner of South America during the Late Cretaceous, following the collision and accretion of a sliver from the Caribbean Large Igneous Province (CLIP) (Kennan and Pindell, 2009; Boschman *et al.*, 2014; Whattam and Stern, 2015). Records of the interaction between the CLIP and the South America continental margin are preserved along its suture zone in the Western Cordillera and SW coastal Ecuador (e.g. Hughes and Pilatasig, 2002; Kerr *et al.*, 2002; Jaillard *et al.*, 2009; Vallejo *et al.*, 2009; Aizprua *et al.*, 2019b) (Figure 3.1). Several lines of evidence suggest that before the collision with South America the CLIP was affected by the emplacement of the tholeiitic San Lorenzo/Naranjal and Rio Cala island arcs, while the western limit of the South American plate (SAP) was most likely a passive margin (Jaillard *et al.*, 2009; Vallejo *et al.*, 2009). Different authors agree on an oblique arc-passive margin collision configuration starting at ~75Ma (Jaillard *et al.*, 2009; Boschman *et al.*, 2014; Braz *et al.*, 2018) with subsequent clockwise block rotations between ~70-75Ma (Roperch *et al.*, 1987; Luzieux *et al.*, 2006; Kennan and Pindell, 2009). However, discrepancies exist about the subduction polarity beneath the CLIP. This aspect and the arc-continent collision geometry, including the tectonic regime of the subduction, may have had a great impact on the preferential preservation or loss of evidence of the Late Cretaceous subduction system (Draut and Clift, 2013).

Stern *et al.* (2012) suggest that ophiolites emplaced along the suture zone provide the best record for understanding subduction initiation processes and forearc composition and magmatic stratigraphy. Such exposures along the Western Cordillera of Ecuador and Colombia have provided key petro-tectonic indicators for the geodynamic reconstruction of the NW South American margin (Figure 3.1). Nevertheless, the low preservation potential of such ancient terranes after an arc-continent collision, together with limited exposure could limit geodynamic reconstructions, leading to controversial interpretations (Clift and Vannucchi, 2004; Draut and Clift, 2013). Despite the records of arc activity in the Western Cordillera,

there are few publications discussing the different pre-collision elements of the subduction system including the location of the trench, forearc, and back-arc systems.

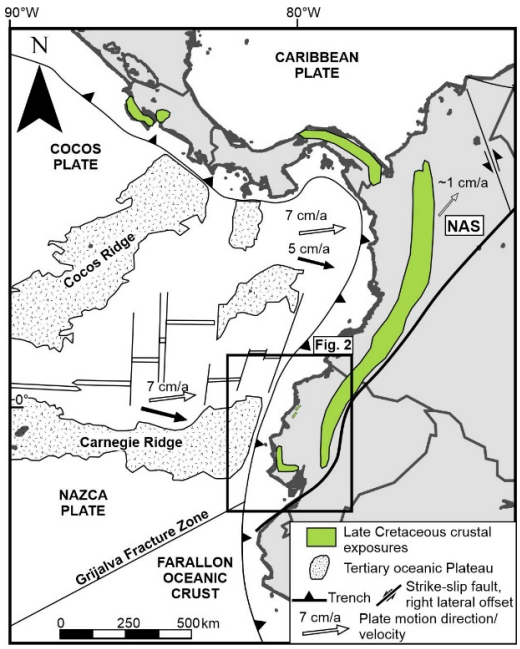

Figure 3.1: Plate configuration of the NW South America and Central America regions, highlighting the surface exposure of ophiolites attributed to the Late Cretaceous Caribbean Large Igneous Province (CLIP). Plate kinematics are derived from relative plate motions according to GPS data (unfilled color arrow) and the NUVEL-1 global kinematic model (filled color arrow). Modified after: **(Gutscher *et al.*, 1999; Aitken *et al.*, 2011; Whattam and Stern, 2015)**

In Western Ecuador, between the Coastal Cordillera and the Western Cordillera (Figure 3.2A), the units associated with the accreted sliver are buried beneath the Cenozoic forearc sediments impairing the reconstruction of the underlying forearc basement. We use an unpublished aeromagnetic/gravity survey of this region (Figure 3.2B), and present a multi-scale data integration approach to uncover the underlying crustal structure of the forearc region in Ecuador and add further constraints on the geodynamic evolution of the region. This work was motivated by the lack of a crustal model for the Ecuadorian forearc region. Indeed, since the presentation of a simple 2D Bouguer's anomaly forward model across the continental margin by Feininger and Seguin (1983), until a recent and similar plate-scale study using satellite potential field

data by Tamay *et al.* (2018), the underlying basement structure of the Ecuadorian forearc remains poorly understood.

In this work, we have defined three main geophysical domains based on the analysis of aero gravity/magnetic anomalies, constraints derived from published geodynamic scenarios (Lebrat *et al.*, 1987; Kerr *et al.*, 2002; Mamberti *et al.*, 2003; Luzieux *et al.*, 2006; Jaillard *et al.*, 2009; Vallejo *et al.*, 2009), and by means of 2D forward models. Our model shows a heterogeneous and structurally complex basement, which may have resulted from the fragmentation of the sliver following the initial accretionary phase. Furthermore, our model sheds light on the nature of the southern suture between the accreted sliver of the CLIP and the continental block.

3.2 REGIONAL GEOLOGY

The Coastal and Western Cordillera regions in Ecuador are characterized by exposures associated with crustal fragments derived from the plume derived Caribbean Large Igneous Province (CLIP) erupted in Early - Late Cretaceous times (e.g., Mamberti *et al.*, 2003; Van Melle *et al.*, 2008; Whattam and Stern, 2015) (Figure 3.2). The arrival and collision of the CLIP along the NW corner of the South American margin has been dated as a Late Cretaceous event (75-65 Ma) based on stratigraphic, paleomagnetic, and radiometric age control (Kerr *et al.*, 2002; Luzieux, 2007; Vallejo *et al.*, 2009). Paleomagnetic studies in Western Ecuador by Roperch *et al.* (1987) and Luzieux *et al.* (2006) concluded that the arc-derived basement in Ecuador was generated at low latitudes. The collision of the CLIP may have been followed by crustal fragmentation and clockwise rotations (ca. 40-50°) during the Campanian to Early Maastrichtian (Roperch *et al.*, 1987; Luzieux *et al.*, 2006). Alternative models propose the presence of at least two different oceanic plateaus emplaced during two accretionary periods between the Late Cretaceous and the Late Eocene (Jaillard *et al.*, 1995; Reynaud *et al.*, 1999; Hughes and Pilatasig, 2002; Kerr *et al.*, 2002).

3.2.1 Western Cordillera crustal blocks

3.2.1.1 Pallatanga block

The block is located along the Western Cordillera and is composed of a series of fault-bounded slices with SSW-NNE direction (Figure 3.2B). It is limited to the west by the Chimbo-Toachi fault, and the east by the Calacalí-Pujilí-Pallatanga fault (Figure 3.2B). It comprises Early to Late Cretaceous mafic to ultramafic rocks, mainly composed of basalts, gabbros, and massive dolerites, overlain by volcaniclastic sediments (Figure 3.2C) (Kerr *et al.*, 2002; Mamberti *et al.*, 2003). Basalts and gabbros from the Pallatanga block have an enriched MORB geochemical signature, possibly related to a mantle plume eruption (Lebrat *et al.*, 1985; Lapierre *et al.*, 2000; Hughes and Pilatasig, 2002; Kerr *et al.*, 2002; Mamberti *et al.*, 2003). Its easternmost part comprises serpentinized peridotites, dolerites, and hornblende-bearing gabbros from the San Juan unit (Kerr *et al.*, 2002; Jaillard *et al.*, 2009). An amphibole-bearing gabbro of this unit yielded an Sm/Nd isochron of 123 ± 1.3 Ma (Lapierre *et al.*, 2000) and a poor Ar/Ar integrated age of 105 Ma (Mamberti *et al.*, 2004). However, zircons from a layered gabbro mapped as the San Juan unit yielded a U/Pb age of 87.1 ± 1.66 Ma (Vallejo *et al.*, 2009), suggesting that the San Juan unit is part of the same oceanic plateau as the Pallatanga unit.

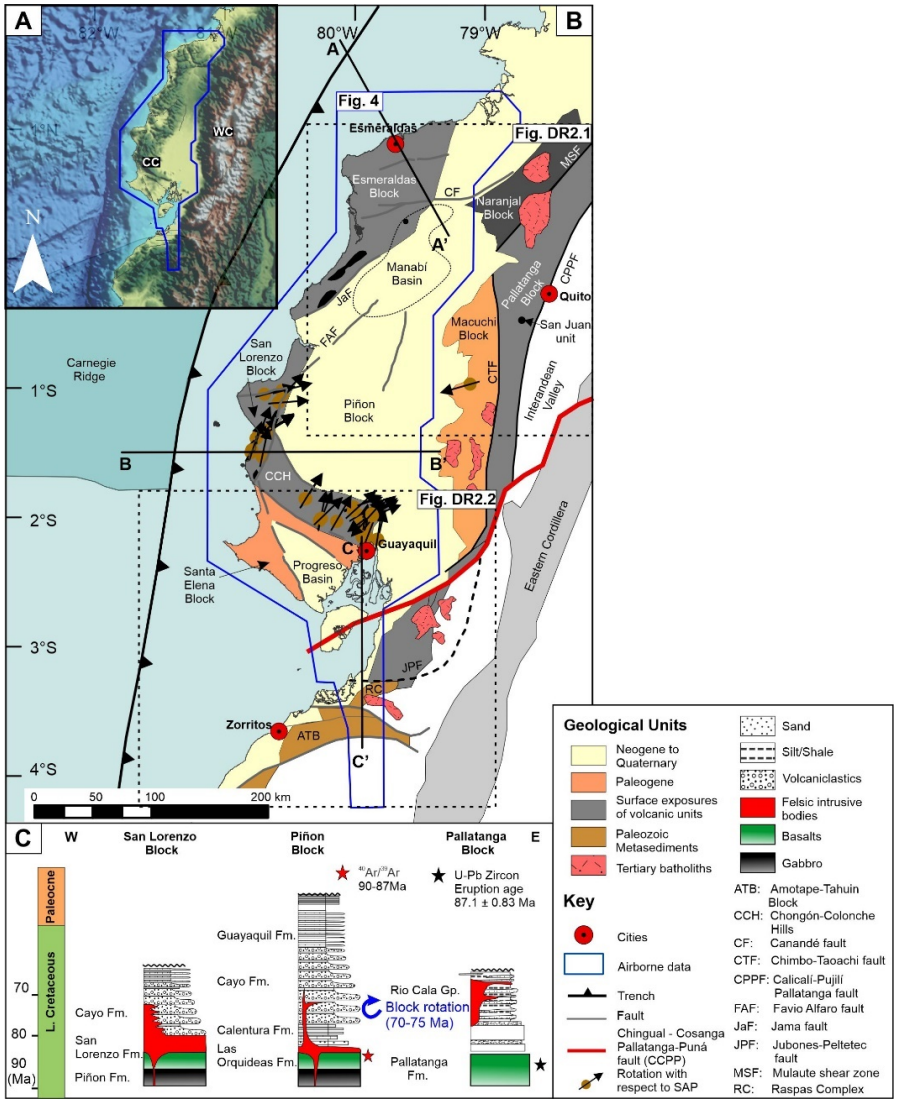

Figure 3.2: Topographic relief map of western Ecuador and NW Peru showing the location and coverage of the aeromagnetic survey. (B) Simplified tectonic terrane map showing the different crustal blocks interpreted along western Ecuador maps (modified after: **Luzieux *et al.* (2006)** and **Vallejo *et al.* (2009)**). The blue outline defines the limits of the gravity and magnetic aeromagnetic survey used in this study. (C) Representative stratigraphic columns for the three main tectonic blocks discussed in this study.

3.2.1.2 Macuchi block

The Macuchi block is in faulted contact with the Pallatanga block along the Chimbo-Toachi fault (Figure 3.2B) (Kerr *et al.*, 2002; Vallejo *et al.*, 2009). Different authors have interpreted the Macuchi block as a volcanic arc accreted during the Eocene (e.g. Lebrat *et al.*, 1987; Kerr *et al.*, 2002). However, Vallejo *et al.* (2009) suggest that this is a difficult model to reconcile given the current position of the Macuchi block, in between the Pallatanga and Piñón blocks that possess a similar radiometric age (ca. 88 Ma).

The Macuchi block is mostly characterized by volcaniclastic material with a small percentage of basaltic pillow lavas, lithic tuffs of basaltic and andesitic composition, basaltic breccias, turbidites of volcanic origin, and cherts (Hughes and Pilatasig, 2002; Vallejo, 2007). The sedimentary units that compose the Macuchi block are interpreted as a product of submarine volcanism transported by gravity flow processes (Hughes and Pilatasig, 2002). Whole-rock K/Ar radiometric data yield an age of 41.6 ± 2.1 Ma for a basaltic andesite sample (Egüez, 1986). Vallejo *et al.* (2009) obtained a similar age of 42.63 ± 1.3 Ma from a plagioclase of an andesitic lava flow. Nevertheless, the age of the base of the Macuchi unit, as well as the age of the volcaniclastic deposits, remains largely unconstrained.

3.2.1.3 Naranjal block

The block is located in the northern part of the study area in faulted contact with the Pallatanga block, along the Mulaute shear zone (Figure 3.2B). The Naranjal block is characterized by rocks with a volcanic arc affinity, which appears to correlate with the interpreted Ricaurte arc in southern Colombia (Spadea and Espinosa, 1996). It is composed of basaltic pillow lavas and andesites with intercalated sedimentary rocks (Vallejo, 2007). Two distinct litho-tectonic units have been interpreted within the block: 1) island arc lavas, towards the north, that may correlate with basalts from the Río Cala group at the Pallatanga block, and 2) to the south by rocks with plateau

affinities (Kerr *et al.*, 2002). The southern extent of the Naranjal block is assumed to be buried under the forearc sediments of the Manabí basin (Figure 3.2B).

3.2.2 Volcanic and oceanic plateau remnants in the forearc region

3.2.2.1 Piñón and Santa Elena blocks

The exposures in the Chongón Colonche Hills in SW Ecuador (Figure 3.2A) are mainly composed of tholeiitic basalts, pillow lavas, and gabbros. The geochemical signature of these mafic rocks supports an oceanic plateau interpretation (Jaillard *et al.*, 1995; Reynaud *et al.*, 1999; Kerr *et al.*, 2002; Mamberti *et al.*, 2003).

The age of the Piñón Formation was initially constrained by foraminifera and nannofossils from the overlying black shales of the Calentura Formation, which yielded a Cenomanian-Early Coniacian age and led Reynaud *et al.* (1999) to propose an Early Cretaceous age for the Piñón Formation. Van Melle *et al.* (2008) then based on more stratigraphic data propose a Coniacian age for the Piñón Formation. Some authors suggest that the Pallatanga and Piñón blocks were fragmented after the Late Cretaceous collision with the South American margin. This is supported by 40Ar/39Ar dating yielding an age between 90-87 Ma for both crustal blocks (Luzieux *et al.*, 2006).

South of the Chongón-Colonche Hills, in the Santa Elena block (Figure 3.2), the stratigraphy is dominated by deformed Late Cretaceous rocks from the Santa Elena Formation, unconformably overlain by folded rocks from the Paleocene Azúcar Formation. These deformed sequences are interpreted as an accretionary wedge, which led to the development of an outer forearc high during the Oligocene, and the development of the restricted Neogene Progreso basin (Figure 3.2B) (Aizprua *et al.*, 2019b; Witt *et al.*, 2019b). It is assumed that volcaniclastic sequences from the Cayo Formation and possibly mafic rocks from the Piñón Formation form the underlying basement of the Santa Elena block.

3.2.2.2 San Lorenzo block

West of the Piñón block and delimited by the Jipijapa, Jama, and Canandé faults (Figure 3.2B), this block forms the medium topography (max. 400 m) Coastal Cordillera (Reyes, 2013). The mafic rocks encountered in the Coastal Cordillera are attributed to the Piñón Formation, commonly overlain by coarse-grained sandstones, ash beds, basaltic flows, dikes, and pillow lavas (Figure 3.2C) (Reynaud *et al.*, 1999; Luzieux *et al.*, 2006). Goossens and Rose (1973) report tholeiites erupted along east-trending fractures from the Late Cretaceous until Early Eocene. These rocks are attributed to a Campanian to Maastrichtian volcanic island arc constituting the San Lorenzo formation (Jaillard *et al.*, 1995; Reynaud *et al.*, 1999; Van Melle *et al.*, 2008; Vallejo *et al.*, 2009). Based on plagioclase from pillow basalts Ar/Ar dated as 72.7 ± 1.4 Ma, leading Lebrat *et al.* (1987) to propose that the island arc-related sequences preserved in the Coastal and the Western Cordillera are coeval and possibly part of the same system. However, several authors report larger age ranges between 87 and 54 Ma (Goossens and Rose, 1973; Jaillard *et al.*, 1995; Luzieux *et al.*, 2006). The San Lorenzo block is also characterized by a clear hiatus between the Late Cretaceous and Middle Eocene carbonaceous formations (Reynaud *et al.*, 1999; Luzieux *et al.*, 2006; Vallejo *et al.*, 2019), which has been attributed to the accretion of the San Lorenzo block to the already accreted Piñon block, during Paleocene-Eocene times (Jaillard *et al.*, 1995; Kerr *et al.*, 2002).

3.2.2.3 Esmeraldas block

Limited to the east by the Canandé fault and mostly covered by Neogene sediments (Figure 3.2B), this is the least well-constrained block in terms of its nature and age. It comprises pillow basalts, dolerites, isotropic gabbros, and hyaloclastites containing glass fragments and picritic compositions (Mamberti *et al.*, 2003). The same authors suggest that the units forming the block appear petrologically and geochemically like the lavas of the CLIP (92-86 Ma).

3.2.3 Amotape-Tahuin Massif along NW Peru

The Amotape-Tahuin massif is an SW-NE oriented morphological feature composed of Precambrian to Paleozoic rocks along the NW coast of Peru, shifting to a NE-SW direction to the south (Mourier *et al.*, 1988). Towards the ENE the Jubones fault separates rocks with a continental affinity from those composed of exhumed high pressure, low-temperature oceanic origin (Arculus *et al.*, 1999; Spikings *et al.*, 2010; Spikings *et al.*, 2015).

Most of the massif between 4°S to 6°S is composed of metasediments. Zircon ages along the metamorphic belt show a very similar pattern of Neoproterozoic age clusters and a younger group around 320 Ma, and suggest a common metasedimentary origin of the entire massif (Witt *et al.*, 2017). Furthermore, these age cluster similarities agree with those in the western parts of the Eastern Cordillera, and the northern section of the Occidental Cordillera of Peru suggesting a wide, polyphase Andean metamorphic belt (Witt *et al.*, 2017); thus excluding previous theories about the allochthonous origin for the Amotape-Tahuin massif (Feininger, 1987; Mourier *et al.*, 1988; Winter *et al.*, 2010). Moreover, its autochthonous origin was previously evidenced by the pervasive presence of Triassic (230-220 Ma) granitoids along the Amotapes Massif and the Cordillera Real of Ecuador (Aspden *et al.*, 1992; Sanchez *et al.*, 2006; Spikings *et al.*, 2015).

Paleomagnetic studies at the Amotapes-Tahuin massif report clockwise rotations in the order of 35° during the Late Cretaceous-Early Paleocene, related to the collision and accretion of the CLIP (Mourier *et al.*, 1988). Fault mapping and displacement data show deformation that might be associated with a post-Paleocene reactivation, block rotations in the order of 25° (Mitouard *et al.*, 1990), of the inherited structures formed during the initial accretionary phase (Aizprua *et al.*, 2019b).

3.3 PREVIOUS STUDIES

The earliest study using aeromagnetic data was carried out during the mid 1960s for the Mineral Project of the United Nations Development Program (Goossens

and Rose, 1973), and identified a series of E-W magnetic anomalies, along the San Lorenzo block, bounded to the west by a major north to NE-trending fault (Jipijapa fault in this study). Goossens and Rose (1973) suggest that these anomalies are caused by tholeiitic basaltic flows (their "Basic Igneous Complex"). Later, these rocks were compared to similar exposures in Colombia and interpreted to form an elongated igneous belt along the NW of South America, from Ecuador to Panamá (Goossens *et al.*, 1977). Subsequent potential field studies along the margins of Ecuador and Peru analysed free-air gravity gradients, both near the trench and along the continental slope (Shepherd and Moberly, 1981). Primary observations along the NW Peru and SW Ecuador margin by Shepherd and Moberly (1981) include: 1) flattened gradients east of the current trench position associated with a wedge of tectonized sediments accumulated by subduction processes; 2) abrupt free-air gravity inflections on the upper slope (NW Peru), related to the granitic basement (correlative to the Amotape-Tahuin block); and 3) a gravity minimum in the Gulf of Guayaquil, which denotes more than 6000 m of Quaternary sediments infilling an inferred pull-apart basin.

Feininger and Seguin (1983) characterized the crust in Ecuador using a 2D forward model (located at ~2°S) based on simple Bouguer gravity data. They concluded that the coastal region in Ecuador must be underlain by an ancient oceanic plate. Based on the correlation between positive (Bouguer) anomalies over the inferred oceanic terrane and negative values over the interpreted continental crust they proposed a possible location for the suture between these two crustal blocks. Nevertheless, the conclusions drawn for the coastal region lacked a more thorough analysis regarding its internal structure.

Tamay *et al.* (2018) studied the extension of the subducted Carnegie Ridge using potential field data analysis, and suggest that the Carnegie Ridge underlies the continental margin reaching the Andes Cordillera based on an elongated E-W negative magnetic anomaly concordant with the position of the aseismic ridge and that it subsequently controlled margin segmentation, seismicity, and volcanism. Free-air gravity anomalies along the off-shore zone have more recently been used to constrain the tectonic development of the offshore forearc basins between 1°N and 2°S

(Hernandez et al., in press). This study shows a clear relationship between depth-to-basement and related faulting and the distribution of gravimetric anomalies.

Despite the different studies using potential field data, none of them present a detailed view of the crustal structure of the entire forearc region in Ecuador. Utilizing recently acquired high frequency aeromagnetic and gravity data along the coastal region, we present a new model of the underlying crustal architecture of the forearc region in Western Ecuador.

3.4 GEOPHYSICAL DATA and METHODS

An aero magnetic/gravity survey, acquired by SANDERS GEOPHYSICS for EP PETROECUADOR in 2010, is available between 2°N to 4°S for the forearc region in Ecuador (Figure 3.2). A total area of ca. 78000 km^2 was covered with N-S oriented acquisition lines and E-W tie lines with a spacing of ca.1500 m and ca. 8950 m respectively, and a nominal flight altitude of 250 m above the terrain. In addition, we had access to unpublished onshore seismic lines acquired and processed by SINOPEC for EP PETROECUADOR in 2009, which aid to define the forearc basin geometry (especially depth to basement) within the study area. Offshore seismic reflection and refraction profiles across the margin (Flueh *et al.*, 2001; Collot *et al.*, 2002; Graindorge *et al.*, 2004; Calahorrano *et al.*, 2008) were integrated into the 2D models to constrain the extent of the forearc basement up to the trench.

3.4.1 Analysis of gravity and magnetic anomalies

Our approach is based on two steps: 1) a spectral analysis of the frequency content to map-out buried geological features, and 2) 2D forward modelling of the anomalies to test plausible geological scenarios. Throughout this approach, we aim to delineate the main geophysical domains and to characterize the interpreted crustal blocks in terms of density and magnetic susceptibility.

Conventional filtering techniques including regional and residual anomalies, analytical signal, and tilt derivative were applied to the data (File DR1), in order to

aid geological interpretations of the sources of the gravity and magnetic anomalies. Due to the poor coverage and low frequency content of global satellite-derived magnetic data in this region, only the aeromagnetic survey was used. A brief description of the different types of filters including the results of their application to the data is further described in the supplementary material (File DR1).

For 2D forward modelling, the GM-SYS module in Oasis Montaj, software developed by GEOSOFT Inc was used. Three key profiles were selected to cover all the major crustal blocks (Figure 3.2): 1) a northern profile to study the Esmeraldas and Naranjal blocks; 2) a central profile across the Santa Lorenzo and Piñón blocks to study the highest Bouguer gravity anomaly observed in the region (Figure 3.3), and 3) a southern profile, coincident with a narrow strip of the high-resolution magnetic data, to study the suture of the accreted sliver across the Gulf of Guayaquil area.

3.4.2 Data Constraints for 2-D forward models

The geometry of the 2D crustal models across the forearc region in Ecuador was mainly constrained using existing velocity models and deep and conventional seismic profiles. The properties of the different blocks to initiate the forward models were derived from velocity analyses, paleomagnetism studies, and borehole data (Table 3-1).

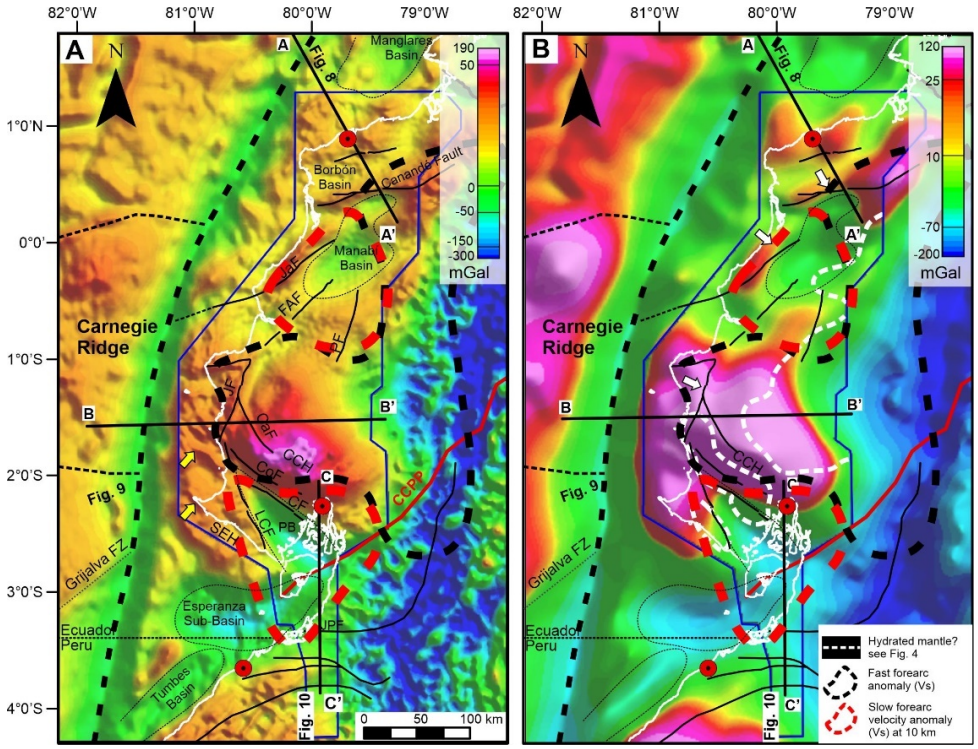

Figure 3.3: (A) A combined Bouguer gravity anomaly map, including satellite gravity data (Sandwell *et al.*, 2014) outside the outline of the aeromagnetic survey, marked in blue. At ca. 2°S, a very high positive anomaly is coincident with the Chongón-Colonche hills (CCH). The negative Bouguer's values to the east are associated with a deep Andean crustal root. To the west of the trench, another high positive anomaly is associated with the oceanic Carnegie Ridge. (B) Tilt derivative anomaly highlighting the sources of anomalies. Continuous lines in black consist of the compilation of surface faults (Reyes, 2013) and the red line represents the CCPP fault system, which is associated with a sharp boundary between the NAS and the Subandean domain overthrusting the SAP (Alvarado *et al.*, 2016). Abbreviations are as follow: CF. Carrizal fault; CaF: Cascol fault; CoF: Colonche fault; FAF: Flavio Alfaro fault; JF: Jipijapa fault; JaF: Jama fault; JPF: Jubones-Peltetec fault, LCF: La Cruz fault; MA: Mulaute Anomaly; PB: Progreso basin; PF: Pichincha fault; SEH: Santa Elena High. Dashed blue lines represent a low-velocity gradient zone and the red dashed lines a low-velocity zone (Cano *et al.*, 2014)

Table 3-1: Model constrains

Element to be constrained	Parameter of constraint	Reference
Tectonic settings	Fieldwork and geophysical studies	This work. Bethoux *et al.* (2011); Aizprua *et al.* (2019b), Calahorrano *et al.* (2008); Feininger and Seguin (1983), Font *et al.* (2013) Gutscher *et al.* (1999); Graindorge *et al.* (2004); Gailler *et al.* (2007); Hernández *et al.* (2020); Jaillard *et al.* (2002); Koch *et al.* (2020); Luzieux *et al.* (2006); Lynner *et al.* (2019); Michaud *et al.* (2009); Vallejo *et al.* (2009); Witt and Bourgois (2010)
Ecuadorian trench	Bathymetry	SRTM30 Plus v7
Subduction slab geometry	Wide-azimuth seismic, OBS	Graindorge *et al.* (2004); Gailler *et al.* (2007)
Density	Density from seismic velocity profiles	Calahorrano *et al.* (2008); Gailler *et al.* (2007); Sanclemente (2014)
Magnetic properties	Paleomagnetic studies	Roperch *et al.* (1987); Luzieux *et al.* (2006),

The densities for basement rocks are derived from the velocity analysis of wide-angle seismic data (Collot *et al.*, 2002; Graindorge *et al.*, 2004; Lynner *et al.*, 2019), using empirical velocity-density relationships for igneous rocks (Hinze *et al.*, 2013). For the sedimentary cover, densities were estimated from industrial borehole logs, located in the Gulf of Guayaquil and the Progreso basins. The different densities used in this study are listed in Table 3-2.

We define the acoustic basement as the Cretaceous oceanic crust underlying the coastal forearc region. Overlying sedimentary packages were roughly averaged with a seismic velocity of 2.3 km/s, to depth convert the top of the acoustic basement. The results of the seismic interpretation of deep and conventional seismic profiles (Graindorge et al., 2004; Calahorrano et al., 2008; Collot et al., 2008; Cano et al., 2014; Lynner et al., 2019; and this work) were used to constrain the forearc basement structural configuration as input geometry for the 2D forward models.

Magnetic susceptibility and remanent magnetization values from outcrops along the Chongón-Colonche Hills (Luzieux, 2007) were used as input parameters for the Cretaceous blocks in our forward magnetic models. For the characterization of the subducting Nazca plate, natural remanent magnetization (NRM) values were used from Ocean Drilling Program (ODP) sites 1238 and 1239 (Mix et al., 2003). Other blocks were initialized with theoretical values (Hinze *et al.*, 2013) and final parameters were determined based on a best-to-fit approach.

Table 3-2: List of parameters used for forward modelling purposes

Initial Parameter					
Earth's magnetic field (December 2011)		29407 nT			
Magnitude (A m^{-1})		20.58°			
Inclination (deg)		-0.78°			
Declination (deg)					
Block's name	Density (kg m^{-3})	Susceptibility (SI)	Remanence magnetization		
			Intensity (A m^{-1})	Inclination (deg)	Declination (deg)
Water	1030	--	--	--	--
Piñón	2850	0.01	1.2	-15	50
Hydrated mantle	2900	0.07	--	--	--
Mantle	3300	--	--	--	--
Volcanic-arc	2900	0.02	1.4	-15	70
Sedimentary basin	2400	--	--	--	--
Volcano-sedimentary	2700	--	--	--	--

3.5 ANALYSIS OF REGIONAL GEOPHYSICAL DATA

3.5.1 Seismic, gravity and magnetic anomalies

The gravity and magnetic data show contrasting anomalies (Figure 3.3 and 5.4), which have been grouped into three main geophysical domains based on their different wavelength and textural characteristics.

3.5.1.1 Outer domain

A series of short-wavelength Bouguer anomalies and elongated in a NNE-SSW direction characterize the SW coast (yellow arrows, Figure 3.3A). This region is coincident with the Santa Elena Block and bounds the Progreso basin to the east. The short wavelength characteristic of the anomalies extends north, but in an irregular pattern (Figure 3.3A). The eastern boundary of this domain is defined by a high positive and elongated anomaly, which appears segmented and rotated clockwise to the north. This last lineament is also highlighted by a series of elongated magnetic anomalies (Figure 3.4A). An analytical filter applied to the total intensity magnetic map highlights a series of positive anomalies (M1, M2, and M3 sections in Figure 3.4B) of similar textural characteristics. The analytical signal highlights the outline of the possible sources of these anomalies with their eastern edges coincident with the major Jipijapa, Jama, and Canandé faults (Figure 3.4B); a set called here the Coastal Range Fault System.

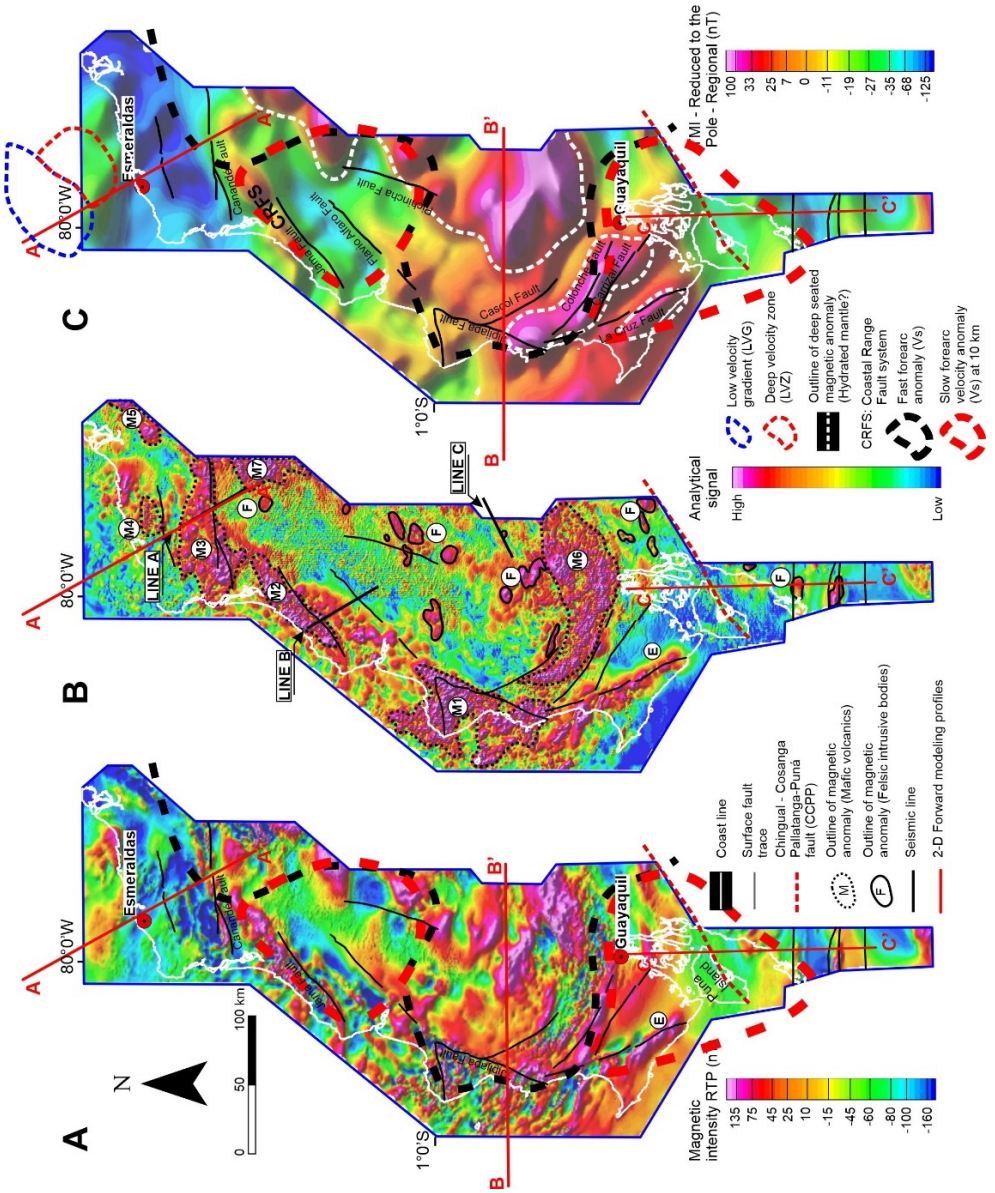

Figure 3.4: (A) Total magnetic intensity (TMI) map reduced to the pole of the forearc region in Ecuador. (B) Analytical signal of the TMI in (A). C) Upward continuation (10km) of the TMI in (A). M-type anomalies are associated with mafic-derived bodies, whereas F-type anomaly relates to felsic intrusive bodies. The E anomaly refers to the Estancia Magnetic high, possibly a M-type anomaly and prominent feature in southern Ecuador coincident with the La Cruz fault.

The same textural characteristic appears to extent southwards into the SEH but shifting to a NW-SE direction. This lineament is coincident with the La Cruz fault, delimiting the outer domain from the Progreso basin. From south to north, this lineament, which appears related to a deep source as shown by Figure 3.3B, has a concave shape and delimits the outer domain from the inner domain to the east. As mentioned above, this lineament is coincident with major faults and bounds Cenozoic forearc depocenters located landwards within the inner domain. The unusual feature (E in Figure 3.4), here termed the Estancia magnetic high, strongly correlates with the La Cruz fault. The Estancia magnetic high (70 nT) suggests that it may be underlain by mafic rocks, presumably from the Piñón formation. Farther south into the Santa Elena High and towards the Puná island, the magnetic intensity has a different anomaly pattern (Figure 3.4), possibly suggesting the transition into the Santa Elena accretionary complex (Aizprua *et al.*, 2019b).

The M1 and M2 anomalies highlighted by the analytical signal are characterized by a discontinuity that correlates to the jump between the Jipijapa and Jama faults (Figure 3.4B). Northward into the M3 anomaly, similar textural patterns are observed with its eastern limit apparently rotated in relation to the same structural trends, the Jipijapa and Jama faults, observed to the south. The near E-W orientation of the eastern limit of the M3 anomaly coincides with the Canandé fault, a major bounding fault to the Cenozoic Manabí basin and the boundary between inner and outer domains (Figure 3.4).

The apparent relationship between the eastern limit of the M1 to M3 anomalies to the major bounding faults suggests that the mafic-associated anomalies may partly control the location of major fault activity, possibly as a rheological factor. A close-up look into the transitional region between M2 and M3 anomalies shows the structural complexity of the area and how this may correlate with exposures of the Esmeralda's block and possibly with the southern extension of the Naranjal block (File DR2). An industrial seismic profile across this area (Figure 3.5A) shows the Canadé fault separating a major structural high to the north from a sedimentary basin to the south. The closely spaced normal faults affecting the top of the basement can be

correlated with the geophysical lineaments derived from the analytical signal (File DR2). A seismic profile farther south (Figure 3.5B) shows similar characteristics to the profile described above suggesting that the Canandé and Jama faults delimit the outer domain landwards and may be of a similar origin.

The M4 anomaly, located farther north, appears to have similar textural characteristics in the analytical signal as those observed for M3, however with a less considerably size (File DR2). The location of the M4 anomaly is coincident with exposures across the structural high called "Businga dome", where rocks of the Late Cretaceous Piñón Formation have been described in the past (Evans and Whittaker, 1982; Reyes, 2013).

3.5.1.2 Inner domain

In contrast to the outer domain, the inner domain is mostly characterized by long-wavelength anomalies (Figure 3.3). It is limited to the west by the convex-shaped lineament forming the eastern boundary of the outer domain (Figure 3.3), to the east by the limit of the survey (i.e. Andean piedmont and related outcrops of the Macuchi block) and to the north by the Canandé fault. This domain accounts for a large portion of the forearc region in Ecuador. A key feature of this domain is the high positive amplitude and long-wavelength Bouguer gravity anomaly, coincident with the exposures along the Chongón-Colonche Hills (Figure 3.3A).

From the inner and towards the outer domain, gravity values decrease considerably reaching up to c. -10 mGal to the north and c. -50 mGal south of the Chongón-Colonche Hills (Figure 3.3). The northernmost gravity low within this domain is associated with the Manabí sedimentary basin, which has an elliptical shape with a NE-SW oriented axis.

The analytical signal of the total magnetic intensity anomaly map (Figure 3.4) shows two major mafic-associated anomalies (M6 and M7). In between these two anomalies, there are a series of patchy circular to elliptical anomalies possibly

associated with felsic intrusions, of similar dimensions as those outcropping farther to the east within the Macuchi block (Figure 3.2). The circular anomalies observed in the analytical signal may likely represent a SW prolongation of the intrusives bodies related to the Macuchi Unit. A seismic profile across this region (Figure 3.5C) shows a localized and irregular acoustic basement relief, typical of igneous intrusions.

The elongated M6 anomaly apparently expanding from the west towards the east, exposed along the Chongón Colonche Hills, accounts primarily for rocks of mafic characteristics (Luzieux *et al.*, 2006; Van Melle *et al.*, 2008). Goossens and Rose (1973) have previously reported elongated magnetic anomalies located along the Chongón-Colonche Hills, with a predominantly E-W orientation and associated them with basaltic lava flows. In contrast, in the northern part of the inner domain near the transition to the Naranjal block, the M7 anomaly coincides well with the exposures that define the Naranjal block (File DR2), suggesting that the anomaly may be a southward prolongation of the former.

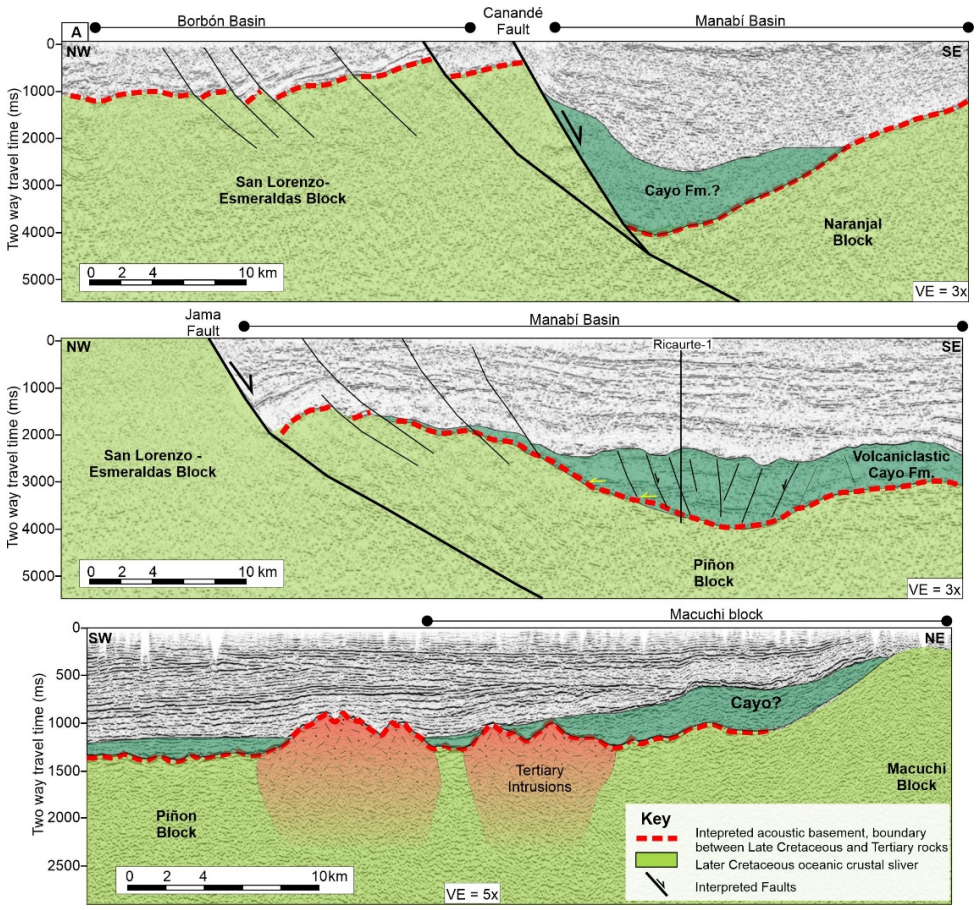

Figure 3.5: Onshore seismic profiles across the San Lorenzo-Esmeraldas and Piñón blocks. (A) a NW-SE profile which shows a series or normal faults dipping landwards west of the major Canande fault, which bounds the Cenozoic Manabí basin. (B) a NW-SE profile showing to the west an uplifted area related to the Cretaceous acoustic basement, and to the east a depocenter possibly underlie by a deformed basement. (C) a NE-SE seismic profile shows an uplifted area towards the north, which corresponds to the exposed Macuchi Block. Notice the likely presence of intrusive bodies possibly emplaced at different ages. Location of seismic profiles in Figure 3.2

3.5.1.3 Southern suture domain (Gulf of Guayaquil)

The positive Bouguer gravity anomaly over the Santa Elena block decreases to the south where it becomes negative over the Esperanza sub-basin (Figure 3.3A). A rapid change related to the thick sedimentary succession of Quaternary deposits in the

Esperanza sub-basin, a depocenter that is associated to the northward migration of the North Andean Sliver (Witt *et al.*, 2006; Aizprua *et al.*, 2019b), whereas along the Tumbes basin the gravity low is likely to be controlled by a s.s. forearc depocenter (Espurt *et al.*, 2018; Aizprua *et al.*, 2019b). Across the Ecuador-Peru border, south of the Tumbes basin (Figure 3.3), the gravity anomaly increases towards the Amotape-Tahuin Massif, which is of continental affinity and marks the southern limit of the suture domain.

The gravity map shown in Figure 3.3A shows an apparent oblique relationship between the Tumbes and Esperanza gravity lows. From the Esperanza sub-basin towards the continent, the gravity low area narrows drastically into a location where it coincides with the major Chingual-Cosanga-Pallatanga-Puná (CCPP) fault system defined by Alvarado *et al.* (2016) (Figure 3.3A). The wider part of the whole negative anomaly may be associated with: 1) the possibly northward displacement of the Santa Elena High, which is part of the North Andean Sliver tectonic scape (Aizprua *et al.*, 2019b), or to 2) the trenchward extension of the Jubones fault. The latest is the southernmost location of the suture between the accreted oceanic terranes of the CLIP and the continent. At the narrow section of the gravity low, Late Cretaceous rocks from the Pallatanga Formation (an age equivalent to the Piñón Formation) are interpreted to underlay the sedimentary basin in this region (Aizprua *et al.*, 2019b).

Despite only partial coverage of the aeromagnetic survey across the eastern part of the Gulf of Guayaquil, this has allowed us to better constrain the deep crustal structure across a major boundary (File DR2). The magnetic intensity map – Reduced To the Pole (RTP) shown in Figure 3.4A shows a decrease of values over the Puná island, pointing towards a reduction in magnetic susceptibility of the region. The disposal of the magnetic anomalies, shown in Figure 3.4A, appears to correlate with some surface exposure of crustal units in the area. For instance, south of the Puná island, a prominent magnetic source correlates with the strike of the ultramafic Raspas Complex, an exhumed fragment from a Late Jurassic - Early Cretaceous subduction system (Arculus *et al.*, 1999; Bosch *et al.*, 2002). This magnetic high is bounded to

the north by a magnetic low striking E-W and coincident with the trend of the Jubones fault (the southernmost identified suture), and to the south by the Late Cretaceous Lancones sedimentary basin.

3.5.2 Forward models

3.5.2.1 Crustal Structure

Overall the model A-A' shows an average thickness of 15 km of crust (Figure 3.6C), based on a best-fit approach, with some variations at the different domains. At the outer domain in profiles A-A' and B-B' (Figure 3.6 and Figure 3.7, respectively) the seaward decrease of the gravity anomaly may be indicative of thickness or density variations. For instance, at profile A-A', this lower gravity anomaly may be associated to a low-velocity zone along the western part of the pre-stacked depth migrated SIS-line 44 presented by Collot *et al.* (2008), who suggest that this block represents an altered outer wedge affected by deep-sourced fluids flowing along crustal faults. East of the low-density zone (Figure 3.6B, C), who suggest that this block represents an altered outer wedge affected by deep-sourced fluids flowing along crustal faults. Indeed, recent tomography-based shear velocity inversion models reveal low-velocity crustal bodies possibly associated with the subduction of the Carnegie Ridge, north of 1°S (Figure 3.3) (Lynner *et al.*, 2019; Koch *et al.*, 2020). East of the low-density zone (Figure 3.6B, C), a high-amplitude magnetic anomaly shows decreasing values towards the Borbón basin. The magnetic contrast towards the east (0.01 SI) extends from 60 to 110 km in profile A-A'. In between 110 – 140 km, both the magnetic and gravity anomalies are characterized by a flat gradient prior to entering into an area of varying magnetic values, associated to the major Canandé fault zone, as observed on the seismic profile shown in Figure 3.5A. A series of faulted blocks with varying magnetic susceptibility are added to match the varying magnetic profile west of the Canandé extensional fault (Figure 3.6A). The blocks are vertically extended from the inferred top basement down to depths of 7-9 km matching the upper boundary of a higher density (2950 kg/m^3) and laterally extended lower crust. The inferred fault system may also be associated with NNE-SSW dyke-shape mafic bodies, considering

the high degree of variability in the TMI-RTP, a typical response encountered at low latitudes (Beard, 2000). The Canandé fault also marks the base of a steep gravity gradient and the eastern edge of the irregular magnetic zone. In our model, the depocenter of the Cenozoic Manabí basin and a less dense Late Cretaceous oceanic crust basement account for this steep gradient marking the boundary between the inner and outer domains.

Along profile B-B' anomalies are matched with a relatively shallow moho with ~10 km depth and up to 15 km depth towards the Andean piedmont (Figure 3.7). The gravity anomaly and derived model show a similar pattern towards the trench as in A-A', except that values are considerably higher compared to profile A-A'. To fit the anomaly, across the outer domain, a thicker block (of ca. 10 km) with a density of 2850 kg/m^3 was introduced into the model. This outer-wedge geometry in the west may correspond to the northern prolongation of the interpreted Santa Elena High, which consists of thick and highly deformed successions of Late Cretaceous to Paleocene sediments (Jaillard *et al.*, 1995; Calahorrano *et al.*, 2008; Aizprua *et al.*, 2019b). The highly deformed nature of the Late Cretaceous and Paleocene series of the Santa Elena block, and the tectonic interaction with the Piñón block (here the inner domain), this last one acting as a backstop (Aizprua *et al.*, 2019b), supports this outer-wedge model (Figure 3.7). The spectral analysis of the total magnetic intensity map indicates that the magnetic anomalies within the inner domain may be originated at different depth levels (Figure 3.4, and File DR1). An initial model test with magnetized bodies at medium to shallow depths (< 10 km) and susceptibilities values between 0.01-0.02 SI account partly for the observed magnetic anomalies (File DR3). An alternative interpretation for this initial model may include faults; however, it still requires the presence of highly magnetized bodies. We do not rule out a combined model, where highly magnetic bodies are associated with deep-seated faults.

The long-wavelength component of the magnetic anomaly has been modelled considering deeper sources, to a depth of 10-15 km (Figure 3.7). Two different scenarios were considered to match the main gravity low in the east part of the model. The first scenario involves a low-density polygon located at the base of the oceanic

crust representing a fragment of the continental autochthonous crust; a low-density polygon is necessary to match the gravity low without reaching an anomalous high thickness for the accreted plateau rocks. The second scenario involves a similar autochthonous polygon with a paleo-hydrated mantle wedge necessary to match the high positive magnetic anomaly. This last scenario is the preferred one, together with the presence of continental crust, as supported by the velocity model presented by Lynner *et al.* (2019). Indeed, partial serpentinization of the lower crust or a remnant hydrated mantle wedge may be the source of the positive magnetic and negative gravity anomaly pair (see next section).

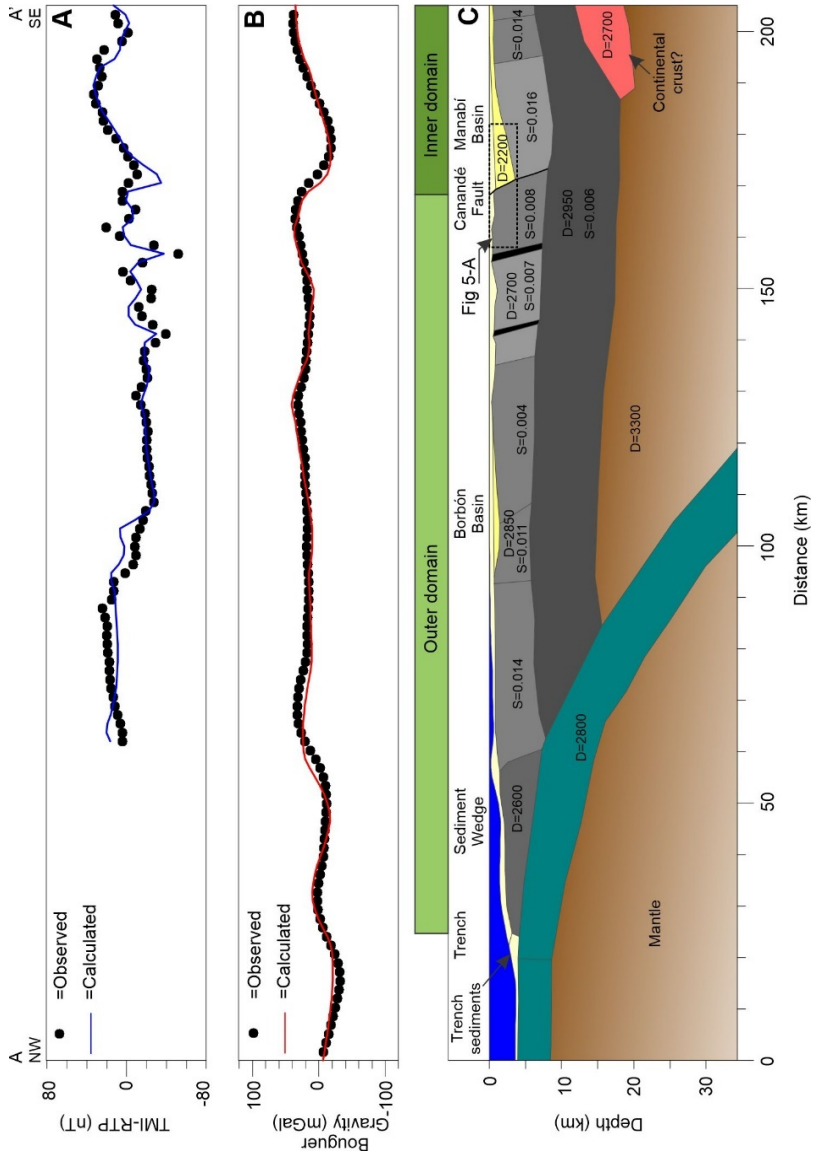

Figure 3.6: Two-dimensional gravity and magnetic forward models along profile A-A', between 2°N - 0°. A) Observed and calculated total magnetic intensity reduced to the pole (TMI-RTP) across the profile, using the international geomagnetic reference field (IGRF) as the initial parameter listed in Table 1. B) Bouguer's gravity observed and calculated anomaly showing very small differences. C) Geological cross-section with the different blocks constrained by surface geology and deep seismic profiles

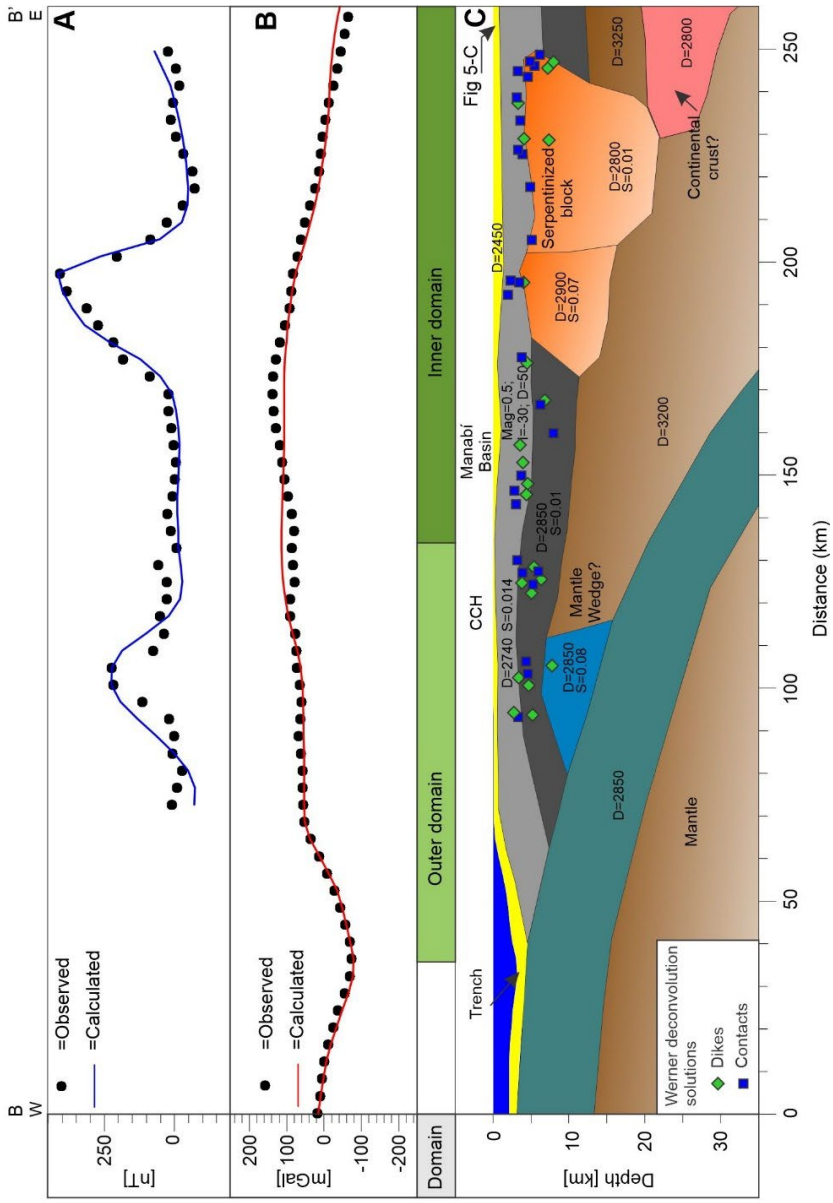

Figure 3.7: Two-dimensional gravity and magnetic forward models along profile B-B', between 1° - 2°S. A) Observed and calculated total magnetic intensity reduced to the pole (TMI-RTP) across the profile, using the international geomagnetic reference field (IGRF) as the initial parameter listed in Table 1. B) Bouguer's gravity observed and calculated anomaly showing very small differences. C) Geological cross-section with the different blocks constrained by surface geology and deep seismic profiles. Density values are shown in the section, and magnetic susceptibility and remanence are listed in Table 3-1.

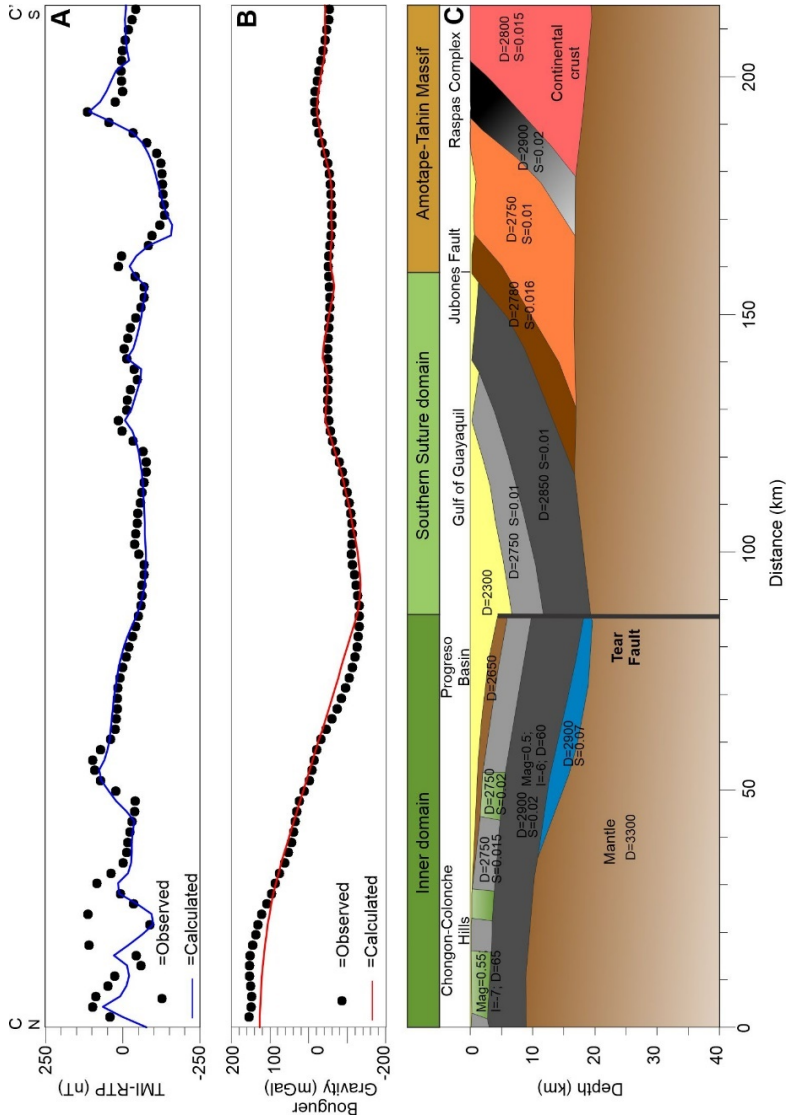

Figure 3.8: Two-dimensional gravity and magnetic forward models along profile C-C', between 2° - 4°S. A) Observed and calculated total magnetic intensity (TMI) across the profile, using initial parameters listed in Table 1. B) Bouguer's gravity observed and calculated anomaly. C) Geological cross-section with the different blocks constrained by surface geology and seismic profiles. Density and magnetic susceptibility are shown in the section.

The magnetic anomaly to the west in profile B-B' (between 80-110 km, Figure 3.7) is located near to a high to low shear velocity zone according to the model proposed by Lynner *et al.* (2019) (Figure 3.4). Considering the gravity decrease in this area, the presence of magnetic underplated material or a hydrated mantle wedge seems as plausible models. Similar observations are reported across other active margin, with presence of an hydrated mantle wedge underlying a forearc basement of oceanic affinity like in Oregon and East Antarctica (Ferraccioli *et al.*, 2002; Blakely *et al.*, 2005).

3.5.2.2 Southern suture of the North Andean Sliver to the continent

To investigate the southern suture between the trapped oceanic sliver and the continental South American Plate, we have integrated the observed tectonic elements of the area and modeled the gravity and magnetic response along profile C-C' (see Figure 3.2 for location). The northernmost segment of profile C-C' (Figure 3.8) partly crosses the eastern extent of the Chongón-Colonche Hills, which are characterized by surface exposures of the Piñón Formation and by the highest gravity anomaly in the region discussed in the previous section (Figure 3.3A). The high-amplitude gravity anomaly decreases towards the center of the profile and coincides with the southeastern extent of the Progreso basin (Figure 3.8). This segment crosses a series of high-magnetic anomalies that were matched by introducing shallow bodies (0.01 SI) and a deeper source of high magnetic susceptibility (0.07 SI) extending to a depth of ca. 15 km comparable to profile B-B'.

Towards the south, at the Gulf of Guayaquil (Figure 3.8), the gravity anomaly drops to a minimum of ca. -120 mGal. Strong lateral contrast in density coincident with the base of the steep gravity gradient was introduced in the model to account for this gradient. Although less constrained than profiles A-A' or B-B', the profile C-C' could be divided and analysed in two main segments: 1) the northern segment characterized by high gravity values as well as long-wavelength magnetic anomalies that extend laterally along the Chongón-Colonche Hills (Figure 3.4), and 2) the southern segment presenting a gentle southward stepping-up trend of gravity values

and lower magnetic contrasts. In between 90 to 125 km (Figure 3.8) gravity values increase to ca. -60 mGal staying almost constant up to 180 km, where it increases again up to -20 mGal. At the lowermost gravity point (at ca. 90 km), the SE extend and deepening of the Progreso basin connects to the eastern extension of the Gulf of Guayaquil basin, without any hint on the eastward presence or continuation of the Santa Elena High, as described byAizprua *et al.* (2019b) (Figure 3.8).

A series of north stepping magnetic highs, in between 120 – 210 km, characterized by steep slopes to the north and gentle gradients to the south (Figure 3.8) are modeled by a stacked series of blocks probably developed during the Late Cretaceous accretionary phase, later reactivated by extensional tectonics. Large basement-faults with an extensional component has been previously reported in this area based on seismic profiles (Benitez, 1995; Witt *et al.*, 2006; Aizprua *et al.*, 2019b). The southernmost part of the model is constrained by the surface exposure from the Raspas Complex that coincides remarkably well with a high magnetic peak (at ca. 190 km) and the slight increase in gravity values forming a bell-shaped geometry. In between this area and the Jubones fault (Figure 3.8), the model is fitted with a block of lower density (2750 kg/m^3) comparable to the block south of the Raspas Complex, suggesting that this area might be considered the continuation to the NE of the metasediments from the Amotape-Tahuin massif or it consist of a transitional zone to the obducted oceanic section (Figure 3.8).

3.6 DISCUSSION

The gravimetric and magnetic anomalies in the Ecuadorian forearc show a clear correlation to the crustal exposures across the coastal region. Furthermore, the structural interpretation based on the anomaly's gradients correlates well with their surface expression allowing to extend the interpretation to buried areas. The compilation of the different lineaments interpreted from the spectral analysis of gravity and magnetic anomalies provide clear evidence of a complex crustal architecture (Figure 3.9), most likely inherited from the Late Cretaceous allochthonous terranes (CLIP) - passive margin collision event.

It is admissible to conceive that the structure of the current Ecuadorian forearc and part of the arc will depend on the preservation degree of the accreted terranes during the arc-continent collision, which is controlled at the first-order by the polarity of subduction (Draut and Clift, 2013). A major discrepancy in the pre-collision settings of the Late Cretaceous arc is related to the subduction polarity. A west-dipping subduction system colliding perpendicular with the South American margin, presented by Vallejo *et al.* (2009), is in accordance with the "forward-facing" arc-continent collision type-1 (the forearc collides first) proposed by Draut and Clift (2013), which may lead to the preferential preservation of the intra - oceanic arc; as observed in the northern part of the Western Cordillera. Suggested evidence for a westward polarity includes regional models proposed for volcanic island arcs located in Colombia and farther north in the Caribbean region and the absence of magmatism older than 85-80 Ma in the Ecuadorian margin (Vallejo *et al.*, 2009). Nevertheless, alternative models based on tomography and supported by a quantitative plate reconstruction, support an east-dipping subduction system in the Northern Andes (Boschman *et al.*, 2014; Braz *et al.*, 2018); a similar polarity has been considered in models across western Ecuador, inferred from a geochemical and stratigraphic approach (e.g. Hughes and Pilatasig, 2002; Kerr *et al.*, 2002; Jaillard *et al.*, 2009). Suggested evidence for an eastward subduction include the lack of a clear magmatic gap from the older oceanic plateau lavas (Piñón Fm.) to younger arc lavas, expected during a polarity reversal as proposed by Vallejo *et al.* (2009). Collision with an eastward polarity is in accordance with the "backward-facing" arc-continent collision type-1 (the back arc collides first) proposed by Draut and Clift (2013), which may lead to the preferential loss of the back-arc system.

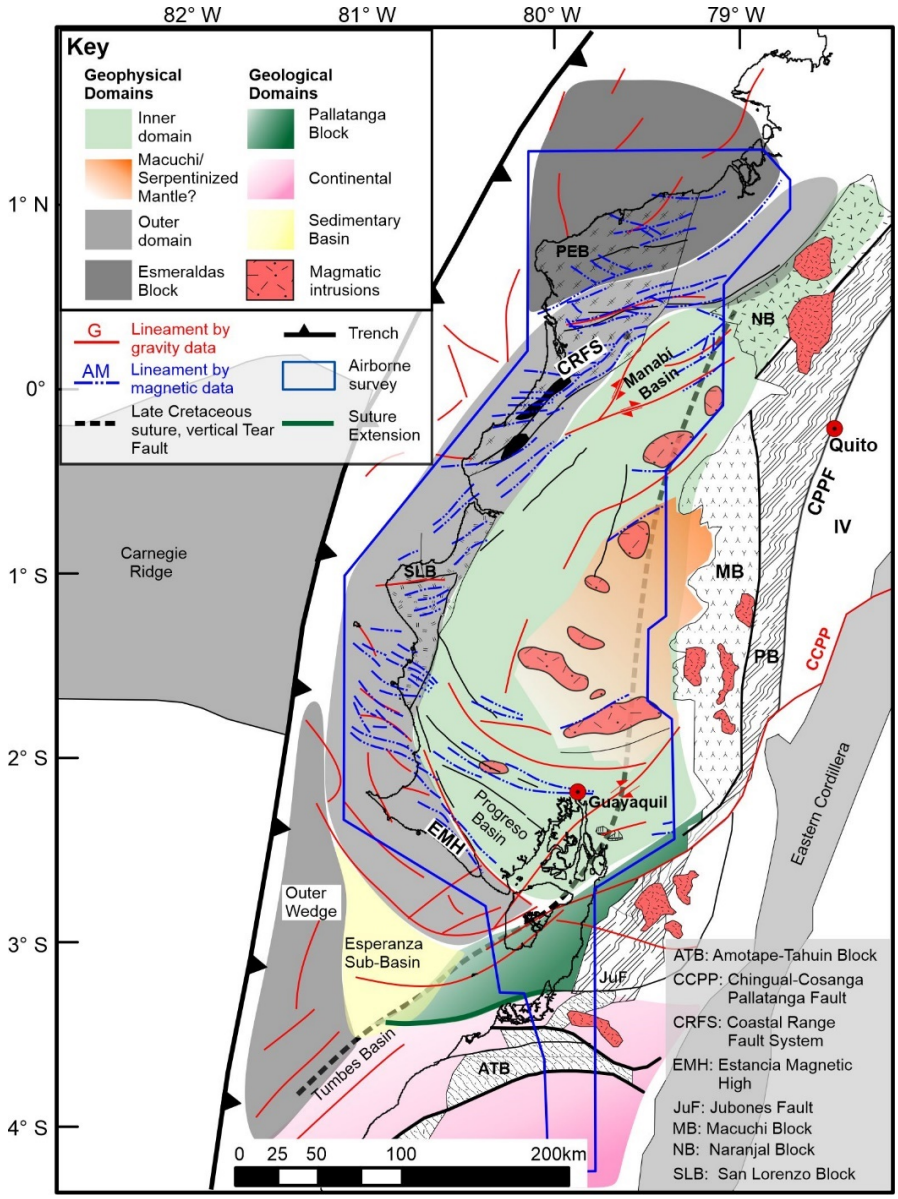

Figure 3.9: Crustal model of the Western Ecuador forearc region depicting the different geophysical domains and buried elements derived from the interpretation of combined gravity and aeromagnetic data.

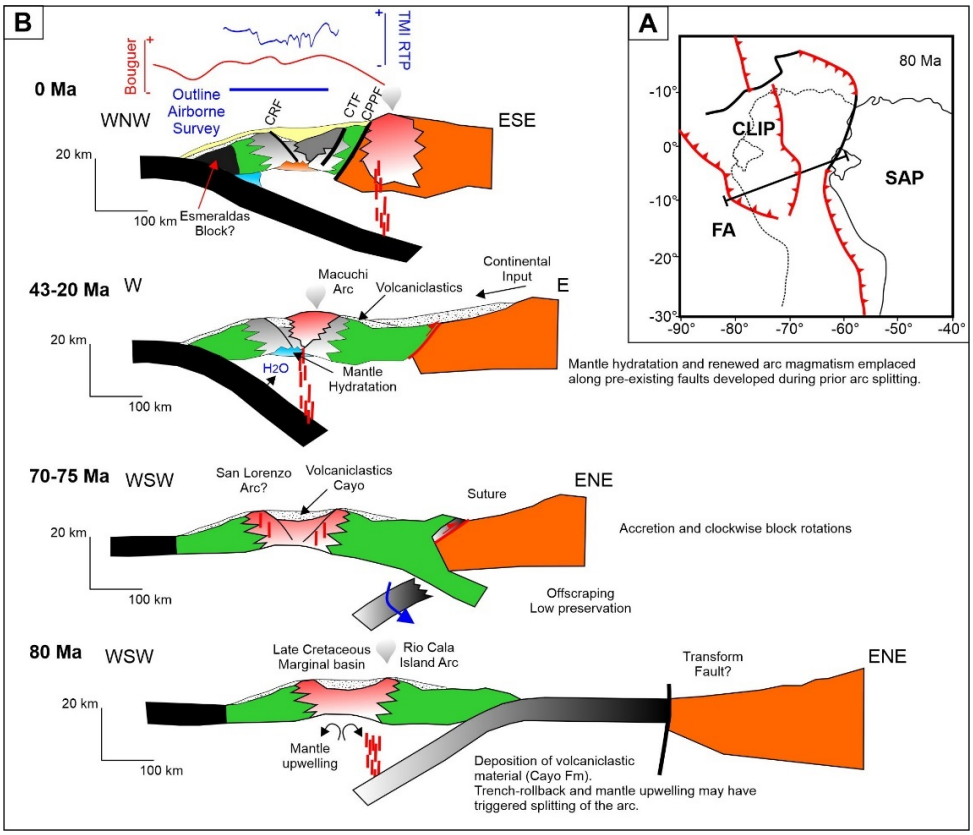

Figure 3.10: Geodynamic model of the oblique collision between the Caribbean Large Igneous Province (CLIP) and the South America passive margin (Western Ecuador). A) Plate reconstruction at 80 Ma **(modified after Braz *et al.*, 2018)**. B) Proposed tectonic evolution of the Western Ecuador subduction system. FA: Farallon Plate; SAP: South American Plate.

3.6.1 Split of Rio Cala-San Lorenzo arc and development of a marginal basin?

Major block rotations took place possibly triggering an initial crustal fragmentation between 70 -75 Ma (Luzieux *et al.*, 2006). The series of high magnetic susceptibility sources along the outer domain (Figure 3.4B) appear to correlate with plateau and island arc associated formations described within the San Lorenzo block (Figure 3.2) (Kerr *et al.*, 2002; Luzieux *et al.*, 2006). The coincidental location of the major faults bounding the eastern limit of the M1, M2, and M3 anomalies (the Coastal

Range Fault System, see Figure 3.4, 3.9, and 3.10) suggest rheological controls on the formation of this major boundary. The patchy and apparent northward change in orientation between the M2 and M3 anomalies, along the Canandé fault, suggests crustal deformation possibly accompanied by block rotation. In addition, the lack of continuity between M1 and M2 anomalies (Figure 3.4) could be explained by fault-related demagnetization process following block fragmentation and strike-slip movements. This area is coincident with the development of the Pedernales basin (Collot *et al.*, 2014; Hernández *et al.*, 2020) within the outer domain.

Both the San Lorenzo and Esmeraldas blocks are characterized by the presence of volcanic rocks from the San Lorenzo Formation unconformably overlain by middle Eocene rocks, marking a clear stratigraphic hiatus (Ordónez *et al.*, 2006). A stratigraphic gap that supports the interpretation of a structural high developed by Late Cretaceous (Luzieux *et al.*, 2006; Marcaillou and Collot, 2008; Lucas and Delgado, 2018). Furthermore, an oil exploratory well located in the inner domain (Ricaurte-1 in Figure 3.5) encountered (near its bottom) a series of volcaniclastic deposits (Coniacian to Campanian) that correlate to the Cayo Formation described farther south along the Chongón Colonche Hills (Benitez, 1995; Deniaud, 2000; Ordónez *et al.*, 2006). The onlapping stratal termination pattern of the lowermost seismic unit onto the Piñón acoustic basement suggests that the depocenter and the bounding structural high were coeval with the sedimentation of the Cayo Formation. Thus, onset of sedimentation in the Cayo Formation may have preceded the main accretion whereas the upper part is synchronous with the major tectonic event during Late Campanian characterized by clockwise block rotations, between 75 and 70 Ma, recorded by paleomagnetic declination (Roperch *et al.*, 1987; Luzieux *et al.*, 2006) and most likely associated with the main Late Cretaceous accretionary period in Ecuador (Kerr *et al.*, 2002; Jaillard *et al.*, 2009; Vallejo *et al.*, 2009). Although the temporal relationships between the San Lorenzo and Rio Cala arcs are poorly constrained (especially because of poorly defined ages for the Rio Cala arc, see Vallejo et al., 2009) the wealth of observations suggest that the outer domain and more specifically the San Lorenzo arc may represent the western section of a split-arc. An

early separation between these two arcs may have developed a marginal Late Cretaceous basin, where sedimentation of volcaniclastic deposits of the Cayo Formation took place. It is, however, difficult to conceive the mechanism leading to the formation of the marginal basin, especially because of doubts about the temporal relationships between the arcs and the subduction polarity during Late Cretaceous. However, the very weak deformation observed at the base of the depocenter, interpreted here as a marginal basin, suggest that the accreted sliver was most likely transferred to the continental margin with little internal deformation. This last aspect may be interpreted as a highly preserved sliver because of forward-facing collision. Nevertheless, a weak deformation may also be conceivable in the context of a thick accreted sliver colliding in a back-ward facing mode.

At the southernmost part of the inner domain, we found one of the most significant positive and long-wavelength Bouguer anomalies in the northern Andes located along the Chongón Colonche Hills. Feininger and Seguin (1983) and this study estimate that a shallow mantle and a thinner crust (ca. 10km) are contributing to the anomaly. This may be considered atypical for an oceanic plateau or for an island-arc, as they commonly exhibit thicknesses above 10 km (Tetreault and Buiter, 2014). Recent studies based on seismic tomography put in evidence a high shear velocity zone that correlated very well with this gravity anomaly, confirming the shallow mantle model (Figure 3.3). Indeed, farther north, the thickness of the accreted sliver increases and reach values of ca. 15 km (Figure 3.6). The very significant positive anomaly seems coincident in the southern limit of the marginal basin, here related to a possible split of the Rio Cala and San Lorenzo arcs. Therefore, crustal thinning and resulting isostatic mantle upwelling may well explain this gravity high in the region. Additionally, preliminary petrological analysis on intrusive rocks at the eastern part of the CCH (Witt *et al.*, 2019a) suggest significant denudation in excess of 2-3 km subsequent to the magmatic activity. Nevertheless, this hypothesis needs further verification, especially regarding the timing of the denudation period and its relationship with better known rotational and accretional periods in SW Ecuador.

3.6.1.1 The regional positive magnetic anomaly: a serpentinized mantle?

We propose that a combination of 1) deep seated faults controlling basalt flow location, and 2) disturbances of the underlying mantle possibly through a serpentinization process, may have considerably modified the density and magnetic properties of the underlying forearc basement or crustal mantle.

It is widely accepted that at depths of ~40-50 km the subducting slab release large amounts of water into the overlying lithosphere producing serpentine (Hyndman and Peacock, 2003; Blakely *et al.*, 2005). Serpentinization can be distributed extensively affecting in some cases the entire forearc mantle (Blakely *et al.*, 2005). It is known that serpentinization reduces the density of peridotites and produces a residual iron oxide, typically magnetite, which imparts a strong magnetic susceptibility to serpentinites, where its value is proportional to the degree of serpentinization and amount of iron derived from source rocks (Toft *et al.*, 1990; Hyndman and Peacock, 2003). Magnetic susceptibilities may increase by several orders of magnitude, remanent magnetization may increase by one order whereas density may decrease from ~3000 kg/m3 to ~2500 kg/m3 (e.g. Saad, 1969; Blakely *et al.*, 2005). Therefore, and as suggested by Blakely *et al.* (2005) long-wavelength magnetic anomalies lacking corresponding positive gravity anomalies may provide evidence to map hydrated mantle in convergent-margin settings. Forearc hydrated mantles may also have a strong influence on deformation partitioning and seismicity at depth (Seno, 2005; Reynard, 2013) and they have been usually discovered by the presence of anomalous low velocities in mantle regions (e.g. Blakely *et al.*, 2005).

The long-wavelength component of the anomalies described within the inner domain suggests that part of the anomalies may be originated at great depths. Thus, the very high positive magnetic anomaly (~250 nT) observed at ~180 km in profile BB' is not paired with a positive gravimetric anomaly, although the gravimetric low may be masked by the vicinity of the continental crust. In addition, the presence of small circular anomalies, highlighted by the analytical signal in (Figure 3.4B), with high magnetic susceptibility may suggest the presence of magnetite-rich igneous intrusions built on the accreted

and composite sliver. Indeed, the apparent serpentinization of the forearc mantle does not appear to correlate to the modern arc (actually, a high-velocity mantle has been defined in the area; Lynner et al., 2020) and instead, it may be related to ancient plutonism. We suggest that part of the inner domain underlying crustal mantle may have undergone a serpentinization process giving rise to this significant magnetic anomaly (Figure 3.4C); most likely coevally with the magmatic intrusions, which east of the piedmont has been dated between 43 to 25 Ma in the Macuchi block (Vallejo *et al.*, 2016). Similar anomaly patterns have been observed along other active margins that share similar characteristics in terms of forearc sliver accretion, like in Cascadia on the Oregon coast (Blakely *et al.*, 2005), East Antarctica (Ferraccioli *et al.*, 2002), and in Japan (Finn, 1994).

The Macuchi block, just east of the inner domain, is characterized by a broad volcanic arc region and marked by pulses of adakite-like magmatism (Chiaradia, 2009). This author attributes the peculiar adakite-like magmas to a process of crustal thickening through the build-up of previous magmatic arcs. Indeed, the hydration of the mantle may have considerably modified the upper crustal structure through the emplacement of volcanism and felsic intrusive material such as the intrusives of the Macuchi block (Hughes *et al.*, 1999; McCourt *et al.*, 1999; Chiaradia, 2009; Vallejo *et al.*, 2016). The intrusions observed beneath the forearc depocenter, considered together with coeval intrusions outcropping in the Western Cordillera, may possibly represent the wider magmatic arc of the Cenozoic history of the Northern Andes of Ecuador (Figure 3.10B). In this context, the serpentinization process may have played a significant role in the generation of mineral deposits during Late Eocene to Oligocene such as the porphyry/epithermal Balzapamba, Chaso Juan and La Plata deposits. Indeed, the suite of porphyry Cu-Au and epithermal Au deposits, such as those encountered in Ecuador, have been related to water-rich, calc-alkaline magmas originated by partial melting of a hydrated mantle wedge (e.g Richards, 2009; Richards, 2011). Alternative models for the serpentinization within the inner domain

may be related to the obduction process of continental crust (Petterson, 2010; Bonnemains *et al.*, 2016). Either process may have led to serpentinization of the mantle and lower crust, diminishing the density and therefore a reduction on the gravity anomaly. This may shed some light onto the up to now disputable Macuchi event (Late Eocene to Oligocene event) in the Ecuadorian geology.

3.6.2 Esmeraldas block – trailing edge of a different accreted sliver?

South of the city of Esmeraldas, the total magnetic intensity map reveals strong negative anomalies oriented in a NE-SW direction, a pattern that differs from those observed along the outer domain (Figure 3.4). Figure 3.4C shows a deep source (>10 km) contributing to the negative anomaly. The southern limit of the anomaly coincides with the major Canandé fault. This long wavelength and negative magnetic anomaly appears to extend trench-wards and landwards to the northeast prolonging into Colombia, where a major strike-slip system and a double forearc basin system have been previously described (Marcaillou and Collot, 2008; Lopez, 2009). The Borbón and Tumaco basins in Ecuador and Colombia, respectively, are coincident with the location of the magnetic low, with major basin development onset by Early Miocene (Marcaillou and Collot, 2008). In Western Ecuador, the set of strike-slip duplex appears limited to the Esmeraldas block and northwards into Colombia. The northern limit of the magnetic low coincides with the southern prolongation of the Buenaventura fault described in Colombia. The latter interpreted as being the suture trace between the Gorgona and the Dagua terrane (equivalent to the Piñón terrane) (Cediel *et al.*, 2003), both of an oceanic plateau origin. However, paleomagnetic data from the Gorgona terrane (MacDonald *et al.*, 1997) may suggest a different plateau origin compared to the CLIP (Kerr, 2005; Kerr and Tarney, 2005).

Farther north at the edge of the aeromagnetic survey, a slight increase in magnetic susceptibility appears to coincide very well with a decrease in gravity (Figure 3.3). Furthermore, the outline of a low-velocity zone, inferred from a tomographic model (Cano *et al.*, 2014) agrees with the gravity/magnetic relationship described above. This relationship may be attributed to a serpentinization process of

mafic rocks, commonly present along the convergent margin, such as the one described in the present work associated to the Macuchi block, and like those observed in south-central Alaska (Mankhemthong *et al.*, 2013) or western Oregon (Blakely *et al.*, 2005).

Thus, we cannot discard that the Esmeraldas block could be the southern prolongation of a different sliver such as the Gorgona sliver described by (Cediel *et al.*, 2003), which extends farther north and possibly giving rise to the development of a double forearc basin system as observed in Western Colombia (Lopez, 2009).

3.6.3 The southern suture zone (Gulf of Guayaquil) – a transform fault boundary

The southern suture, across the Gulf of Guayaquil, between the oceanic crustal sliver from the CLIP and the South American Plate, remains uncertain giving rise to different interpretations. For instance, Bourgois (2013) proposes two end-members tectonic reconstructions for the underlying crustal structure across the Gulf of Guayaquil-Tumbes basin to better explain the movement of the North Andean Sliver through 1) reactivation of ~75-65 Ma ophiolite suture by simple shear, or 2) through pure shear along the Inter Andean depression. Onshore, south of the Puná Island, the depression coincides with the Jubones-Peltetec fault (Figure 3.2). Giving the partial coverage of this area by the airborne survey, we discuss the possible location of the suture based on the forward model presented in Figure 3.8, and the spatial distribution of the different tectonic elements (Figure 3.4), which may be inferred as inherited from the underlying crustal configuration.

The forward model along profile C-C' (Figure 3.8), was geological constrained based on surface and subsurface observations (Bosch et al., 2002; John et al., 2010; Herms et al., 2012; Bourgois, 2013; Aizprua et al., 2019b). We consider that the gravity low south of the major long-wavelength gravity high described along the Chongón Colonche Hills may be caused by a great lateral density variation possibly controlled by a major transform fault. Considering that the Gulf of Guayaquil area

may be the southernmost region where an east-dipping subduction system from the CLIP interacted with another subduction system along northern Peru (Figure 3.10A), it is plausible that both systems connect through a transform fault as shown by analogue modelling (Boutelier and Chemenda, 2011). Fault segments with a possible shear character, such as the Puná segment (Dumont *et al.*, 2005; Alvarado *et al.*, 2016), are apparently rooted in this major transform fault, which is defined as a vertical tear fault.

Farther to the west, there are two key elements to consider for positioning the suture. First, the presence of the Santa Elena High, which consists of deformed Late Cretaceous to Paleocene sequences possibly conforming an outer wedge remnant of an east-dipping subduction system (Aizprua *et al.*, 2019b). And second, the clear oblique relationship between the Tumbes and Esperanza associated gravity lows (Figure 3.3). This may suggest that the underlying crustal structure across the Tumbes basin differs from the Esperanza sub-basin. Indeed, Aizprua *et al.* (2019b) and Espurt *et al.* (2018) propose that the Tumbes basin may conform to a forearc s.s basin controlled to the north by the Banco Peru outer forearc high and underlain by the offshore continuation of the continental Amotape-Tahuin Massif.

Forward modelling seems insufficient to define the southern suture zone of the CLIP. Nevertheless, putting together all the element, we considered that suture zone across the Gulf of Guayaquil is composed of both a suture and a vertical tear fault (Figure 3.9), both inherited from the collision and accretion process during Late Cretaceous, a model composed of both end-members proposed by Bourgois (2013).

3.7 CONCLUSIONS

We put forward the first crustal model for the forearc region in Ecuador that integrates spectral analysis of gravity and magnetic data along with 2D forward models and seismic data. It incorporates previous geochemical, stratigraphic, and structural observations mostly derived from the ophiolites emplaced along the

Western Cordillera and Coastal regions. It is noteworthy that the analyses and interpretation of the geophysical data were tied to geological constraints at least for the shallowest sources of the anomalies. The crustal structure model of an exceptionally well-preserved remnant sliver from the CLIP provides additional constraints when building a geodynamic model for Western Ecuador.

Our model is composed of at least three main geophysical domains, which are 1) the inner domain, 2) the outer domain and 3) the southern suture domain. The spatial distribution of the different igneous-associated bodies may be in direct relationship to the structuring of the forearc basement following the entrapment of a sliver from the CLIP (Aizprua et al., 2019b), and the post-Oligocene deformation due to oblique subduction that may have resulted in the development of strike-slip systems (Witt and Bourgois, 2010; Reyes, 2013; Aizprua et al., 2019b; Hernández Salazar et al., 2019). We propose that the inner and outer domains are most likely controlled by the inherited structure. The disposal and alignment of the magnetic anomalies along the outer domain with the series of faults, here defined as the Coastal Range Fault System, supposed an underlying rheological control. Furthermore, the presence of Coniacian to Campanian volcaniclastic deposits, within the inner domain, onlapping onto a structural high, which is delimited by the fault system mentioned above suggests the development of a marginal basin prior to the collision and accretion of the plateau. The presence of a high positive gravity anomaly and 2D forward models support a very shallow moho in this region with a thin crust atypical of an oceanic plateau. Therefore, it is plausible to consider that the San Lorenzo arc may be a split-arc segment of the Rio Cala arc to the east, possibly triggered by isostatic mantle upwelling and trench rollback (Figure 3.10); transferred almost undeformed to the continental margin during the accretionary phase.

Another key factor of our interpretation is related to a regional long-wavelength magnetic anomaly across the inner domain, apparently pair with a gravity low, which may suggest the presence of an underlying serpentinization process, with intrusions built on the accreted and composite sliver. Based on the irregularities of the magnetic anomaly, the serpentinization process may have altered the lower crust or the mantle

crust underlying the CLIP as suggested by forward modelling. The general disposition of the high magnetized area seems to coincide with the western edge of the exposed Macuchi block, suggesting that magmatism type present in the block may be at least partly related to the serpentinization process. Notably, prominent magnetic anomalies have been identified in other regions in adakite-rich arcs such as the Palmer Land section of the Antarctic Peninsula (Ferraccioli et al., 2006). The identification of a serpentinized lower crust beneath the forearc of Ecuador may have crucial significance, for instance in the definition of metallogenic zones (Richards, 2009). A similar autochthonous magmatic arc process has been proposed for the early Paleozoic subduction system of Victoria Land in Antarctica, with the aid of gravity and magnetic data (Ferraccioli *et al.*, 2002).

Forward modelling seems insufficient to define the southern suture zone of the CLIP. However, by considering the different tectonic elements at the surface and subsurface, we propose that the suture zone across the Gulf of Guayaquil is most likely composed of a suture and superimposed vertical tear fault.

Throughout the use of potential field methods and the integration of different types of data, we have shown the key importance of geophysics to uncover the forearc crustal structure in Western Ecuador, such as the similar cases of southern Alaska (Mankhemthong *et al.*, 2013), Antarctica (Ferraccioli *et al.*, 2002), Cascadia (Blakely *et al.*, 2005), and the northeast of Japan (Finn, 1994) where buried volcanic arcs and serpentinized mantle have also been identified based on the analyses of gravity and aeromagnetic anomalies.

Acknowledgments

This study was conducted as part of a Ph.D. thesis by C. Aizprua at the Norwegian University of Science and Technology (NTNU) in cotutelle with the University of Lille (France). The funding for this work was provided by the Statoil's (currently called Equinor) AKADEMIA agreement. We are grateful to Petroamazonas EP (Quito, Ecuador) for kindly providing access to unpublished data, such as airborne

gravity/magnetic and seismic data from the Coastal region in Ecuador. We are thankful to Ulrike Freitag, Sofie Gradmann, Terje Solbakk, and Galo Montenegro for constructive comments and corrections to the initial versions of the manuscript. Thoughtful reviews by Fabio Speranza, Fausto Ferraccioli, and editor Andrea Billi are much appreciated. Geosoft is thanked for the provision of Oasis Montaj and the GM-SYS module used for the analysis and modelling of gravity and magnetic data. The data used for this study are accessible at the NTNU Open Research data repository (https://dataverse.no/).

Chapter 4

Cenozoic tectonic evolution of SW Ecuador

The content of this chapter is published in: ***Aizprua, C.****, C. Witt, S. E. Johansen, and D. Barba (2019), Cenozoic stages of forearc evolution following the accretion of a sliver from the late Cretaceous-Caribbean Large Igneous Province: SW Ecuador-NW Peru, Tectonics, 38(4), 1441-1465.*

In this work, we present an integrated study revisiting old data and results from recent studies dealing with the dynamics of allochthonous terrane accretion along continental margins. Our integrated approach shows that SW Ecuador was dominated by a Late Cretaceous deforming outer wedge, which may have constituted a remnant of a northeast or northwest-dipping obliquely obducted oceanic block at the edge of the CLIP. This tectonic phase was governed by plate instability, affecting NW Peru and SW Ecuador, followed by re-establishment of the margin by early Eocene. The resulting margin configuration and the spatial distribution of the different tectonic elements seem to have played a key role in the further Cenozoic development of the forearc region. The model presented in this study proposes that the accretion of buoyant oceanic terranes may have had a profound impact on the early margin configuration of SW Ecuador and NW Peru and led to the development of localized but genetically related forearc depocenters.

4.1 Introduction

Forearc basins along convergent margins are characterized by complex structural configurations and sedimentary infilling that are primarily governed by the erosional versus accretionary tectonic regime along the margin (Seely, 1979; Beck, 1983; Von Huene and Scholl, 1991; McCaffrey, 1992; Pinet and Cobbold, 1992; Platt, 1993; Haq and Davis, 2010; Kopp, 2013; Noda, 2016). The sedimentary record can provide valuable information about past episodes, but the information may be biased by the better preserved geological evidence (Draut and Clift, 2013). Ancient forearc regions are commonly composed of amalgamations of continental fragments, intra-oceanic island arcs, or the entrapment of oceanic plateau slivers (NW South America, Kerr and Tarney, 2005; Great Basin, Dickinson, 2013; e.g. Costa Rica margin, Andjić *et al.*, 2018), making it imperative to account for their role in the tectonostratigraphic evolution of forearc basins.

Recent numerical models of the dynamics of oceanic plateau accretion versus subduction along continental margins show a strong link with the topographic evolution of the forearc region (Moresi *et al.*, 2014; Vogt and Gerya, 2014). Moresi *et al.* (2014) suggest that the dynamics of the accretion of buoyant and/or exotic plates or microplates are marked by three stages: 1) a collision stage leading to the accretion of the crust; 2) a transitional stage marked by coeval advance and trench retreat in different parts of the margin; and 3) the re-initiation of a stable subduction system behind the accreted microplate.

The seaward flanks of the Northern Andes are underlain by allochthonous oceanic terranes derived from the Caribbean Large Igneous Province (CLIP) (Whattam and Stern, 2015) that were episodically accreted to the South American continent from the Late Campanian to the Paleocene (Jaillard *et al.*, 1997; Reynaud *et al.*, 1999; Hughes and Pilatasig, 2002; Mamberti *et al.*, 2003; Luzieux *et al.*, 2006; Vallejo *et al.*, 2009), which led to the entrapment of the North Andean Sliver (Kennan and Pindell, 2009; Alvarado *et al.*, 2016). At the trailing edge of the North Andean Sliver, the peculiarly oriented Gulf of Guayaquil-Tumbes and Progreso basins are located along a major shear zone coincident with a complex suture zone between

oceanic and continental crustal terranes, which probably marks the southern edge of the CLIP (Figure 4.1) (Deniaud *et al.*, 1999; Witt *et al.*, 2006; Jaillard *et al.*, 2009; Aizprua *et al.*, 2017).

The collision and accretion of the CLIP to the margin is well documented along the Western Cordillera (Reynaud *et al.*, 1999; Mamberti *et al.*, 2003; Vallejo *et al.*, 2009). However, the initial interaction between the trailing edge of the CLIP and the margin and its role into the further Cenozoic forearc basin development in SW Ecuador and NW Peru have not been discussed in detail (Benitez, 1995; Jaillard *et al.*, 1995; Fildani *et al.*, 2008; Witt and Bourgois, 2010; Espurt *et al.*, 2018).

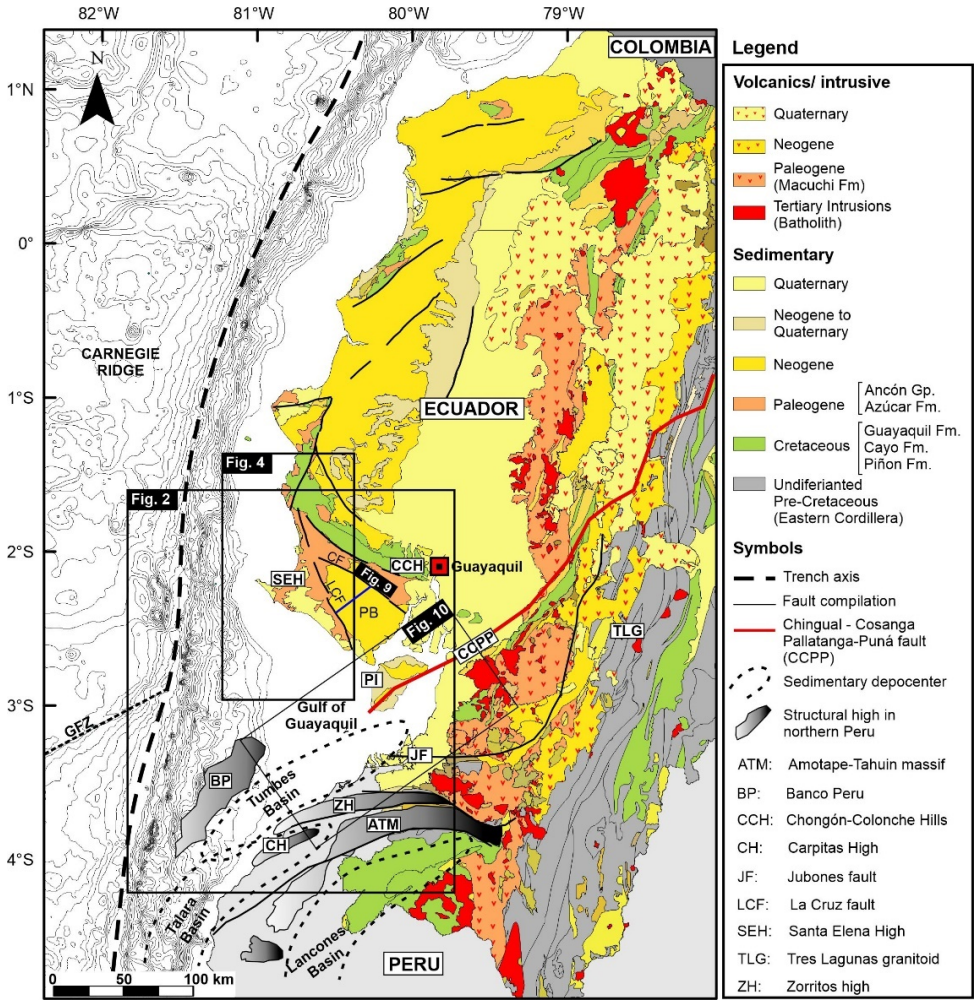

Figure 4.1: Regional geology of southwestern Ecuador displaying the present-day spatial relationship of the different geological units. Black lines show the major structural lineaments of the study area. Geological units and major faults are compiled from previous studies (Reynaud *et al.*, 1999; Bosch *et al.*, 2002; Hungerbühler *et al.*, 2002; Kerr *et al.*, 2002; Mamberti *et al.*, 2003; Spikings *et al.*, 2005; Fildani *et al.*, 2008; Vallejo *et al.*, 2009; Winter *et al.*, 2010; Witt and Bourgois, 2010; Herms *et al.*, 2012; Espurt *et al.*, 2018)

Using an integrative data approach, we present a model depicting the tectonostratigraphic response to the accretion of an oceanic plateau along the transform boundary between its southern edge and the NW South American continental margin. The distribution of the different tectonic elements across the study

area suggests a natural example of the numerical simulations proposed by Moresi *et al.* (2014) and Vogt and Gerya (2014), at least until the mid to late Eocene. Since at least the Oligocene, the resulting margin configuration appears to have controlled the development of the Gulf of Guayaquil-Tumbes Basins through transtensional movements, and the Progreso Basin as a sensu stricto forearc basin that was controlled by the development of an outer forearc high buttress to a remnant of the CLIP (Piñon Block) acting as a backstop (Figure 4.2). These aspects bring new insights into the evolution of the Ecuador-Peru forearc region, which have general implications for the tectonostratigraphicarchitecture of forearc regions affected by the accretion of allochthonous terranes.

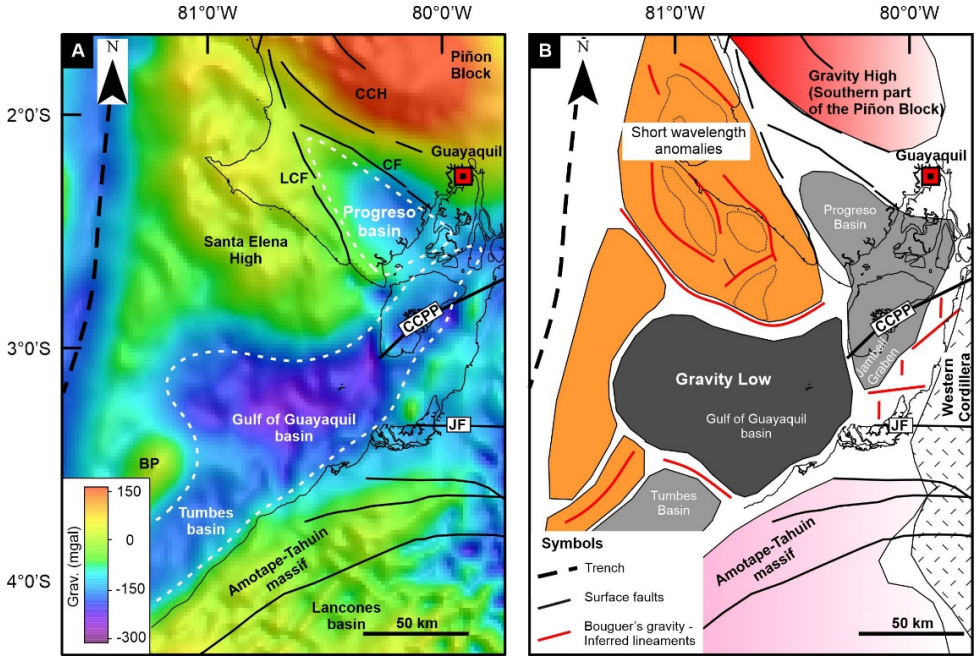

Figure 4.2: (a) Bouguer's gravity anomaly map in SW Ecuador (Sandwell *et al.*, 2014). (b) Main structural lineaments derived from gravity gradients are highlighted in red. Notice the three main domains derived from the Bouguer's gravity anomaly: 1) in red an area of long wavelength anomaly which corresponds to surfaces exposures from the Piñon block, 2) in orange an area dominated by short wavelength anomalies directly linked to the Santa Elena High, and 3) negative values corresponding to the thick sedimentary successions along the Gulf of Guayaquil-Tumbes basin. BP: Banco Peru; CCH-Chongón Colonche Hills; CCPP: Chingual-Cosanga-Pallatanta-Puná; CF-Carrizal fault; JF: Jubones fault; LCF: La Cruz fault.

4.2 Geodynamic and Geological Settings

4.2.1 North Andean Sliver

Coastal Ecuador is composed of terranes with plateau and island-arc affinities based on the geochemical fingerprints of the magmatic products (e.g. Kerr *et al.*, 1997; Reynaud *et al.*, 1999; Hughes and Pilatasig, 2002; Kerr *et al.*, 2002). Paleomagnetic studies along the Chongón Colonche Hills (Figure 4.1) reveal a low latitude (~ 0-10°S) origin for the Cretaceous mafic rocks exposed in coastal Ecuador and clockwise rotations ranging from 20-70° during the Late Campanian, which were likely triggered by the collision with the South American Plate (Roperch *et al.*, 1987; Luzieux *et al.*, 2006). Potential-field models across the North Andean Sliver supports the presence of an underlying oceanic crust (Feininger and Seguin, 1983; Kellogg *et al.*, 1995). Feininger and Seguin (1983), propose a sharp and vertical boundary between the oceanic terrane and the South American continental crust and suggest a shallow mantle interpretation to explain the high positive Bouguer gravity anomaly coincident with the strike of the Chongón Colonche Hills (Figure 4.2). Kellogg *et al.* (1995) instead propose a low angle obduction of the oceanic crust supported by velocity inversion results along a refraction profile farther north, along the border between Ecuador and Colombia.

The accreted mafic rocks form the basement of coastal Ecuador, and they are mainly confined between the major dextral Chingual-Cosanga-Pallatanga-Puná fault system to the east (Alvarado *et al.*, 2016), the trench to the west, and a complex suture zone to the south that runs along the Gulf of Guayaquil (Aizprua *et al.*, 2017) (Figure 4.1). Despite several studies on the nature and origin of the basement of coastal Ecuador, its emplacement along the margin is still a topic of debate. This has led to two main and opposing models for its emplacement: one incorporates a single accretionary episode during the Maastrichtian (e.g. Vallejo *et al.*, 2009), and the other includes multiple accretionary episodes between the Late Cretaceous and the Eocene (Hughes and Pilatasig, 2002; Kerr *et al.*, 2002; Jaillard *et al.*, 2009).

Deformation partitioning affected the Northern Andes from southwest Ecuador to northern Colombia and formed the regional "North Andean Sliver" (Ego *et al.*,

1996; Nocquet *et al.*, 2014; Alvarado *et al.*, 2016; Yepes *et al.*, 2016). The northeastward movement of the North Andean Sliver resulted in clear north-south-striking transpressive deformation along the eastern boundary of the sliver (Winkler *et al.*, 2005), which suggests that the deformation was induced by oblique subduction. A fault analysis performed in the Western Cordillera led Alvarado *et al.* (2016) to propose that the northward migration of the sliver may have started during the middle Miocene (~ 15 Ma). Furthermore, rapid subsidence resulting in thick Quaternary basin formation in the Gulf of Guayaquil was associated with an acceleration of the tectonic "escape" of the sliver for at least the last 1.8 Ma in a process that may have resulted from a stronger coupling with the subducting Carnegie Ridge (Witt *et al.*, 2006; Michaud *et al.*, 2009; Egbue and Kellogg, 2010).

4.2.2 Basin Stratigraphy of SW Ecuador

The Bouguer gravity anomaly map of the study area (Figure 4.2) highlights the locations and extents of the different forearc basins. Both the Santa Elena High and the Chongón-Colonche Hills are prominent features that played key roles in the segmentation of the forearc region.

The Piñon Block, which is part of the CLIP region, outcrops along the Chongón-Colonche Hills (Figure 4.1 and 4.2). Near the city of Guayaquil, the Piñon Block contains a nearly complete volcanoclastic sequence with stratigraphic contacts striking ESE-WNW (Figure 4.1 and 4.3). Figure 4.3 shows the stratigraphy of the area, from tholeiitic basalts and pillow lavas of the Piñon Formation to flysch and volcaniclastic deposits of the Cayo Formation, which are unconformably covered by chertized turbidite deposits of the Guayaquil Formation (Benitez, 1995). Farther to the SW, highly deformed equivalents of the Guayaquil Formation are exposed along the Santa Elena Peninsula (Figure 4.3).

4.2.2.1 Santa Elena Peninsula

A significant tectonostratigraphicchange occurs south of the Chongón-Colonche Hills (Figure 4.4 and 4.5-A), where highly deformed layers of the Late Cretaceous Santa Elena Formation, which are age equivalent to the Guayaquil Formation, are unconformably overlain by acidic rocks of the late Paleocene Azúcar Formation (-B). This formation is only present south of the Chongón-Colonche Hills, which is evidence of input from a localized continental source during this period.

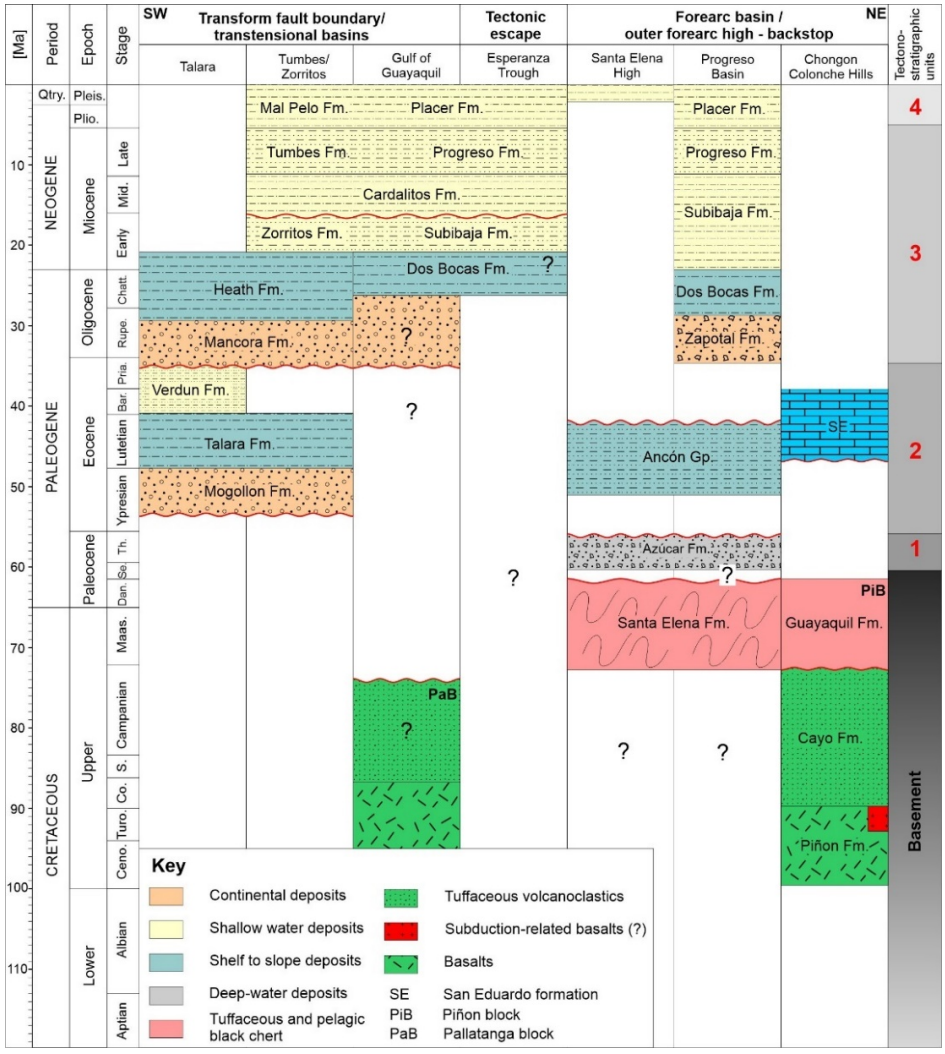

Figure 4.3: Chronostratigraphic chart of the SW Ecuador and NW Peru (modified after Benitez, 1995; Jaillard *et al.*, 1995; Fildani *et al.*, 2008; Espurt *et al.*, 2018). The upper part of the chart displays the structural domains interpreted from this study and the location of the different stratigraphic columns. Towards the NE, within the forearc basin domain, the stratigraphy of the accreted oceanic terrane (Piñon Block) is displayed. At the center, the Esperanza trough is within the tectonic escape domain, which is characterized by very negative Bouguer's anomaly values (Figure 4.2) and thick Pleistocene sequences (Witt *et al.*, 2006). Towards the SW, the Eocene sequences found within the Talara and Tumbes basins lies unconformably over Paleozoic metasediments (not displayed). Numbers 1 to 4 indicate the tectonostratigraphic units discussed in this study: 1 = high density deep marine deposits and highly deformed Paleocene sequences; 2 = slope sedimentary sequences; 3 = shallow sedimentary sequences, and 4 = thick Quaternary sequences following the tectonic escape of the North Andean Sliver.

Paleocene outcrops near the city of Playas (Figure 4.4 and 4.5-C) show a sequence of conglomerates alternating with coarse sand layers within a channelized conforming geometry, which are likely part of a submarine canyon architecture with a major paleocurrent direction pointing northward (Moreno, 1983; Benitez, 1995; Jaillard *et al.*, 1995). Similar surface exposures show vertically dipping layers, indicating that a relatively high degree of post sedimentary deformation occurred by the end of the Paleocene or early Eocene (Figure 4.5).

Farther to the west, middle Eocene rocks unconformably overlie the Azúcar Formation (Figure 4.5-A). Middle Eocene rocks of the Ancón Group are characterized by minor normal faulting and major gravitational sedimentary structures (at least in the basal part; Figure 4.5-E) during a period that may have resulted from a relaxation process accommodated by extensional tectonics (Jaillard *et al.*, 1995). These authors suggest that during the Eocene, sediments were deposited on top of an accretionary slope-basin and were subsequently affected by several deformation phases with different orientations that derived from an oblique subduction system. The latest possibly within a tectonic framework influenced by the generation of a triple junction at the interaction of the Gorgona Plateau (Late Cretaceous), the east-dipping Farallon plate (affecting western Ecuador) and the North Andean Sliver (Kerr and Tarney, 2005). By the end of the Eocene, the entire area emerged,and the sedimentary infilling

of the basin evolved to a more continental setting (Benitez, 1995; Jaillard *et al.*, 1995; Jaillard *et al.*, 1997; Witt *et al.*, 2019b).

4.2.2.2 Progreso and Gulf of Guayaquil-Tumbes Basins

The Progreso Basin is an Oligo-Pliocene basin located between the Chongón-Colonche Hills and the Santa Elena High (Figure 4.1 and 4.2). The basin has a NW-SE axis and a triangular shape that expands towards the SE (Figure 4.2). Its southwestern limit coincides with the La Cruz Fault (Figure 4.1). Benitez (1995) summarizes the main stratigraphic units, which reflect a restricted basin with localized sediment input derived from the Chongón-Colonche Hills and the Santa Elena High. The underlying basement is believed to have been formed of the same complex and deformed sequences of Late Cretaceous to Paleocene age that are observed along the Santa Elena High. After emersion of the Santa Elena High during the late Eocene-early Oligocene, the Progreso Basin began to form as a restricted area with a rapid shift to a continental to shallow marine environment (Witt *et al.*, 2019b). This is supported by the immature sediments of the Oligocene Zapotal Formation (Figure 4.3), which have paleocurrent directions that point towards the center of the basin (Benitez, 1995). The Miocene and Plio-Quaternary sedimentary rocks continued to develop in a restricted shallow marine environment with a marine influence possibly through the Gulf of Guayaquil.

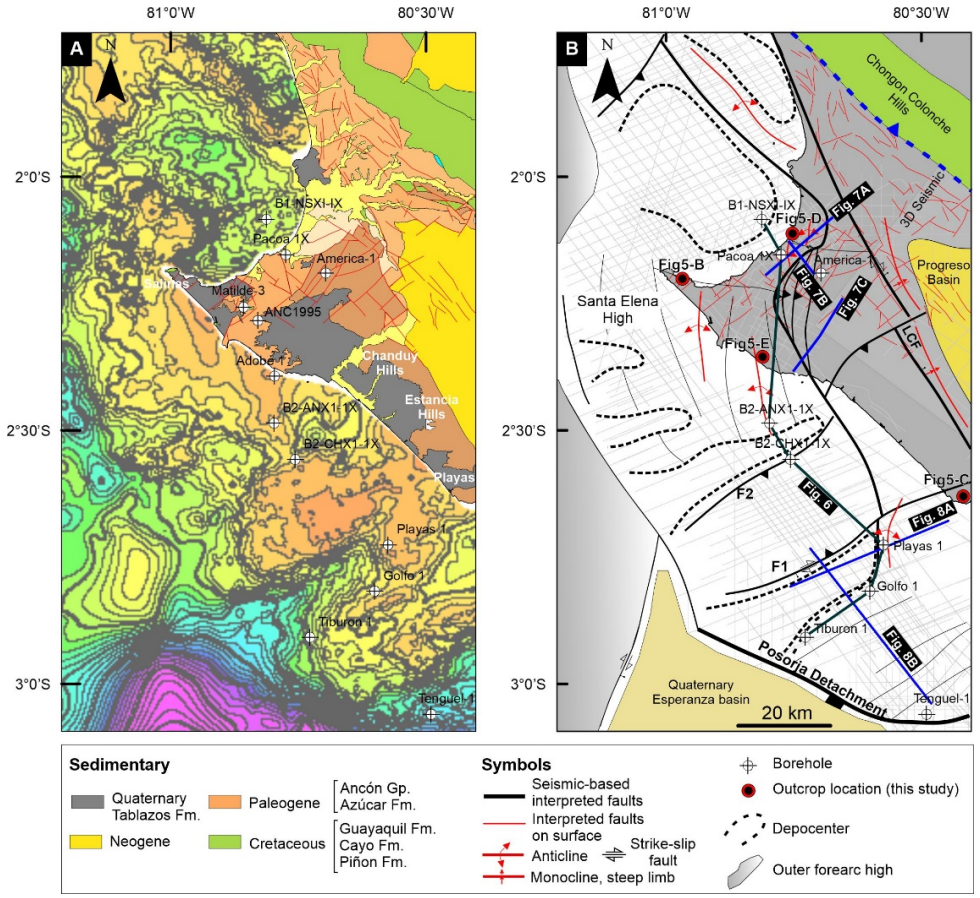

Figure 4.4: Geological map and two-way travel time (TWT) map of the major unconformity (U1/U2) across the Santa Elena High. (b) Structural map showing the main structural lineaments identified from interpreted seismic profiles. Faults identified on seismic sections in black, folded structures in thick red lines, and faults identified on surface on thin red lines.

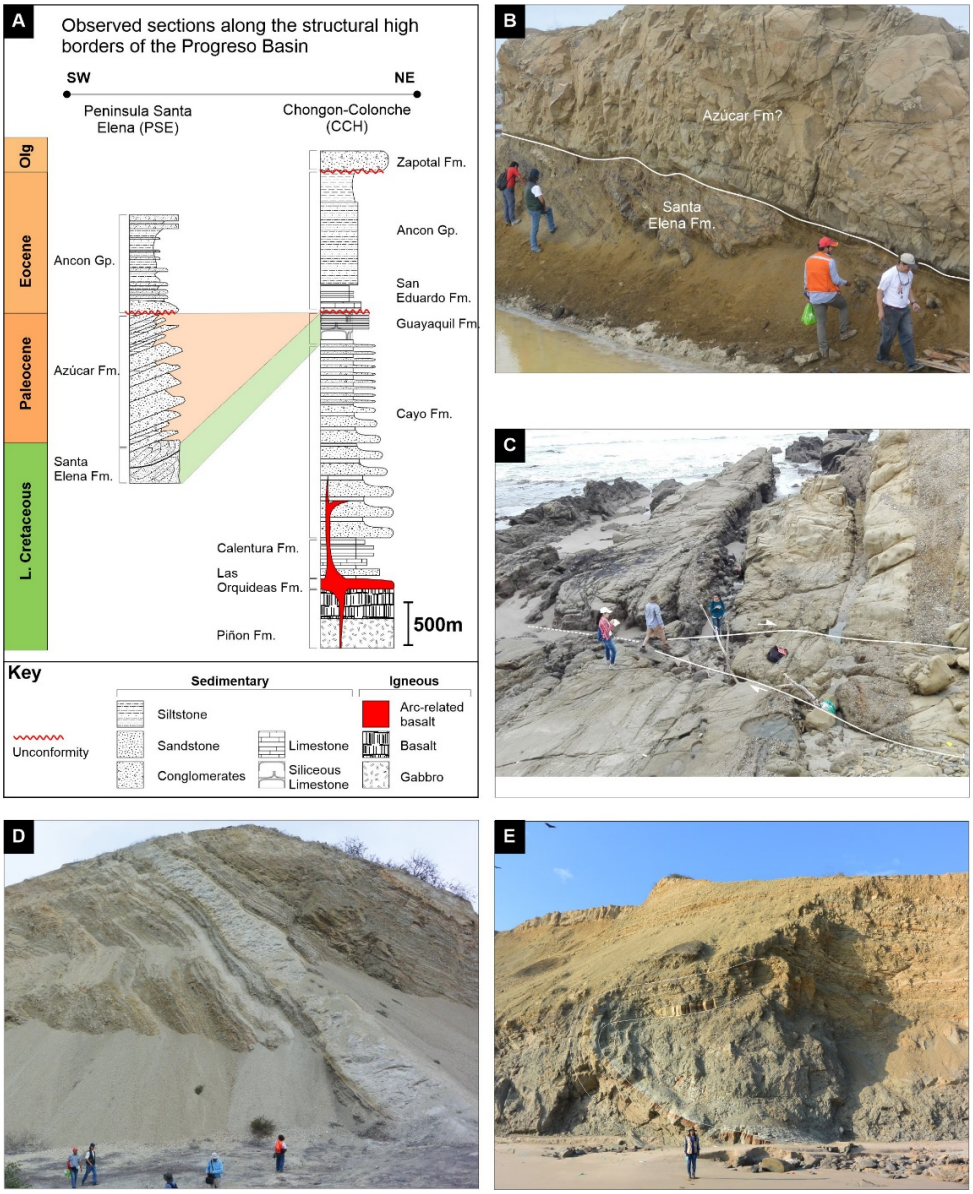

Figure 4.5: (a) Stratigraphy column of SW Ecuador for the Santa Elena Peninsula and Chongón Colonche Hills areas. (b) Chertified sediments of the Santa Elena Formation overlain discordantly by deposits of the Azúcar Formation near the city of Salinas (location on Figure 4.4). (c) Vertical strata of the Paleocene Azúcar Formation, outcrop located near the city of Playas showing high dense turbiditic deposits possibly in a confined channelized architecture. (d) Southern flank of a tight folded structure near the Pacoa oil field, deposits classically associated to the Ancón Group E) Middle Eocene sequences of the Ancón Group (within the Ancón oil field) showing a gravitational and mass transport complex structure.

South of the Santa Elena High, the Gulf of Guayaquil-Tumbes Basin is described as an elongated basin, oriented in NE-SW direction, which is coincident with a marked gravity low (Figure 4.1 and 4.2). It includes the so-called Jambelí channel or graben, the offshore Tumbes Basin, and the deep Esperanza sub-basin (part of the Gulf of Guayaquil basin) (Figure 4.2) (Benitez, 1995; Deniaud *et al.*, 1999; Witt and Bourgois, 2010). It is bounded to the north by the Posorja detachment, to the south by the Tumbes detachment, to the west by the Domito fault system, and to the east possibly by Late Cretaceous oceanic terranes (see details in Witt and Bourgois, 2010).

The area has experienced a very high subsidence rate at least since the late Pliocene. Seismic profiles and borehole data clearly indicate a thick sedimentary succession of Quaternary sediments (Witt *et al.*, 2006). Witt and Bourgois (2010) conclude that the thick Quaternary section of the Gulf of Guayaquil is the result of an acceleration of the NE migration of the North Andean Sliver (approx. 1 cm/yr), which is possibly explained by the arrival of the Carnegie Ridge at the subduction zone.

4.2.3 Northern Peru

4.2.3.1 The Amotape-Tahuin Massif

The Amotape-Tahuin massif is a mountain range that trends E-W at the Ecuador-Peru border and changes to a NE-SW trend to the southwest (Figure 4.1). A series of positive Bouguer gravity anomalies have been identified along the NW coast of Peru, suggesting a very dense underlying basement along the Amotape-Tahuin massif that may indicate an allochthonous origin for the massif (Feininger, 1987). Mourier *et al.* (1988) list some of the main geological processes and stratigraphic sequences that have been identified along the Amotape-Tahuin massif and how they differed from those observed farther east along the Eastern Cordillera, which supports the analysis of Feininger and Seguin (1983). Furthermore, paleomagnetic studies from the Amotape-Tahuin massif indicate clockwise rotations of approximately 35 to 90° during the Late Cretaceous-Early Paleocene (Mourier *et al.*, 1988), a rotation probably associated to the collision and accretion of the CLIP observed north of the massif in western Ecuador (Luzieux *et al.*, 2006). However, geochemical and

thermochronological data from rock samples along the Amotape-Tahuin massif complex show affinities with the Tres Lagunas Triassic granitoids (TLG) that are located farther northeast along the Eastern Cordillera (Figure 4.1), which suggest that the Amotape-Tahuin massif is a translated sliver by clockwise rotation during the Early to Late Cretaceous (Aspden *et al.*, 1992; Spikings *et al.*, 2005; Sanchez *et al.*, 2006). This is corroborated by recent similarities between age clusters and the maximum depositional ages of metasediments of the Amotape-Tahuin massif and the Eastern Cordillera of Ecuador and Peru (Witt *et al.*, 2017).

4.2.3.2 Lancones-Talara Basins

The Lancones and Talara basins in NW Peru comprise a series of NE-SW forearc depocenters bounded by thrust-related structural highs with a sequential northwestward progradation (Figure 4.1) (Espurt *et al.*, 2018). Paleomagnetic results from the Lancones Basin show clockwise rotations on the order of ~38° (Mitouard *et al.*, 1990), indicating that the basin was affected by dextral movements that were probably coincident with the increased exhumation rates in the Amotape-Tahuin massif at 75 - 65 Ma (Jaillard *et al.*, 1999; Spikings *et al.*, 2005).

The Talara Basin, which is located northwest of the Amotape-Tahuin massif (Figure 4.1), is overlain by Eocene deposits comprising fluvial to deep marine strata that are mainly sourced from Paleozoic basement of the Western Cordillera of Peru and the Amotape-Tahuin massif (Fildani *et al.*, 2008; Hessler and Fildani, 2015; Witt *et al.*, 2017; Espurt *et al.*, 2018). The Talara Basin is bounded to the north by the subsurface Carpitas High, which separates it from the Tumbes Basin (Figure 4.1). The sedimentary succession thickens to the south from ~ 3.5 km to 9 km, where exploration boreholes penetrated Paleocene strata (Fernández *et al.*, 2005). Fildani *et al.* (2008) provide a detailed stratigraphic study of the Eocene deposits, which record a tectonically abrupt deepening of the basin in the middle Eocene that controlled the transition from deltaic and fluvial deposits to deep water strata; these authors attributed this event to collisional tectonics and terrane accretion along the Ecuadorian

margin. Mitouard *et al.* (1990) reported post-Paleocene clockwise rotations for northern Peru, an event that Spikings *et al.* (2005) suggest was coincident with the high exhumation rates of the Amotape-Tahuin massif during the middle Eocene to early Oligocene.

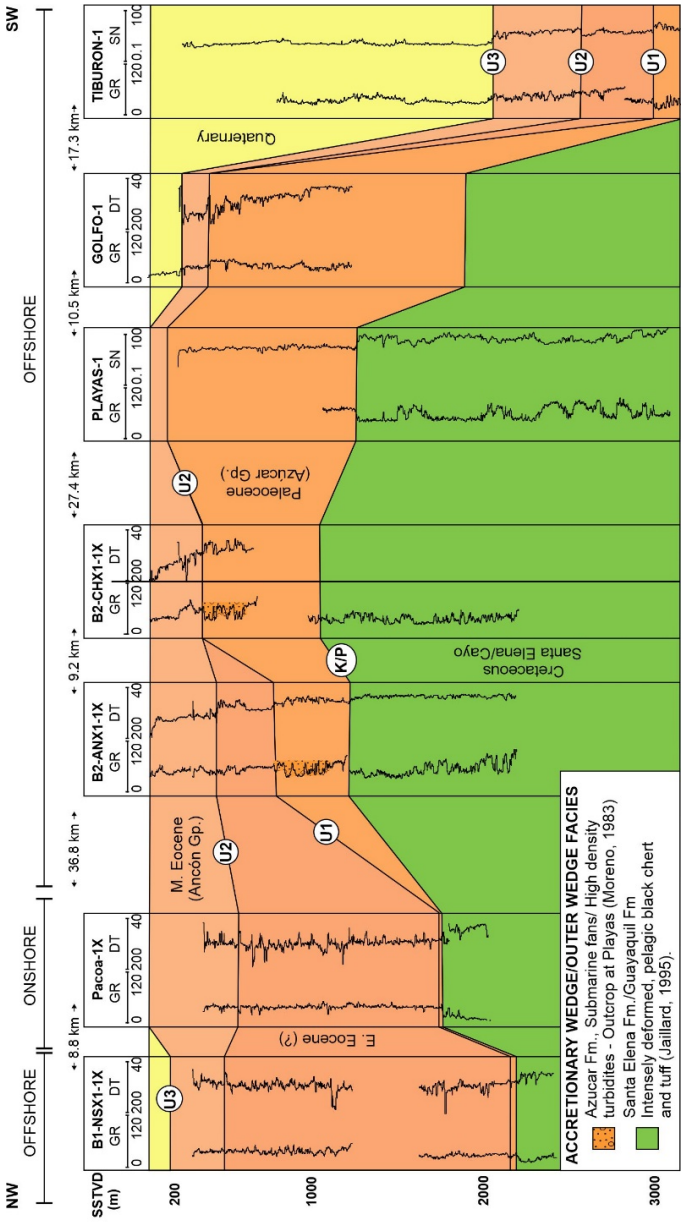

Figure 4.6. N-S well log correlation along the Santa Elena High. Major unconformity U2 is identified by an increase in velocity and it is dated (accordingly to unpublished well reports) as late early Eocene. Pacoa-1 and B1-NSX1-1X penetrated and confirmed the presence of the deformed Santa Elena Formation of Late Cretaceous age. The Late Cretaceous and Paleocene sequences form the Santa Elena High outer wedge (this work). GR – Gamma ray (API units); DT – Sonic (us/ft); RHOB – Density (g/cc); SN – Short normal resistivity log (ohm.m).

4.3 Dataset and Methodology

Hydrocarbon exploration has been performed in the study area for at least a century. The discoveries were mainly based on oil seeps along the southern coast of the Santa Elena Peninsula, which triggered further exploration campaigns. This study is based on the compilation of 2D industrial seismic profiles, borehole data, and internal unpublished reports provided by Petroamazonas EP, the Ecuadorian national oil and gas company (Aizprua *et al.*, 2019a). In NW Peru, we used two 2D seismic survey campaigns and four exploration boreholes to delimit the Tumbes Basin. The industrial multi-channel seismic reflection data in Ecuador and Peru are mainly composed of 2D seismic surveys and processing sequences with varying qualities from good to fair. Additionally, we used information from two unpublished 3D seismic surveys within the study area, one covering the offshore Amistad gas field and the second located onshore in the central Progreso Basin. The borehole data are sparse in the area but in some cases provide relatively poor age control, especially in the deepest part of the Gulf of Guayaquil and on the Santa Elena High. In NW Peru, the age control for the different seismic units was obtained from a public report written by Perupetro, the national oil and gas company in Peru (Fernández *et al.*, 2005).

A structural seismic interpretation across the offshore domain was performed to define the possible link between the offshore subsurface structures with structures that have been mapped onshore. A special focus was placed on mapping the southern extension of the Santa Elena High and its transition into the Gulf of Guayaquil (Figure 4.4). The stratigraphic interval encountered across the Santa Elena High plays a key role in the geology of southwestern Ecuador due to its interaction with the South American Plate during the emplacement of the CLIP. The definition of the main structures and their orientations is discussed in detail in the next section.

The results from previous studies of the surface geology of the Santa Elena Peninsula have been incorporated to discuss the structural styles and deformational phases that may have affected the region. The geological markers obtained from these studies were included in the definition of the stratigraphic tops. During this study, the main outcrop localities along the southern coast of Ecuador were visited for structural

and stratigraphic investigations. This study also benefited from radiometric ages, mostly zircon U-Pb ages (see Witt *et al.* (2017) and Witt *et al.* (2019b) for additional details).

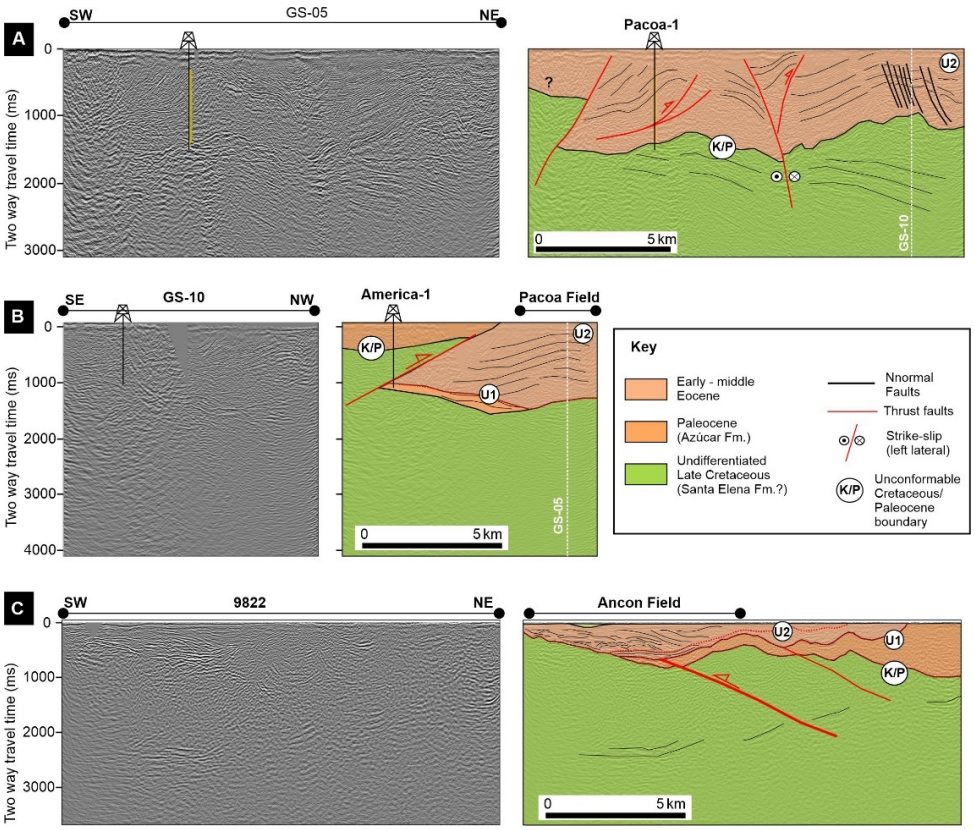

Figure 4.7: (a) (a) Seismic profile across the Pacoa field showing the presence of folded and thrusted structures unconformably overlying the deformed Late Cretaceous series of the Santa Elena Formation. (b) Seismic profile perpendicular to A) showing an overthrust of the Late Cretaceous/Paleocene series onto possibly early to middle Eocene sedimentary successions. (c) Seismic profile showing a possible piggy-back basin with middle Eocene deposits from the Ancón Group Noticed at the base the chaotic and inland seismic reflection packages overlain by more parallel to sub-parallel reflections.

4.4 Results

The results of the mapping include: 1) a late Paleocene unconformity (U1), which, based on exploration boreholes, defines an unconformable contact between early Eocene and Paleocene rocks; 2) an early Eocene unconformity (U2), which is a major boundary with the late Paleocene U1 across the different structural highs (Figure 4.6); 3) a mid to late Eocene unconformity (U3) that is recognized mainly in the Santa Elena and Progreso regions, and 4) an early Miocene unconformity (U4) in the Gulf of Guayaquil, which was identified from industrial boreholes and long amplitude incisions on the eastern side of the Tumbes Basin. The latter event corresponds to one of the main hydrocarbon reservoir intervals within the Gulf of Guayaquil-Tumbes Basin. The acoustic basement identified on seismic profiles, underlying the main tectonostratigraphic units, is characterized by at least two different seismic facies that can be traced locally: 1) thick packages of high amplitude and subparallel reflections, which, according to borehole Pacoa-1, correspond to the Late Cretaceous Santa Elena/Guayaquil Formation (Figure 4.7-A), and 2) chaotic and dipping discontinuous reflections that possibly correspond to the crustal Piñon Block. Based on our analysis, we subdivided the study area into different forearc regions characterized by their structural styles and sedimentary infilling, which are described further in the following sections.

4.4.1 Santa Elena High

It is a region characterized by positive and short wavelength gravity anomalies, located south of a gravity high, this latest one coincident with surface exposures of the Piñon Block (Figure 4.2). Its northeastern limit is defined very well by the “La Cruz Fault” and the Progreso basin, a boundary that is laterally changing to the northwest, into an apparent direct contact between the Santa Elena High and the Chongón Colonche Hills (Figure 4.2). Based on the study of surface exposures (Figure 4.1), and the analysis of well and seismic data, we present the results dividing the Santa Elena High into the region exposed along the Santa Elena Peninsula and its offshore continuation.

4.4.1.1 Ancón-Pacoa area

The Pacoa-1 borehole penetrated early to middle Eocene sequences and reached the Late Cretaceous Santa Elena Formation (Figure 4.6 and 4.7). A series of continuous high amplitude reflections concordant with the top of the Santa Elena Formation are present locally across the onshore Santa Elena High (Figure 4.7-A). This package of high amplitude reflections was tracked to guide the interpretation of acoustic basement and infer its likely structural control on the Santa Elena High configuration. These reflections are observed farther to the south across the Ancón Field and offshore along the continuation of the Santa Elena Peninsula, where well correlation and seismic profiles show a deepening of the Cretaceous units towards the south (Figure 4.6).

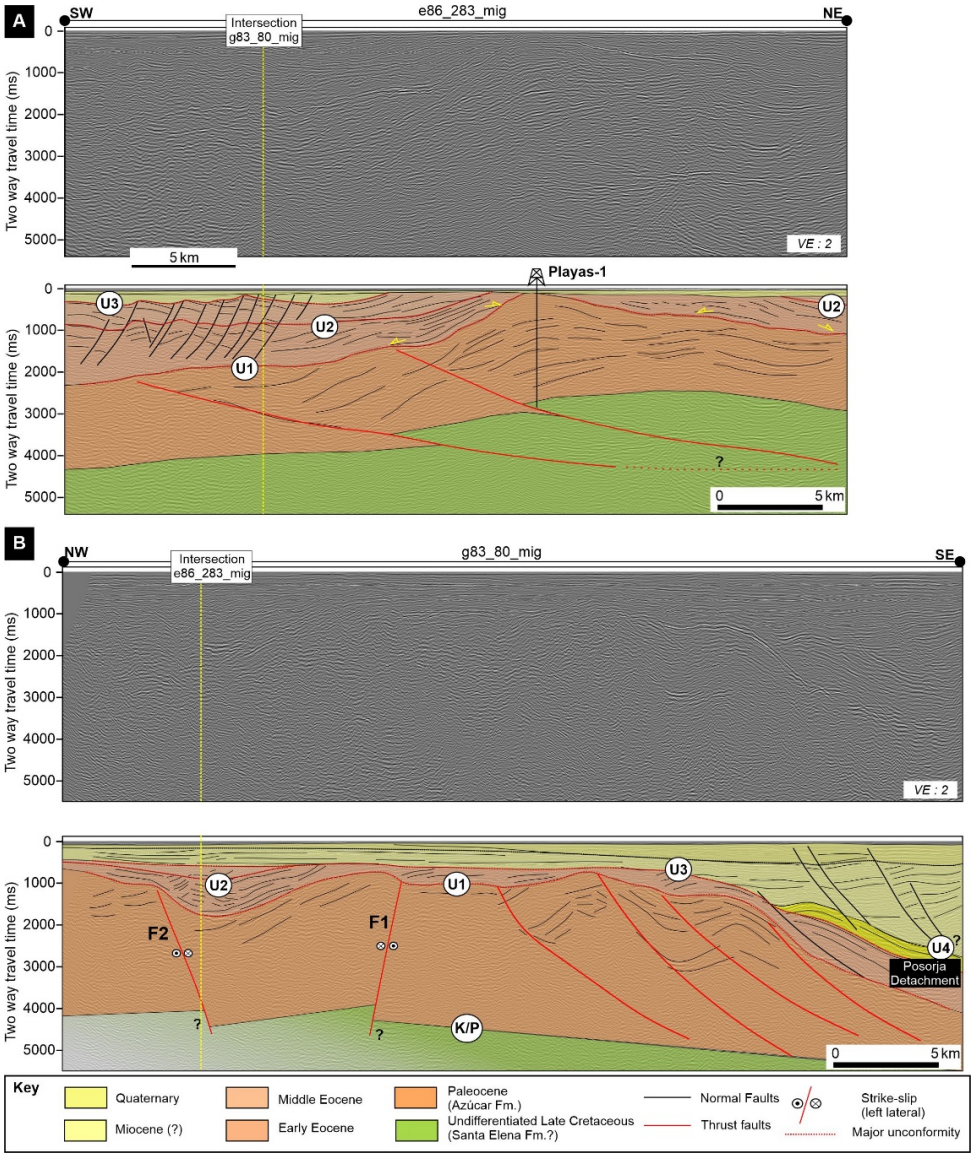

Figure 4.8: (a) NE-SW composite seismic profile, located south of the Playas outcrops location. A folded structure is observed with seaward dipping layers overlying a strong amplitude erosional event, associated to the main unconformity U1. Playas-1 was drilled on top of the structure founding a very thin Eocene sedimentary sequence. Highly dipping reflections underneath the unconformity U1 are associated to sequences from the Paleocene Azúcar Formation. (b) NW-SE composite seismic profile highlighting lateral ramp structures sealed by major unconformity U3. Towards the south, the Santa Elena High dips southward, affected by a series of low angle faults conforming the Posorja detachment.

Along a NE-SW seismic profile across the Pacoa Field, the basement-associated continuous reflections are overlain discordantly by folded structures of possible early Eocene age (Figure 4.7-A). Between the two folded structures, a deformed area with steeply dipping reflectors is present and strikes NW-SE. This structure outcrops north of the Pacoa oil field near the coastline (Figure 4.5-D). On seismic line GS-10, which is perpendicular to GS-5 (Figure 4.7-B), parallel slightly folded reflections dip to the southeast, where they are interrupted and apparently overthrust by older rocks. Borehole America-1 (Figure 4.7-B) penetrated Paleocene rocks that are probably thrusted over early Eocene rocks.

Surfaces U1 and U2 are characterized by increases in velocity and are clearly defined in borehole B2-ANX1-1X (~ 400 m and 700 m TVDSS, respectively; Figure 4.6). The stratigraphic sequences deposited above the U2 unconformity are exposed along the coastal cliffs in the Ancón region, north of borehole B2-ANX1-1X (Figure 4.4), and have been dated paleontologically and radiometrically as early (?) to middle Eocene (Ordoñez, 1995; Witt *et al.*, 2019b). We can link the surface exposures of the Ancón Group to the parallel and subparallel seismic facies above unconformity U2 observed on the seismic profile of Figure 4.7-C. The major unconformity (U2) appears to be intensified near locally deformed structures of the underlying Azúcar Formation, which disrupt the parallelism of the reflections observed elsewhere and suggest syntectonic sedimentation in the basal part of the early-middle Eocene Ancón Group. The lateral changes of the sedimentary facies along the coastal cliffs in the Ancón area (Figure 4.5-E) and the chaotic and downlapping reflections onto unconformity U2 (Figure 4.7-C) may indicate localized syntectonic sedimentation for the area.

The basement-associated continuous reflections observed on Figure 4.7 show a general shallow position across the Ancón-Pacoa area, where exposures of the Late Cretaceous Santa Elena Formation have been reported previously (Figure 4.5-A, Jaillard *et al.* (1995)). Figure 4.5-B shows the Late Cretaceous Santa Elena Formation overlain unconformably by the Paleocene Azúcar Formation, the boundary of which is poorly defined on seismic profiles farther to the south on the offshore continuation of the Santa Elena High (Figure 4.8).

4.4.1.2 South of Playas

South of the Ancón-Pacoa area along the extension of the Santa Elena High, a series of structural highs are observed in several seismic profiles. Exploration boreholes Playas-1 and Golfo-1 targeted the folded structures as shown in Figure 4.4 and 6.8. The seismic profile in Figure 4.8-A shows a stratigraphic gap at the position of Playas-1, passing from thin Quaternary deposits into the Paleocene Azúcar Formation. Along the western limb of the Playas structure, a thick (~ 2 s TWT) series of parallel to sub-parallel reflections overlie the major unconformity U1 with an apparent progradation and thickening of this interval (Figure 4.8-A). This thick package is divided into two intervals: the lower one characterized by rapidly varying dipping reflections that are apparently affected by the underlying structure, and the upper interval defined by minor dip changes and more parallel reflections. Unconformity U2 is located between these two sequences (Figure 4.8). Both sequences conform the early-middle Eocene sequence, which is characterized by parallel to sub-parallel seismic facies (distorted around structural highs) and small normal faulting displacements.

Figure 4.8-B shows a NW-SE-oriented seismic section perpendicular to the seismic profile described previously, which shows the transition towards the Gulf of Guayaquil Basin by deepening of the Santa Elena High. The seismic reflections underlying the major unconformity (U1) are chaotic with varying dip directions, which were probably caused by significant deformation. In addition, a series of near vertical structures, which are interpreted as strike-slip faults (F1 and F2) and are oriented ENE-WSW, appears to segment the Santa Elena High possibly through lateral transfer fault-ramps (Figure 4.4-B). The apparent onshore continuation of these structures appears to coincide with outcropping structures; the vertically dipping layers of the Azúcar Formation (Figure 4.5-C) at the location of the Playas outcrop (see location in Figure 4.4) well appear to coincide with the possible northward extension of fault F1 (Figure 4.4). A comparable situation occurs with fault F2, which has similar characteristics to F1; it appears to extend onshore and coincides with the location of the Chanduy Hills (Figure 4.4). There is an apparent direct link between

the subsurface structures interpreted offshore and those observed onshore as shown in Figure 4.4.

4.4.2 Progreso Basin

A seismic inline (derived from a 3D cube; Figure 4.9) shows the underlying geological units of the Progreso Basin. Towards the NE, possible SW-dipping acoustic basement reflections represent undifferentiated Late Cretaceous volcanoclastic sequences of the Cayo to Guayaquil Formations. Overlying this unit, a series of high amplitude and steep reflections dipping in different directions (below unconformity U1/U2) may indicate increasing degrees of deformation towards the SW. Similar reflection packages with lower dip angles are present to the NE. These reflection packages are clearly truncated by an erosional surface (coincident with the U1/U2 unconformity), which may mark the limit of an active deformational phase during the Paleocene. Overlying the major and semi-regional unconformity (U1), steeply dipping reflections with chaotic to sub-parallel seismic characteristics are attributed to early - middle Eocene deposits of the Ancón Group. Towards the center of the basin, the reflections become sub-parallel and onlap onto the underlying Paleocene highly deformed area.

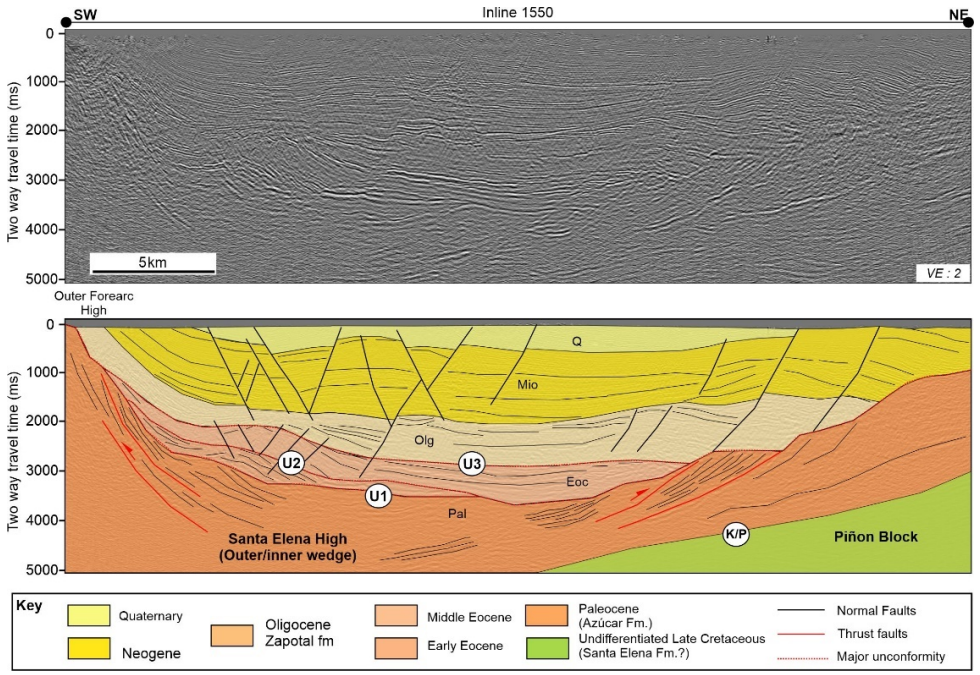

Figure 4.9: Time migrated seismic (Inline 1550) across the Progreso basin. Towards the SW, high dipping reflections coincide with outcropping sequences of the Azúcar Formation along the Estancia Hills (Figure 4.4). Unconformity U3 seems to mark the uplift and erosion of the Eocene Ancón Group, and deposition of the coarse sediments from the Oligocene Zapotal Fm, toward the Progreso basin.

Up-section, laterally varying high amplitude reflections may represent the Oligocene shallow-water to continental deposits of the Zapotal Formation, which are probably interbedded with silty deposits (low amplitude reflection seismic facies). The Zapotal Formation consists of coarse sediments derived from the emerged and subaerially exposed Santa Elena High (Figure 4.3).

Less deformed reflections characterized by extensional tectonics overlie the Oligocene series of the Zapotal Formation. This seismic stratigraphic unit corresponds to Miocene sequences that, based on outcrop exposures, are described as shallow marine deposits (Benitez, 1995). On the seismic profile shown in , this unit maintains a relatively equal thickness in the direction perpendicular to the basin axis and expands slightly southward (Benitez, 1995), suggesting a very low subsidence rate or deformation during the Miocene in this area.

4.4.3 Gulf of Guayaquil-Tumbes Basin

From east to west, the Gulf of Guayaquil-Tumbes Basin is defined by a NNW-dipping monoclinal structure and can be subdivided into a series of blocks bounded by approximately E-W-striking and north-dipping normal faults (Figure 4.10). The crustal fault blocks that apparently fragmented the Amotape-Tahuin massif, and subdivide the Tumbes from the Talara basin in NW Peru (Figure 4.1), appear to extend offshore as observed on Figure 4.10-A. Moving to the east, the offshore extension of the Jubones Fault is diffuse in the Gulf of Guayaquil, marking an apparent boundary between the Tumbes and Jambelí sub-basins. At the eastern offshore limit of the Jambelí area, a similar expression of these crustal lineaments is identified in Figure 4.10-A. This steep fault system seems to extend onshore into the Pallatanga Block (Figure 4.10-B) and may be genetically related to the tectonic process of block fragmentation due to shear lateral movements, as those reported in NW Peru.

Tight anticlinal structures separate the shallower Tumbes and Jambelí sub-basins from the deep Esperanza sub-basin (Figure 4.11-A). Towards the eastern limit of the Tumbes sub-basin, an antiform forms the Corvina structure, which is apparently affected by strike-slip movements (Figure 4.11-B). Industrial boreholes in the Corvina and Delfín hydrocarbon fields (Figure 4.11-B) reached late Oligocene/early Miocene sequences without penetrating the deeper high amplitude reflections, which may correspond to the underlying Eocene sequences of the Talara Basin (lower wedge according to Espurt *et al.* (2018)).

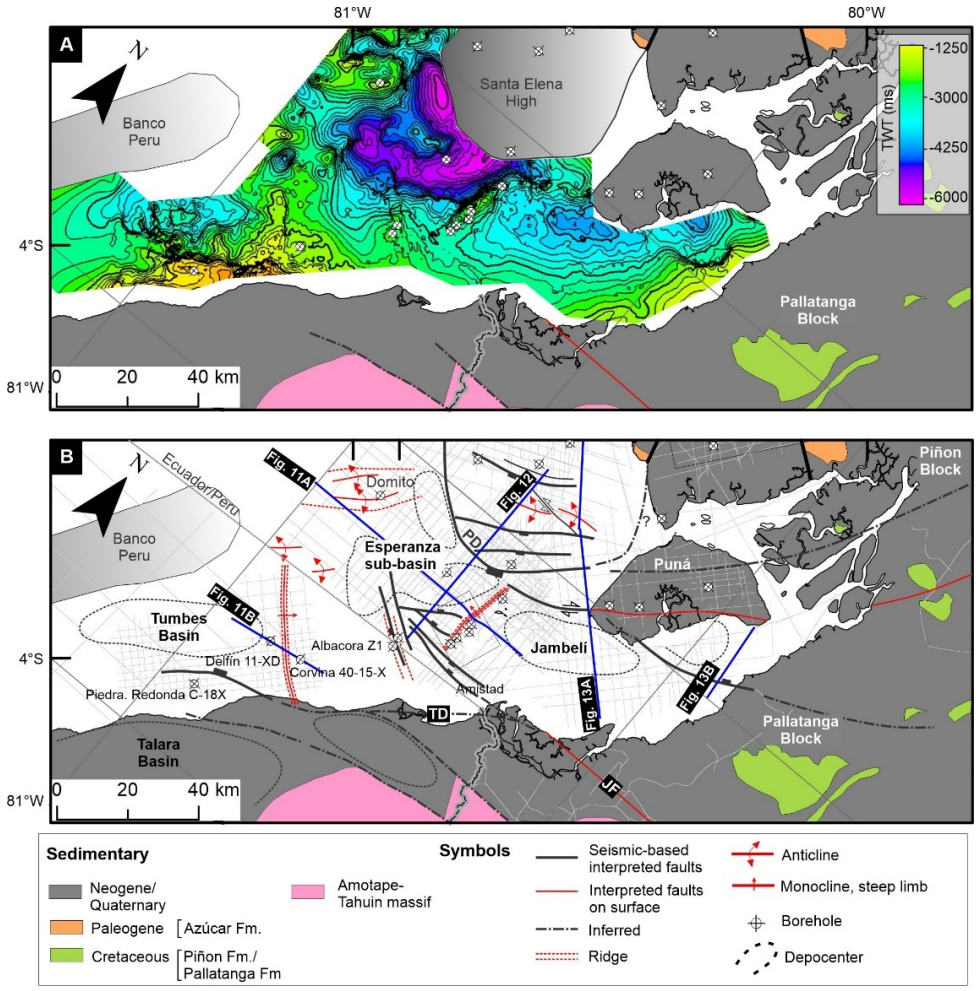

Figure 4.10: (a) Two-way travel time (TWT) map for the early-middle Miocene unconformity (U4). (b) Structural map showing the main lineaments identified from seismic profiles, and their inferred onshore continuation. Notice the local extend of the Santa Elena High with respect to the Gulf of Guayaquil-Tumbes basin. JF: Jubones fault; PD: Posorja detachment; TD: Tumbes detachment.

Farther to the east, the Amistad antiform structure defines the eastern boundary of the deepest Esperanza sub-basin. Figure 4.11-A shows the Amistad and Domito antiforms separating the deepest Esperanza sub-basin from the Jambelí sub-basin. There is apparent thinning of the late Miocene interval, although the seismic quality precludes studying this issue properly. A seismic profile across the deepest part of the Gulf of Guayaquil-Tumbes Basin shows a thick succession of Plio-Quaternary

sediments (Figure 4.12). The northern limit of these successions is defined by the Posorja detachment (Deniaud *et al.*, 1999; Witt and Bourgois, 2010) (Figure 4.12). Based on our seismic interpretation and the results from the Esperanza-1 borehole, we estimate a thick Quaternary sedimentary succession (at least 3.5 km to 5 km thick) in the main depocenter area, south of the Posorja detachment (Figure 4.12). This seismic profile shows an anticlinal structure characterized by crestal extension, oriented NE-SW, at the center of the Esperanza sub-basin. These extensional faults dipping towards the center of the structure are apparently layer-bounded along the top of the Late Miocene surface (in red), suggesting that the structure is not basement–controlled and thus formed during the Plio-Quaternary time interval (Figure 4.12).

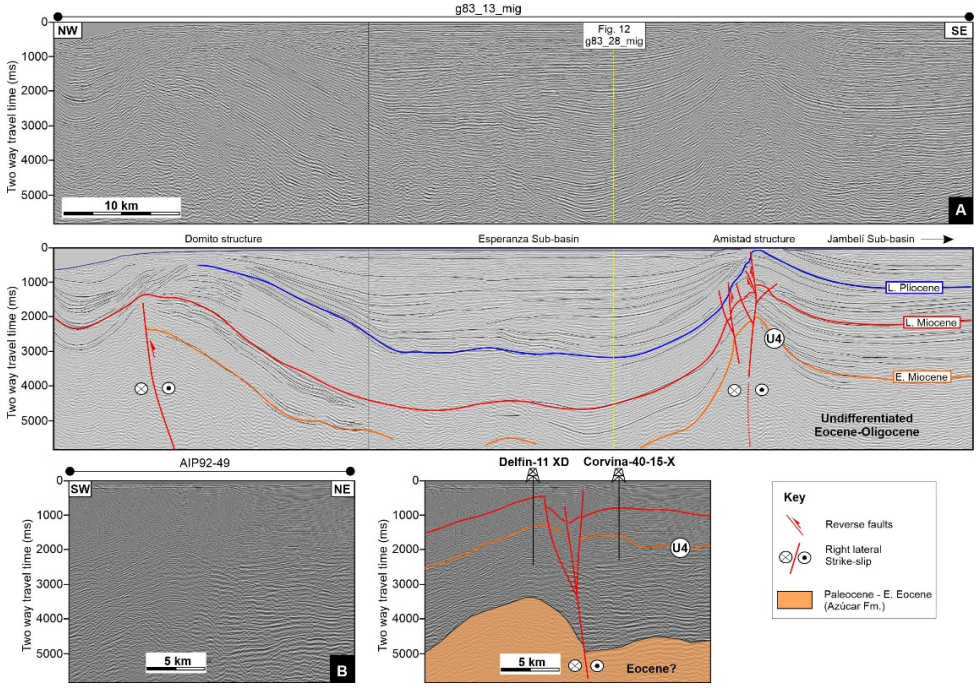

Figure 4.11: (a) Seismic profile across the Amistad and Domino antiforms showing the Esperanza sub-basin in between. (b) SW-NE profile across the Corvina structure, a structure likely to be connected to the Domito fold trend farther to the north (Figure 4.10)

An industrial borehole located in the Gulf of Guayaquil (Gulf of Guayaquil-1, Figure 4.12) penetrated early Miocene and possibly late Oligocene deposits. Although the seismic profile in Figure 4.12 shows deeper reflections, we suspect that those

reflections correspond to Oligocene and possibly older sequences. Following these deepest reflections from the location of Gulf of Guayaquil-1 towards the east, a significant pinch-out of the sequences is observed in Figure 4.13. This NW-SE-oriented seismic profile across Puná Island reveals early Miocene sequences above the inferred Late Cretaceous acoustic basement (characterized by chaotic and varying dipping directions reflections). To the north, the structural styles are different, transitioning from a monoclinal and north-dipping structure into a complex area with tightly folded structures similar to those observed in Figure 4.8-B. The series of thrust faults and shear zones interpreted in Figure 4.13 probably root at the transition between the Santa Elena High and crustal basement rocks attributed to the Pallatanga Block.

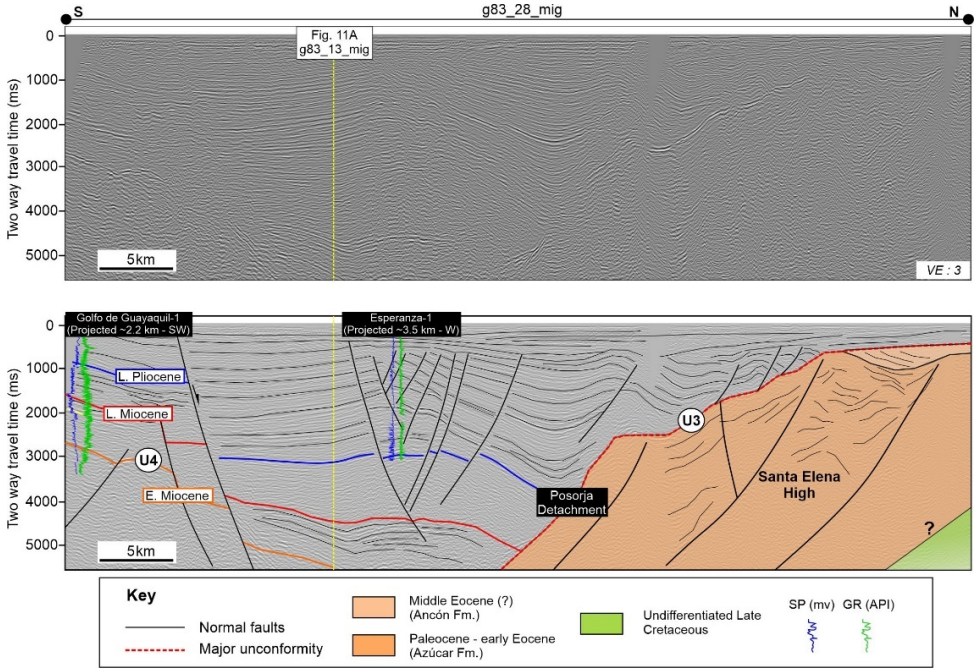

Figure 4.12: Interpreted seismic section across the Gulf of Guayaquil basin and the Santa Elena High. Towards the south, a series of Miocene sequences are penetrated by the Gulf of Guayaquil -1 borehole. At the center, the Esperanza sub basin, a depression mark by a thick succession of Plio - Quaternary sediments.

The surface expression of the tightly folded structure observed near the transition from the southern limit of the Santa Elena High and possibly northern extend of the Pallatanga Block is defined by the Puná Island, which is located a few kilometers to the east of the profile (Figure 4.10). A fault analysis at the surface on Puná Island characterized this deformation as a positive flower structure (Dumont *et al.*, 2005).

4.5 Discussion

Two major acoustic basement units were identified in this study: 1) a westward extension of the Pallatanga Block that interacts to the west with the Amotape-Tahuin massif, and 2) highly deformed Late Cretaceous sediments that accreted onto the CLIP crustal fragments. Both basement domains are characterized by different structural expressions and different seismic facies. This study defines at least four tectonostratigraphic units (Figure 4.3) overlying these inferred acoustic basement units: 1) a highly deformed Paleocene sequence, 2) an early to middle Eocene sedimentary succession that accumulated on the slope segment of unit 1; 3) an Oligocene to late Miocene sequence that was deposited in a transtensional setting in the Gulf of Guayaquil-Tumbes area and as a forearc sensu stricto setting in the Progreso Basin; and 4) a thick Plio-Quaternary sedimentary sequence within an subsiding depocenter (Esperanza sub-basin, Figure 4.2). Units 1 and 2 are mainly identified across the Santa Elena High, and units 3 and 4 are mainly identified in the Gulf of Guayaquil-Tumbes and Progreso area; unit 2 is also possibly present in the Gulf of Guayaquil-Tumbes area.

4.5.1 Possible effects on the margin following the arrival of the Caribbean Large Igneous Province (CLIP)

Following the results presented by Moresi *et al.* (2014) and Vogt and Gerya (2014) from numerical models of the dynamic of oceanic plateau accretion and subduction, we discuss the collision stage of the CLIP and its possible effects on the

margin that led to the following stages of margin instability (stage 2) to re-initiation of a stable subduction system (stage 3) discussed within the next section.

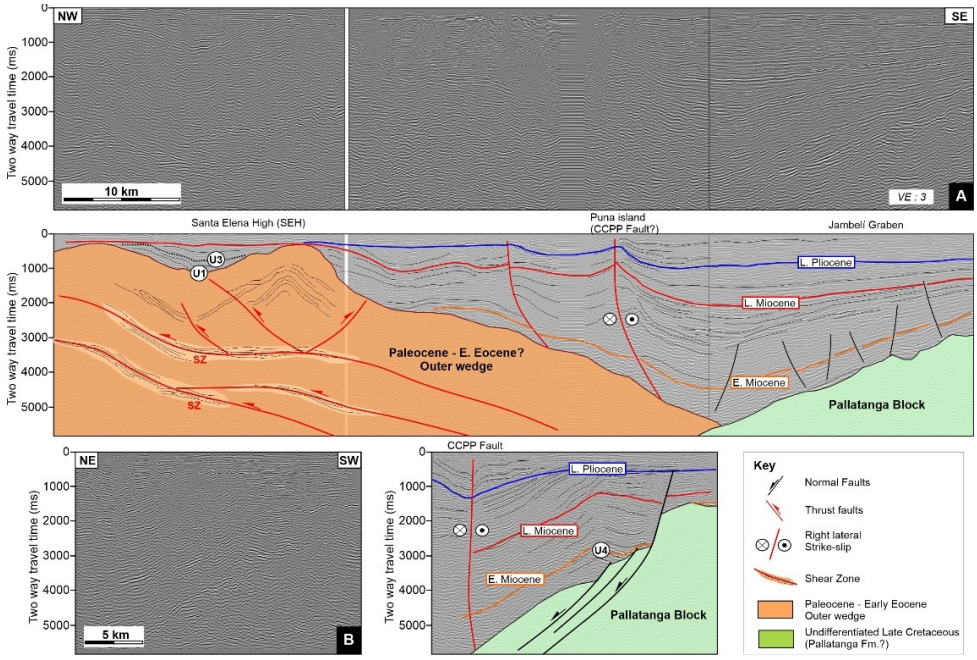

Figure 4.13: (a) NW-SE composite seismic profile across the Jambelí area and the Puna island, and into the southern part of Santa Elena High. Towards the south, a series of siliciclastic sequences of Miocene to Quaternary age are correlated and tied to boreholes located farther west. The sedimentary successions thin towards the south and apparently onlap onto Pallatanga Block. The series of high amplitude reflections associated to shear zones (SZ) may represent the high deformation related to the formation of the Santa Elena High. (b) Seismic section farther to the northeast, which shows the possibly displacement of the underlying Pallatanga block occurring since early-middle Miocene.

Thermochronological indications suggest significant cooling and exhumation rates along the Eastern Cordillera (Spikings *et al.*, 2010) at ca. ~73-70 Ma, which mark the onset of the collision of the Caribbean Large Igneous Province (CLIP) with the proto-NW South American margin in Ecuador (Vallejo *et al.*, 2009). However, south of the study area, Jaillard *et al.* (1999) reports that the Lancones Basin underwent a phase of deformation marked by compressional tectonism, dextral shear

movements, and erosion of the Amotape-Tahuin massif during Coniacian to Santonian times. This tectonic phase may represent an early interaction of the CLIP with the margin farther south in NW Peru. The transition from a stable and subsiding Lancones Basin during the late-early Cretaceous to an unstable forearc with trenchward uplift of the Amotape-Tahuin massif and block rotations (Mourier *et al.*, 1988) may be directly associated with an unstable plate configuration that was possibly created by the interaction between the leading edge/southern limit of the CLIP, the subducting oceanic Farallon Plate, and the NW South American Plate (Figure 4.14-A) in a scenario similar to those predicted by numerical modelling (Moresi *et al.*, 2014; Vogt and Gerya, 2014). If the plate instability was linked to the arrival of the CLIP at the margin, its collision may have occurred diachronically from Coniacian-Santonian times in NW Peru to Maastrichtian times in Ecuador. This indentation process of the CLIP to the NW South American margin may have exerted a torque on the overriding plate (Wallace *et al.*, 2005; Wallace *et al.*, 2009), which may have caused significant margin variations across the transform fault boundary between the southern limit of the CLIP and the NW South American plates. It has been recognized that oceanic plateau-trench collisions can strongly influence the shape of the trench; depending on the density of the plateau, this may cause significant trench retreat and advances in the region surrounding the plateau (Mason *et al.*, 2010).

Therefore, we propose that the CLIP played a key role in defining a tectonic framework for further Cenozoic development of the forearc region, including crustal fragmentation, block rotations, and backstop effects in both SW Ecuador and NW Peru.

4.5.2 From an unstable to a stable margin (Paleocene-Eocene stage)

Surface exposures of the Azúcar Formation provide evidence of the first sialic-derived deposits in SW Ecuador, after the accretion of the CLIP. The sedimentary facies, architectural elements, and paleocurrent indicators (Moreno, 1983; Benitez, 1995), along with heavy mineral provenance analysis, suggest a southern provenance of the Azúcar Formation, probably from the Amotape - Tahuin massif; this model was

recently corroborated by Witt *et al.* (2017). A problematic aspect of the Paleocene series is its local distribution. The Paleocene series (60-55 Ma) are observed neither north of the Chongón-Colonche Hills nor in NW Peru, where the oldest sedimentary rocks above the basement have ages of 54 - 53 Ma (Witt *et al.*, 2018). The depositional record and location of the Paleocene series with respect to the continental margin suggest a different configuration of the margin south of the Chongón-Colonche Hills, which was possibly controlled by the remnant of an ancient subduction system related to the previous deformation of the Santa Elena Formation (Figure 4.14-B).

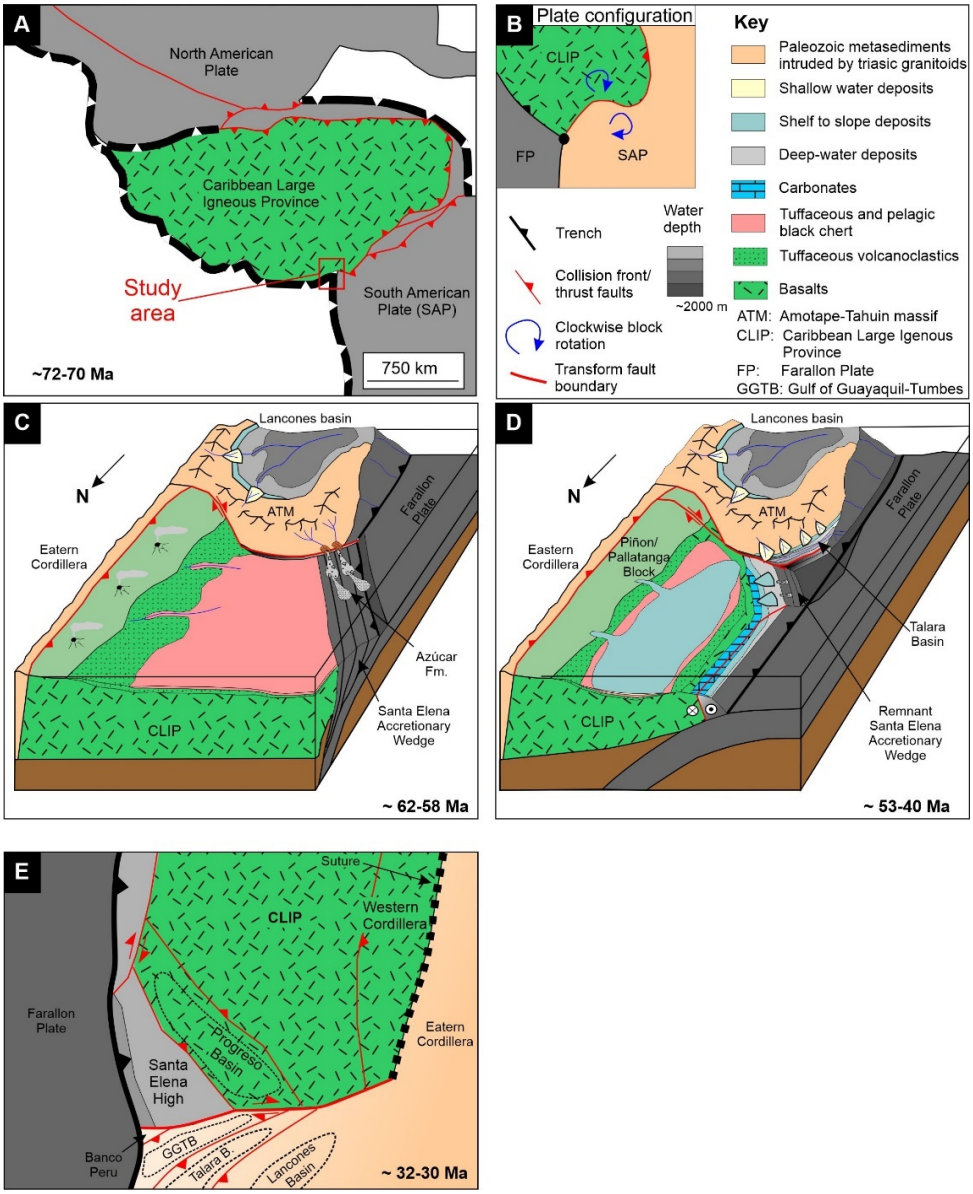

Figure 4.14: Series of sketches showing the proposed tectonic evolution of SW Ecuador and NW Peru. (a) a possible scenario of accretion of the CLIP against the South American Plate, showing the possible location of a triple plate junction (modified after Boschman *et al.*, 2014). (b) deposition of the Paleocene Azúcar Formation, over a Late Cretaceous accretionary wedge. (c) re-establishment of a stable subduction system with trench retreat and development of the Talara basin in NW Peru. (d) simplified sketch highlighting the spatial relationship of the main tectonic elements post-accretionary phase at 32-30 Ma. Notice the development of the Progreso basin limited to the west by the Santa Elena High.

Although difficult to define in seismic data and on the field, the vergence of the main structures is most likely to the ENE, although local structures, such as those in the Playas area, may be related to secondary structures like accommodation faults or oblique ramps. Furthermore, our integration of borehole, seismic, and outcrop data throughout the Santa Elena High shows that the Azúcar Formation grades to the north into fine and deeper water facies that apparently pinch out across the Pacoa area (Figure 4.6).

The relatively local character of the deformed series of the Azúcar Formation (approx. 100-150 km in extent) prevents defining the unit as part of a regional accretionary prism; instead, a more local model is proposed in which the Azúcar Formation was deposited across a margin offset resulting from the instability of a triple plate junction (Figure 4.14-B).

Subsequent basin reconfiguration and forearc uplift within a stable and re-established margin may have taken place following the accretion of remnants from the ancient Santa Elena accretionary wedge and overlying Paleocene deposits, which is currently called the Santa Elena High. Along the Chongón Colonche Hills and farther north, early to middle Eocene carbonaceous deposits of the San Mateo Formation and equivalents were unconformably deposited on Late Cretaceous volcanoclastic deposits of the Cayo Formation (Jaillard *et al.*, 1995), defining the limit of the Paleocene depocenter and a major shift in the sediment source at this time (Figure 4.14-C).

South of the Chongón - Colonche Hills, upper slope to deepwater slope sandstones of the Ancón Group overlie the highly deformed Azúcar Formation or sit directly on the Late Cretaceous Santa Elena Formation. The Ancón Group was deposited unconformably across a combined late Paleocene-early Eocene surface (U2, Figure 4.6). A clear structural and stratigraphic change is observed across the boundary between the Azúcar Formation and the Ancón Group, as revealed by outcrop and seismic data (Figure 4.5 and 4.8). This change has been proposed to be related to the emergence of the Santa Elena High following the collision of the Cayo Arc during the Late Paleocene (Jaillard *et al.*, 1995). However, the Cayo Arc had

already accreted onto the margin prior to the deposition of the Azúcar Formation (Van Melle *et al.*, 2008). Furthermore, both the basal part of the Ancón Group and the Azúcar Formations are characterized by deep water facies, precluding the idea of sub-aerial exposure of the late Paleocene Azúcar Formation. The Ancón Group is marked by extensional deformation that is most likely related to gravitational instability. Thus, we propose that the deformation of the Azúcar Formation is related to an accretionary event, very likely through reactivation of the ancient Santa Elena accretionary wedge (Figure 4.14-B), during late Paleocene-early Eocene with quiescence during the deposition of the middle Eocene Ancón Group (Figure 4.14-C), which represents the switch from a trench jump (stage 2) to the re-initiation of a stable subduction system (stage 3) farther to the west. This event is correlated with the end of the cooling and exhumation phase events recorded in the Amotape-Tahuin massif and is highly coincident with the end of sedimentation of the Azúcar Formation at ~55 Ma (Witt *et al.*, 2018).

4.5.3 Preservation of the Santa Elena accretionary wedge in SW Ecuador

The underlying mechanism that led to the localization of the thick wedge related to the Azúcar Formation may be related to the resulting margin configuration after the collision and indentation of the CLIP (Figure 4.14), possibly causing a tear-faulted subducting slab that was able to accommodate thick Paleocene sedimentary sequences. Similar observations of a deepening and thickening wedge oblique to the convergence direction that was controlled by a physical boundary at one edge (in our case, this boundary is represented by the Amotape- Tahuin massif) have been reported in the Sumatra, southern Ryukyu, and Hikurangi trenches (Heuret *et al.*, 2012; Malatesta *et al.*, 2013).

Furthermore, the location of the Santa Elena High compared to the autochthonous Amotape-Tahuin massif and the allochthonous Piñon Block cannot be disregarded. We suggest that variations in the material strengths of the different crustal blocks involved in the region may have played a significant role in the location

and orientation of the Santa Elena High and in the formation of the Progreso Basin. Therefore, we propose that the Piñon Block may have acted as a backstop since the early Paleocene under an oblique subduction regime. The interaction between the ancient Santa Elena accretionary wedge and the Piñon Block resulted in the formation of an outer wedge, known as the Santa Elena High. The early outer wedge configuration may have developed a west to northwest-dipping slope along the seaward margin, where gravity-driven sediments from the middle Eocene Ancón Group were deposited over unconformity U2, as observed in seismic profiles and the well correlation presented within this study (Figure 4.6). During the Oligocene, a second major uplift of the accretionary prism may have formed the restricted Progreso forearc basin, which is indicated by the deposition of the immature sediments of the Zapotal Formation along the La Cruz Fault (Witt *et al.*, 2019b). This continuous uplift of the Santa Elena High, which played a key role in the forearc basin evolution, may have been possible due to the inherited margin configuration, which allowed the accumulation of significant quantities of sediments that prevented an erosional regime of subduction beneath the Santa Elena High and instead created a local outer forearc high since the Oligocene.

4.5.4 Development of the Progreso and Gulf of Guayaquil – Tumbes basins

Following the deposition of the middle Eocene Ancón Group, a major uplift of the entire forearc region occurred in the Oligocene. This is supported by the coarse-grained and immature sediments of the Zapotal Formation that were deposited at 32-30 Ma (Figure 4.3) (Witt *et al.*, 2019b) along the axis of the restricted Progreso Basin. Similar conditions occurred in the Tumbes and Talara depocenters, where coarse-grained fluvio-deltaic Oligocene sequences have been identified in the field and in the subsurface (Mancora Formation; Figure 4.3) (Fernández *et al.*, 2005; Espurt *et al.*, 2018). The deposition of continental coarse-grained sediments marked the first major subaerial unconformity in the region, which is defined in this study as the U3 unconformity (Figure 4.6 and 4.8). This may represent the principal evidence of a transition from trench to forearc deposition due to the development of outer forearc

highs, such as the Santa Elena High in SW Ecuador and possibly Banco Peru in NW Peru.

The forearc region within the study area is underlain by different crustal units of oceanic and continental affinities; thus, a focus on identifying the suture appears to be critical. The quasi-perpendicular relationship between the orientations of the Progreso and Gulf of Guayaquil-Tumbes basin axes (Figure 4.14-D) suggests that different underlying processes controlled their structural development.

The suture between the remnants of the CLIP and the South American Plate is well documented along the Western and Eastern Cordilleras (Alvarado *et al.*, 2016) but has been poorly constrained in the Gulf of Guayaquil. Its location is still uncertain and debated (Aizprua *et al.*, 2017). Nevertheless, a unique vestige of the contact between these two crustal blocks occurs at the Jubones Fault (Figure 4.1 and 4.10), which is the closest location of the suture to the offshore Gulf of Guayaquil. The offshore continuation of this structure appears to be deeply buried and below the depth of investigation of the current seismic profiles. Nevertheless, our integration across the Jambelí, Gulf of Guayaquil and NW Peru () allowed us to point out three key elements that may support the location of the suture across the Gulf of Guayaquil: 1) a northwest-dipping surface, which may represent the offshore continuation of the oceanic crustal rocks of the Pallatanga Block (age equivalent to the Piñon Block) north of the Jubones Fault (Figure 4.13); 2) shallow expressions of potentially reactivated or basement-controlled normal faults (potentially along the suture) with diffuse patterns and E-W orientations (Figure 4.10); and 3) continental crustal fault-bounded blocks observed at the surface south of the Jubones Fault, which delimit the forearc depocenters in NW Peru (Figure 4.1 and 4.10).

Our model proposes that during the initial stage of forearc development, the Tumbes and Progreso basins formed an embayment with a sea inlet possibly located between the Banco Peru and the Santa Elena High, an area which is coincident with the change in strike of these two structural highs and may coincide with the position of the transform boundary (Figure 4.14-D). The Jubones Fault at this stage is inferred

to have played a significant role in the development of the forearc, possibly by acting as a major conduit of sediments towards the basin.

A second stage of forearc basin development is inferred to have taken place by the late early to middle Miocene (~ 15 Ma) and may represent the first vestige of the opening of the Gulf of Guayaquil. Seismic profiles on the eastern side of the Tumbes sub-basin and across the Jambelí sub-basin show two key elements: 1) an erosional event along the eastern border of the Tumbes Basin (unconformity U4, Figure 4.11-B), which may extend farther to the southeast and link to the inferred Tumbes detachment (Figure 4.10), and 2) a possible fault jump from the Jubones Fault to the Jambelí detachment via further fragmentation of the underlying Pallatanga crustal block (Figure 4.10 and 4.13-B), producing the local late-early Miocene erosion (U4) (Figure 4.10-A). Our analysis also suggests that the Santa Elena High outer wedge may have controlled the development of both the Progreso and Gulf of Guayaquil basins through the development of an outer forearc high, which generated restricted conditions, especially in the Progreso Basin (32-30 Ma, Witt *et al.*, 2019b), and acted as the northern bounding block for the Gulf of Guayaquil area (Figure 4.12 and 4.13). An interaction between the Santa Elena High and the north-dipping successions overlying the Pallatanga Block may have resulted in local transpressional movements, which possibly gave rise to the development of some of the ridges and the Puná Island observed in Figure 4.10. An interaction that may correspond to an initial stage of tectonic escape of the North Andean Sliver.

4.6 Conclusions

In this study, we used an integrated and multidisciplinary approach with different scales of observations to propose an updated tectonic model for SW Ecuador and NW Peru. The structural interpretation linking onshore and offshore structures allowed us to delineate an ancient and preserved Late Cretaceous-Paleocene accretionary wedge that may have formed at a concave margin at the trailing edge of the Caribbean Large Igneous Province along the Northern Andes (Figure 4.14).

The process that led to a concave margin during the Late Cretaceous is uncertain, but we propose that the southern limit of the CLIP may have created an unstable triple plate junction with the oceanic Farallon Plate and the South American Plate. Plate instability may have resulted in a tearing of the Piñon Block creating a localized depocenter, NW of the Amotape-Tahuin massif, where deposition of the Paleocene Azúcar Formation overlying the Santa Elena accretionary wedge took place. Plate stability may have been reached by the end of the Eocene, through translation of the junction farther north into Colombia. A movement that is possibly reflected in NW Peru by sequential trench retreat in both NW Peru and SW Ecuador. This is in agreement with trench retreat and seaward advance of the forearc depocenters proposed in NW Peru by Espurt *et al.* (2018).

The accretion and preservation of an ancient accretionary wedge along the southern trailing edge of the CLIP, post re-establishment of a stable subduction system, seems to have controlled the post-accretionary forearc basin configuration in the region. Further oblique subduction and strike-slip fault movements along the western edge of the Santa Elena High outer wedge may have taken place, controlling the development of the forearc region. These processes may have led to a strong interaction between the Santa Elena High outer wedge and the crustal sliver of the CLIP, this last one acting as a backstop, and resulting on the development of a local sensu stricto forearc basin (Progreso Basin) controlled by development of a local outer forearc high.

The results from this study may represent a natural example of recent numerical models of the dynamic of allochthonous terrane accretion along continental margins (Moresi *et al.*, 2014; Vogt and Gerya, 2014). Therefore, we propose that the accretion of oceanic plateaus may have had a great impact on the early margin configuration of ancient forearc basins, such as in SW Ecuador and NW Peru, where we found the development of localized but genetically related forearc depocenters.

Acknowledgments

The authors wish to thank Petroamazonas EP (Quito, Ecuador) for kindly providing all of the subsurface data used in this study. We are particularly grateful to Marco Rivadeneira for encouraging this study and to the exploration team from Petroamazonas for rewarding discussions about the subsurface geology of the study area. We are in debt to Galo Montenegro for his insights into the geology of SW Ecuador and for fruitful discussions in the field. Associate Editor Federico Rossetti; Reviewers Adrian Pfiffner, James Kellogg and an anonymous referee, and Journal Editor John Geissman are acknowledged for their thorough review and constructive comments. This research was conducted as part of a Ph.D. thesis by C. Aizprua at the Norwegian University of Sciences and Technology (NTNU) jointly with the University of Lille in France and was supported by funds from Statoil's AKADEMIA agreement (Norway). Schlumberger is thanked for provision of Petrel® for seismic interpretation. The data used for this study are accessible at the NTNU Open Research data repository (https://doi.org/10.18710/BYZIZX).

Chapter 5

Stratigraphy controlled by the local development of an outer-forearc-high: Progreso basin

*The content of this chapter is published in: C. Witt, J.Y. Reynaud, D. Barba, M. Poujol, **C. Aizprua**, M. Rivadeneira, C. Amberg (2019), From accretion to forearc basin initiation: The case of SW Ecuador, Northern Andes, Sedimentary Geology, 379, 138-157.*

The SW of Ecuador offers a great opportunity to study the long-term behavior of an almost entire forearc system, from the external accretionary prism to the landward limit of the forearc basin. A combination of field observations, LA-ICP-MS U-Pb dating on zircon and interpretation of different vintages of unpublished industrial seismic records are used to study the evolution of the forearc system of SW Ecuador including the accretionary prism and the forearc depocenter. The youngest dates, obtained from U-Pb dating on zircon grains believed to be derived from the arc, define the best estimate for the age of sedimentation and permit a clear description of the temporal and spatial evolution of the accretionary, post accretionary and forearc basin series between 60 Ma and 10 Ma. This reinforces the idea that forearc sediments can be dated by U-Pb on zircon provided that the arc is active at the moment of sedimentation. The Azúcar Formation reflects the accretion of SW Ecuador against the South American continental margin from 61 Ma to 55 Ma. This event is post-dated by the formation of an accretionary prism which may have started at circa 55 Ma. Deformation of the accretionary prism may have been less active during

sedimentation of the Ancón Group from ~54 Ma (?) to ~40 Ma which shows evidence of normal faulting and other extensional processes. The transition from the Azúcar Formation to the Ancón Group is marked by a significant decrease of the topographic profile, which in turn resulted in sedimentary series that shallow upwards. The forearc basin sensu strictu develops coevally with the uplift of the outer forearc high (Estancia Hills) and the sedimentation of the Zapotal Formation at 32–30 Ma; the latest marking a significant differentia- tion in the sedimentary style of the area to shallower and even continental environments. From 30 Ma to 10 Ma the forearc basin was defined by shallow water deposits, progressively influenced by tidal dynamics, most likely related to a protected triangular bay symbolizing the shape of the forearc basin. Evidence presented here suggests the existence of a stable outer forearc high limiting the forearc depocenter for at least 20 My and creating, at least in part, the accommodation necessary for an ~3 km thick forearc sedimentary package. The architecture of SW Ecuador is typical of a forearc basin setting including an accretionary prism and an outer forearc high such as those observed in the Kumano (Japan) and the Coast Range and Great Valley basins (USA). The Estancia Hills may correspond to one of the best-preserved exposures of an ancient outer forearc high worldwide.

5.1 Introduction

During the recent years, our knowledge about how forearc areas evolve trough time has significantly increased thanks to thoughtful examinations of their tectonic and sedimentary evolution (e.g Noda and TuZino, 2007; Takano *et al.*, 2013; Moore *et al.*, 2015). However, because forearc areas show a great variability (including their accretion or erosional related subduction regime) and a complex history of subsidence very often partitioned in space and time (Xie and Heller, 2009; Noda, 2016), it is still noticeable that the knowledge about how forearc basins evolve through time in the wake of the subduction system, especially in long-lived subduction systems, remains poor. Indeed, variations in convergence kinematics (velocity, direction and slab angle), variations of the overburden resulting from erosion of the arc, slab roll-back, subduction-erosion and sediment thickness at the trench, time since initiation of subduction and tectonic escape along partitioned systems are just some of the mechanisms believed to control the forearc basin evolution (Jarrard, 1986; Moxon and Graham, 1987; Einsele *et al.*, 1994; Clift and Vannucchi, 2004; Melnick and Echtler, 2006; Clift and Hartley, 2007; Mitchell *et al.*, 2010; Takano *et al.*, 2013; Moore *et al.*, 2015). The forearc basins might be a clue to hierarchize these varied tectonic controls, but their unravelling is still a challenge because most of them have uncomplete stratigraphic records. Moreover, because tectonic episodes (especially uplift) in the forearc seem to be very short in duration (see review of Pedoja *et al.*, 2014) the record of deformation in forearc basins is often difficult to understand. Consequently, some forearc basins have been interpreted as evolving independently from the kinematics of subduction (Clift and Hartley, 2007; Takano *et al.*, 2013), whereas others may be strongly coupled to plate kinematics (e.g Daly, 1989; Regalla *et al.*, 2013).

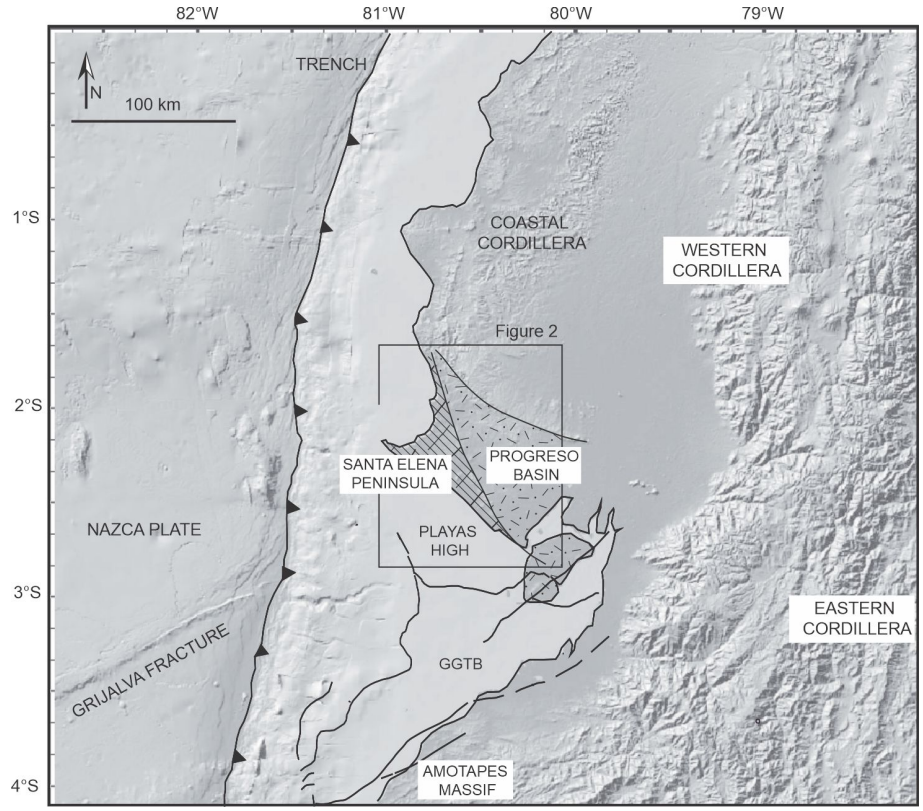

Figure 5.1: Geodynamic sketch of the Andes of Central-South Ecuador and North Peru including the forearc area. The rectangle shows location of the studied zone shown in detail in Figure 5.2. GGTB, Gulf of Guayaquil-Tumbes Basin. Topography and bathymetry from GeomapAPP. (http://www.geomapapp.org/). Offshore structures in the GGTB compiled from Witt and Bourgois (2010).

It is beyond doubt that a clear definition of basin evolution depends on how accurate the chronology of sediment deposition is defined. Obtaining depositional ages by using U-Pb age spectra of zircon grains acquired from volcanoclastic sediments depends mainly on the presence of an active arc at the moment of sedimentation (Cawood *et al.*, 2012; Gehrels, 2014). The Ecuadorian forearc is an excellent candidate to unravel the complicated structuring of forearc areas in the realm of the arc-trench system. Indeed, the

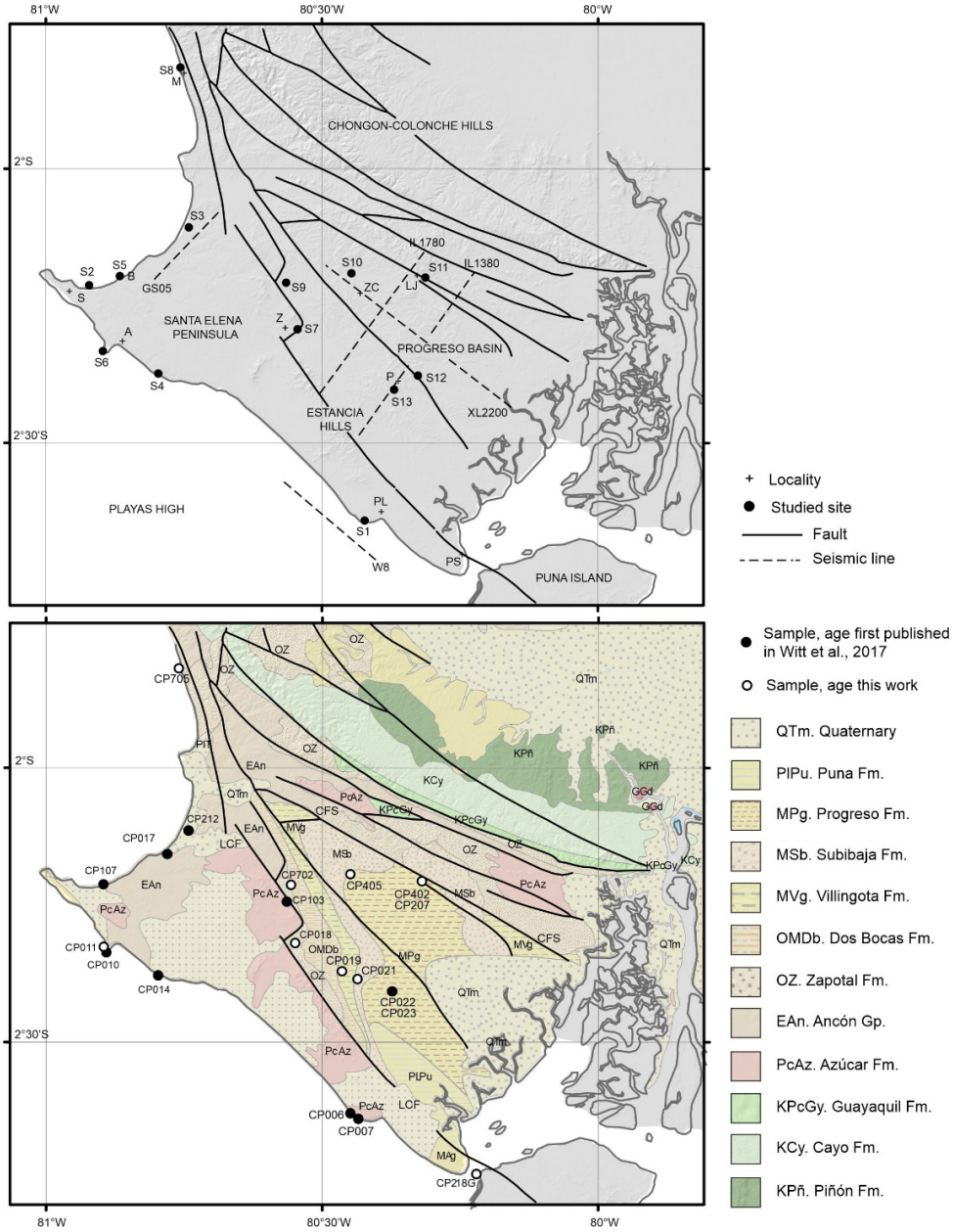

Figure 5.2: The SW Ecuadorian forearc. A) SRTM-derived topography showing geologic features, main localities (crosses) and sites discussed in the text (black dots). CFS, Carrizales Fault System; LCF, La Cruz Fault. Localities abbreviations are as follows: A, Ancón; B, Ballenita; LJ, Las Juntas; M, Montañita; P, Progreso; PL, Playas; PS, Posorja; S, Salinas; Z, Zacachun. B) Geological map modified from the 2017 1:1000000 Inigemm Map including sample location. Black circles are U-Pb zircon ages first published in Witt et al. (2017). White circles represent new analysis.

SW Ecuadorian margin shows long-lived forearc sedimentation that evolved conjointly with an active volcanic arc since at least the Early Paleocene (Hall and Calle, 1982; Benitez, 1995; Jaillard et al., 1995; Vallejo et al., 2009; Schutte et al., 2010). Furthermore, the SW of Ecuador represents a dichotomy in the shared vision of what forearc areas represent, since it shows high sediment preservation, both the accretionary prism and the forearc basin outcrop and, finally, it has been studied, for oil and gas exploration purposes, by the industry. To examine the evolution of the forearc system, we have analysed in detail the sedimentological features of the Paleocene - Late Miocene forearc infilling in SW Ecuador. Chrono- logic insights are obtained from in situ dating of zircon by LA-ICP-MS.

The combination of sedimentological observations and U-Pb dating allow clarifying the chronostratigraphic evolution of SW Ecuador, including the temporal evolution of depositional environments and forearc basin initiation. Seismic records are used to define the regional architecture of the area, including the relationships between a newly defined outer forearc high (OFH) and the forearc basin depocenter. The evolution of the SW Ecuadorian margin resembles that of better studied forearc systems in the Nankai trough (Japan) and in the Great Valley basin (USA). Thus, the SW Ecuadorian margin offers an exceptional opportunity to study an outcropping OFH, a feature whose importance in forearc basin development has gained relevance in recent years (Clift and Hartley, 2007; Takano et al., 2013; Moore et al., 2015; Noda, 2016).

5.2 Forearc development during the Cenozoic

The forearc of SW Ecuador (Figure 5.1 and 5.2) is central to the debate about the evolution of the southern part of the Northern Andes as it records the oceanic subduction of the Nazca plate, the accretion of allochthonous terranes, Paleogene and Neogene arc magmatism, exhumation of the coastal area and the tectonic escape of the North Andean block. The SW Ecuadorian forearc was formed after the accretion of oceanic terranes with plume and/or island arc affinity such as the Pallatanga and Piñon terranes and their related volcanoclastic covers (Feininger, 1987; Hughes and

Pilatasig, 2002; Kerr et al., 2002; Jaillard et al., 2009; Vallejo et al., 2009). There is a major debate about the definition of the nature, number and timing of accretions that led to crust addition and the construction of the Western Cordillera in Ecuador. For some authors, a single Caribbean type accretion may have occurred between 75 and 65 Ma (Vallejo et al., 2009), whereas other hypotheses suggest multi-episodic oceanic accretions (some of them with no Caribbean affinities) at ~75 Ma, ~68 Ma, and ~58 Ma (Feininger, 1987; Hughes and Pilatasig, 2002; Kerr et al., 2002; Vallejo et al., 2006; Jaillard et al., 2009). The oceanic basement has been dated at ~90 Ma close to the northern border of the studied zone (Luzieux et al., 2006). In this context, forearc basins most likely evolved in relation with an oceanic crust impinged to the South American margin and which may have acted, at least in part, as an undeformable backstop (Aizprua et al., 2018).

Major tectonic processes (some of them interrelated or competitive) affecting the continental margin of southern Ecuador during the Cenozoic include: 1) Breakup of the Farallon plate at ~25 Ma (Handschumacher; Hey, 1977); 2) Subduction of ocean plate asperities, such as the Carnegie Ridge and the Grijalva Fracture System (Collot et al., 2002; Sage et al., 2006; Michaud et al., 2009); 3) Tectonic escape of the North Andean block and related formation of the Gulf of Guayaquil-Tumbes basin (Witt *et al.*, 2006; Witt and Bourgois, 2010) and 4) A subduction-erosion regime working at the plates interface (Bourgois et al., 2007). All of these processes resulted in basin formation or disruption. Thus, the variable localisation and timing of these processes lead to the superimposition of basin depocenters, a process currently poorly understood for the Andean forearc.

The sedimentary record of SW Ecuador starts during the Late Cretaceous with the deep-water volcaniclastic deposits of the Cayo, Santa Elena and Guayaquil Formations (Figure 5.3) in an island arc setting. It is believed that afterwards, SW Ecuador was accreted at ~58 Ma, a process resulting in the quartz-rich turbiditic deposits of the Azúcar Formation, which constitutes the infilling of an early trench slope basin (Benitez, 1995; Jaillard et al., 1995). After accretion, the forearc of SW Ecuador may have been under extension during the sedimentation of the Ancón

Group. It is suggested that compression was then renewed during the Eocene (Jaillard et al., 1995; Jaillard et al., 1997), although this deformation period remains unconstrained. The Paleocene and Eocene series crop out along the Santa Elena Peninsula and along its offshore extension (the Playas High; Figure 5.2A). The modern forearc started during the Oligocene with the onset of the Progreso basin, a fault-bordered triangular-shaped depocenter located between the Chongón-Colonche hills and the Estancia hills (Figure 5.2) and mainly exposing in ascending order the Zapotal, Villingota, Dos Bocas, Subibaja and Progreso Formations (Figure 5.3). The forearc sediments show a shoaling trend trough time which has been attributed to several geodynamic factors, such as the kinematics of the subduction system (including accretions) and the subduction of the Carnegie ridge (Benitez, 1995; Jaillard et al., 1995). One of the most accepted models suggests that the extensional deformation leading to the formation of the Progreso basin (mainly controlled by the Carrizal Fault; Figure 5.2) resulted from the northwards displacement of a forearc sliver (Benitez, 1995). The entire evolution of the forearc is believed to be strongly correlated with plate kinematics (Daly, 1989). Furthermore, uplift is active in several zones of the Peninsula and marked by the presence of Pleistocene marine terraces (Pedoja et al., 2006).

U-Pb ages younger than 100 Ma obtained from detrital zircon grains show that the forearc sediments of SW Ecuador were mainly sourced from the Western (Occidental) Cordillera (Ecuador and Peru), which acted as a topographic barrier from ~60 Ma to ~10 Ma and prevented sourcing from inner (eastwards) sections of the Andean Cordillera (Witt et al., 2017). The input of older zircon grains (i.e. older than 100 Ma) is related to the Amotapes Massif or similar terranes. The onset of exhumation of such a topographic barrier is most likely coeval with the early accretion of oceanic terranes, which took place between 75 and 65 Ma (Jaillard et al., 2009; Vallejo et al., 2009) although evidence for the accretion in the forearc is, at least in part, younger and dated at ~60–55 Ma (Benitez, 1995; Jaillard et al., 1995, Jaillard et al., 1997; this work).

5.3 Sampling and methods

The chronologic data set used in this work consists of ten new sets of U-Pb detrital zircon analyses and ten sets of previously published analyses (Witt et al., 2017) for which the younger age spectra (e.g. <100 Ma) were not previously examined. The twenty samples were collected from the Paleocene to the Upper Miocene sedimentary outcrops in the Peninsula de Santa Elena and Progreso basin (Figure 5.2). Sampled localities are shown in Figure 5.2 and listed in Table 5-1. Samples are tuffs, reworked tuffs and medium-grained sandstones with evidence of significant volcanic components. Detailed sedimentary constraints come from field observations, whereas tectonic constraints were obtained from field observations and unpublished industrial seismic records. 2D lines in the Peninsula area were obtained during the eighties whereas seismic lines along the Progreso basin were derived from a 3D seismic cube obtained in 2010. More details are provided in the seismic interpretation section.

U-Pb geochronology of zircon grains was conducted by in-situ laser ablation inductively coupled plasma mass spectrometry (LA-ICPMS) at Géosciences Rennes using an ESI NWR193UC Excimer laser coupled to a quadrupole Agilent 7700x ICP-MS equipped with a dual pumping system to enhance sensitivity (Paquette et al., 2014). Concordia ages and diagrams were generated using Isoplot/Ex (Ludwig, 2012). Follow- ing the recommendations of Faure and Mensing (2005) and Talavera *et al.* (2012), the % of concordance in our study are calculated as % Conc = Age(206Pb/238U) × 100/Age(207Pb/235U) for apparent ages younger than 1Ga and as %Conc = Age(207Pb/235U) × 100/Age (207Pb/206Pb) for apparent ages older than 1 Ga. Dates are displayed ei- ther in Tera-Wasserburg concordia diagrams or histograms. Weighted average 206Pb/238U dates for the younger clusters are shown in the sup- plementary materials. All errors given in Table 1 are provided at 1 sigma. In all the diagrams (concordia and weighted average) the data are re- ported at 2 sigma as well as when ages are calculated. When a concordia age (as of Ludwig, 1998) is calculated, the MSWD value is reported as “concordance + equivalence”. Further

information on the protocol used in this work can be found in Manzotti *et al.* (2015), Witt et al. (2017) and in the Complementary Table 1.

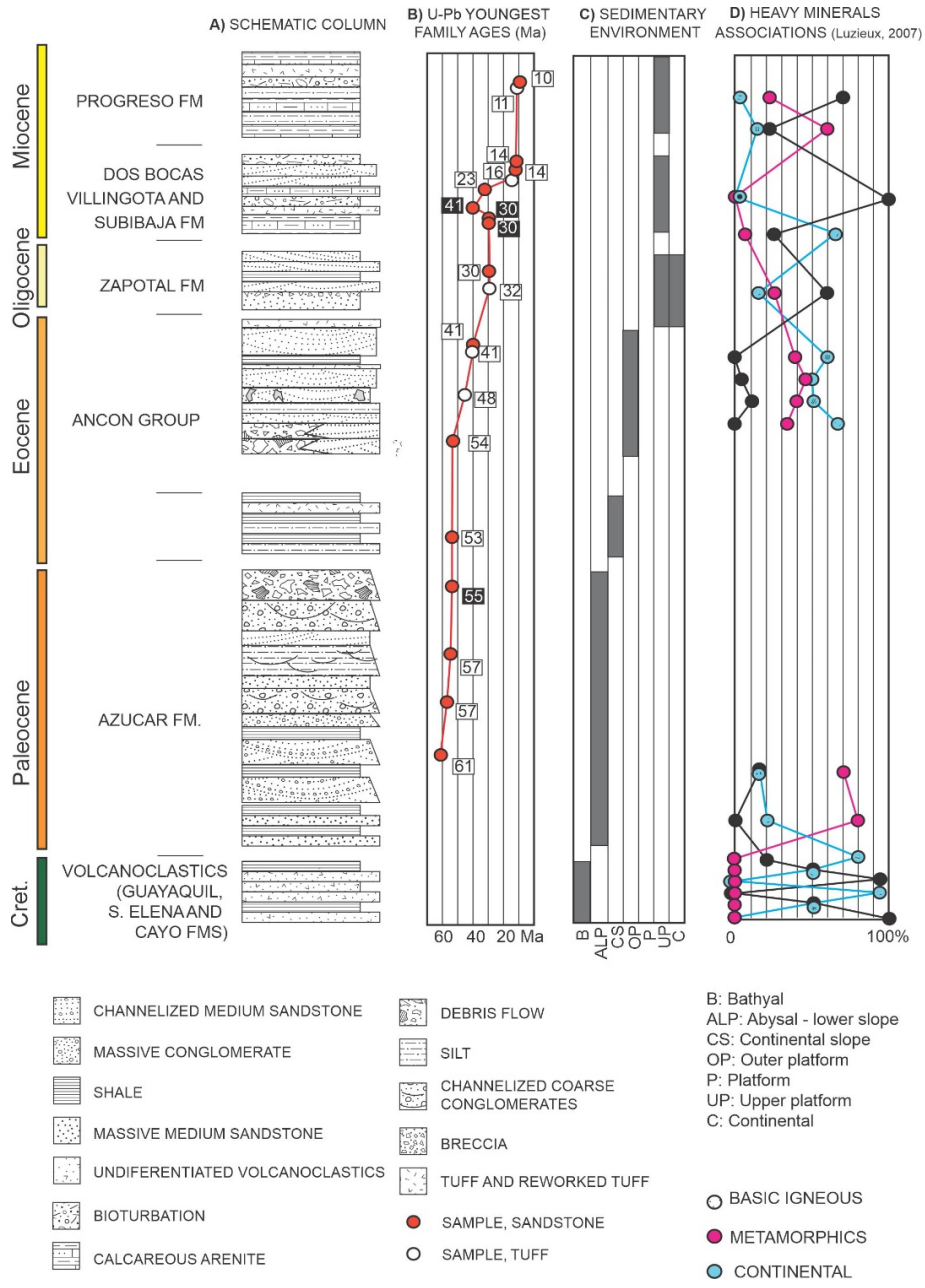

Figure 5.3: Stratigraphy, age constraints and sediment depositional environment in SW Ecuador. A) Schematic stratigraphic column showing main litho-tectonic units. Thickness of the column does not reflect true sediment thickness. B) U-Pb zircon youngest ages for all

samples shown on Figure 5.2B; including those published in Witt et al. (2017). Ages in white rectangles represent the age of sedimentation. Black rectangles are ages most likely coming from recycled rocks or zircons. C) Sedimentary environment at time of deposition obtained from paleontological records (Ordoñez et al., 2006). Abbreviations are explained on the legend. D) Heavy mineral associations obtained from Luzieux (2007).

5.4 Stratigraphic evolution and U-Pb constraints

5.4.1 Youngest U-Pb zircon dates point to depositional age

Detrital zircon age spectra are controlled mainly by the presence of: 1) igneous activity coeval with deposition (primary zircon); 2) the potential of zircon grains preservation and 3) the degree of incorporation of older zircon grains into the sedimentary record (Cawood *et al.*, 2012; Gehrels, 2014; Schoene, 2014). Detrital zircon ages in forearc sedimentary rocks generally show a unimodal distribution with a main population provided by zircon derived from magma emplaced during sediment deposition (Cawood et al., 2012). Gehrels (2014) suggested that if the youngest age decreases progressively up-section, a reasonable interpretation is that measured ages record volcanism during sedimentation. Data presented here come from reworked tuffs and volcanic-rich sandstones with high potential to show a syn-sedimentary volcanic input. Furthermore, the obtained youngest ages, apart from three exceptions, are systematically younger up-section (Figure 5.3) and show a good correlation with paleontological records mainly those of Ordoñez et al. (2005; see Comp. Figure 5.1). We consider that the analyses presented here define the ages of deposition, or ages very close to the deposition age.

To further constraint the relationship between youngest age and depositional ages we double dated three outcrops (samples CP010-CP011, CP207-CP402 and CP022-CP023). These samples gave comparable ages within error (or very similar ages), thus giving further support for primary zircon input being coeval with sedimentation. Data presented here reinforces the idea that U-Pb detrital zircon dating is an excellent tool to date sedimentary series in forearc basins that developed synchronously with and in proximity to an active magmatic arc. Additionally, several

grain size fractions (60–100 μm, 100–160 μm and 160–200 μm) were dated separately in one sample (CP402) and no differences in age clusters were observed between them.

Table 5-1: Sample information. All tuffs are reworked tuffs. The calculated age corresponds to the weighted average age (Ludwig, 1991) obtained from the youngest zircon family. N.D = non-defined.

Sample	Formation	Lithology	Lat (°S)	Long (°W)	Youngest cluster TW Concordia (Ma)	Younger cluster weighted average (Ma)
CP007	Azúcar	Sandstone	2°38′25.74″	80°26′1.92″	61.2 ± 2.0 (N = 3)	60.7 ± 0.6 (N = 10)
CP006	Azúcar	Sandstone	2°37′49.22″	80°26′53.79″	61.3 ± 0.7 (N = 35)	59.9 ± 0.3 (N = 42)
CP103	Azúcar	Sandstone	2°14′31.82″	80°33′25.52″	57.1 ± 1.2 (N = 5)	57 ± 1.3 (N = 7)
CP107	Azúcar	Sandstone	2°13′13.91″	80°54′55.73″	55.2 ± 1.6 (N = 3)	57.5 ± 1.3 (N = 7)
CP212	N.D	Tuff	2° 6′53.33″	80°44′30.18″	52.8 ± 1.3 (N = 4)	53.7 ± 1.4 (N = 7)
CP014	Ancón	Sandstone	2°22′44.23″	80°47′47.60″	54.5 ± 1.9 (N = 3)	53.4 ± 1.1 (N = 4)
CP017	Ancón	Tuff	2° 9′28.19″	80°46′48.85″	48.6 ± 0.6 (N = 6)	48.5 ± 1 (N = 6)
CP010	Ancón	Sandstone	2°20′13.24″	80°53′25.85″	40.9 ± 0.5 (N = 4)	40.9 ± 0.4 (N = 5)
CP011	Ancon	Tuff	2°19′58.10″	80°53′25.92″	40.5 ± 0.6 (N = 4)	40.5 ± 0.5 (N = 4)
CP018	Zapotal	Tuff	2°19′11.25″	80°32′54.32″	32.5 ± 0.3 (N = 4)	32.5 ± 0.3 (N = 10)
CP218	Zapotal	Sandstone	2°44′27.03″	80°13′13.73″	29.5 ± 0.4 (N = 5)	29.5 ± 0.4 (N = 15)
CP705	Dos Bocas	Sandstone	1°49′8.74″	80°45′32.40″	23.5 ± 0.4 (N = 3)	22.9 ± 0.6 (N = 8)
CP702	Dos Bocas	Tuff	2°13′2.40″	80°34′22.17″	Recycled	Recycled
CP019	Villingota	Tuff	2°22′17.04″	80°27′50.84″	Recycled	Recycled
CP021	Subibaja	Sandstone	2°23′8.33″	80°26′8.24″	Recycled	Recycled
CP405	Subibaja	Tuff	2°11′40.41″	80°26′55.16″	15.6 ± 0.2 (N = 7)	15.9 ± 0.27 (N = 11)
CP207	Subibaja	Sandstone	2°12′24.41″	80°19′9.38″	14.2 ± 0.2 (N = 11)	14.3 ± 0.31 (N = 13)
CP402	Subibaja	Sandstone	2°12′28.45″	80°19′10.22	14.3 ± 0.1 (N = 36)	14.2 ± 0.12 (N = 50)
CP022	Progreso	Sandstone	2°24′29.29″	80°22′22.69″	Subconcordant	~11.5 (two grains)
CP023	Progreso	Tuff	2°24′29.29″	80°22′22.69″	10.3 ± 0.2 (N = 3)	10.2 ± 0.41 (N = 5)

Additionally, how accurately the youngest zircon dates constrain the age of sedimentation depends on several aspects including zircon recycling, Pb-loss and uncertainties related to the dating method (1–2% for LA ICPMS; Dickinson and Gehrels, 2009; Schoene, 2014). It has been proposed by these authors that the difference between the age of deposition and the younger U-Pb age may be significantly reduced with high sampling density, especially in areas where significant volcanic input is present. Nevertheless, as pointed out by (Dickinson and Gehrels, 2009), the youngest date from a sample will be younger than the true age in almost all cases. The same authors propose that a solution to this too-young bias is to use the age of the youngest group of ages from a sample. Here we consider the youngest clusters defined by at least three analyses that are concordant within error as recommended by Dickinson and Gehrels (2009).

The forearc evolution of SW Ecuador is defined by three main stratigraphic successions that define the accretion, post-accretion, and forearc basin series. Thirteen different sites are described. Site and sample locations are shown in Figure 5.2. Complementary field pictures and age constraints are shown in Complementary

Figure 5.2 and weighted average 206Pb/238U ages, where possible, are shown in Complementary Figure 5.3.

5.4.2 The accretion series: the Paleocene Azúcar Formation

The Azúcar Formation contains the first products of erosion resulting from the accretion of SW Ecuador against the continental South American margin (Benitez, 1995; Jaillard et al., 1995). The accretion event is marked by the first appearance of metamorphic clasts in the forearc sediments (Figure 5.3D; Luzieux, 2007), as well as the presence of Paleozoic and Triassic detrital zircon U-Pb ages (Witt et al., 2017). The last two aspects are believed to constrain sourcing resulting from the erosion of the Amotapes Massif (or other terranes sharing the same age affinities; e.g. Olmos Terrane or Western Cordillera of Peru) located south of the studied area (Witt et al., 2017). Because of different degrees of deformation between the Azúcar Formation and its underlying and overriding series, it has been proposed that both the base and the top of the Azúcar Formation are erosional boundaries (Benitez, 1995). The Azúcar Formation yielded the assemblage of benthic foraminifera such as Rzehakina epionga and Bathysiphon gerochi, the calcareous nannoplankton Heliolithus kleimpellii, Fasciculithus involutus, Cruciplacolithus tenui and Chiasmolithus bidens and palynomorph Foveotriktes margaritae, which are diagnostic of a Paleocene age (Comp. Fig. 1; Ordoñez et al., 2006). Fossil associations suggest a deep sedimentation environment up to 2000–3000 m deep (Ordoñez et al., 2006).

The best outcrops of the Azúcar Formation are located in the SE part of the Peninsula at site 1 (Figure 5.2). They display steep NW-SE directed (strike) strata of siliciclastic facies, ranging from shale to conglomerate. The lowermost sections of the Azúcar Formation at site 1A exhibit typical flysch-like facies (Figure 5.4A). The monotonous interbedding, the aggradational pattern and the distribution of strata suggest a low confinement environment, probably related to the depositional fringe of a deep, turbiditic system. The common occurrence of Bathysiphon foraminifera species in these deposits argue in favor of a deep marine setting. A more proximal

setting of this system crops out at site 1B, where the facies is composed of unsorted conglomeratic and thicker sandstone beds (Figure 5.4B). The degree of confinement is stronger than at site 1A.

Sandstone beds are pervasively laminated (flat at the base, grading upward to arcuate to crossbeds) with locally fluidization at the top (Comp. Fig.2A) and bioturbated interval observed at the sand-to-sand contacts. These conglomerate-sandstone successions can be interpreted as Lowe sequences of coarse-grained gravity flows emplaced on a westward dipping submarine slope. The feeders of the turbiditic system, found at site 1C (Figure 5.4C), correspond to N10 m deep channels infilled by conglomerates and coarse-grained sandstones with numerous evidences of by-pass (traction carpets). Conglomerate clasts are mainly composed of well-rounded quartz and dark quartzite or chert. In some places imbrications and crossbeds show a SW directed current. Summarising, the Azúcar Formation at site 1 corresponds to a classical submarine fan sequence of (Walker, 1976), ranging from outer fan sequences at site 1A to to suprafan lobes at site 1B and inner fan channel fill at site 1C. In site 2, the Azúcar Fm exhibits syn- sedimentary mass wasting structures in conglomeratic facies similar to that at site 1C (Figure 5.4D). North of site 6 very fine-grained series affected by intense penetrative deformation may be ascribed to the Azúcar Formation (Comp. Fig.2B). Alteration patterns suggest the presence of a great amount of fluids. The sedimentary rocks are intensively sheared; although some folded structures are still noticeable. Sedimentary facies and deformation are very different from those observed in other nearby outcrops of the Azúcar Formation (or the Ancón Group, see below).

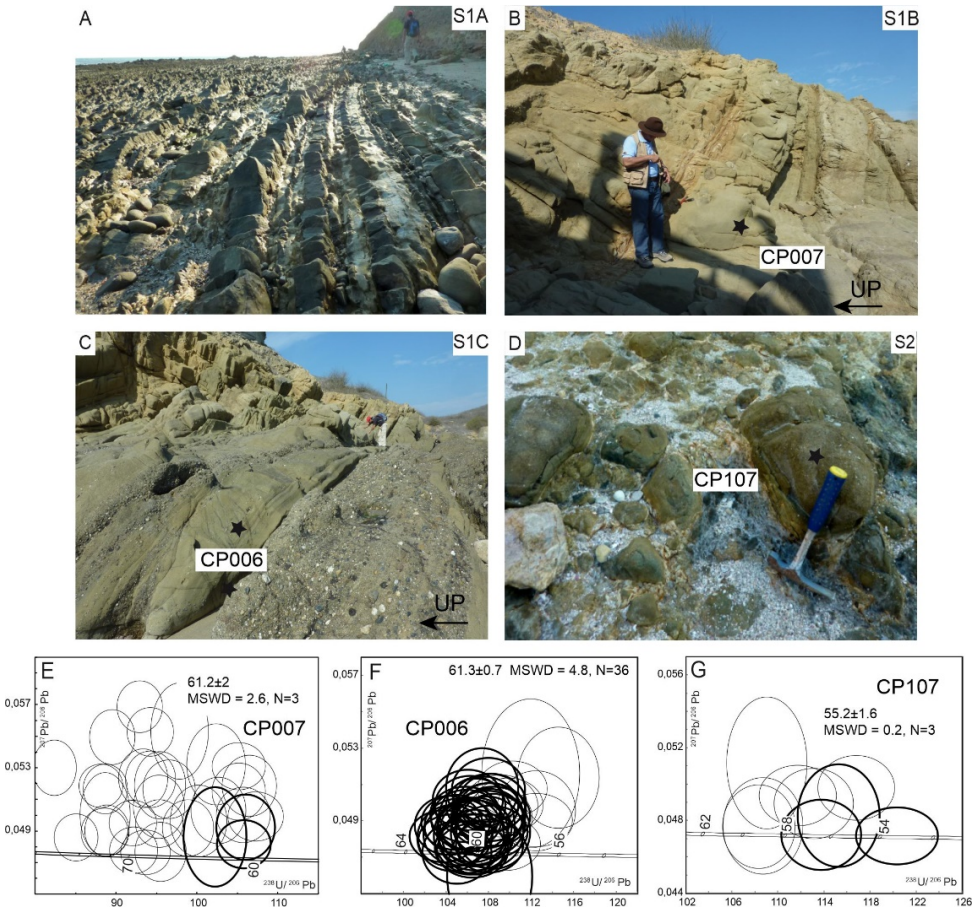

Figure 5.4: The Azúcar Formation A) Flysh-like deep series. B) Slope deposits showing flat-base sandstones and fine conglomerates, location of CP007 sample. C) Large conglomerate channel incised in sandstones, location of CP006 sample. D) Boulder of the Azúcar Formation (sample CP107) obtained from a debris-flow near La Libertad locality. E to G) Tera-Wasserburg concordias showing the youngest dates obtained from sediments of the Azúcar Formation (location of samples on Figure 5.2B and Table 1). Dates used for age calculations are shown with thicker black lines. Additional figures shown in Comp. Figs. 2A to 1D.

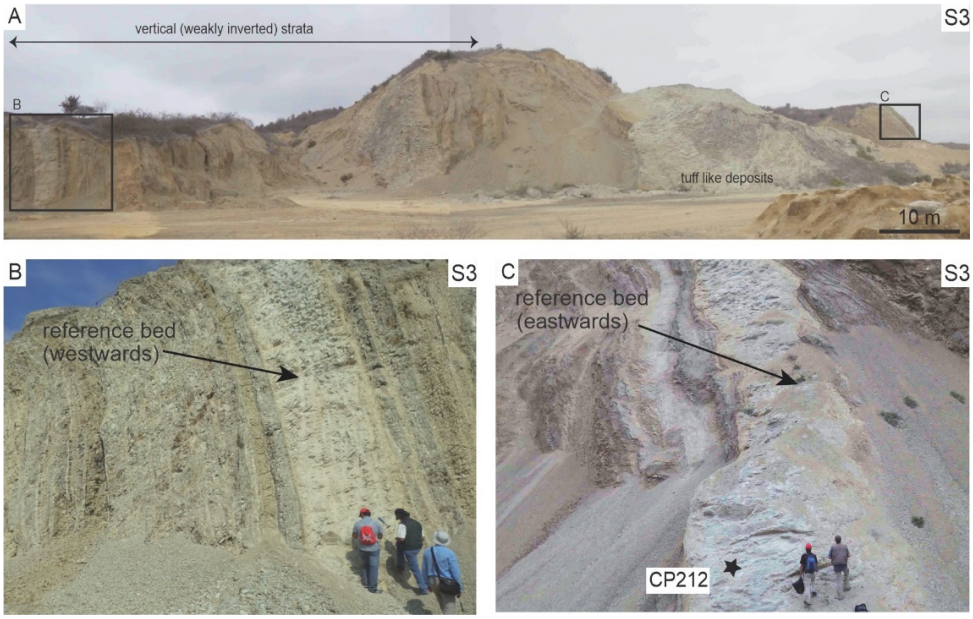

Figure 5.5: Outcrop near the Pacoa locality at site 3. A) General view of the folded outcrop showing the reference tuffaceous layer at the left and the right of the picture. B) Slightly overturned series at the north flank of the antiform showing the reworked tuffaceous layer. C) The southern part of the anticline showing the tuffaceous layer and location of sampling. Age constrains shown in Comp. Fig.2E.

Four samples of the Azúcar Formation provided zircon dates of various quality, especially with regard to the concordance of youngest grains. This is true for sample CP007 (a massive sandstone; Figure 5.4B) as only three of the 10 youngest analyses are concordant within error (Figure 5.4E). These three concordant analyses yield a concordia age of 61.2 ± 2 Ma (MSWD = 2.6). The ten youngest analyses return a weighted average 206Pb/238U date of 60.7 ± 0.6 Ma (MSWD = 1.2). Sample CP006 (Figure 5.4C) yielded 42 apparent ages between 61.8 ± 0.8 Ma and 56.0 ± 0.8 Ma with a weighted average 206Pb/238U date of 59.9 ± 0.3 Ma (MSWD = 1.5; Comp. Fig. 3). Sample CP103 (a thick sandstone deposit near the Estancia hills; Comp. Fig. 1C) yields a Concordia age of 57.1 ± 1.2 Ma (MSWD = 2.8, N = 5) which is con- firmed by the weighted average 206Pb/238U date of 57.0 ± 1.3 Ma (MSWD = 3.7; Comp. Fig.3) obtained from the seven youngest grains (Comp. Fig. 2D). In site 2 (Figure

5.2), mass transport deposits include centimetric boulders (Figure 5.4D) with characteristics very similar to the sediments of the Azúcar Formation found at site 1B. One boulder (sample CP107) was sampled from this debris flow. The three youngest concordant data yield a Concordia age of 55.2 ± 1.6 Ma (MSWD = 0.2, Figure 5.4G). In the light of these data, the Azúcar Formation was deposited between ~61 Ma and ~55 Ma in good agreement with the Late Danian – Late Lutetian age proposed from paleontological records (see Comp. Fig.1; Ordoñez et al., 2006).

5.4.3 The Upper Paleocene – Lower Eocene accretionary series close to the Chongón-Colonche hills

Deformed sediments located at site 3 (Figure 5.2) have been classically correlated with the Ancón Group by Benitez (1995), although as shown in this work, its sedimentary and compositional characteristics differ from those observed in that group. The outcrop is arranged in a long wavelength antiform with a reference reworked white (tuffaceous) layer observed in the eastward and westward borders (Figure 5.5A). The deposit is mostly composed of monotonous whitish volcano sedimentary material with some meter-thick tuff layers in the antiform core. Due to the mineral composition, the fine grain size and conformable parallel bedding, these deposits were likely formed by fallout of volcanic ash in a quiet submarine setting. The western flank of the antiform is slightly overturned (Figure 5.5B), whereas the eastern flank dips gently (Figure 5.5C). Several normal faults were rotated during the main compressional step, and as for the Azúcar Formation deformation in this sedimentary series is most likely younger than the sedimentation.

A thick ~4 m laminated tuffaceous layer was sampled (sample CP 212; Figure 5.5). The four youngest zircon analyses return a concordia age of 52.8 ± 1.3 Ma (MSWD = 2.4). This age is slightly younger than the ages obtained for the Azúcar Formation. The sample also yielded a significant population between 75 and 70 Ma. Because of significant sedimentary differences, the fine-grained sediments of the Pacoa area found in site 3 should probably be considered as a different formation, not related with neither the Azúcar Formation nor the Ancón Group.

5.4.4 The post-accretionary Eocene Ancón Group

The Ancón Group outcrops along kilometer-scale cliffs in sites 4, 5 and 6 in the west of the Peninsula (Figure 5.2A); whereas its lowermost part has hitherto only been observed in seismic records. Outcrops of the Ancón Group have been related to the Seca, Socorro and Punta Ancón formations (see Benitez, 1995; Ordoñez et al., 2006; Figure 5.6), all of them being defined in the past as lithological rather than chrono-stratigraphic units. Because of the absence of clear stratigraphic criteria, we made no difference between the Socorro and Seca Formations which are treated as the same unit in the present work. The Ancón Group yielded the calcareous nannoplankton Tribrachiatus orthostylus and Discoaster lodoensis from the eponymous biozones indicating a late Early Eocene (Comp. Fig.1; Ordoñez et al., 2006). In detail, the Socorro Formation corresponds to the Discoaster binodosus and the lower Tribrachiatus orthostylus calcareous nannoplankton biozones, the Seca Formation to the Tribrachiatus orthostylus calcareous nannoplankton Biozone and the Punta Ancón Formation to the Discoaster lodoensis calcareous nannoplankton Biozone (Comp. Fig. 1; Ordoñez et al., 2006).

In site 4, outcrops of the Seca-Socorro sequence exhibit a mud breccia unit, starting by an intraformational conglomerate and passing upward to an olistostrome (Figure 5.6A and Comp. Fig. 2F). The intraformational conglomerate is matrix-supported, with angular to sub-rounded pebbles/cobbles of greyish, laminated sandstones. The matrix is a massive grey silty mud rich in bitumen but some dm-thick, lense-shaped layers have a sandy matrix and a higher abundance of small pebbles. The absence of lamination in the matrix suggests a high density, rapid flow (mudflow). This deposit, ascribed in the literature to the so called Clay-pebble beds unit (see Benitez, 1995), is interpreted as a large debris flow forming a submarine mass-transport complex (MTC). The MTC is truncated at the top by a N 10 m deep channel system infilled by flat-bedded sandstones passing upward to heterolithic strata (Figure 5.6A). The massive sandstone beds would correspond to high density bottom flows confined with the channel, whereas the heterolithic beds indicate low density turbiditic spillout deposits. The perfect parallel bedding and very large lateral extent of even the

thinnest beds suggest that they are distal, low density turbidites. Many bedsets of the finest grained facies show convolute bedding with shear structures (that does not affect their thickness regularity), which is consistent with a high sedimentation rate on a submarine slope with the mud breccia beds and slumps being associated with slope failure. Although some meter scale reverse faults are observed (Figure 5.6B), deformation at site 4 is mostly extensional and related to meter scale normal faults (Figure 5.6C). As no clear extensional regime is observed and deformed series are rapidly sealed, deformation is most likely related to instability pulses of the depositional profile. Further sedimentary observations in site 4 are detailed in Comp Fig. 1G and H.

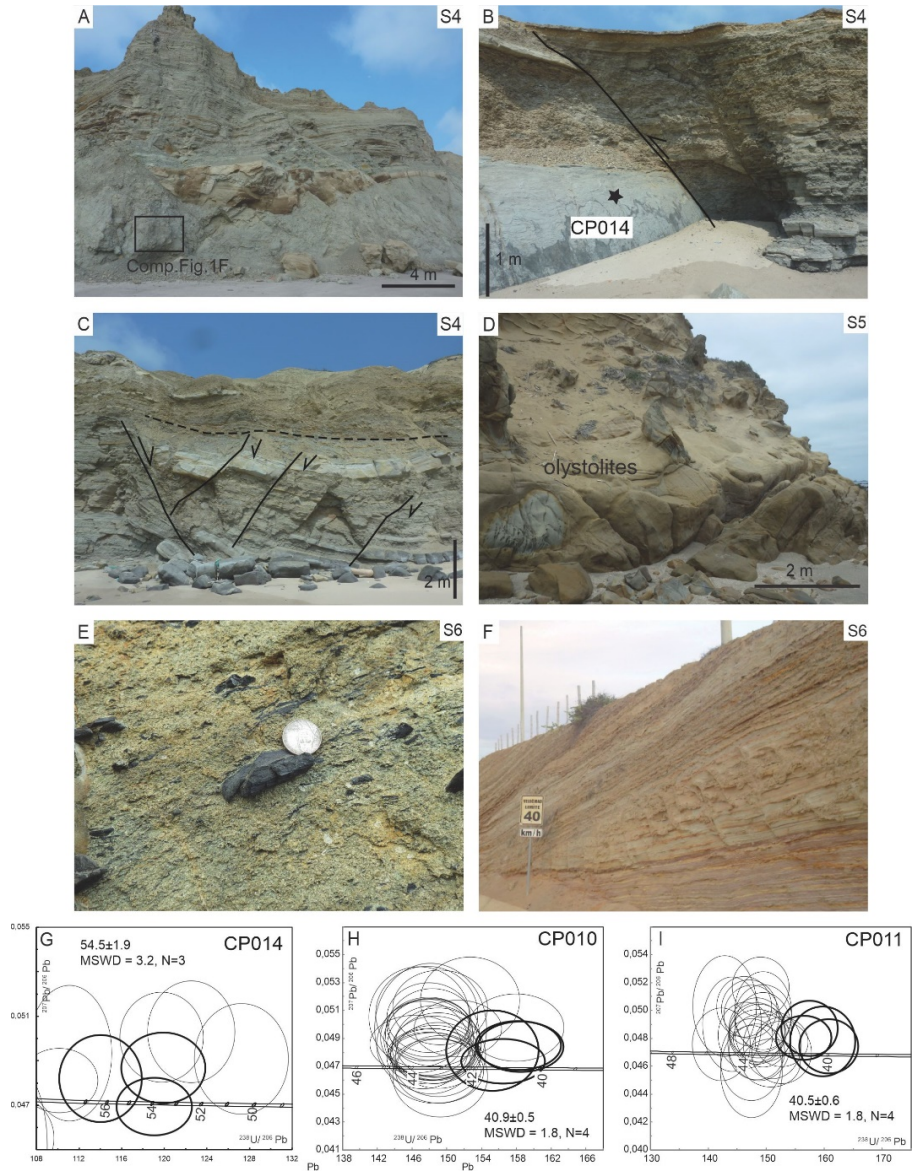

Figure 5.6: Outcrops of the Ancón Group in the cliffs of Ancón (site 4), Ballenita (site 5) and Anconsito (site 6) areas. A) Sandstone channels incising the debris flows. B) Reverse fault and location of sample CP014. C) Extensional *syn*-tectonic faulting, the layer defined by the dashed line seal the deformation. D) Channel incision above a massive olistolith-bearing sandstone. Flaky lignite-rich layers. F) Deltaic plane channel-bars at the top of the succession at site 6. G to I) Tera-Wasserburg concordias showing the youngest dates obtained from sediments of the Ancón Group (location of samples on Figure 5.2B). Dates used for age calculations are shown with thicker black lines. Additional figures shown in Comp. Fig. 2F to 1M.

Site 5 shows a 50 m thick succession of massive sandstones overlying, with an erosional disconformable surface, a succession of fine- grained, ripple-laminated sandstone and locally organic-rich (peat-like) claystone facies. Olistoliths of the claystone facies, N1 m in size, are present at the bottom of the massive sandstone unit (Figure 5.6D), which grades upward to the ripple-laminated sandstone and claystone facies. The idealized succession of the facies at this place is a large-scale channel-fill with the massive sandstone, passing upward to the lami- nated sandstone and claystone forming levee and overbank deposits. A strong energy and discharge are indicated by the supercritical regime in the massive sandstone (namely hummocky cross stratification, HCS) and by the climbing ripples in the overlying laminated deposit (Comp. Fig. 2I). The organic-rich clay, together with the abundance of trace fossils of the Skolithos assemblage, suggests a deltaic setting. Paleocurrents, indicated by the ripples, were towards the south and may be consistent with the paleoslope of the basin. The deformation is related to cm-scale normal faults most likely younger than sedimenta- tion (Comp. Fig. 2J).

In site 6, a N200 m thick section has been correlated with the upper- most series of the Ancón Group (e.g. Punta Ancón Formation; Benitez, 1995). At the base, the series are mostly dominated by an alternation of cross-bedded sandstones and flaky, lignite rich layers, delivering a various collection of large burrows with passive fills (Comp. Fig. 2K). Several beds show Thalassinoid sp. assemblages, whereas others show lignite beds and wood fragments (Figure 5.6E). This succession is overlain by a massive sandstone bed (15–20 m) with metric olistolits and float- ing coal clasts, where sample CP010 (sandstone) was collected. The massive sandstone grades upward to a poorly stratified, lithic-rich coarse sandstone with stringers of gravels and finally to a massive grav- elly conglomerate with lignite clasts and an iron-rich matrix. A metric channeled deposit is observed in this deposit, the base of which being coincident with sample CP011 (tuff, Comp. Fig. 2L). The section terminates by an alternation of sand-mud layers with abundant volcaniclasts, mud pebbles and Ophiomorpha. These heterolithic deposits are organized in 2 m-thick sigmoidal bedsets, laterally stacked and truncating each other (Figure 5.6F), with superimposed

smaller-scale oblique trough crossbedding. The entire section can be interpreted as a forced regres- sive succession across a fluvial-dominated deltaic margin, in concordance with previous observations (Benitez, 1995). The proximity of a terrestrial source is testified by the abundant lignite-rich beds and wood fragments. The heterolithic deposits at the top are interpreted as sinuous channel bars of the deltaic plain, whereas the underlying conglomerate would correspond to the delta front or mouth bar. The overall coarse grain size for this deposit may indicate a still active uplift of the sourcing region.

Sample CP014 was obtained from the base of the sandy series at site 4. The three youngest zircon analyses yield a concordia age of 54.5 ± 1.9 Ma (MSWD = 3.2) confirmed by the weighted average 206Pb/238U date of 53.4 ± 1.1 Ma (MSWD = 3.3) given by the four youngest grains (Figure 5.6G and Comp. Fig. 3). Paleontological assemblages suggest a younger age (~46–44 Ma) for the sandy sedimentation at this site (Ordoñez et al., 2006), although the major debris flow shown in Figure 5.6A may be older and deposited between ~50 and ~46 Ma. Although the low number of young zircon grains dated for sample CP014 prevents to clearly define a true depositional age, the dated grains here are in relatively good correlation (within errors) with the paleontological ages proposed for the debris flow at the base of the unit. The sequence of site 5 is overlain by a volcanic rich tuffaceous deposit, most probably reworked. We collected a similar reworked tuffaceous deposit 10 km to the north of this area (sample CP017). The six youngest grains are all concordant and define a concordia age of 48.6 ± 0.6 Ma (MSWD = 1.2). (Comp. Fig. 2M). Because of the facies similarities and similar structural position of the two tuffaceous outcrops we suggest that deposition of the sedimentary series observed in the site 4 may have occurred at ~48 Ma, an age slightly older than the ~46 Ma, which was proposed by Ordoñez et al. (2006) as the older age for these units, based on paleontology. Samples CP010 and CP011 yielded a very significant young component of zircons ranging between 45 and 40 Ma, with most likely two different clusters in this range (Figure 5.6H and I). For sample CP010 (Figure 5.6H), the 4 youngest concordant data yield a concordia age of 40.9 ± 0.6 Ma (MSWD = 1.8). In sample CP011 (Figure 5.6I), the four youngest

concordant analyses return a concordia age of 40.5 ± 0.6 Ma (MSWD = 1.8). These ages are in very high concordance with paleontological analysis (Ordoñez et al., 2006), which indicate a 41–40 Ma age (zone P13 of planktic foraminifera; Bolli et al., 1989; Comp. Figure 5.1) for the Punta Ancón succession. Samples CP010 and CP011 yielded very important clusters of ages weighted at 43.1 ± 0.2 Ma and 43.1 ± 0.4 Ma, respectively (Figure 5.6H and I). Based on these results, the Ancón Group records the transition from the deep-water slope to the deltaic shelf edge of the basin that occurred between ~55 Ma to ~41 Ma, although further constraints are necessary to better date the base of the group.

5.4.5 The Progreso forearc basin and coeval sediments in the North Peninsula

The Zapotal Formation marks the transition from the accretionary and post-accretionary system to the forearc basin depocenter. Outcrops of the Zapotal Formation are located on the western edge of the Progreso Basin (including its southernmost extension through Puná Island) and are bounded to the west by the Estancia Hills. Indeed, the Estancia hills separates the Paleocene – Eocene series of the Peninsula (west) from the Oligocene-Miocene series of the forearc depocenter (east). In the basin border, eastwards from the Estancia Hills the sedimentary infilling is highly deformed (including sub-vertical strata) and composed of a mixture of typical Azúcar and Ancón facies including some cherts most presumably of the Late Cretaceous Santa Elena Formation (Comp. Fig. 2N). The Zapotal Formation holds marine fossils and plants, but there is a lack of diagnostic fossil for biozone. However, some benthic foraminifera were determined at the species level, such as Gyriodina sp., Cibicides sp., Bathysiphon sp. and Rhabdamina sp. The relative age is determined with the position of the sediments and estimated as Oligocene (Comp. Fig. 1; Ordoñez et al., 2006).

Sediment thickness of the Zapotal Formation decreases from approximately 1000 m in the center of the basin to ~220 m at the basin border (Estancia Hills;

Benitez, 1995). At the type-locality, the Zapotal Formation is composed of tuffaceous sandstone and polygenic, massive, clast-supported conglomerates with rounded elements (Site 7, Figure 5.7A). Chert fragments observed in the conglomerate facies are most probably derived from the deeper rocks exposed at the Estancia Hills. The bottom of the conglomerate beds above the sandstones is commonly marked by burrows infilled by gravels, suggesting a kind of firm or hard ground and the sandstones are commonly cross-bedded (Figure 5.7B). These facies have been interpreted as deposits related to fluvial and marine shallow-water environments (Benitez, 1995).

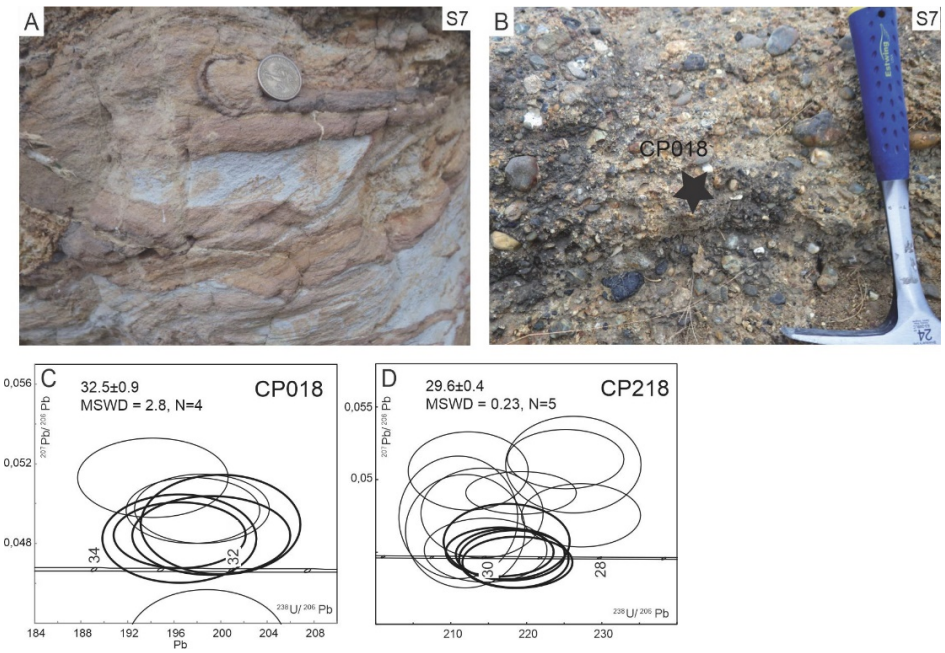

Figure 5.7: A) Conglomeratic facies of the Zapotal Formation at the locality type near the Estancia Hills at site 7. B) Volcanic-rich clastic deposits of the Zapotal Fm, location of sample CP018. C, D) Tera-Wasserburg concordias showing the youngest dates obtained from sediments of the Zapotal Formation. Dates used for age calculations are shown with thicker black lines. Additional figures shown in Comp. Figs. 2N to 1P.

Sample CP018 (reworked tuff; Figure 5.7B), yielded a concordia age of 32.5 ± 0.9 Ma (MSWD = 2.8, N = 4; Figure 5.7C) and a weighted average date of 32.5 ± 0.3 Ma (MSWD = 0.4; Comp. Fig. 3) calculated with the 10 youngest grains (Figure 5.7C). The sandstone sample CP218 obtained from NW Puná Island (Comp. Fig. 2O) yielded a concordia age of 29.6 ± 0.4 Ma (MSWD = 0.2; N = 5; Figure 5.7D) and a weighted average date of 29.5 ± 0.4 Ma (MSWD = 2.5) obtained with the 15 youngest grains. The ages obtained here suggest that the Zapotal Formation was deposited during the earliest Oligocene; thus, redefining the Oligocene undifferentiated age proposed from paleontological assemblages and constraining the forearc basin initiation at around 32–29 Ma.

The forearc basin deposit continued in the early Miocene with the sedimentation of the Dos Bocas and Villingota Formations. Outcrops of the Dos Bocas and Villingota Formations are very sparse in the Progreso basin depocenter and confined to a strip parallel to the Estancia hills (Figure 5.2). In the northernmost areas of the Santa Elena Peninsula, a shallow-water series ascribed to the Dos Bocas Formation outcrop in Site 8 in the Montañita area (Figure 5.2A). The outcrop consists of a succession of units of yellowish litharenites and sandstones bounded by low angle unconformities (Figure 5.8A). The deposits are parallel bedded or structureless, with locally large diagenetic nodules. The beds are bounded and traversed by boxworks of large arthropod burrows (Comp. Fig. 2Q). They also exhibit marine mammal bones (Comp. Fig. 2R) and some patch reefs of bivalves and worms are locally found. These beds were deposited in a protected shallow-water setting, likely under a period of strong tectonic deformation (as indicated by the progressive unconformities). Near the axis of the Progreso basin, outcrops ascribed to the Dos Bocas Formation (Figure 5.2) are observed in site 9 (Figure 5.8B); it consists of a flat bedded tuff arenite with superimposed symmetrical ripples, passing upward to hummocky crossbeds. It is incised at the top by a channel, several meters deep, floored by a tuff conglomerate. These facies are typical of the succession expected in shoreface bars and rip channels.

Sample CP705 (sandstones attributed to the Dos Bocas Formation) yielded a concordia age of 23.5 ± 0.4 Ma (MSWD = 0.7; N = 3; Figure 5.8C and Comp. Fig.

3). The eight youngest grains return a weighted average date of 22.9 ± 0.6 Ma (MSWD = 4; Comp. Fig. 3). This depositional age is in high concordance with paleontological records. Indeed, the Dos Bocas Formation shows a great abundance and diversity of fossils; there are planktic foraminifera, radiolarians and numerous calcareous nannoplankton. The base of the formation yielded diagnostic fauna indicating the Early Miocene Cyrtocapsela tetrapera radiolarian Biozone (Comp. Fig. 1; Ordoñez et al., 2006). The U-Pb age is also coincident with the age proposed for a dolphin skeleton recently found in the same unit in the Montañita area and dated as Chatian (upper Oligocene, 26–24 Ma; Tanaka et al., 2017); and 2) previous macro and micro fauna observations from Bristow (1975). Sandstones samples, CP702 (Dos Bocas Formation) and CP019 (Villingota Formation), near the basin border, did not yield a depositional age component (Figure 5.8D and E) and the extensive record of ~30 Ma and ~43 Ma zircons is believed to be derived from erosion of the Zapotal Formation and the Ancón Group, respectively. Similarly, an outcrop attributed to the Subibaja Formation (sample CP021; Comp. Fig. 2P) showed a representative family at ~60 Ma and 3 zircon grains at ~30 Ma, which are ascribed to the Azúcar and Zapotal Formations, respectively. From all our dated samples, CP702, CP019 and CP021 are the only ones in which the youngest dates are not related to the depositional age. Not coincidentally, these samples are: 1) close to the main structural high of the Progreso basin, which suggests that reworking processes are stronger within sedimentary rocks located near to the structural high and coeval with basin-inversion processes taking place at the NE basin limit (see seismic interpretation section). Furthermore, three other analysed samples of the same formations near the Estancia Hills did not contain any zircon grain.

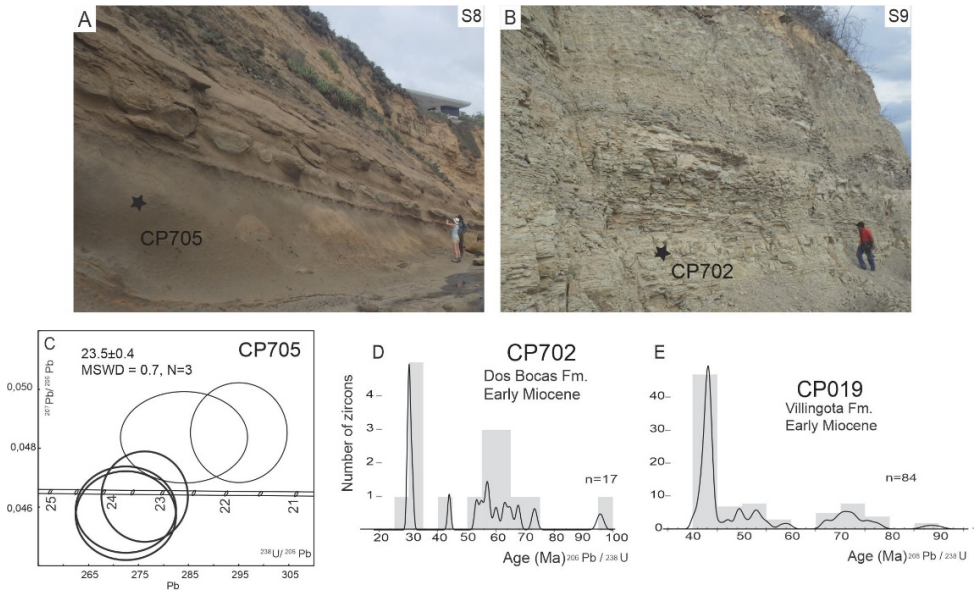

Figure 5.8: Yellowish litharenites and sandstones (Dos Bocas Formation) bounded by low angle unconformities. Additional pictures of this outcrop are shown in Com. Fig. 1Q and R. B) White sandstones of the Dos Bocas Formation C) U-Pb dating performed on sample CP705 D, E) Recycled zircon component of Lower-Middle Miocene sedimentary rocks cropping out near the Estancia Hills; major peaks are related to the Zapotal Formation (~30 Ma), Ancon Group (~43 Ma) and Azúcar Formation (~60 Ma). An additional histogram related to the same recycled component is shown in Com. Fig. 1P.

Site 10 corresponds to the type-locality of the Subibaja Formation The Subibaja Formation show diagnostic foraminifera from the Globigerinatella insueta, Globorotalia foshi peripherodonda and Globorotalia foshi foraminifera biozones, indicating a Middle Miocene age for that formation (Comp. Fig. 1; Ordoñez et al., 2006). The lower part of the section is composed of a silty, volcaniclast-rich mudstone (Figure 5.9A) with numerous nodules and pipes that are likely related to early diagenesis. Due to the absence of tractive bedforms, and the occurrence of many floating bivalve shells in connection, this facie is interpreted as a lower offshore setting. The overlying deposits are coarsening upward and show a progressive return of current action at the seabed, by way of offshooting ripples, interpreted as wave ripples, which indicate an upper offshore setting (Comp. Fig. 2S). The offshore deposits are overlain by a regressive facies tract, composed of a volcaniclastic litharenite comprising hummocky cross-stratification (HCS), Ophiomorpha and cross

strata infilling channels at the top. The HCS would correspond to shoreface deposits and the cross strata, which comprise upper-plane bedding, is interpreted as foreshore runnel infill. The sharp erosion at the bottom of the coastal facies and the lesser preservation of the shoreface argue in favor of a forced regression at this point. Similar downward shifts of facies are observed near the Zacachun locality (Figure 5.2A), where oyster patch reefs overlie the shoreface deposits by way of a regressive surface of marine erosion. These features are the hint of a reduced subsidence in these formations. Sample CP405, taken from a tuffaceous interval in this outcrop, yielded a concordia age of 15.6 ± 0.2 Ma (MSWD = 1.5; N = 7; Fig. 5.9E) identical within error with the weighted average date of 15.9 ± 0.3 Ma (MSWD = 1.7; Comp. Fig. 3) calculated with the 11 youngest grains. Similar downward shifts of facies are observed near the Zacachun locality (Figure 5.2A), where oyster patch reefs overlie the shoreface deposits by way of a regressive surface of marine erosion.

Three outcrops of the upper part of the Subibaja Formation are exposed at site 11, near Las Juntas (Figure 5.2A). Although it was not possible to structurally correlate these outcrops, they show similar successions of facies and might represent lateral equivalents. The lower part of the section exhibits loose, gravelly sand and litharenite with a gastropod fauna indicative of freshwater to brackish water. It is therefore interpreted as a fluvial to estuarine proximal channel deposit (Figure 5.9B). This facies is erosionally overlain by a finer-grained facies, either sandy or structureless, with long vertical burrows (Rosselia?), crossbedded with mud drapes (Figure 5.9C), or locally flat bedded with rhythmic mud drapes interstatified. A Glossifungites facies lies in between, infilling large arthropod burrows (Comp. Fig. 2T). The mud drapes (Figure 5.9C) is interpreted as the effect of tidal dynamics, and the Glossifungites surface as a transgressive surface. The dominant tidal paleocurrent measured in this level is towards the east, which indicates a flood dominance. The upper part of the outcrops is composed of cross-bedded gravelly sandstone with mud pebbles at the bottom, and locally containing silicified wood logs. The crossbeds indicate paleocurrents towards the west. It is interpreted as the return to a fluvial or deltaic setting. We collected two sandstone samples from site 11A (CP207 and

CP402), from which eleven concordant grains from sample CP207 yield a concordia age of 14.2 ± 0.3 Ma (MSWD = 1.6, Comp. Fig. 5.2W) and in sample CP402, 36 grains yield a concordia age of 14.3 ± 0.1 Ma (MSWD = 1.5). The 50 youngest grains return a similar weighted average date of 14.2 ± 0.1 Ma (MSWD = 2). Thus, at site 10 and 11, spanning about 2 Ma, the Subibaja Formation records relative sea-level falls in a siliciclastic setting ranging from the outer shelf to the shoreline, with incised valleys and embayments influenced by tidal dynamics.

The Progreso Formation is exposed at Sites 12 and 13. According to the literature (Benitez, 1995) it corresponds to the last marine transgression over the area, after a fluvial-dominated sedimentation at the top of the Subibaja Fm (Zacachun Mb.). The base of the Progreso Formation holds Globigerina nepenthes and Globorotalia siakensis, an assemblage corresponding to the Middle Miocene, whereas the upper part of the formation has a Late Miocene age (Comp. Fig. 1; Ordoñez et al., 2006). The two studied outcrops exhibit aggradational units of large lateral extent. In site 12, each unit (about 2–5 m thick) has a sharp bottom, underlined by a dense network of Thalassinoides (Comp. Fig. 2U). This surface is overlain by oyster patches, grading upward to a muddy calcarenite with numerous Skolithos and Cylindrichnus burrows (Figure 5.9D). The upper part of the unit is a fine-grained calcarenite with mud drapes. These units are interpreted as high frequency, transgressive systems tracts. In site 13 (Comp. Fig. 2V) the deposits are more siliciclastic and tuff-rich. They are dominantly composed of poorly bedded muds, with a sharp bounded, 8 m-thick interstratified sandy unit composed at the bottom by convolute beds, grading upward to large-scale trough crossbeds, the bottom of which is underlined by thick mud drapes. The muddy background is interpreted as a shelf highstand deposit, and the interstratified sandy unit as a forced regressive delta-front, the top of which being reworked into dunes in a tide-influenced setting (mud drapes). Two samples, CP022 and CP023, were collected in the deltaic facies from a reworked tuff and a sandy layer, respectively. Dating on sample CP022 shows three subconcordant grains with ages comprised between 11.5 Ma and 10.5 Ma (Comp. Fig. 2X). In sample CP023, three concordant grains yield a concordia age of 10.3 ± 0.2 Ma (MSWD = 0.9; Figure 5.9G) whereas

the five youngest grains return a weighted average date of 10.2 ± 0.4 Ma (MSWD = 4.5; Comp. Fig. 3). These data confirm the Tortonian depositional age obtained for the CP022 sandy sample.

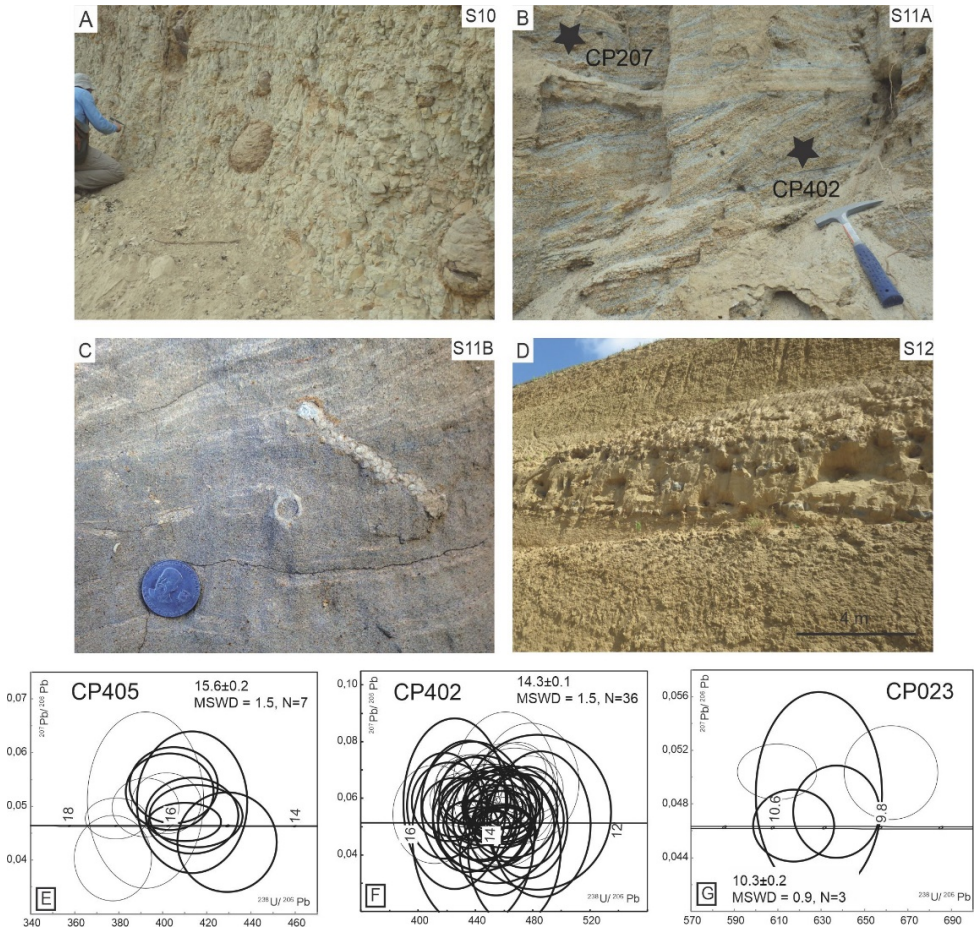

Figure 5.9: The Neogene infilling of the Progreso forearc basin. A) White tuffaceous sandstones of the Subibaja Formation. B) Littoral deposits of the limit between the Subibaja and Progreso formations, location of samples CP207 and CP402. C) Tidal deposits of the Subibaja Formation and ophiomorpha sp. D) Oyster patches and muddy calcarenites typical of the Progreso Formation E, F) Age spectra of youngest zircons of the Subibaja and Progreso formations.

5.5 Seismic interpretation

Five key lines (Figure 5.10 and 5.11) have been chosen from a set of hundreds (including different 3D seismic cubes) to show the accretionary, post accretionary and forearc basin series (line location is shown in Figure 5.2). The seismic lines of Figure 5.10 were obtained during the 1980's whereas the 2D seismic lines shown on Figure 5.11 were derived from a 3D seismic cube (30 m trace separation) coincident with the Progreso basin; obtained in 2010 by Petroamazonas. Although there is poor stratigraphic control on exploratory wells, a relatively good correlation of chronological markers (i.e. formation tops) were derived from well data (Petroamazonas confidential data and internal reports) and from facies analysis performed in the present work. Furthermore, the chronology of superficial reflections was constrained by the U-Pb ages presented here. The seismic line W8 (Figure 5.10A) is located in the south of the Peninsula and parallels the coastline coincident with site 1. Although the quality of reflections is relatively poor, the seismic line is mainly divided into three main units. The lowermost unit may correspond to the Upper Cretaceous volcaniclastics deposits, the top of which is tentatively related to the angular unconformity roughly observed in the line and that may correspond to a décollement-surface. Above the unconformity, the Azúcar Formation consists of very chaotic high amplitude reflections with illegible geometries. The deformed series are bounded upwards by an angular unconformity interpreted to dip towards the south, as the Azúcar Formation reaches the surface 2 km towards the north of Line 1 at site 1. The upper unit consists of less deformed sedimentary units located above the unconformity and attributed to the post accretionary series of the Ancón Group, the difference in deformation between the lower and upper series being similar to that observed in the field. The horizontal uppermost series are most probably of Quaternary age.

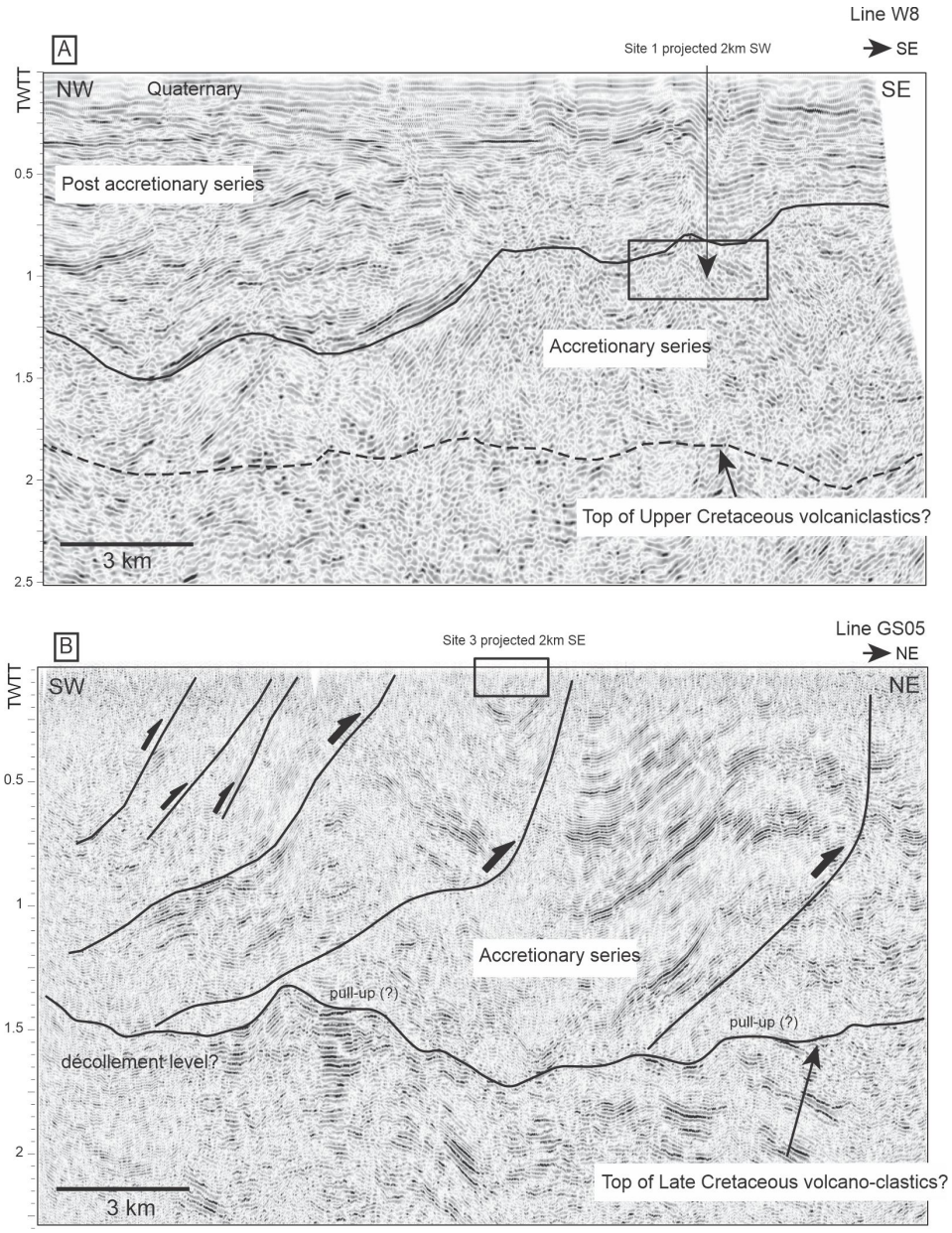

Figure 5.10: Time migrated seismic lines of key sections of the accretionary prism. Location of lines in Figure 5.2A. A) NW-SE directed line W8 showing the main unconformity between the Azúcar Formation (accretionary series) and the Ancón Group (post-accretionary series). B) NE-SW directed line GS05 showing the main thrust and fold systems near the Pacoa area (site S3). Note the difference between the scale of local observations performed in the field compared with the regional distribution of tectonic structures and sedimentary units observed in seismic lines.

The NE-SW directed Line GS05 (Figure 5.10B) is located in the westernmost part of the study area. It clearly displays two major thrust systems with a northeastward vergence formed by mostly parallel reflections. Deformation seems more pronounced towards the southern limit of the line, where closely-spaced highly dipping reflections may be related to thrust faults. The décollement level seems coincident with the major angular unconformity observed at approximately 1.5 s TWTT (two-way travel time), the local shallowing of reflectors at this surface most likely being artificial and related to velocity pull-ups. Well data constrained the location of the limit between the accretionary series and the Upper Cretaceous volcano-clastic deposits along the unconformity shown on seismic line GS05 (Aizprua et al., 2018).

The inlines 1780 and 1380 and the cross-line 2200 (Figure 5.11) are located in the Progreso forearc basin and generally display: 1) a non- reflective zone related to the topographic and structural high related to the Estancia Hills; 2) a shallowing of reflectors towards both the SW and the NE basin limits and 3) a south-eastwards deepening of reflectors. In lines 1780, 1380 and 2200 the accretionary and post-accretionary series of the Azúcar Formation and the Ancón Group are related to thick high amplitude reflections showing little internal structure. They are limited upwards by a basin-scale high amplitude seismic marker defining a strong to moderate angular unconformity. Upwards, forearc basin infilling is related to several facies assemblages which are mostly defined by parallel reflections with moderate to high amplitude and high continuity reflectors. Early forearc series such as those of the Villingota and Dos

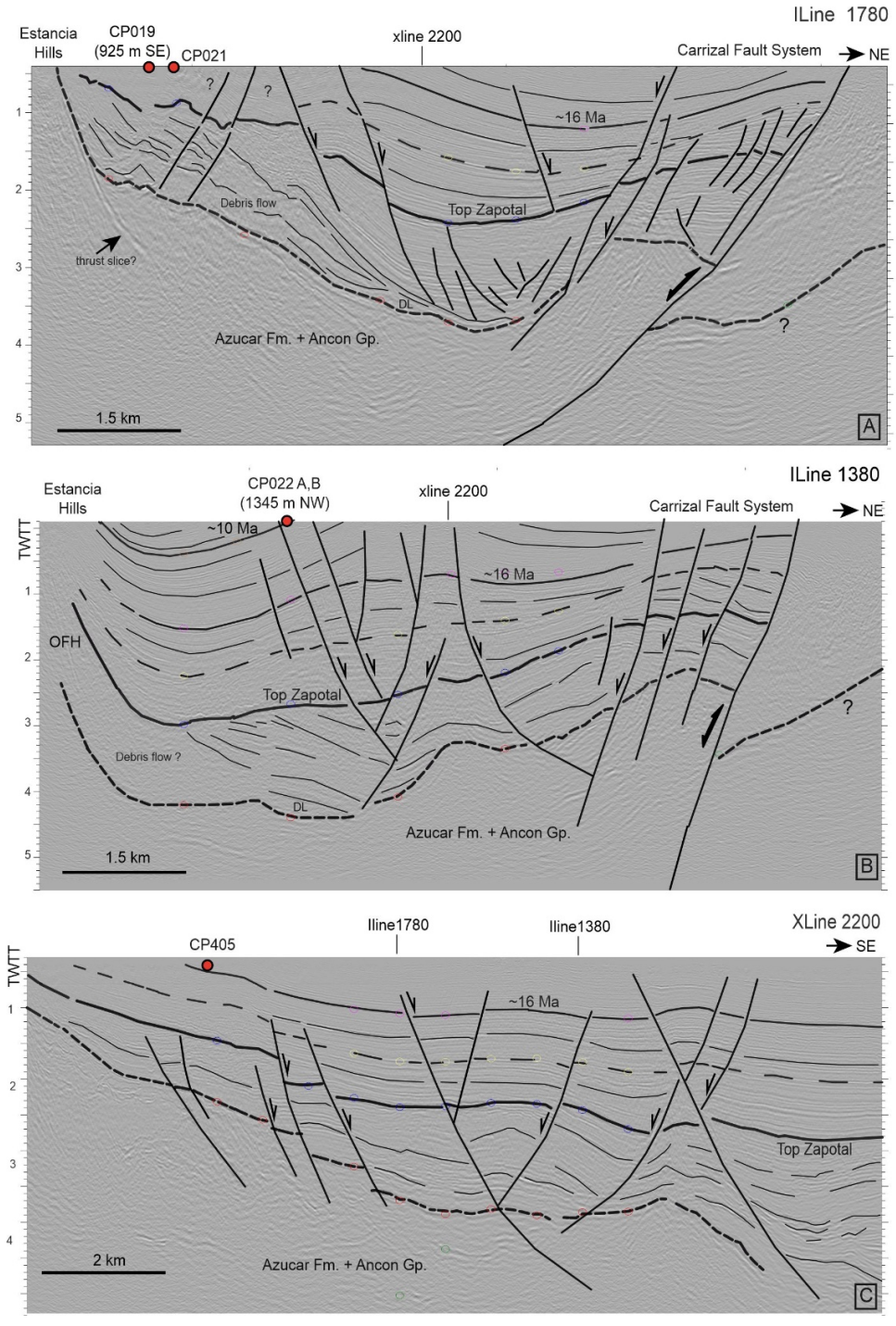
ILine 1780
Estancia Hills
CP019 (925 m SE)
CP021
xline 2200
Carrizal Fault System
NE
~16 Ma
Debris flow
Top Zapotal
thrust slice?
DL
Azucar Fm. + Ancon Gp.
1.5 km
A
ILine 1380
Estancia Hills
CP022 A,B (1345 m NW)
xline 2200
Carrizal Fault System
NE
TWTT
~10 Ma
~16 Ma
OFH
Top Zapotal
Debris flow ?
DL
Azucar Fm. + Ancon Gp.
1.5 km
B
XLine 2200
SE
CP405
Iline1780
Iline1380
TWTT
~16 Ma
Top Zapotal
2 km
Azucar Fm. + Ancon Gp.
C

Figure 5.11: Time migrated seismic lines and line drawing of key sections of the Progreso basin and its related outer forearc high (OFH) coincident with the Estancia Hills. Location of lines in Figure 5.2A. A) Inline 1780 showing debris flow deposits that are believed to represent the first products resulting from the erosion of the OFH. B) Inline 1380 showing slight thickness variations of reflectors near the OFH suggest a long-lived and continuous uplift along the high. Note the down-lapping reflectors (DL) of the Zapotal Formation next to the structural high. C) Crossline 2200 showing the southwards deepening of reflectors. Note that the displacement along normal faults is only partially related to the SE basin deepening.

Bocas Formations crop out near the OFH (Estancia Hills) and at the northwest basin border (cross-line 2200); otherwise they are covered by sediments younger than ~16 Ma (inlines 1780 and 1380; Figure 5.11) as constrained by the age of sample CP405. Several angular unconformities are of local to regional character and are believed to be related to sealevel changes and in a lesser extent to fault activity, in concordance with field observations.

The seismic characteristics of the zone close to the Estancia Hills vary along strike. Along inline 1780 (Figure 5.11A), a thick sigmoid package (~1.5 s TWTT, two-way travel time; ~5 km long) of mostly chaotic reflections lies unconformably above the units related to the Azúcar Formation and the Ancón Group We interpret these zones as debris-flows resulting from the onset of uplift of the Estancia Hills. Reflectors attributed to the Zapotal Formation are parallel equivalents of the non-reflective zone attributed to the debris flow (see also inline 1380). These aspects show that the Zapotal Formation is coeval with the onset of uplifting of the Estancia Hills, as suggested in the previous stratigraphic sections. The Zapotal Formation shows pervasive evidence of normal faulting, most of them being sealed down the upper limit of the group. In inline 1780 sedimentary units younger than the Zapotal Formation (e.g. younger than 32–30 Ma, see previous sections) are arranged in a more or less parallel way in the basin depocenter but show chaotic geometries next to the Estancia Hills, suggesting ongoing deformation at the topographic high. Along inline 1380 (Figure 5.11B), next to the structural high, reflections are observed deeper than in inline 1780 and they appear less chaotic. Seismic reflectors located above the top of the Zapotal Formation systematically thin towards the topographic high, most

likely defining syn-tectonic sedimentation and hence constant uplift of the Estancia Hills since 32–30 Ma, the age proposed in this work for the Zapotal Formation.

The NE limit of the forearc basin is related to the Carrizal fault system. Inlines 1780 and 1380 show that the Carrizal fault system has followed an inversion period, which disrupted the basin floor. Inversion is related to uplifted growth sediments at the basin border and onlapping terminations basinwards. Onset of inversion is coeval with the onlaping reflections above the black dashed thin marker (Figure 5.11A and B) and seems to be older than ~16 Ma.

5.6 Discussion

5.6.1 The accretionary prism and the post-accretion series

The compressional deformation observed at the Santa Elena Peninsula and the Playas high, beneath the depocenters of the Miocene Progreso basin and most likely beneath the Miocene-Quaternary Gulf of Guayaquil-Tumbes basins, define an accretionary prism (Figure 5.12B). This definition is mostly related to the deformation style and the position of the fold-and-thrust series between the active arc in the Western Cordillera and the trench. Besides the eventual loss of some parts of the prism via subduction-erosion processes, the current extension of this accretionary prism is considered as relatively local. Indeed, no coeval deformed series have been observed north of the Chongón-Colonche hills and further south in North Peru, where the older sediments of the modern forearc (i.e. the Salinas Formation) are younger than the Azúcar Formation (i.e. Early Eocene) and are significantly less deformed (Witt et al., 2018).

The Guayaquil Formation may contain the oldest sediments having a sialic composition in the entire Ecuadorian forearc (whole-rock geochemistry analysis; Witt et al., 2018); an aspect also evidenced by the presence of heavy minerals with continental affinity (Luzieux, 2007; Figure 5.3). Nevertheless, although this could be tentatively defined as an early proximity of SW Ecuador to a continental magmatic

arc, other aspects such as the presence of acid intrusions in the Pascuales area (e.g. north Guayaquil) may have resulted in the acid geochemistry of the Guayaquil Formation Regardless of the origin of the continental- like affinity of the Guayaquil Formation, the detrital character and deformation of the Paleocene Azúcar Formation recorded the main event related to the accretion of SW Ecuador against continental South America. Furthermore, the Azúcar Formation recorded the first metamorphic input as shown in their heavy mineral record (Figure 5.3D; (Luzieux, 2007). The U-Pb ages presented here, in combination with former paleontological data, suggest that the accretion of SW Ecuador took place between 61 and 56 Ma. Thus, confirming (at least partially) former hypotheses that account for a multi-episodic construction of the Ecuadorian forearc basement through several accretion events (Hughes and Pilatasig, 2002; Jaillard et al., 2009; Kerr et al., 2002).

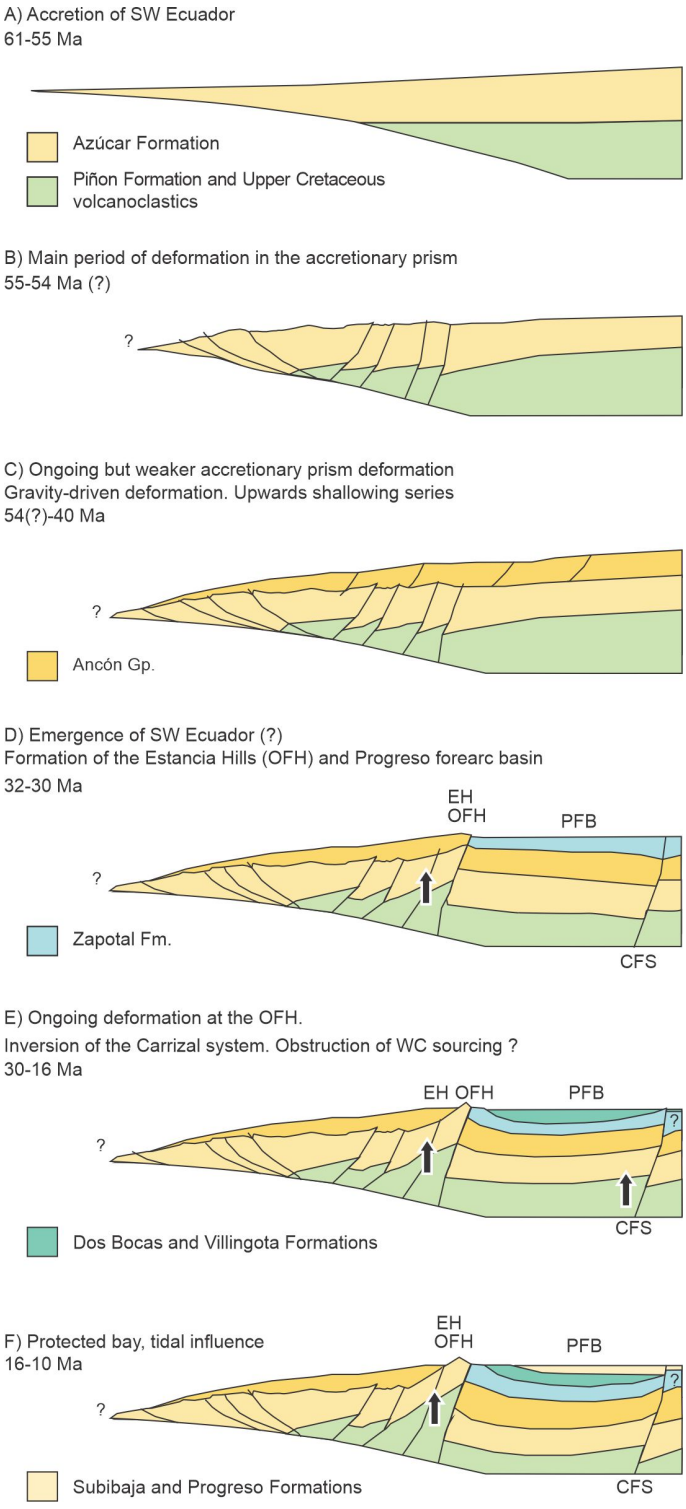

Figure 5.12: A to E) Schematic cartoons showing the evolution of the Peninsula and Progreso Basin. Sections are related to the architecture observed in a NE-SW direction near the center of the Progreso basin. Sections are not balanced and are used here only for qualitative schematic purposes, this includes the vergence of thrust-fold systems and the frontal/basal accretionary processes taking place at the very front of the system. DB, debris flow; EH, Estancia Hills; OFH, outer forearc high; PB, Progreso basin.

Both the Azúcar Formation and sediments in the Pacoa area are devoid of evidence of syn-sedimentary deformation, which suggests that construction of the accretionary prism occurred after ~55 Ma (Figure 5.12B). This aspect is corroborated by the parallelism of deformed reflectors in seismic lines and by the presence of boulders of the Azúcar Formation in highly deformed series related to the accretionary prism (Figure 5.4D), which confirms the post ~55 Ma age for the deformation (Figure 5.4D and G). The high degree of deformation, the relative scarcity of outcrops and the poor quality of seismic reflections prevent a clear characterization of the internal geometry of the prism including its main vergence. Thus, strain directions seem to have rotated through time as evidenced by structural analysis of the Santa Elena Formation (Jaillard et al., 1997). Although a clear NE vergence may be defined in the westernmost parts of the Peninsula, to the SE, near site 1 the thrust vergence is not clear in the field or in seismic records. Formation of the accretionary prism may have raised deep sediments in concordance with the N2000 m water depth depositional paleoenvironment proposed for some parts of the Azúcar Formation (Ordoñez et al., 2006). Although more evidence is required the highly penetrative deformed sediments observed near Ancón (Comp. Fig. 2B) may represent parts of an outer prism in which deformation was more assisted by fluids. Accretionary prisms are common features of the upper part of subduction zones. Based on the reviews of (Clift and Vannucchi (2004) and Noda (2016) the presence of an accretionary prism may result from a significant amount of sediments at the trench (excess of ~1 km) and a great convergence velocity (greater than ~60 mm/yr). Nevertheless, the development of more local prisms is believed to result from other factors such as oblique convergence and terrane accretion. A new model for the formation of an accretionary wedge related to the Azúcar Formation has been recently proposed in new paleogeographic models for the evolution of SW Ecuador and NW Peru (Aizprua et al., 2018). Also, an accretionary-type model has been recently proposed for the evolution of the forearc of NW Peru (Espurt et al., 2018).

Up-section, deformation in the Ancón Group is mainly related to extensional tectonics (Figure 5.12C), although small-scale compressional deformation has been

observed in several locations (Figure 5.6B). The syntectonic style characterized by mass-transport deposits, cliff-scale slump features and extensional faulting most likely defines gravity-driven structures (Figure 5.6C). The presence of instability features and the absence of major compressional deformation suggest that the sedimentation of the Ancón Group occurred after the main period of formation of the accretionary prism. In this context and taking into account that U-Pb ages for the Ancón Group are between ~54 and ~40 Ma it is suggested that the accretionary prism was active mainly between ~55 and ~54 Ma and that probably ongoing, but significantly weaker deformation characterized the prism from ~54 to ~40 Ma. Nevertheless, more efforts are needed to properly constraint the age of the base of the Ancón Group.

The accretion to post-accretion stages form a first depositional stage during which the basin was a turbiditic slope with currents mostly directed in a north south axis (Sites 1 to 3). The overall fining-upward deposits in this system, from the Azúcar Formation to the Ancón Group, marks a progressive decay of the southward tilting linked to the decrease of the activity of the accretionary prism. The final progradation of the slope fan leads to the build-up of a shelf margin where shallower deltaic systems develop as those observed in Sites 4 and 5. Furthermore, the slope may have been directed westwards by the end of deposition of the Ancón Group (Jaillard et al., 1997). The provenance of these sediments is in strike relationship with the magmatic arc developed in the Western Cordillera (Witt et al., 2017). A comparison of the zircon record found in the Paleocene – Eocene sediments of the forearc and the age of intrusive arc-related bodies in the Cordillera may shed some light on detailed provenance aspects and should be considered in further studies.

5.6.2 The outer forearc high

The seaward part of accretionary active margins (accretionary forearcs) is often divided into two parts; the first one, an inner forearc basin usually showing flat-topped or low slope surfaces and related to depocenters evolving between the arc and the

outer forearc high (OFH; a structural high usually coincident with the slope break) and the second one, the outer forearc system which is often coincident with the continental slope. From the earliest works dealing with forearc evolution the OFH was regarded as a major factor controlling the evolution of forearc areas (Dickinson and Seely, 1979). The strong control being simple in nature and related first to the rate at which the OFH rises and second to how the sedimentation rate can pace with it (Dickinson and Seely, 1979; Mitchell et al., 2010). Thus, the trapping of sediments at the inner forearc or the by-pass of sediments through the outer forearc and trench is a major aspect controlling the subduction regime and therefore the architecture of the outer margin. Nevertheless, with some remarkable exceptions as the Nankai accretionary margin in Japan (Moore et al., 2007; Takano et al., 2013; Buchs et al., 2015) or the Great Valley basin in USA (Mitchell et al., 2010) the relationships between the OFH and the forearc basin remain relatively unexplored. Shoaling sedimentation from bathyal or slope to shallow water environments has been observed in many forearc basins with most hypothesis suggesting driving factors ascribed to the uplift of the outer forearc high or to basal sediment accretion (Encinas *et al.*, 2012; Buchs *et al.*, 2015). The river and shallow-water deposits of the Zapotal Formation are bounded to the west by the Estancia Hills (Figure 5.12D). Evidence showed here constrain a compressional regime for the formation of the topographic high; they include: 1) the pervasive thinning of stratigraphic series towards the structural high; 2) the absence of normal faults near the structural high; 3) important erosion related to the presence of debris flows downlapping ancient reflections; 4) onlapping of the Zapotal Fm above the upper part of the debris flow and 5) the high degree of zircon recycling, as evidenced in Miocene series of the Villingota and Subibaja Formations. All of this evidence suggests the activity of a thrust fault, which may be related to the accretionary prism described in the previous sections, although not directly observed in seismic data. It is proposed in this work that the Estancia Hills acts as an outer forearc high (OFH) separating the forearc basin to the west from the accretionary and post-accretionary series to the east (Figure 5.12D). Uplift along this OFH may be important as deep rocks of the Upper Cretaceous volcaniclastics series (cherts of the Santa Elena Formation) crop out near the surface to the southwest of site 7 (Comp.

Fig. 2N). The activity of the OFH seems pervasive during the Neogene as seismic records shows constant thinning of series younger than 32–30 Ma and no Oligocene or younger sediments are observed west of the OFH.

OFHs are crucial features in the evolution of trench-forearc systems.It is believed that formation of an OFH results in a landward increase of accommodation space (Moore et al., 2007; Buchs et al., 2015; Noda, 2016). The evolution of accretionary prims, as other types of fold-and- thrust belts, is controlled by the interaction between internal factors such as the slope of the basal décollement and the topographic surface (the addition of both being the taper), the strength of the materials forming the prism and the décollement and by external factors such as sedimentation and erosion. Thus, fold-and-thrust belts will grow by frontal accretion only when a critical taper is reached. When sedimentation modifies the taper angle deformation often migrates away from the deformation front in order to reconstitute a critical taper. This is the critical taper theory (Dahlen, 1990) extensively used during the last 50 years to analyse the evolution of fold-and-thrust belts. OFHs have been generally ascribed to out-of-sequence deformation (e.g. that resulting from a sub-critical taper in order to gain taper and return to growth by frontal accretion). It is difficult to clearly define what caused the OFH in SW Ecuador to be formed during Oligocene times, but a decrease of the taper angle, inferred here from 54 to 41 Ma and probably subsequently related with a yet-to-be defined non-depositional step during 41–32 Ma may be an option, as no sedi- mentation has been observed for this period. The difficulty in defining the origin of the OFH in the wake of the accretionary prism comes first from the impossibility to clearly define the geometry of the prism and its vergence near the OFH, the vergence of structures shown in Figure 5.12 being related to the clearest vergence observed between sites 3 and 5. Nevertheless, a relationship between the Estancia Hills and the activity of a deep thrust fault was already proposed in the early work of Benitez (1995).

Uplift along the OFH, caused the depositional locus to move eastwards (Figure 5.12E) with syn-tectonic growth strata on-lapping former slope deposits. This is a mechanism very similar to that observed in other forearc – OFH assemblages, such as

the Great Valley Basin (USA; Mitchell et al., 2010) and the Kumano basin (Japan; Moore et al., 2015; Takano et al., 2013). The direction of the OFH probably changed trough time, as extensional and strike slip systems affected the zone during the opening of the GGTB during Miocene to Quaternary times (Witt et al., 2006; Witt and Bourgois, 2010). In any case, based in our knowledge, the Estancia Hill may correspond to one of the best-preserved exposures of an ancient outer forearc high worldwide.

5.6.3 The shallow-water forearc basin infilling

As in other forearc basins related to the formation of an OFH, the Progreso basin depocenter consists of shallow water sediments lying unconformably on deep slope sediments. The onset of the basin resulted from the definite rise of the OFH, isolating the semi-enclosed triangular Progreso basin (protected bay) which fills up mainly with shallow marine sediments (Figure 5.12E), whereas the Peninsula area may have been emerged ever since. The OFH remains stable during the entire basin evolution from ~32 to ~10 Ma, as there is no evidence of basin dissection and outcrops of Oligocene – Miocene deposits in the Peninsula area.

The protected geographic configuration produced by the OFH favours the development of tidal dynamics, which is recorded for the first time in the Subibaja Formation (site 10) at ~16 Ma. The tidal currents running through the Progreso Basin would then have been trending WNW-ESE. Owing to the likelihood that the north-western boundary of this basin (i.e. Chongón-Colonche Hills) was already uplifted, the tides might have entered in the basin from the east (Guayas area). Depending on the local configuration and systems tracts, either flood currents (to the WNW, ex. within channels) or ebb currents (to the ESE, ex. within sand bars) would have dominated. Open coast shoreline deposits might still have existed at this time (e.g. site 10). During the Progreso Formation, the tectonic quiescence of the basin brings about a decrease of the coarse clastic supply, favouring the onset of a carbonate system where oyster patch reefs develop close to the shoreline (site 12). Although the

sedimentary evidence points to forced regression periods a thorough examination of forearc sedimentation in the wake of the eustatic variations during the last 30 Ma is difficult to achieve as field evidence is sparse and the early period of the forearc basin evolution comprised between 30 and 16 Ma has not been yet dated accurately, because of absence of primary zircons. The necessary accommodation for the deposition of the 2–3 km forearc sediments may have resulted from the formation of the OFH (a process suggested for other forearc basins) although the south-eastwards deepening of reflectors may also attest for an increase of subsidence towards the Gulf of Guayaquil-Tumbes basin, which opening period may have started and clear tidal dynamics reached at least in Quaternary times (Reynaud et al., 2018). The sedimentary succession in the upper part of the Progreso basin looks similar to that of other forearc Andean embayments, as those observed in the Valdivia complex in Chile (le Roux and Elgueta, 2000).

The Progreso basin records at least one episode of tectonic inversion as evidenced by the shallowing of reflectors at the Carrizal fault system (structural limit between the Chongón-Colonche Hills and the Progreso basin). Seismic evidence suggests that the main tectonic inversion step took place before ~16 Ma (Figure 5.11B), the basin floor was probably flatter before the inversion. Although, more work is needed to constrain the timing of uplift of the Chongón-Colonche Hills and its eventual relationships with the sedimentary input in the Peninsula and Progreso basin, it seems reasonable that topographic growth in the hills is probably linked with the recycled zircon component from 30 to 16 Ma in the basin; the hills acting as a semi-regional topographic barrier preventing direct sourcing from Andean derived primary zircons. Moreover, this process was of lesser importance or inexistent in the westernmost sections of the hills (Montañita area; site 8) where primary 23 Ma zircons are present.

5.7 Conclusions

The SW of Ecuador exposes a Paleocene to Upper Miocene accretionary, post-accretionary and forearc basin system. Youngest age clusters obtained by LA ICP-MS U-Pb dating on detrital zircon indicate the age of sedimentation, thus outlining the importance of the U-Pb method on zircon for dating sediments that are, at least in part, derived from active volcanic arcs.

Sedimentary and seismic-derived tectonic analysis as well as detrital zircon dating on the Paleocene Azúcar Formation indicates that SW Ecuador represents an oceanic block accreted against the continental margin between 61 and 55 Ma. The Azúcar Formation and coeval deposits located near the Chongón-Colonche Hills were deposited prior to the formation of a complex and regional fold-and-thrust belt system that defines an accretionary prism, whose main activity may have taken place between 55 and 54 Ma. The Ancón Group, the post accretionary series, deposited from ~54 Ma to ~40 Ma and shows pervasive normal faulting and gravitational deposits related to slope instabilities, suggesting a significant decrease of the activity of the accretionary prism. The Azúcar Formation would correspond to the junction of a steepening submarine slope with a basin floor fan (large conglomeratic channels and coarse-grained turbidites). Then, the Ancón Group would record the progressively finer grained turbidites of a slope fan, finally undergoing to mass-transport (mud-dominated turbidites and mass- transport complexes). The transition from the Azúcar Formation to the Ancón Group is denoted by a significant decrease of the topographic profile resulting in shallowing upwards sedimentary series.

The structural high of the Estancia Hills shows Late Cretaceous to Eocene rocks at surface levels. It is characterized in seismic records by debris flows downlapping older and deeper sedimentary units and by continental to shallow water sediments unconformably covering those debris flows. Thus, the degree of zircon recycling is manifestly higher next to the structural high. It is proposed in this work that the structural high defines an outer forearc high (OFH), typical of forearc basin such as those observed in the Kumano (Japan) and Great Valley (USA) basins. The evolution

of the OFH is most likely related to the uplift of a thrust slice during 32–30 Ma, coeval with deposition of the coarse-grained shallow-water to continental Zapotal Formation. Evidence presented here suggests the existence of a stable outer forearc high limiting the forearc depocenter for at least 20 Ma and creating the necessary accommodation for a ~3 km thick forearc sedimentary package. The forearc sediments are related to shallow water environments (Formations Dos Bocas, Villingota, Subibaja and Progreso) ranging from littoral to tidal facies most likely related to a triangular protected bay that mimics the architecture of the forearc depocenter. The youngest sediments dated here belong to the Progreso Formation and yielded a ~10 Ma age. Supplementary data to this article can be found online at https://doi.org/10.1016/j.sedgeo.2018.11.009.

Acknowledgements

We would like to thank Petroamazonas, and especially Manuel Rivera for letting us to publish the seismic material. Patrice Baby, Galo Montenegro, Juan Abella and Nelson Jimenez are kindly thanked for helpful discussions in the field. Reviews of A. Noda and G. Moore were very appreciated and improved the quality of this paper. This work was fund by Petroamazonas (Ecuadorian Petroleum Company) and INSU (Institut National de Sciences de l'Univers, France).

Chapter 6

Tectonostratigraphic evolution at the termination of a trench-linked continental transform boundary: Gulf of Guayaquil-Tumbes Basin, southernmost Northern Andes

The content of this chapter is in preparation for submission: ***Aizprua, C****., Reynaud, J-Y, Witt, C., Barba, D. Tectono-stratigraphic evolution at the termination of a trench-linked continental transform fault boundary: Gulf of Guayaquil-Tumbes, southernmost Northern Andes*

The lithospheric stress imposed at convergent margins under oblique subduction may result in strain partitioning both normal and parallel to the trench. Indeed, trench-parallel large scale strike-slip faults can prolong for hundreds of kilometres, very likely bounding different forearc crustal slivers. The mechanisms for its development are well documented in offshore Sumatra, Western North America, to mention some examples. However, few cases discuss the formation of sedimentary basins at the trailing edge of such large-scale trench-linked faults in the presence of trapped oceanic slivers and their link to the trench. Based on multi-channel seismic profiles, industrial well data, surface rock exposures, and preliminary radiometric age results, we attempt to make a palinspastic reconstruction of one of such structures at the southernmost Northern Andes, where basin geometry have characteristics of a

continental transform basin controlled by a paleo-obduction suture and the lateral movement of a remnant accretionary wedge.

6.1 Introduction

The strain partitioning imposed by the lithospheric stress at convergent margins under oblique subduction is well documented from surface and geodetic studies (e.g. the Kuril arc, Kimura (1986); Sumatra, Fitch (1972); Huchon and Pichon (1984); Philippines, Barrier et al. (1991); Peru-Chile trench, Hoffmann-Rothe et al. (2006)) and by physical analogue modelling (e.g. Chemenda et al., 2000; Haq and Davis, 2010). The resulting trench-parallel deformation under oblique subduction is characterized by large-scale strike-slip faults, known as trench-linked strike-slip faults (Sylvester, 1988), which can prolong for hundreds of kilometres (Teyssier et al., 1995; Haq and Davis, 2010). Transtensional and transpressional structures characterize these areas, commonly located ~100 to 300 km inboard the trench (Fitch, 1972; Woodcock, 1986; Berglar et al., 2017). Indeed, trench-linked fault subsiding corridors are at the origin of major active margin sedimentary basins (Mann, 2007; Noda, 2013). Their location and evolution, still poorly understood, may reflect inherited mechanical heterogeneities of the margin basement (Vauchez *et al.*, 1998), together with the interplay of active magmatic processes (Philippon and Corti, 2016).

Active margins may also involve the accretion and trapping of oceanic crustal sliver along the margin, possibly leading to transform faults associated basins. Their structural configuration and the sedimentary infill across continental transform basins are well documented from the study of outcrop and subsurface studies (e.g. the Northern Anatolia fault, Aksu *et al.* (2000); Okay *et al.* (2000); Lake Izabal in Central America, Bartole et al. (2019); the Northern Andes, Audemard (2009); Escalona et al. (2011)). Commonly described as pull-apart basins (Ben-Avraham, 1992; Seeber et al., 2010), they seem to share some common characteristics like 1) an asymmetric shape, 2) migrating depocenter opposite to that of sediment supply direction, 3) coarse-grained marginal facies along the active master fault, and 4) predominance of fine-grained facies (e.g. Ben-Avraham, 1992; Seeber et al., 2010; Noda, 2013). Analog

modelling of the transtensional faulting patterns at pull-apart and transform fault associated basins, presented by Basile and Brun (1999), suggest a strong dependence on the rheological layering.

Despite our general knowledge of sheared zones at convergent margins under oblique subduction, the linkage between the trench-linked fault systems or reactivated major lithospheric boundaries towards the trench remains under-research. The east limit of the Northern Andes is a clear example of a trench-linked fault system controlled by a lateral rheological variation, inherited from the accretion of an oceanic crustal sliver from the Caribbean Large Igneous Province during Late Cretaceous (Whattam and Stern, 2015). A rheological boundary that appears to control, at least partly, the location of the trench-linked fault system since Middle Miocene (e.g. Ecuador, Alvarado et al. (2016); Venezuela, Audemard (2009)). This fault system may have developed in response to a change in the subduction direction and velocity during the Miocene (Pardo-Casas and Molnar, 1987). In Ecuador, the system is known as the Chingual-Cosanga-Pallatanga-Puna (CCPP) fault system, more commonly known as the Guayaquil-Dolores megashear zone between the North Andean Sliver (NAS) of oceanic affinity and the South American Plate (Figure 6.1-A).

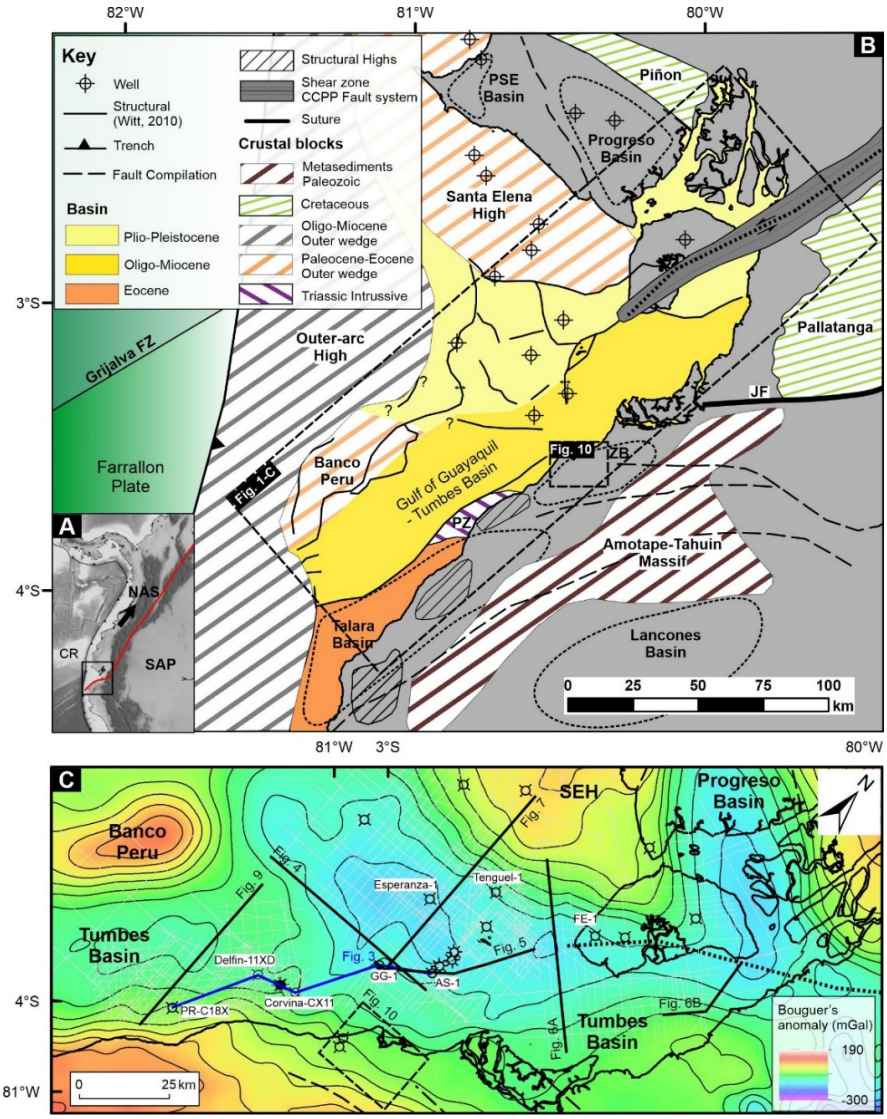

Figure 6.1: Location map of the study area. A) regional shaded topographic map of the Northern Andes indicating the location of the study area. The red line delimits the North Andean Sliver (NAS) from the South American Plate (SAP). B) Close-up look to the study area showing the location of the Gulf of Guayaquil-Tumbes basin, and the main structural elements. C) Bouguer's gravity anomaly map along the Gulf of Guayaquil – Tumbes basin. High positive anomaly values coincide with the location of the Banco Peru to the southwest and the Santa Elena High and southern extent of the Chongón Colonche Hills to the north. In between these two-last anomalies, a gravity low with a triangular-shape coincides with the Progreso s.s basin. The GGTB is bordered by the described anomalies and governed by negative values, that become positive farther south near the location of the exposed Amotape-Tahuin Massif. CR: Carnegie Ridge.

Both, the suture and the CCPP fault system diverge from each other towards the south, at the Gulf of Guayaquil-Tumbes basin (Aizprua et al., 2019b), where the deformation becomes diffuse. This area and its westward continuation along the Tumbes area is characterized by the development of Cenozoic basins, which have been attractive for hydrocarbon exploration purposes. Most of the existing published work has focused on the thick upper Pleistocene depocenter, attributed to a process of tectonic escape (Deniaud et al., 1999; Witt et al., 2006; Aizprua et al., 2019b), and less attention on the Miocene or older intervals.

In this study, we use primarily 2D industrial seismic reflection data, wireline logs, and outcrops descriptions to investigate the temporal and spatial evolution of the main structural elements and to provide insights on the role they have played in the development of the main gross depositional environments in the area.

6.2 Regional Geological Framework

6.2.1 Structure

The Gulf of Guayaquil - Tumbes basin (GGTB) may be considered a sub-basin of the Progreso Basin Province (Higley, 2004b), located between 3°S and 4°S at the southwestern region of the Northern Andes. The GGTB is located at the border between northwest Peru and southwest Ecuador, in a region characterized by a broad continental shelf and large tidal systems, atypical of actives margins (Reynaud et al., 2018). The GGTB is a ca. 90 km wide by ca. 230 km long monoclinal to half-graben structure, subdivided by the Amistad and Corvina ridge structures (Aizprua et al., 2019b) (Figure 6.1-B). A particular aspect of the GGTB is its NE-SW orientation, oblique to most of the area's forearc basins (Figure 6.1).

Different tectonic elements delimit the basin, possibly originated following the accretion of a sliver from the Late Cretaceous-Caribbean Large Igneous Province (Aizprua et al., 2019b). From west to east, the basin is bounded towards the north by 1) a flat top structural high called “Banco Peru” of possibly oceanic origin (Espurt et al., 2018; Aizprua et al., 2019b); 2) the Domito outer forearc high, which consist of a

series of en-echelon folds possibly controlled by deep sitting faults and mud diapirism (Witt and Bourgois, 2010); 3) at the centre by the most distinct element, the Santa Elena High (SEH), a structural high bordering a great portion of the basin; and 4) an unclear structural relationship and connection to the southern prolongation of the Progreso s.s. basin through the northern area of the Puna island (Benitez, 1995; Aizprua et al., 2019b).

The Banco Peru high has not been penetrated by any well yet. In contrast, the SEH outcrops along the SW coastal area of Ecuador and the offshore prolongation has been subject to hydrocarbon prospection. Both surface and subsurface data across the SEH account for highly deformed Late Cretaceous to Paleocene rocks evidencing the collisional stage of oceanic terranes and the arrival of the first continental-sourced sediments to the forearc region (Benitez, 1995; Jaillard et al., 1995; Aizprua et al., 2019b; Vallejo et al., 2019; Witt et al., 2019b). Recent studies of the area suggest that the Progreso s.s. basin, east of the SEH, is controlled by the local development of an outer forearc high (the so-called "Santa Elena High") at least since the Oligocene (Aizprua et al., 2019b; Witt et al., 2019b) and possibly genetically connected to the GGTB (Aizprua et al., 2019b).

Southward of the SEH, from east to west, the basin is delimited by rocks of oceanic plateau origin (Pallatanga Formation), accreted to the margin during Late Cretaceous; and both geochemical and age equivalent to the underlying basement in the Progreso s.s. basin (Vallejo et al., 2009; Witt et al., 2019b). The Jubones fault delimits the southwestward inland extent of these oceanic rocks (Figure 6.1), considered the southern suture's vestige between the Late Cretaceous oceanic rocks and the metasediments and crystalline rocks forming the continental Amotape Tahuin Massif. The latter extends to the west, shifting from a near E-W to NE-SW orientation. South of the Banco Peru, the GGTB is delimited by the Pilar de Zorritos basement uplift. This boundary coincides with the southern edge of the Dolores-Guayaquil megashear zone and delimits to the south the Eocene Talara basin (Higley, 2004a).

The formation of the GGTB has been linked to different plate tectonic processes that range from terrane accretion and docking (Aizprua et al., 2019b), subduction

dynamics with a strong sediment accumulation and recent ridge subduction (Espurt et al., 2018), and tectonic scape (Daly, 1989; Egbue and Kellogg, 2010; Witt and Bourgois, 2010; Aizprua et al., 2019b). The latest leading to the development of a large depocenter (Esperanza through), marked by a strong negative Bouguer anomaly (Witt and Bourgois, 2010; Bourgois, 2013; Aizprua et al., 2019b). Several authors (Deniaud, 2000; Witt et al., 2006; Witt and Bourgois, 2010) seem to have a consensus on the main phase of the opening of the basin by the Pliocene reaching its climax at the upper Pleistocene. However, major discrepancies appear in the mode of deformation. For instance, Deniaud et al. (1999) locates the basin at the southern tip of the Dolores-Guayaquil megashear (Campbell, 1974), and interpreted it as a pull-apart type basin. In contrast, Witt and Bourgois (2010) argue that the fault system along the Gulf of Guayaquil is disconnected from the trench and proposes that the GGTB is a particular type of pull-apart basin controlled by major detachments that prolong at depth and may follow a proto-obduction suture zone.

Recently there has been a distinction between the Gulf of Guayaquil and the Tumbes basins, the latter being related to a northwestward propagation of thrust-related structural highs involving continental/oceanic basement rocks (Espurt *et al.*, 2018; Stéphane *et al.*, 2018). However, Aizprua *et al.* (2019b) suggest that those depocenters are genetically related through a margin configuration inherited from a plate instability and trench retreat process generated by the collision and accretion of a sliver from the CLIP, which stabilized by the Eocene. Evidence for such processes are encounter across the SEH and the Progreso basin (Jaillard *et al.*, 1995; Aizprua *et al.*, 2019b; Witt *et al.*, 2019b).

6.2.2 Stratigraphic framework

North of the GGTB (Figure 6.1), the region is characterized by the infilling of a Late Cretaceous marginal basin, possibly associated with an intra-arc basin developed previous to the collision and accretion of a sliver from the Caribbean Large Igneous Province (Jaillard *et al.*, 1995; Van Melle *et al.*, 2008). The outcrop exposures along the northern limit of the Progreso basin (Figure 6.1) evidence the presence of

volcaniclastic material overlying the mafic units from the Piñon Formation, which constitutes the forearc basement of the Progreso s.s. basin. Towards the south, across the Santa Elena High, the late Cretaceous succession appears highly deformed and overlain by a Paleocene accretionary succession, dominated by a series of high-density turbidities with evidence of the first sialic input (Jaillard *et al.*, 1997). This stratigraphic interval is interpreted as an accretionary outer wedge possibly following the collision and accretion of an oceanic sliver (Aizprua et al., 2019b). Such successions are not observed farther south, and instead, the metamorphic and crystalline Paleozoic basement appears unconformably overlain by Eocene rocks, south of the GGTB at the Talara Basin (Fildani *et al.*, 2008). Lithological similarities between the Eocene successions across the Talara basin and the Santa Elena High may suggest its presence deeply buried across the GGTB. The deepest successions encountered both onshore and offshore within the GGTB are the early Oligocene coarse-grained clastic successions of the Mancora formation, an equivalent to the Zapotal formation in the Progreso basin (Figure 6.2). These series probably represent the onset of the Progreso forearc s.s. basin development in the area and possibly of the GGTB (Aizprua et al., 2019b; Witt et al., 2019b). During the Late Oligocene – Early Miocene, the basin may have been subjected to accelerated rates of subsidence or transgressions, resulting in its drowing and deposition of an open marine mudstone-dominated succession (Heath/Dos Bocas formations) (Figure 6.2). At the GG-1 well (Figure 6.1) the Middle Miocene succession (Subibaja/Zorritos Formation) consists of two units, a lower one dominated by multicolour siltstones deposited near the littoral and an upper one dominated by continental lacustrine facies, marking the end of a prolonged transgression according to Benitez (1995). The two main members of the Subibaja formation are top-bounded by a semi-regional unconformity that appears to be enhanced near the structural highs (Aizprua et al., 2019b). This succession is overlain by deposits from the Progreso/Tumbes Formation, characterized by shallow marine deposits at the base that shallow upward into estuarine conditions towards the top (Benitez, 1995). The uppermost section, previously interpreted as a part of the Progreso Formation, has been redefined as the lower Puna formation, deposited within a continental shelf environment (Benitez, 1995). This interval is then overlain by the

Pleistocene Upper Puna formation (Placer/Mal Pelo Fm., Figure 6.2), coincident with an increase of sediment input and significant subsidence in the basin, representing up to 3000 m of estuarine-deltaic to shallow marine deposits (Benitez, 1995).

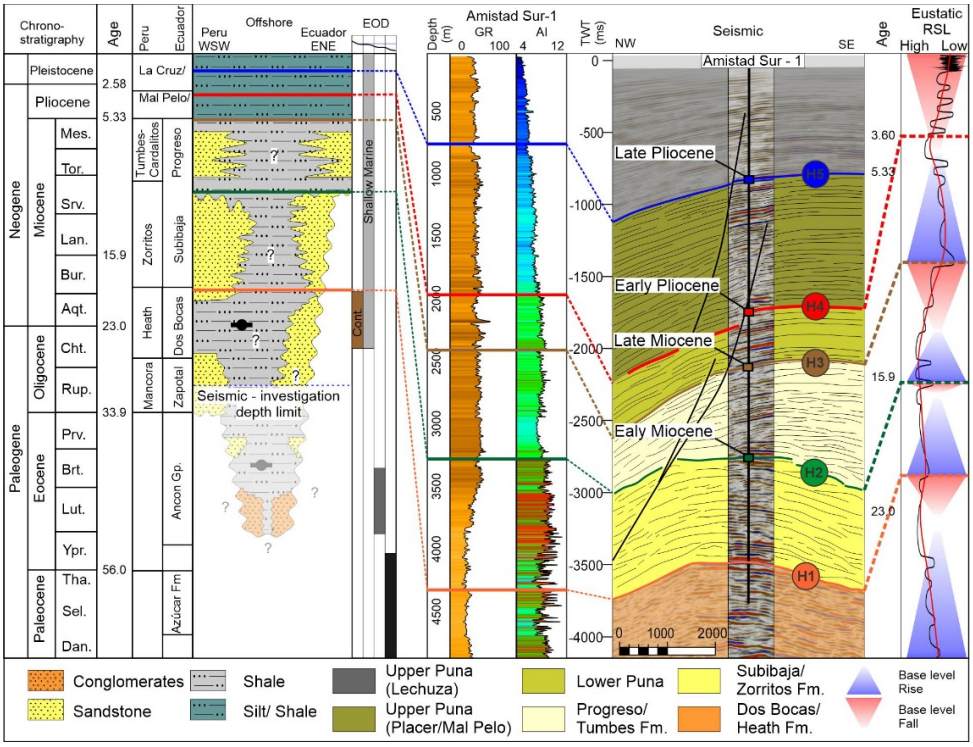

Figure 6.2: Chronostratigraphic chart for the Gulf of Guayaquil – Tumbes shelf (based upon Aizprua *et al.*, 2019b) highlighting the Early Oligocene to recent Pleistocene stratigraphy along a WSE-ENE trend. Seismic reflections to stratigraphy correlation at well Amistad Sur-1. The gamma-ray log is displayed next to the environment of deposition interpreted in Benitez (1995). Top U1 is characterized by an erosional character and an increase in acoustic impedance. Top U2 is defined by a decrease in acoustic impedance and is aged as Late Miocene (Ordónez *et al.*, 2006).

6.3 Data & Methods

Different 2D seismic surveys are used for this study, with a total length of ca. 7000 km of interpreted seismic profiles. The seismic consist of post-stack time migrated and unmigrated data of varying quality. The different seismic surveys were

acquired at different periods, between the ’80s and ’90s, by the different operating companies. As the GGTB lies in between Ecuador and Peru, a key challenge is posed by the lack of data continuity across the border. From east to west, the study area is covered by 2D profiles oriented in NW-SE and NE-SW direction and a separation of ca. 2.5-3 km. Before carrying out the mapping of the different reflections, a series of post-stack seismic attributes were applied to the different seismic surveys to homogenize the profiles for interpretation purposes. First, an amplitude dynamic range balance was applied followed by a structural smoothing and an Ormsby frequency filter with a central frequency of 20 Hz. Upon this procedure, the different seismic profiles were comparable in their frequencies and amplitudes across the different seismic surveys.

The work carried out during this study consisted of two main components: 1) interpretation of existing industrial seismic profiles to outline the tectonostratigraphic configuration of the basin to define its evolution across the offshore area, and 2) an analysis of the structures and sedimentary facies of middle Miocene age found along the NW onshore Peru. The observations made at the surface then linked to the regional interpretation to elucidate the main controlling parameter on the sediment dispersal across the basin.

6.3.1 Structural & stratigraphic seismic interpretation

The approach here to define the main horizons to interpret is based on detecting clear acoustic impedance boundaries at the well position and linking them to their near geological or formational top definition. The well to seismic tying was carried out at offshore exploration wells located near the NW margin of Peru (Figure 6.1). The Amistad Sur-1 well shows the interpreted horizons together with their age equivalent for demonstration purposes of the interpretation strategy. This same well is key to expanding the mapping towards the east throughout the Jambelí area, which lacks well control. For the Tumbes area, a well located in the Corvina field was tied to the seismic following the same procedure described above. The northward extension of the mapping across the Esperanza through or the Puna Island was highly uncertain due to

the quality of the seismic and the complex structuring of the area. Nevertheless, regional trends on thicknesses from the Progreso basin, and surface exposures located across the Puna Island aid to better constrain the dubious areas.

6.3.2 Outcrop exposures

The onshore area of NW Peru consists of exposures from Cenozoic successions, allowing a direct recognition of the different sedimentary facies to interpret plausible depositional environments. Different field campaigns were carried out during 2015 and 2016 for mapping the different sedimentary facies in an attend to reconstruct the paleogeographic environment of the area and linked it to the offshore to build a regional tectonostratigraphic interpretation. The association of the different sedimentary facies and their interpretation was later constrained in the age of deposit through radiometric age dating of U/Pb in zircons.

6.4 Tectono-stratigraphic units of the GGTB

Four tectonostratigraphic units have been identified from seismic data and characterized using electrofacies and former lithological descriptions both at surface and subsurface. The oldest unit here mapped through the study area is of early to middle Miocene age, corresponding to the Zorritos/Subibaja Formation. Despite seismic profiles showing reflectivity below this unit, the lowermost interval is poorly defined to be mapped across the study area. Thus it is considered as an undefined Eocene to Late Oligocene unit. It is not fully described in this work; however, key observations have been incorporated into the proposed model.

The different seismic units have been mapped across the offshore area, partly extending it north across the Santa Elena High and the southernmost extent of the Progreso basin (Figure 6.1). In Figure 6.2, we can observe a well that penetrated all the units here presented, along with its log responses and seismic section along the wellpath.

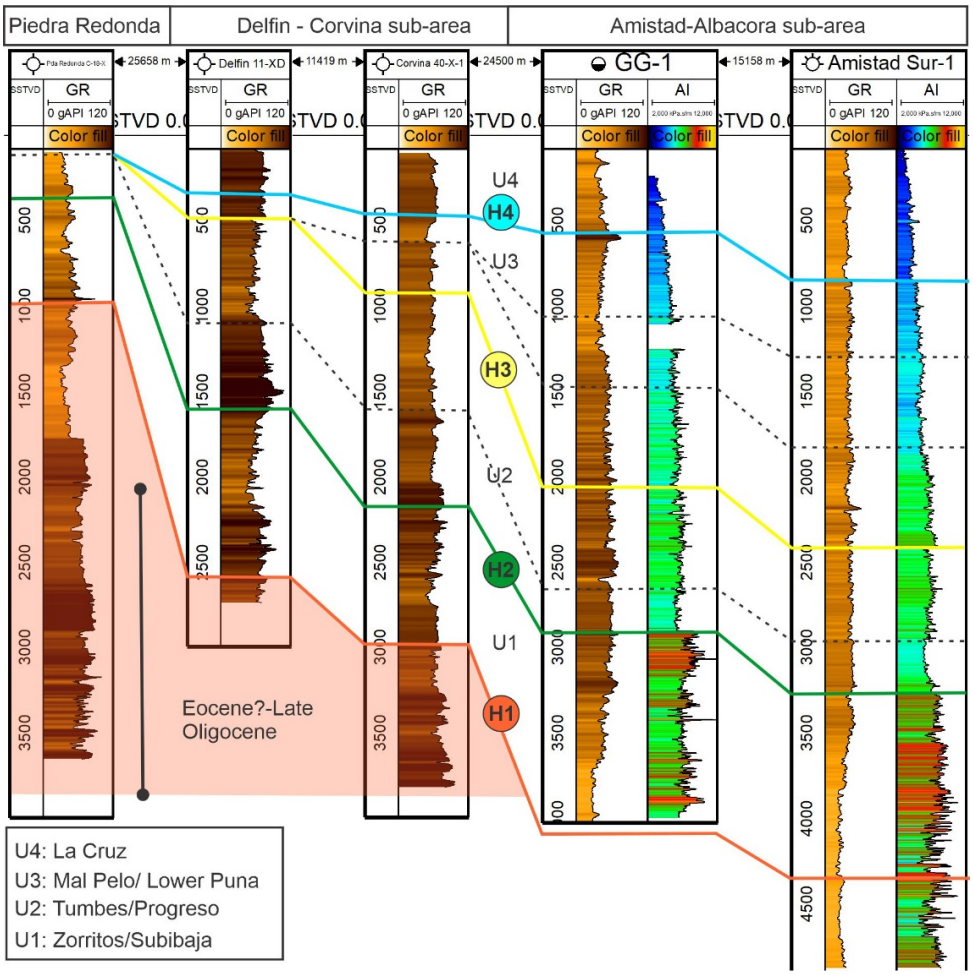

Figure 6.3: NE-SW well log correlation from the Amistad field to the Piedra Redonda structural high. AI: Acoustic impedance.

6.4.1 Early to Middle Miocene (Unit 1)

The hydrocarbon fields located at 10 to 20 km north of the coastline have targeted the early to middle Miocene deposits, presented as unit 1. At the centre of the basin, at the Albacora/Amistad area, 2 wells with a good set of well logs are available for this study (GG-1 and AS-1, Figure 6.1). These wells are our reference point for expanding the interpretation farther to the east, where there are not well observations (Figure 6.1). Both wells reached the base of the seismic unit U1 (Figure 6.3), which

on seismic profiles appears to tie to a reflection event captured on the 3D data but poorly resolved on the 2D data. Hence, the base of U1 is uncertain, especially north-westward into the Esperanza through. Seismic profiles across the Albacora/Amistad area show deeper reflections to those associated with U1 (Figure 6.4), however, as mentioned previously, the 2D seismic profiles are poorly imaged below 4s (Figure 6.4), apparently, the depth of investigation of the survey campaigns, impairing the regional mapping of deeper units.

The well Amistad Sur-1, located in the Albacora/Amistad area at ca. 20 km north of the coastline (Figure 6.2), penetrated the entire section of U1. A calculated acoustic impedance log marks an interval of high acoustic impedance (Figure 6.2) comparable to the one observed in the GG-1 well, 15 km to the west (Figure 6.3). U1 is characterized by an upward increase in gamma-ray, which slightly differs from the Corvina area farther to the west (Figure 6.3). The basal section of U1 at the Corvina well has higher values than the Amistad-1 well, possibly indicating a homogeneous silty clay and very likely a much coarser-grained interval in the Albacora/Amistad area (Figure 6.3). Figure 6.4, shows an E-W oriented seismic profile, with its eastern section located in between wells AS-1 and GG-1 (3 and 5 km of distance respectively to the profile). At the same location, two apparent folded and narrow structures with continuous reflections, within U1, appear to be truncated by an erosional surface, characterized by strong amplitudes (white arrows, Figure 6.4). Similar structures with a higher fold amplitude are observed farther west into the South Domito area; however, the seismic quality impairs to properly recognized internal reflections or geometrical relationship that may indicate truncation of U1. It is worth to highlight that the fold structure, defining the Albacora field, appears to be controlled by a decollement fold, as deeper reflections are weakly deformed or folded (Figure 6.4).

Farther to the east and northeast from the Albacora/Amistad, a composite seismic profile running from west to northeast, tie to the GG-1 and AS-1 wells, shows the transition into the Jambelí area, highlighting an increase in the thickness of unit U1 (Figure 6.5). Furthermore, across the Jambelí area, U1 is marked by the lack of folded structures, as shown in Figure 6.5. Instead, it is characterized by a monoclinal

geometry such as an asymmetrical graben dipping to the northwest (Figure 6.6), a similar description is presented previously by Benitez (1995). U1 shows a tabular-shaped geometry with a slight thickness increasing towards the north, near the location of the Puna island (Figure 6.6-A). This unit decreases in thickness across the CCPP fault system and become structurally shallower with surface exposure at the Puna island (Puna-1, Figure 6.3). U1 is internally characterized by discontinuous to continuous reflections. Some apparent bi-directional downlap terminations and short distance-high angle progradation packages up-dip, topped by high amplitude reflections (Figure 6.6-A) as those shown in Figure 6.4. Northward, U1 is up to ~1 s with low amplitude and broken reflections. U1 is onlapping onto what is interpreted as the southern prolongation of the Paleocene Santa Elena High (SEH), an outer forearc high controlling both the Gulf of Guayaquil-Tumbes and Progreso basins according to Aizprua et al. (2019b).

Towards the west at the Tumbes sub-basin, a seismic profile oriented in a SW-NE direction crosses the southern realm of the basin controlled by a large E-W fault (F4, Figure 6.10). The footwall of F4 is penetrated by the Piedra Redonda well at the location of a narrow horst, bounding to the south a north dipping half-graben structure, conforming the Carpitas - Zorritos High (Figure 6.10). This structural high continues landward to the east, where exposures of the offshore equivalent U1 and underlying deposits are found (Figure 6.7).

6.4.1.1 Surface exposures

The eastward extend of the F4 footwall, shown in Figure 6.10 correlated with an E-W trending basin of Neogene age, the Zorritos sub-basin, located in the transition between the GGTB and the Talara basin to the south (Figure 6.7). Near the coastline and landwards, a series of gullies provide direct access to surface exposures of middle Miocene age equivalent to the offshore U1. Two main sections have been studied in the present work to assess the main depositional facies of the succession deposited during this time and their possible interplay with the underlying structure.

The present-day N-S Bocapan river, located to the west of the Zorritos town, allows direct access to the different sedimentary processes within U1 and underlying units (Figure 6.7). The Bocapan gulley in the southward direction follows half-graben configuration observed south of the Piedra Redonda well location (Figure 6.7), with a gentle northward and decreasing dip of the different sedimentary units.

At the Bocapan gulley we encounter thick sequences of gray silts changing into a chocolate-colour silt with laminae and interbedded primary-gypsum veinlets, followed by a discontinuous surface containing meter scale sandstone layers marked by the presence of bivalves defining the contact to the overlying U1. A NS outcrop-oriented profile, in Figure 6.9, shows apparent large-scale downlaps onto the brownish silts from the Heather Formation, with an accretion geometry towards the north. The coarsening upward pattern from the Heath into the Zorritos Formation can be interpreted as a progradational tract of facies. An overall deltaic interpretation can be proposed for the Zorritos Formation at this location. The presence of gravelly channels cutting across the HCS beds would correspond to delta-front deposits.

Northeastward of the Bocapan gulley, along the coastal road, the surface exposures are characterized by a series of discontinuous cliffs near the Zorritos town (Figure 6.7), apparently affected by a system of transverse faults to the main E-W depositional strike. One of the most striking outcrops near the Zorritos town, is shown in Figure 6.9-B, which highlights a steep surface bounding the yellowish coarsening upward succession of the Zorritos Formation from the brownish sediments of the Heath Formation. This outcrop together with another one 600 m farther to the ENE near the coastline account for sedimentary facies associated with shoreface to upper shoreface settings. The Zorritos Formation sediments appear to onlap onto the mentioned surface, which may indicate a possible syn-sedimentary deformation of the Heath Formation, which internally shows shear deformation characteristics.

Approximately at 5km southeast from the Zorritos town, and along the Casitas gully (Figure 6.9-*C*), we found a complex sedimentary setting, characterized by conglomerates' presence within a dominantly marly background. From base to top, the succession is overall finning upward and can be split into two intervals. The lower

interval is dominated by erosional to scour surfaces and the presence of large heterolithic blocks, in a. finning upward sucession. (Figure 6.9-C). The conglomeratic fraction decreases upwards, where it becomes dominated by sandstones lenses within a silty to muddy background, suggesting an overall transgressive tract. This interval is also characterized by the presence of sand injectites, present as cm scale-dikes. The chaotic interval observed in the lower part of the outcrop shown in Figure 6.9-B may represent a mass transport deposit originated or partly controlled by underlying reactivated faults. According to seismic profiles presented by Espurt *et al.* (2018), located near the study area, these faults were active during the Oligocene and sealed by the Miocene. An interpretation that is in accordance with ours offshore near the Albacora/Amistad area along the seismic profile is presented in Figure 6.5.

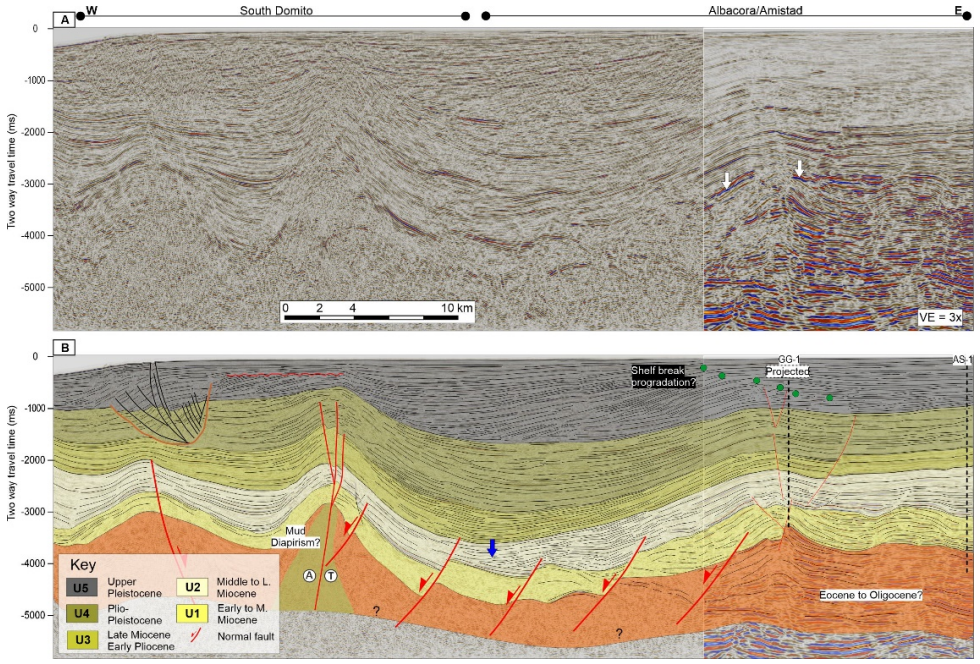

Figure 6.4: a) E-W seismic section across the Amistad-Albacora sub-area to the east, and the Domito domain to the west. (b) Interpreted seismic section in (a), showing the main seismic units covered in this study.

6.4.2 Middle to Late Miocene (Unit 2)

The lowermost part of U2 seems to fill in the topographic relief that resulted from the erosional event at the end of U1. Typically characterized by continuous reflections across the Albacora/Amistad are and towards the Jambelí area (Figure 6.5). U2 appears to be controlled to the west by an eastward tilted structure, as U2 seem to onlap onto U1 (blue arrow, Figure 6.4)

At the Jambeli area, U2 is the thickest of the units (up to ~2s) with internal seismic reflections apparently folded against the SEH structure (Figure 6.6-A). The latter possibly associated with an extensional fault-propagation fold mechanism. U2 is characterized by internally low amplitude reflections in its lower part onlapping updip onto the top of U1, with an increase in reflection continuity and amplitude strength (Figure 6.6-A). The upper part of U2 becomes more aerial extensive primarily characterized by continuous reflections across the half-graben. At the deepest part of the graben, there is an interruption on the continuity of the reflections, characterized by a feature with a chaotic pattern that expands from bottom to top across the stratigraphy, possibly related to either hydrocarbon migration pathways or mud diapirism, or a combined mechanism (Figure 6.6).

Towards the east, U2 decreases in thickness apparently unconformably overlying the acoustic basement, as U1 and underlying units pinch-out against the possible northward continuation of the Pallatanga block (Aizprua *et al.*, 2019b) (Figure 6.6-B). The interpretation of U2 across the down faulted block of F2 is uncertain, however the onset of F2 is estimated as an ealy Pliocene event, thus not major thickness increase of U2 is expected.

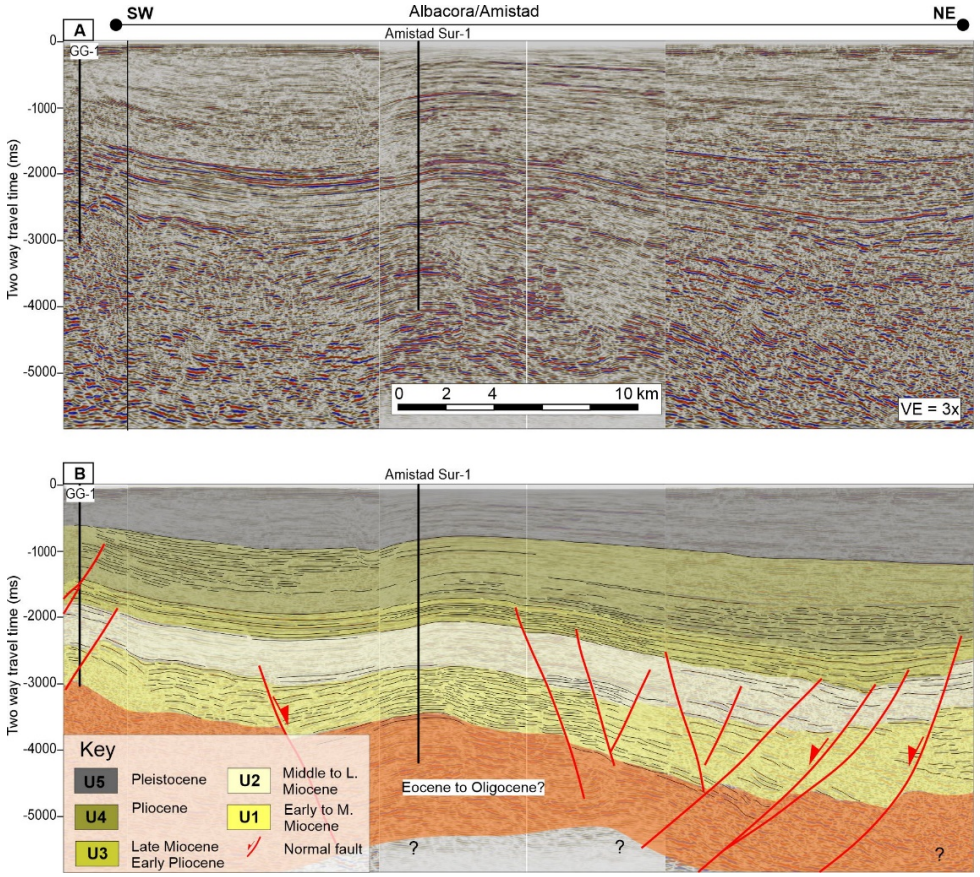

Figure 6.5: a) WSW-ENE composite seismic section across the Amistad structure into the Jambelí sub-area (b) Interpreted seismic section in (a), showing the main seismic units covered in this study.

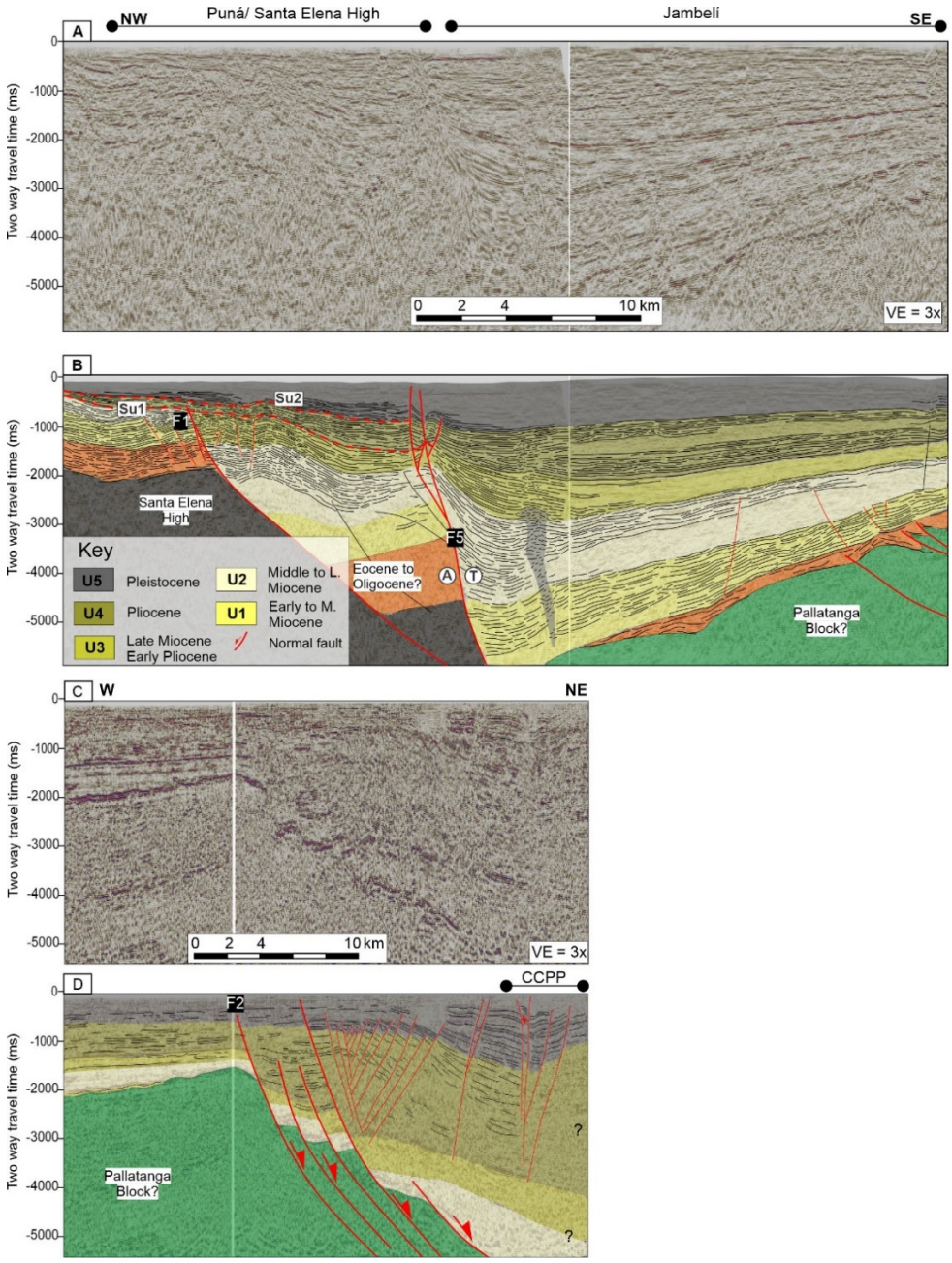

Figure 6.6: a) NW-SE seismic section across the Jambelí area into the Santa Elena High. (b) Interpreted seismic section in (a), showing the structural configuration of the Jambelí area characterized by a half-graben geometry. Notice the growth strata towards the footwall of F5, and the down faulted block from the Santa Elena High with thickness of units U1 and U2

comparable to the hangingwall. There is a lesser thickness expansion of U3 across the Puna fault suggesting a quiescence fault activity period at this time.

6.4.3 Early Pliocene (Unit 3)

Opposed to the units U1 and U2, U3 seems to be a period of relative tectonic quiescence, as it appears as a blanket of even thickness over large areas (Figure 6.5 and Figure 6.7) and with a maximum thickness of up to 1s. U3 follows a pattern observed on the upper section of U2 with continuous reflections, however, of lower amplitude across the Jambelí area. This unit is tight to the AS-1 well as the early Pliocene Puna Formation (Figure 6.2).

Across the Esperanza through, however somehow uncertain, unit U3 appears to have similar characteristics like those presented in the Jambelí area, with thicknesses slightly increasing in a wedge-shaped geometry northward into chaotic-low amplitude reflections that seem to onlap onto an acoustic basement, most likely the southward prolongation of the SEH (Aizprua *et al.*, 2019b). These units appear to be characterized by a series of continuous reflections at the hanging wall of F3, which connects to the Amistad fold structure to the east.

6.4.4 Plio-Pleistocene (Unit 4)

The onset of a NE-SW extensional regime is marked at the top of U3 (Early Pliocene), by the expansion of the unit U4 across the Esperanza though (Figure 6.10). The faults F1 and F3 appear as boundary faults for the location of the depocenter. Across the Esperanza through U4 and overlying unit are characterized by extensional faults, apparently conformable to the crest of an E-W low amplitude fold at the centre of the Esperanza trough. The fault systems within U4 and above appear disconnected, layered bounded, from the fault system affecting the underlying units U1 to U3, oriented in a NE-SW direction. A very similar structural style is observed at the east of the Jambelí area, across a clear NW-SE crustal fault (Figure 6.6-B).

Towards the west of the Albacora/Amistad area, there is a clear structural control on the development of the U4 depocenter and units above by the uplift and development of tight folds (Figure 6.4), an area attributed to the development of an

outer-wedge through deep sitting faults and mud diapirism (Collot *et al.*, 2002; Witt and Bourgois, 2010; Bourgois, 2013; Aizprua *et al.*, 2019b). The seismic unit overlying U4, which is not described in this study presents a rapid progradational pattern clearly observable by the westward migration of interpreted shelf break points (Figure 6.4). This unit may represent the Lechuza member, in the upper Puna formation, described by (Benitez, 1995).

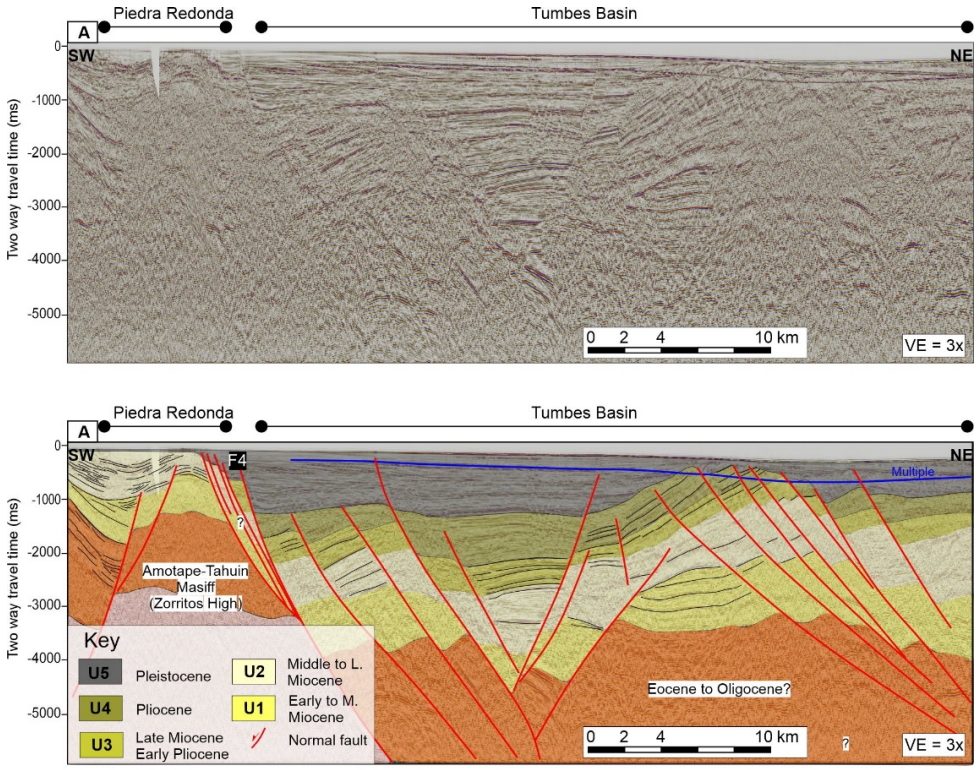

Figure 6.7: a) SW-NE seismic section across the Tumbes sub-basin (b) Interpreted seismic section in (a), showing the structural configuration of the Tumbes sub-basin showing an area of an apparent symmetric graben geometry at the centre. The footwall of fault F5 is approximately 10km west of the onshore Zorritos sub-basin, allowing for a direct onshore-offshore comparison.

.

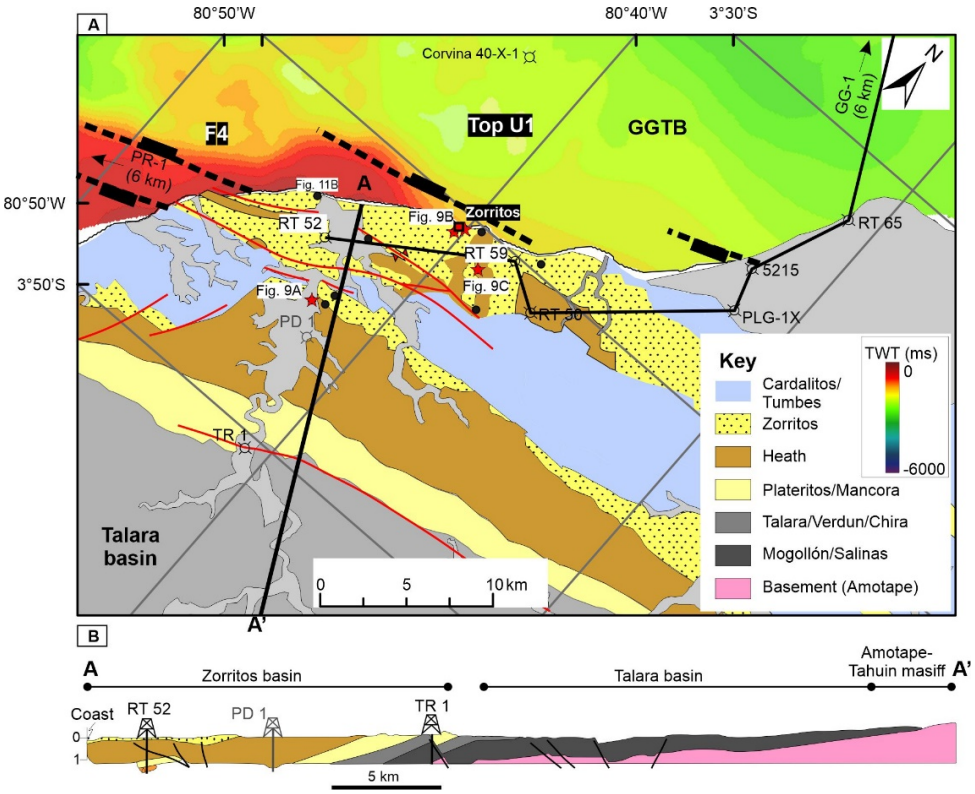

Figure 6.8: a) Geological map of the Zorritos sub-basin, located south of the Gulf of Guayaquil-Tumbes basin. This sub-basin correlates to the Piedra Redonda structure to the west, defined by faulted blocked. b) An NNW monoclinal dipping structure with upward decreasing dip of the sedimentary successions. The Amotape-Tahuin massif conforms the basement of this sub-basin.

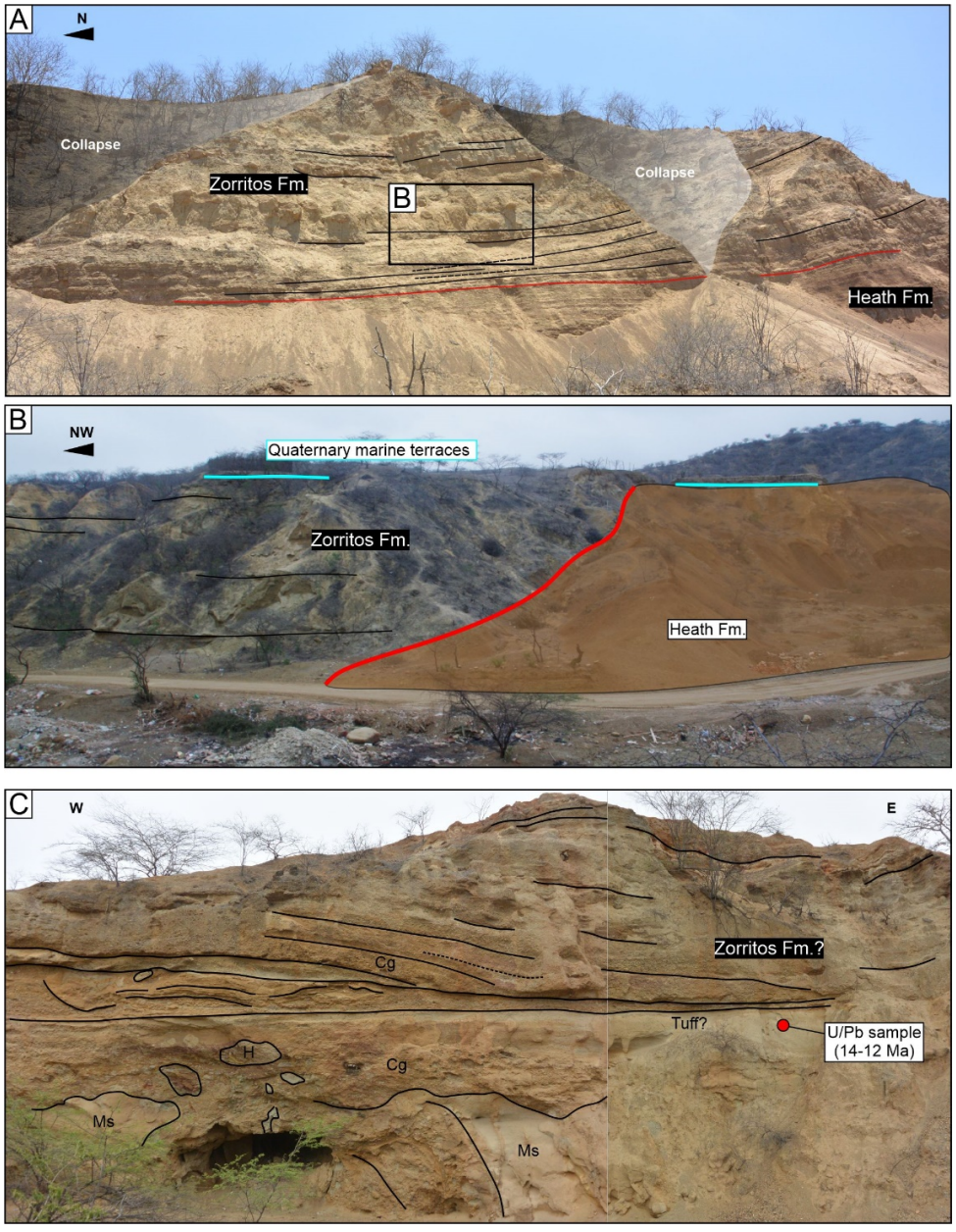

Figure 6.9: a) Outcrop exposure at the upper part of the Bocapan gulley showing large-scaled downlap onto the Heath Formation. b) Cross section at the Casitas gulley showing two main intervals, the lower one characterized by a of disrupted to chaotic blocky, and a lower one dominated by conglomeratic bed downlapping onto the unit below. In between these two intervals there is presence of a fine material layer possibly associated with tuff deposits that has been sampled for U/Pb dating measurement.

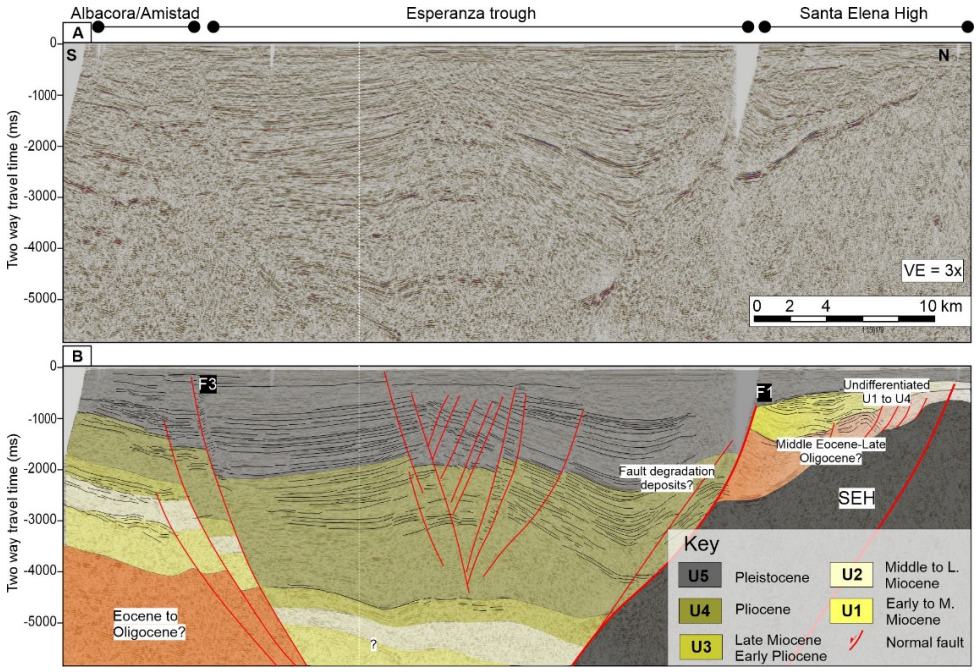

Figure 6.10: N-S seismic section across the Esperanza trough (b) Interpreted seismic section in (a), showing the structural configuration of the Esperanza through area characterized by an apparent symmetric graben geometry. There is a clear expansion of U5 of ca. 2s. TheNotice the growth packages of U1 and U2 towards the footwall, and the down faulted block from the Santa Elena High with thickness of units U1 and U2 comparable to the hangingwall. There is a lesser thickness expansion of U3 across the Puna fault suggesting a quiescence fault activity period at this time.

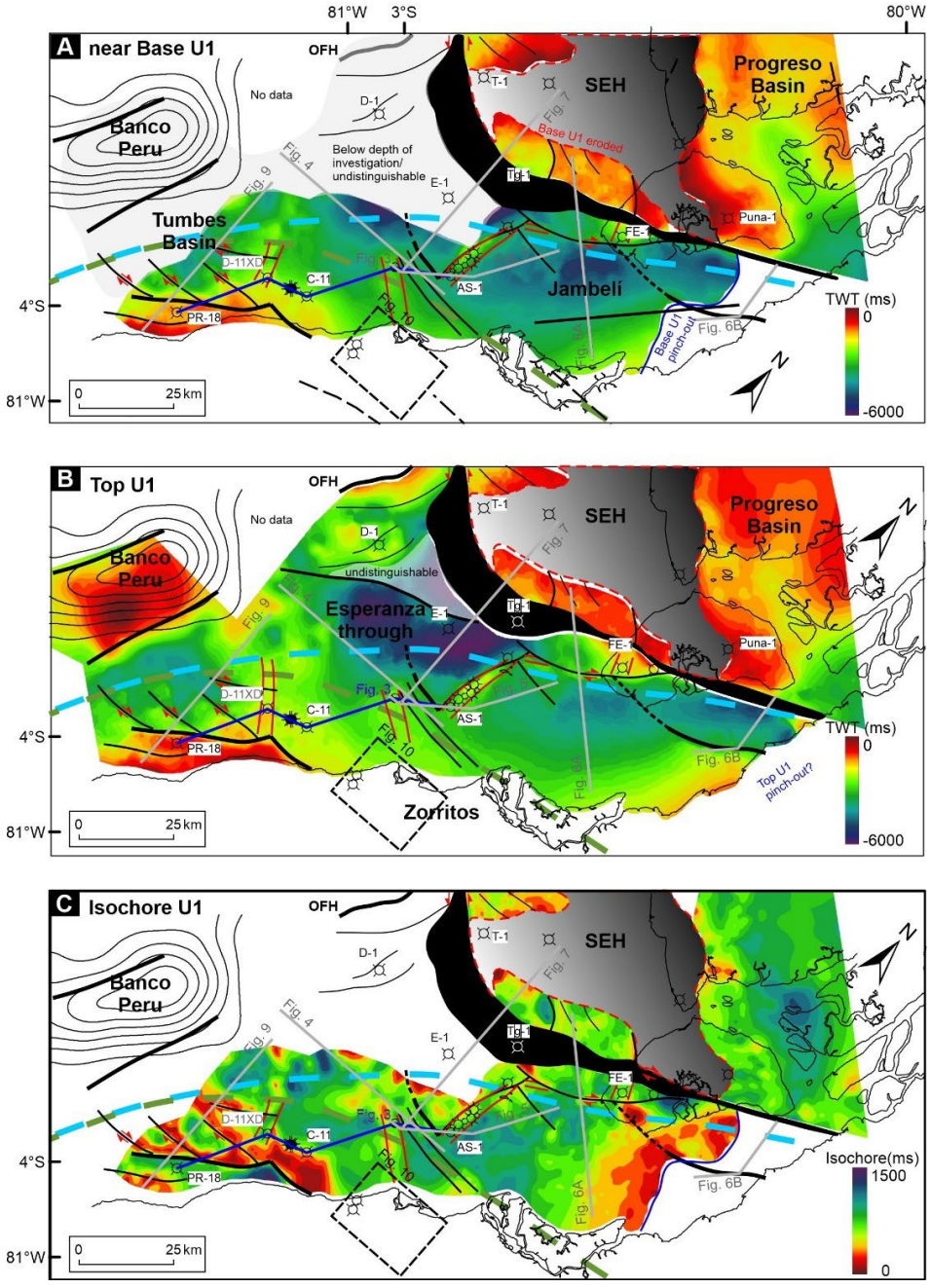

Figure 6.11: a) TWT surface of the near base of U1. b) TWT surface map of U1, and c) Isochrone map of U1.

6.5 Discussion

There are two main elements involved in the evolution of the Gulf of Guayaquil-Tumbes basin here presented 1) being situated across a transform boundary whose nature is associated to a proto obduction suture zone, and 2) the lateral slip movement along a trench-linked fault (CCPP fault system) that may have controlled the northern realm of the basin by the eastward and northward drift of the North Andean Sliver. Through an integrated and holistic analysis of seismic profiles, well data and surface exposures, we elucidate the post Oligocene tectonostratigraphic evolution of the basin.

6.5.1 Basin type development at the termination of a trench-linked continental transform boundary

The GGTB is clearly defined by some major boundaries that appear spatially disconnected and of different nature. The crustal affinity of the basin underlying blocks has been barely considered in the past. Instead, there has been a strong focus on the thickest depocenter of the basin across the Esperanza through. This led to initially catalogue the GGTB as a pull-apart basin (Deniaud *et al.*, 1999; Dumont *et al.*, 2005), but later Witt and Bourgois (2010) argue that it is not a classical pull-apart basin, and instead a particular type of basin primarily controlled by the northward tectonic escape of the NAS. However, the model proposed is based on the analysis of the high subsidence rate Plio-Pleistocene interval across the Esperanza trough.

For the earliest Miocene period less is known about the basin configuration. A model, without supporting evidence, is proposed by Hungerbühler *et al.* (2002), which consist of a large slip movement along the CCPP fault system of ca. 100 km for the middle to late Miocene period. In such scenario, the Jambelí area may have been connected to the Progreso basin to the north, forming a single embayment, constrained at least partly to the open marine environment by the Santa Elena High. Such model does not offer further details on the strain distribution across the basin and nature of faults controlling the proposed lateral movement. Nevertheless, the ca. 100 km lateral

movement and presence of the SEH proposed by Hungerbühler *et al.* (2002) is in accordance with our model and displacement estimation.

Some of key aspect that we have considered in our interpretation, based upon the quality of the data here presented are 1) the estimated variations of the Eocene to Oligocene interval in terms of its presence and likely thickness across the basin, 2) a clear pinch-out of the early to Late Miocene units (U1/U2) at the Jambelí area, and 3) the possible role of underlying crustal faults. These first two aspects suggest that the Jambelí area may have acted as an eastern basin border until the middle Miocene. Farther north, across the Puna island into the Progreso basin, the eastern basin boundary is controlled by the Chongon Colonche Hills (CCH). Hence, a simple assumption is that both limits were close to each other during the middle Miocene, resulting in a displacement of ca. 100 km, as proposed by Hungerbühler *et al.* (2002). This is in line with the isochrone map here presented for U1, which suggests an apparent offset of the depocenter of the same magnitude (Figure 6.11). However, the possible structural kinematics of the basin leading to that lateral displacement have not been fully investigated. A key element of the study area is the underlying crustal structure which is poorly constrained. As pointed out by Aizprua *et al.* (2019b), the Gulf of Guayaquil-Tumbes basin may have been formed during a NE-SW extensional stress field resulting from an oblique subduction regime that reactivated the proto suture, or developed the trench-linked fault system (CCPP fault system, (Alvarado *et al.*, 2016)) during the middle Miocene or earlier. However, this may have been a second phase or even a diminishing on the extensional displacement as observed in Figure 6.5, where the main onset of fault activity is during the early Miocene or Oligocene period. In NW Peru, the main onset of extension is estimated as an Oligocene event sealed during the Miocene, which is in accordance with our interpretation of the offshore area.

There are several aspects of this region to consider when defining the type of basin, such as: 1) the involvement of the proto obduction suture zone, 2) development of a principal deformation zone, and 3) the Santa Elena High and Banco Peru structural highs. South of the Jambelí sub-area, we encountered the unique vestiges of

a suture zone, the Jubones fault delimiting the Late Cretaceous accreted oceanic terrane and the South American continental margin (Figure 6.1). At this location, the PDZ and the suture do not coincide. The PDZ developed farther north, very likely underlying the GGTB axis, possibly inherited from the tearing of the Piñon Block to the east (Aizprua *et al.*, 2019b). The nature of bounding faults differs from normal bounding faults developed along continental transform faults (e.g. the Marmara Sea, Aksu *et al.* (2000)). The northern boundary is controlled by the uplift of the Santa Elena High, a remnant of a Late Cretaceous-Paleocene accretionary outer wedge and to the west by the Banco Peru likely developed in response to the strike-slip movement and the subduction accretion process. However, if we remove the latest phase of tectonic escape, the resulting basin is a combination of a pull-apart and transform parallel strike-slip basin, characterized by an asymmetric geometry and depocenters migrating eastward from the direction of sediment supply, which is to the north.

6.5.2 Oblique ridge development and implication to the depositional environment

A particular aspect of the GGTB, at least evident during the early to middle Miocene and onward is the presence of oblique or transverse folds, subdividing the basin into sub-basins. Present-day transtensional basins, such as the case along the North Anatolian fault zone (Aksu *et al.*, 2000; Rangin *et al.*, 2001) , show similarities to the structures observed during the Miocene in the GGTB. Bathymetry maps of the Marmara Sea along the Anatolian fault zone shows water depth differences of up to 1km. These bathymetric differences may significantly impact sediment dispersal across the basin, and the type of depositional environments and their extension. This is currently observed in the Guayas estuary, where tidal channel incisions and shoreface deposits may coexist around these uplifted structures (Reynaud *et al.*, 2018). The formation of these layer folded structures, in transtensional settings, seems to be supported by analogue modelling (Venkat-Ramani and Tikoff, 2002; Fossen *et al.*, 2013). The erosional event observed at the top of U1 may be related to the local surface exposure of the Corvina, Albaroca and Amistad ridges. As shown in Figure

6.4, the folded structures appear to be decouple from a lower stratigraphic interval and very likely detached at the Heath/Dos Bocas formation level, which is characterized by the presence of plastic shales capable of remobilization.

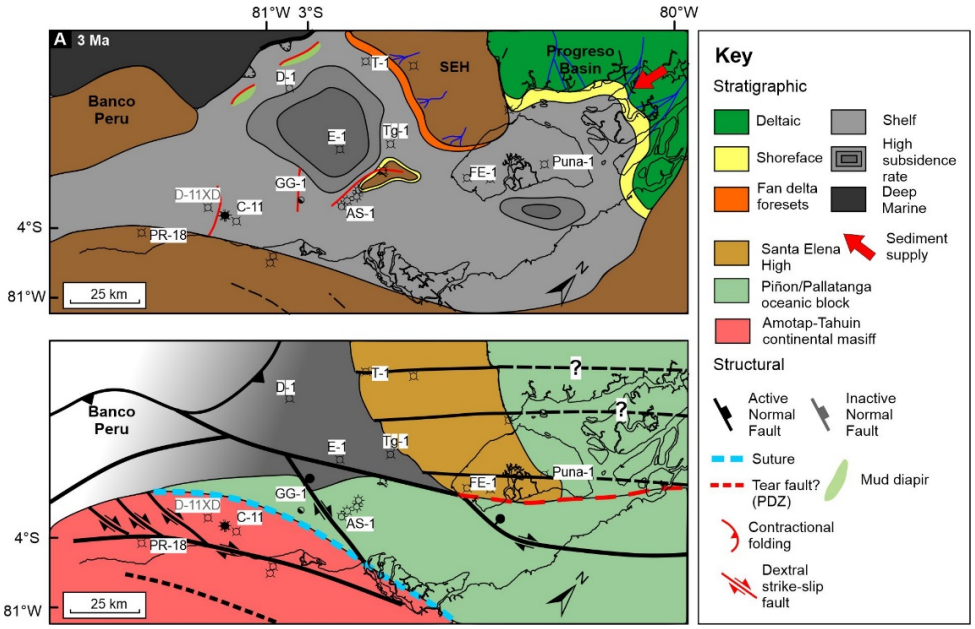

Figure 6.12: a) Proposed palinspastic reconstruction of the southernmost Northern Andes during the Pleistocene. b) distribution of the inferred crustal blocks underlying the area together their fault activity.

6.5.3 Basin evolution of the GGTB

In this work, we elucidate the tectonostratigraphic evolution of a basin across a paleo obduction suture zone (Witt and Bourgois, 2010), which connects landwards to a trench-linked fault system (CCPP fault system) (this work). The Gulf of Guayaquil-Tumbes basin may have developed at least since the late Oligocene, following a phase of plate instability and trench reestablishment (Aizprua *et al.*, 2019b). In this section, we list the main phases of tectonism and infilling evolution of the basin. Despite of the oldest Paleogene sequences not being fully described in this work; we consider this stratigraphic interval, at least the Oligocene, to be of relevance to elucidate the kinematic opening phase of the Gulf of Guayaquil-Tumbes basin. Based on seismic

profiles, surface exposures, well information and previous studies, we present a plausible basin configuration for the Late Oligocene period onward. The depocenter migration towards the east, at least from Early to Late Miocene, away from a NS sediment supply direction, together with the asymmetrical basin shape and the ca. 100 km offset of the early to middle Miocene U1 supports the development of a transform boundary basin. Post Miocene, the basin appears to be controlled by high subsidence rates related to the northward migration of the NAS, with subsequent reactivation of the underlying crustal faults controlling depocenter and transverse ridge location, which has a great impact on sediment dispersal across the basin.

6.6 Conclusions

The Gulf of Guayaquil-Tumbes basin has recorded the evolution of strike-slip movements associated with a major lithospheric boundary at least since the late Oligocene. To catalogue the basin as a pure strike-slip pull-apart of transtensional pull-apart basin is not straightforward and this may be the origin of discrepancy between previous works (Deniaud *et al.*, 1999; Dumont *et al.*, 2005; Witt and Bourgois, 2010). The tectonic escape model proposed by Egbue and Kellogg (2010) and Witt and Bourgois (2010) for the Pleistocene to present, is a clear example that in the presence of a free-face and an oblique angle of the stress field to the Principal Deformation Zone (PDZ), large surface area creation follow by large subsidence may take place (Mann, 1997). By removing this last phase of tectonic escape, we end-up with a shingled array of three basins and two main transverse ridges. Across the Jambelí and Tumbes basins we can observed that the basins have an asymmetric shape with depocenter from U1 to U3 migrating eastward of the sediment supply direction which is towards the north, classical characteristics of a continental transform basins (Seeber *et al.*, 2010). The two ridges are very likely controlled by a combination of transtensional movement, possible domino step style of the underlying crustal units, and shale remobilization seems all together play a key role on the sedimentation dynamics of the basin, allowing certain depositional environment to extent farther north across the ridges, which is an important consideration for reservoir presence.

Chapter 7

Conclusions and Further Perspectives

The model herein proposed further our understanding of the tectonostratigraphic relationships across the southernmost region of the Northern Andes. The compilation of published studies carried out in the past, together with the analysis and interpretation of the available data presented in this work, brings a new perspective on forearc basin development on the wake of accretion and entrapment of an oceanic plateau sliver.

The results from this work, presented holistically from the crustal-scale down to the meter scale, suggest that the underlying crustal structure of the forearc may have a central role on the development of the forearc region, since its emplacement. It is known or conceived that first order controlling factors involved in the development and infilling of forearc basins are linked to the processes occurring at the trench. However, many of these processes may be lost from the geological record when studying ancient forearc basins. Thus, the analysis of the stratigraphic record in forearc basins has been a prime for constraining the processes that may have shaped the forearc.

Nevertheless, this work outlines that elucidating the underlying crustal structure of the forearc, in addition to the stratigraphic record may provide us with better constrained models when studying forearc basins. The conclusions drawn from each of the chapters may have broader implications in our understanding of forearc basins, which I discuss next.

7.1 Revealing the underlying forearc crustal structure: from an early split-arc to a built-in magmatic event

The work presented by Draut and Clift (2013), document the existence of a preferential preservation of some intra-oceanic arc sedimentary and tectonic processes following an arc-continent collision. Indeed, this may bias or impair our attempts to reconstruct the geodynamic processes that have shaped the margin. In the Northern Andes, surface exposures along the Western Cordilleras of Ecuador and Colombia have provided the key petro-tectonic constraints for defining the region's pre-collision palaeogeography. However, the great vast of the allochthonous oceanic terrane is buried under Cenozoic sediments across the forearc region.

The results presented in chapter 3 reveal the underlying crustal structures and discuss their role on shaping the forearc region. The presence of Coniacian to Campanian volcaniclastic deposits revealed by seismic reflection data within the inner domain is crucial. The onlapping geometrical relationship of such reflections onto a pre-existing structural high may indicate the presence of an intra-arc basin developed prior to or synchronous to the collisional event between 75 and 70 Ma Figure 7.1.

Another key element is related to a regional long-wavelength magnetic anomaly across the inner domain, at least partly pair with a gravity low, which may suggest the presence of an underlying serpentinization process, with intrusions built on the accreted and composite sliver. This process may have led to the alteration of the lower mafic to ultramafic crust underlying the forearc basement. The general disposition of the high magnetized area seems to coincide with the western edge of the exposed Macuchi block across the Western Cordillera. This suggests that the possible serpentinization process may be partly associated with a magmatic event (Figure 7.1).

The accretion of the Macuchi arc during the Eocene has been a topic of dispute in the Geology of the Northern Andes. However, the results presented in chapter 3 based on gravity and magnetic data do not reveal or support any buried suture between this terrane and the Piñon block to the west. Furthermore, it has been highlighted the

difficulty reconciling a late Eocene accretion of the Macuchi arc, given its position between the Piñon and Pallatanga blocks accreted during the Late Cretaceous (Vallejo *et al.*, 2009). The so-called "Macuchi" block appears built on pre-existing accreted oceanic terrane possibly following the east-dipping subduction establishment and the increase in convergence velocity (Figure 7.1) (Pardo-Casas and Molnar, 1987).

7.2 An inherited accretionary wedge and its interaction to the Piñon backstop

The updated tectonic view of the southernmost region of the Northern Andes presented in chapter 4 reveals that a localized and preserved outer wedge may significantly impact the development and compartmentalization of the forearc depocenters. Surface exposures, seismic profiles, and gravity anomaly map allowed to delineate an ancient and preserved Late Cretaceous-Paleocene accretionary wedge that may have formed at the trailing edge of the Caribbean Large Igneous Province along the Northern Andes since ~65 Ma (Figure 7.1).

I propose that the CLIP's southern limit may have created an unstable triple plate junction between the Farallon, CLIP, and the South American plates. The strain partitioning imposed by the CLIP's oblique collision may have resulted in a tearing of the Piñon Block creating a localized depocenter, NW of the Amotape-Tahuin massif, where late Cretaceous deposits (Santa Elena Fm.) accumulated (Figure 7.1). The possible surface of weakness created by the tearing off and northward migration of the CLIP may have controlled the location of an east-dipping subduction initiation. The gradual variation of the wedge size towards the south (Figure 7.1) may be explained by numerical models that suggest a lateral tectonic migration of sediments until they reach a physical barrier (Malatesta *et al.*, 2013). In the southernmost Northern Andes case, this barrier is defined by the Amotapes - Tahin Massif.

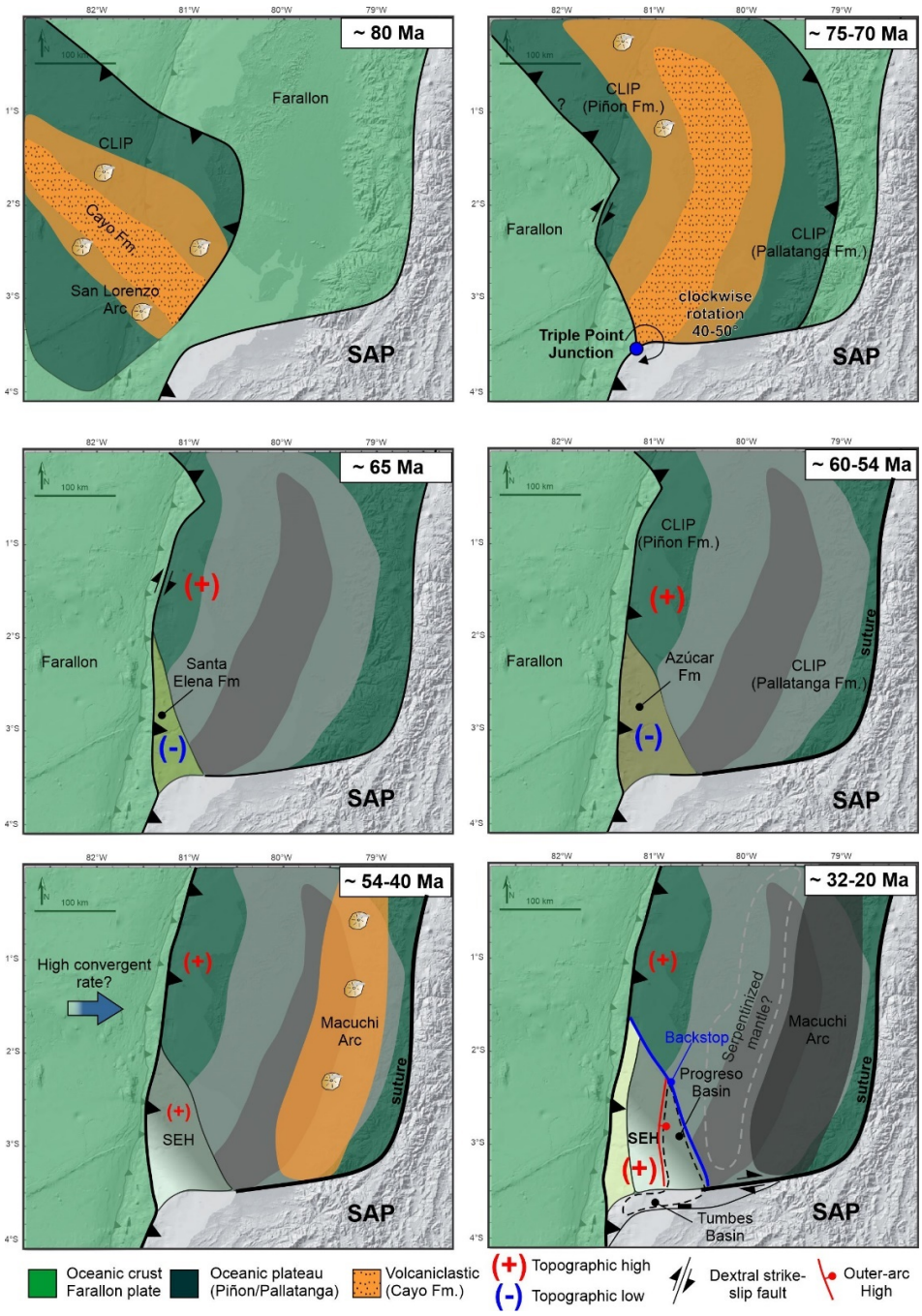

Figure 7.1: Schematic map view of the tectonic reconstruction of the southernmost region of the Northern Andes since pre-collision of a sliver from the Caribbean Large Igneous Province (CLIP). The main tectonic elements discussed in each chapter are highlighted in this schematic reconstruction.

The re-establishment of a stable subduction system by Eocene times seems to have controlled the region's post-accretionary forearc basin configuration. Further oblique subduction and strike-slip fault movements along the southern edge of the Santa Elena High outer wedge may have taken place, controlling the development of the forearc region (Figure 7.1). These processes may have led to a strong interaction between the Santa Elena High outer wedge and the crustal sliver of the CLIP, this last one acting as a backstop, and resulting on the development of a local sensu stricto forearc basin (Progreso Basin) controlled by development of a local outer forearc high.

7.3 Development of a localized outer forearc high (OFH) and further control on forearc basin development

The development of a localized outer wedge and its interaction with the Piñon block, which acts as a backstop, seems to have altered the bathymetric profile from the Paleocene into the Eocene. This resulted in the deposition of shallowing upwards sedimentary series from ~54 Ma to ~40 Ma, showing gravitational deposits related to slope instabilities, suggesting a significant decrease of the activity of the accretionary prism.

The outer wedge – backstop interaction may have resulted in the Estancia Hills structural high development, which shows Late Cretaceous to Eocene rocks at surface levels. It is characterised in seismic profiles by chaotic facies (e.g. debris flows) downlapping older and deeper sedimentary units and continental to shallow water sediments unconformably covering those chaotic facies. This is manifest in the degree of zircon recycling next to the structural high. It is proposed in this work that the structural high defines an outer forearc high (OFH), typical of forearc basins such as those observed in the Kumano (Japan) and Great Valley (USA) basins. The evolution of the OFH is most likely related to the uplift of a thrust slice during 32–30 Ma (Figure 7.1), coeval with deposition of the coarse-grained shallow-water to continental Zapotal Formation. Evidence presented here suggests the existence of a stable outer

forearc high limiting the forearc depocenter for at least 20 Ma and creating the necessary accommodation for a ~3 km thick forearc sedimentary package. The forearc sediments are related to shallow-water environments (Formations Dos Bocas, Villingota, Subibaja and Progreso) ranging from littoral to tidal facies most likely related to a triangular protected bay that mimics the architecture of the forearc depocenter.

7.4 Further perspectives

The interpretation and models presented in this thesis have diverse possible extensions. In the same holistic order that I presented the results of this research work; I propose some further research lines.

The results obtained in chapter 3 provide further questions regarding the crustal structure (and mantle component) within the inner domain, which we explained by a remnant hydrated mantle. However, the crustal model herein presented is expected to improve through time with additional constraints. For instance, future lines of research may consider: 1) the implementation of seismologic data (earthquake hypocentres), which may provide further constraints on the geometry and heterogeneities within the outer domain; 2) the acquisition of additional paleomagnetic data, in particular, to account for remnant magnetization and a better dataset of magnetic susceptibility measurements is a must; 3) the acquisition of long-offset reflection-refraction lines across the inner domain to build a velocity model which then can be interpreted in terms of crustal units. The interpretation can benefit tremendously by assuring the S-wave measurement to obtain a Poisson's ratio that may allow constraining on lithology; and 4) build a 3D model of the crustal structure in the inner domain.

In Chapter 4, the proposed model for the Cenozoic evolution of the SW Ecuador provides an integrated view of the different tectonic elements, their possible origin and their role on the development of sedimentary basins. One of the key elements is the role of the Santa Elena High (SEH), both on the development of the Progreso and the Gulf of Guayaquil basins. Nonetheless, the accretionary-type character of the high and its limited extent may be further study using numerical models. This particular

area is considered to have formed at or near a triple plate junction (e.g. this work; Kennan and Pindell, 2009; Spikings *et al.*, 2015) and therefore is uncertain whether the Santa Elena High developed 1) onto a remnant of a NE accretionary-type subduction system of Maastrichtian age (Santa Elena Fm., Figure 4.3), or 2) the SEH constitutes a singularity developed at a triple plate junction (see Fig. 12 in Kimura *et al.*, 2014), triggered by collision and plate instability as we proposed, followed by a flexural bulge along NW Peru resulting in rapid uplift of the Amotape-Tahuin massif promoting rapid sedimentation during the Paleocene. Numerical models may shade further light into this local aspect of SW Ecuador's geology, but highly relevant on the posterior development of sedimentary basins.

The following chapters 5 and 6 address how the resulting configuration, post accretion, may have controlled the development of the Progreso and the Gulf of Guayaquil-Tumbes basins since the Oligocene. Basin geometry and paleogeography of both basins will be better constrained as new seismic data is acquired, as currently the quality of the available seismic may lead to misinterpretations. However, in my opinion, a relevant area of study is related to heat-flow of the area as a driven mechanism for source rock maturation understanding in the area and future exploration purposes. Back to chapter 3, the high positive anomaly along the NW Peru (not discussed in this work), and the interpreted tear fault should be considered when defining a heat flow model for the area.

There are several variables involved in the development of active margins and forearc basins, and the hidden or lost elements of a subduction system sometimes impair the geodynamic reconstruction of active margins. Therefore, any attempt to study in detail these systems either for understanding continental growth processes or for commercial purposes such as hydrocarbon exploration or metallic resources, these systems should be approached in a multidisciplinary and integrated way, from crustal to pore scales.

References

Agard, P. *et al.* (2012) Long-term coupling along the subduction plate interface; insights from exhumed rocks and models, *Geophysical Research Abstracts*, 14.

Aitken, T. *et al.* (2011) Evolution of the Grenada and Tobago basins and implications for arc migration, *Marine and Petroleum Geology*, 28(1), pp. 235-258. doi: http://dx.doi.org/10.1016/j.marpetgeo.2009.10.003.

Aizprua, C. *et al.* (2017) Forearc basin structuring and seismicity patterns controlled by a trapped sliver from the Caribbean Large Igneous Province (CLIP): Northern Andes, *William Smith meeting 2017; Plate Tectonics at 50, abstract book*. Geological Society of London, London, United Kingdom, pp. 122-123.

Aizprua, C. *et al.* (2019a) Replication Data for: Cenozoic stages of forearc evolution following the accretion of a sliver from the Late Cretaceous-Caribbean Large Igneous Province (CLIP): SW Ecuador-NW Peru, i Norwegian University of, S. and Technology (ed.) (V1 edn.): DataverseNO. doi: https://doi.org/10.18710/BYZIZX.

Aizprua, C. *et al.* (2019b) Cenozoic Stages of Forearc Evolution Following the Accretion of a Sliver From the Late Cretaceous-Caribbean Large Igneous Province: SW Ecuador-NW Peru, *Tectonics*, 38(4), pp. 1441-1465. doi: https://doi.org/10.1029/2018TC005235.

Aksu, A. E., Calon, T. J. and Hiscott, R. N. (2000) Anatomy of the North Anatolian fault zone in the Marmara Sea, western Turkey; extensional basins above a continental transform, *GSA Today*, 10(6), pp. 3-7.

Alvarado, A. *et al.* (2016) Partitioning of oblique convergence in the Northern Andes subduction zone: Migration history and the present-day boundary of the North Andean Sliver in Ecuador, *Tectonics*, 35(5), pp. 1048-1065. doi: https://doi.org/10.1002/2016TC004117.

Andjić, G., Baumgartner, P. O. and Baumgartner-Mora, C. (2018) Rapid vertical motions and formation of volcanic arc gaps: Plateau collision recorded in the forearc geological evolution (Costa Rica margin), *Basin Research*, 30(5), pp. 863-894. doi: https://doi.org/10.1111/bre.12284.

Arculus, R. J., Lapierre, H. and Jaillard, É. (1999) Geochemical window into subduction and accretion processes: Raspas metamorphic complex,

Ecuador, *Geology*, 27(6), pp. 547-550. doi: https://doi.org/10.1130/0091-7613(1999)027%3C0547:GWISAA%3E2.3.CO;2.

Aspden, J. A. *et al.* (1992) Regional S-Type Granites in the Ecuadorian Andes - Possible Remnants of the Breakup of Western Gondwana, *Journal of South American Earth Sciences*, 6(3), pp. 123-132. doi: https://doi.org/10.1016/0895-9811(92)90002-G.

Audemard, F. A. (2009) Key issues on the post-Mesozoic Southern Caribbean Plate boundary, *Geological Society, London, Special Publications*, 328(1), pp. 569-586. doi: https://doi.org/10.1144/SP328.23.

Barrier, E., Huchon, P. and Aurelio, M. (1991) Philippine fault: A key for Philippine kinematics, *Geology*, 19(1), pp. 32-35. doi: https://doi.org/10.1130/0091-7613(1991)019<0032:PFAKFP>2.3.CO;2.

Bartole, R. *et al.* (2019) Sedimentary architecture, structural setting, and Late Cenozoic depocentre migration of an asymmetric transtensional basin: Lake Izabal, eastern Guatemala, *Tectonophysics*, 750, pp. 419-433. doi: https://doi.org/10.1016/j.tecto.2018.12.004.

Basile, C. and Brun, J. P. (1999) Transtensional faulting patterns ranging from pull-apart basins to transform continental margins: an experimental investigation, *Journal of Structural Geology*, 21(1), pp. 23-37. doi: https://doi.org/10.1016/S0191-8141(98)00094-7.

Beard, L. P. (2000) Detection and identification of north–south trending magnetic structures near the magnetic equator, *Geophysical Prospecting*, 48(4), pp. 745-761. doi: https://doi.org/10.1046/j.1365-2478.2000.00214.x.

Beck, M. E. (1983) On the Mechanism of Tectonic Transport in Zones of Oblique Subduction, *Tectonophysics*, 93(1-2), pp. 1-11. doi: https://doi.org/10.1016/0040-1951(83)90230-5.

Ben-Avraham, Z. (1992) Development of asymmetric basins along continental transform faults, *Tectonophysics*, 215(1), pp. 209-220. doi: https://doi.org/10.1016/0040-1951(92)90082-H.

Benitez, S. (1995) *Évolution géodynamique de la province côtière sud-équatorienne au Crétacé supérieur-Tertiaire*, Université Joseph-Fourier - Grenoble I. doi: https://tel.archives-ouvertes.fr/tel-00542421.

Berglar, K. *et al.* (2017) The Mentawai forearc sliver off Sumatra: A model for a strike-slip duplex at a regional scale, *Tectonophysics*, 710-711, pp. 225-231. doi: https://doi.org/10.1016/j.tecto.2016.09.014.

Bethoux, N. *et al.* (2011) Seismological study of the central Ecuadorian margin: Evidence of upper plate deformation, *Journal of South American Earth Sciences*, 31(1), pp. 139-152. doi: http://dx.doi.org/10.1016/j.jsames.2010.08.001.

Blakely, R. J., Brocher, T. M. and Wells, R. E. (2005) Subduction-zone magnetic anomalies and implications for hydrated forearc mantle, *Geology*, 33(6), pp. 445-448. doi: https://doi.org/10.1130/G21447.1.

Bonnemains, D. *et al.* (2016) Magnetic signatures of serpentinization at ophiolite complexes, *Geochemistry, Geophysics, Geosystems*, 17(8), pp. 2969-2986. doi: https://doi.org/10.1002/2016GC006321.

Bosch, D. *et al.* (2002) Geodynamic significance of the Raspas Metamorphic Complex (SW Ecuador): geochemical and isotopic constraints, *Tectonophysics*, 345(1–4), pp. 83-102. doi: http://dx.doi.org/10.1016/S0040-1951(01)00207-4.

Boschman, L. M. *et al.* (2014) Kinematic reconstruction of the Caribbean region since the Early Jurassic, *Earth-Science Reviews*, 138, pp. 102-136. doi: https://doi.org/10.1016/j.earscirev.2014.08.007.

Bourgois, J. (2013) A Review on Tectonic Record of Strain Buildup and Stress Release across the Andean Forearc along the Gulf of Guayaquil-Tumbes Basin (GGTB) near Ecuador-Peru Border, *International Journal of Geosciences*, 4(3), pp. 618-635. doi: http://dx.doi.org/10.4236/ijg.2013.43057.

Boutelier, D. and Chemenda, A. (2011) Physical Modeling of Arc–Continent Collision: A Review of 2D, 3D, Purely Mechanical and Thermo-Mechanical Experimental Models *Arc-Continent Collision.* Berlin, Heidelberg: Springer Berlin Heidelberg, pp. 445-473. doi: https://doi.org/10.1007/978-3-540-88558-0_16.

Braz, C. *et al.* (2018) Geodynamic reconstruction of an accreted Cretaceous back-arc basin in the Northern Andes, *Journal of Geodynamics*, 121, pp. 115-132. doi: https://doi.org/10.1016/j.jog.2018.09.008.

Brown, D. *et al.* (2011) Arc–Continent Collision: The Making of an Orogen *Arc-Continent Collision.* Berlin, Heidelberg: Springer Berlin Heidelberg, pp. 477-493. doi: https://doi.org/10.1007/978-3-540-88558-0_17.

Buchs, D. M. *et al.* (2015) Sediment flow routing during formation of forearc basins: Constraints from integrated analysis of detrital pyroxenes and stratigraphy in the Kumano Basin, Japan, *Earth and Planetary Science Letters*, 414, pp. 164-175. doi: https://doi.org/10.1016/j.epsl.2014.12.046.

Burov, E. and Cloetingh, S. (2010) Plume-like upper mantle instabilities drive subduction initiation, *Geophysical Research Letters*, 37(3). doi: https://doi.org/10.1029/2009GL041535.

Byrne, D. E., Wang, W. H. and Davis, D. M. (1993) Mechanical Role of Backstops in the Growth of Fore-Arcs, *Tectonics*, 12(1), pp. 123-144. doi: https://doi.org/10.1029/92TC00618.

Calahorrano, A. *et al.* (2008) Nonlinear variations of the physical properties along the southern Ecuador subduction channel: Results from depth-migrated seismic data, *Earth and Planetary Science Letters*, 267(3-4), pp. 453-467. doi: https://doi.org/10.1016/j.epsl.2007.11.061.

Campbell, C. J. (1974) Ecuadorian Andes, *Geological Society, London, Special Publications*, 4(1), pp. 725-732. doi: https://doi.org/10.1144/GSL.SP.2005.004.01.44.

Cano, L. C. G. *et al.* (2014) Three-dimensional velocity structure of the outer fore arc of the Colombia-Ecuador subduction zone and implications for the 1958 megathrust earthquake rupture zone, *Journal of Geophysical Research: Solid Earth*, 119(2), pp. 1041-1060. doi: https://doi.org/10.1002/2012JB009978.

Cawood, P. A., Hawkesworth, C. J. and Dhuime, B. (2012) Detrital zircon record and tectonic setting, *Geology*, 40(10), pp. 875-878. doi: https://doi.org/10.1130/G32945.1.

Cediel, F. *et al.* (2003) Tectonic Assembly of the Northern Andean Block *The Circum-Gulf of Mexico and the Caribbean: Hydrocarbon Habitats, Basin Formation and Plate Tectonics.* American Association of Petroleum Geologists, pp. 0. doi: https://doi.org/10.1306/M79877C37.

Chemenda, A., Lallemand, S. and Bokun, A. (2000) Strain partitioning and interplate friction in oblique subduction zones: Constraints provided by experimental modeling, *Journal of Geophysical Research-Solid Earth*, 105(B3), pp. 5567-5581. doi: https://doi.org/10.1029/1999JB900332.

Chemenda, A. I., Mattauer, M. and Bokun, A. N. (1996) Continental subduction and a mechanism for exhumation of high-pressure metamorphic rocks: new modelling and field data from Oman, *Earth and Planetary Science Letters*, 143(1), pp. 173-182. doi: https://doi.org/10.1016/0012-821X(96)00123-9.

Chiaradia, M. (2009) Adakite-like magmas from fractional crystallization and melting-assimilation of mafic lower crust (Eocene Macuchi arc, Western Cordillera, Ecuador), *Chemical Geology*, 265(3-4), pp. 468-487. doi: https://doi.org/10.1016/j.chemgeo.2009.05.014.

Clift, P. and Vannucchi, P. (2004) Controls on tectonic accretion versus erosion in subduction zones: Implications for the origin and recycling of the continental crust, *Reviews of Geophysics*, 42(2). doi: https://doi.org/10.1029/2003RG000127.

Clift, P. D. and Hartley, A. J. (2007) Slow rates of subduction erosion and coastal underplating along the Andean margin of Chile and Peru, *Geology*, 35(6), pp. 503-506. doi: https://doi.org/10.1130/G23584A.1.

Collot, J.-Y. *et al.* (2014) The Neogene forearc basins of the Ecuadorian Shelf (1 degrees N-2 degrees 20'S); preliminary interpretation of a dense grid of MCS data, *American Geophysical Union Fall Meeting*, 2014.

Collot, J. Y. *et al.* (2002) Exploring the Ecuador-Colombia Active Margin and Interplate Seismogenic Zone, *Eos, Transactions American Geophysical Union*, 83(17), pp. 185-190. doi: https://doi.org/10.1029/2002EO000120.

Collot, J. Y. *et al.* (2008) Origin of a crustal splay fault and its relation to the seismogenic zone and underplating at the erosional north Ecuador-south Colombia oceanic margin, *Journal of Geophysical Research-Solid Earth*, 113(B12). doi: https://doi.org/10.1029/2008JB005691.

Dahlen, F. A. (1990) Critical taper model of fold-and-thrust belts and accretionary wedges, *Annual Review of Earth and Planetary Sciences*, 18(1), pp. 55-99. doi: 10.1146/annurev.ea.18.050190.000415.

Daly, M. C. (1989) Correlations between Nazca Farallon Plate Kinematics and Fore-Arc Basin Evolution in Ecuador, *Tectonics*, 8(4), pp. 769-790. doi: https://doi.org/10.1029/TC008i004p00769.

Deniaud, Y. *et al.* (1999) Opening and tectonic and sedimentary evolution of the Gulf of Guayaquil: Neogene and Quaternary fore-arc basin of the south Ecuadorian Andes, *Comptes Rendus De L Academie Des Sciences Serie Ii Fascicule a-Sciences De La Terre Et Des Planetes*, 328(3), pp. 181-187. doi: https://doi.org/10.1016/S1251-8050(99)80094-9.

Deniaud, Y. (2000) *Enregistrements sédimentaire et structural de l'évolution géodynamique des Andes équatoriennes au cours du Néogène : étude des bassins d'avant-arc et bilans de masse*, Université Joseph Fourier. doi: http://www.documentation.ird.fr/hor/fdi:010027994.

Dickinson, W. R. and Gehrels, G. E. (2009) Use of U–Pb ages of detrital zircons to infer maximum depositional ages of strata: A test against a Colorado Plateau Mesozoic database, *Earth and Planetary Science Letters*, 288(1), pp. 115-125. doi: https://doi.org/10.1016/j.epsl.2009.09.013.

Dickinson, W. R. (2013) Phanerozoic palinspastic reconstructions of Great Basin geotectonics (Nevada-Utah, USA), *Geosphere*, 9(5), pp. 1384-1396. doi: http://dx.doi.org/10.1130/GES00888.1.

Dilek, Y. and Furnes, H. (2011) Ophiolite genesis and global tectonics: Geochemical and tectonic fingerprinting of ancient oceanic lithosphere, *GSA Bulletin*, 123(3-4), pp. 387-411. doi: https://doi.org/10.1130/B30446.1.

Draut, A. E. and Clift, P. D. (2013) Differential preservation in the geologic record of intraoceanic arc sedimentary and tectonic processes, *Earth-Science Reviews*, 116, pp. 57-84. doi: https://doi.org/10.1016/j.earscirev.2012.11.003.

Dumont, J. F., Santana, E. and Vilema, W. (2005) Morphologic evidence of active motion of the Zambapala Fault, Gulf of Guayaquil (Ecuador), *Geomorphology*, 65(3–4), pp. 223-239. doi: http://dx.doi.org/10.1016/j.geomorph.2004.09.003.

Egbue, O. and Kellogg, J. (2010) Pleistocene to Present North Andean "escape", *Tectonophysics*, 489(1-4), pp. 248-257. doi: https://doi.org/10.1016/j.tecto.2010.04.021.

Ego, F. *et al.* (1996) Quaternary state of stress in the Northern Andes and the restraining bend model for the Ecuadorian Andes, *Tectonophysics*, 259(1–3), pp. 101-116. doi: http://dx.doi.org/10.1016/0040-1951(95)00075-5.

Egüez, A. (1986) Evolution Cenozoique de la Cordillere Occidentale septentrionale d'Equateur (0°15' S - 01°10' S), les mineralisations associetees, *Doc. Thesis*, UPMC, Paris, pp. 116.

Einsele, G. *et al.* (1994) The Xigaze forearc basin: evolution and facies architecture (Cretaceous, Tibet), *Sedimentary Geology*, 90(1), pp. 1-32. doi: https://doi.org/10.1016/0037-0738(94)90014-0.

Encinas, A. *et al.* (2012) Major forearc subsidence and deep-marine Miocene sedimentation in the present Coastal Cordillera and Longitudinal Depression of south-central Chile (38°30′S–41°45′S), *GSA Bulletin*, 124(7-8), pp. 1262-1277. doi: https://doi.org/10.1130/B30567.1.

Escalona, A., Mann, P. and Jaimes, M. (2011) Miocene to recent Cariaco basin, offshore Venezuela: Structure, tectonosequences, and basin-forming mechanisms, *Marine and Petroleum Geology*, 28(1), pp. 177-199. doi: http://dx.doi.org/10.1016/j.marpetgeo.2009.04.001.

Espurt, N. *et al.* (2018) Deciphering the Late Cretaceous-Cenozoic structural evolution of the North Peruvian forearc system, *Tectonics*, pp. 251-282. doi: https://doi.org/10.1002/2017TC004536.

Evans, C. D. R. and Whittaker, J. E. (1982) The geology of the western part of the Borbón Basin, North-west Ecuador, *Geological Society, London, Special Publications*, 10(1), pp. 191-198. doi: https://doi.org/10.1144/GSL.SP.1982.010.01.12.

Feininger, T. and Seguin, M. K. (1983) Simple Bouguer Gravity-Anomaly Field and the Inferred Crustal Structure of Continental Ecuador, *Geology*, 11(1), pp. 40-44. doi: https://doi.org/10.1130/0091-7613(1983)11%3C40:SBGAFA%3E2.0.CO;2.

Feininger, T. (1987) Allochthonous terranes in the Andes of Ecuador and northwestern Peru, *Canadian Journal of Earth Sciences*, 24(2), pp. 266-278. doi: http://dx.doi.org/10.1139/e87-028.

Fernández-García, C., Guillaume, B. and Brun, J.-P. (2019) 3D slab breakoff in laboratory experiments, *Tectonophysics*, 773, pp. 228223. doi: https://doi.org/10.1016/j.tecto.2019.228223.

Fernández, J. *et al.* (2005) Tumbes and Talara basins hydrocarbon evaluation, Perupetro S.A., *Basin Evaluations Group Exploration Department*, internal report, Retrieved from www.perupetro.com.pe, pp. pp. 130.

Ferraccioli, F., Bozzo, E. and Capponi, G. (2002) Aeromagnetic and gravity anomaly constraints for an early Paleozoic subduction system of Victoria Land, Antarctica, *Geophysical Research Letters*, 29(10). doi: https://doi.org/10.1029/2001GL014138.

Ferraccioli, F. *et al.* (2006) New aerogeophysical view of the Antarctic Peninsula: More pieces, less puzzle, *Geophysical Research Letters*, 33(5). doi: https://doi.org/10.1029/2005GL024636.

Fildani, A., Hessler, A. M. and Graham, S. A. (2008) Trench-forearc interactions reflected in the sedimentary fill of Talara basin, northwest Peru, *Basin Research*, 20(3), pp. 305-331. doi: https://doi.org/10.1111/j.1365-2117.2007.00346.x.

Finn, C. (1994) Aeromagnetic evidence for a buried Early Cretaceous magmatic arc, northeast Japan, *Journal of Geophysical Research: Solid Earth*, 99(B11), pp. 22165-22185. doi: https://doi.org/10.1029/94JB00855.

Fitch, T. J. (1972) Plate Convergence, Transcurrent Faults, and Internal Deformation Adjacent to Southeast Asia and Western Pacific, *Journal of Geophysical*

Research, 77(23), pp. 4432-&. doi: https://doi.org/10.1029/JB077i023p04432.

Flueh, E. R. *et al.* (2001) Cruise report SO159 SALIERI, *GEOMAR*, Kiel.

Font, Y. *et al.* (2013) Seismicity patterns along the Ecuadorian subduction zone: new constraints from earthquake location in a 3-D a priori velocity model, *Geophysical Journal International*, 193(1), pp. 263-286. doi: https://doi.org/10.1093/gji/ggs083.

Fossen, H., Teyssier, C. and Whitney, D. L. (2013) Transtensional folding, *Journal of Structural Geology*, 56, pp. 89-102. doi: https://doi.org/10.1016/j.jsg.2013.09.004.

Frisch, W., Meschede, M. and Blakey, R. (2011) Subduction zones, island arcs and active continental margins *Plate Tectonics: Continental Drift and Mountain Building.* Berlin, Heidelberg: Springer Berlin Heidelberg, pp. 91-122. doi: https://doi.org/10.1007/978-3-540-76504-2_7.

Gailler, A., Charvis, P. and Flueh, E. R. (2007) Segmentation of the Nazca and South American plates along the Ecuador subduction zone from wide angle seismic profiles, *Earth and Planetary Science Letters*, 260(3-4), pp. 444-464. doi: https://doi.org/10.1016/j.epsl.2007.05.045.

Gehrels, G. (2014) Detrital Zircon U-Pb Geochronology Applied to Tectonics, *Annual Review of Earth and Planetary Sciences*, 42(1), pp. 127-149. doi: https://doi.org/10.1146/annurev-earth-050212-124012.

Goossens, P. J. and Rose, W. I. (1973) Chemical Composition and Age Determination of Tholeiitic Rocks in Basic Igneous Complex, Ecuador, *Geological Society of America Bulletin*, 84(3), pp. 1043-1051. doi: https://doi.org/10.1130/0016-7606(1973)84%3C1043:CCAADO%3E2.0.CO;2.

Goossens, P. J., Rose, W. I. and Flores, D. (1977) Geochemistry of tholeiites of the Basic Igneous Complex of northwestern South America, *GSA Bulletin*, 88(12), pp. 1711-1720. doi: http://dx.doi.org/10.1130/0016-7606(1977)88<1711:GOTOTB>2.0.CO;2.

Graindorge, D. *et al.* (2004) Deep structures of the Ecuador convergent margin and the Carnegie Ridge, possible consequence on great earthquakes recurrence interval, *Geophysical Research Letters*, 31(4). doi: https://doi.org/10.1029/2003GL018803.

Gutscher, M. A. *et al.* (1999) Tectonic segmentation of the North Andean margin: impact of the Carnegie Ridge collision, *Earth and Planetary Science*

Letters, 168(3-4), pp. 255-270. doi: https://doi.org/10.1016/S0012-821X(99)00060-6.

Hall, M. L. and Calle, J. (1982) Geochronological control for the main tectonic-magmatic events of Ecuador, *Earth-Science Reviews*, 18(3), pp. 215-239. doi: https://doi.org/10.1016/0012-8252(82)90038-1.

Handschumacher, D. Post-Eocene Plate Tectonics of the Eastern Pacific *The Geophysics of the Pacific Ocean Basin and Its Margin.* pp. 177-202. doi: https://doi.org/10.1029/GM019p0177.

Haq, S. S. B. and Davis, D. M. (2010) Mechanics of fore-arc slivers: Insights from simple analog models, *Tectonics*, 29. doi: https://doi.org/10.1029/2009TC002583.

Herms, P. *et al.* (2012) Evidence for channelized external fluid flow and element transfer in subducting slabs (Raspas Complex, Ecuador), *Chemical Geology*, 310–311, pp. 79-96. doi: http://dx.doi.org/10.1016/j.chemgeo.2012.03.023.

Hernández, M. J. *et al.* (2020) Evolution of the Ecuador offshore nonaccretionary-type forearc basin and margin segmentation, *Tectonophysics*, 781, pp. 228374. doi: https://doi.org/10.1016/j.tecto.2020.228374.

Hernández Salazar, M. J. *et al.* (2019) *Neogene evolution of western boundary of the Manabí basin controlled by the Jama Fault System*. Unpublished paper presented at 8th International Symposium on Andean Geodynamics (ISAG). Quito-Ecuador.

Hessler, A. M. and Fildani, A. (2015) Andean Forearc Dynamics, as Recorded by Detrital Zircon from the Eocene Talara Basin, Northwest Peru, *Journal of Sedimentary Research*, 85(6), pp. 646-659. doi: https://doi.org/10.2110/jsr.2015.45.

Heuret, A. *et al.* (2012) Relation between subduction megathrust earthquakes, trench sediment thickness and upper plate strain, *Geophysical Research Letters*, 39(5). doi: https://doi.org/10.1029/2011GL050712.

Hey, R. (1977) Tectonic evolution of the Cocos-Nazca spreading center, *GSA Bulletin*, 88(10), pp. 1404-1420. doi: https://doi.org/10.1130/0016-7606(1977)88%3C1404:TEOTCS%3E2.0.CO;2.

Higley, D. (2004a) *The Talara Basin province of northwestern Peru; Cretaceous-Tertiary Total Petroleum System*. U. S. Geological Survey, Reston, VA, United States.

Higley, D. (2004b) *The Progreso Basin province of northwestern Peru and southwestern Ecuador; Neogene and Cretaceous-Paleogene total petroleum systems*. U. S. Geological Survey, Reston, VA, United States.

Hinze, W. J., von Frese, R. R. B. and Saad, A. H. (2013) *Gravity and Magnetic Exploration: Principles, Practices, and Applications*. Cambridge: Cambridge University Press.

Hoffmann-Rothe, A. *et al.* (2006) Oblique Convergence along the Chilean Margin: Partitioning, Margin-Parallel Faulting and Force Interaction at the Plate Interface, in Oncken, O.*, et al.* (ed.) *The Andes: Active Subduction Orogeny.* Berlin, Heidelberg: Springer Berlin Heidelberg, pp. 125-146. doi: https://doi.org/10.1007/978-3-540-48684-8_6.

Huchon, P. and Pichon, X. L. (1984) Sunda Strait and Central Sumatra Fault, *Geology*, 12(11), pp. 668-672. doi: https://doi.org/10.1130/0091-7613(1984)12%3C668:SSACSF%3E2.0.CO;2.

Hughes, R. A., Bermúdez, R. and Espinel, G. (1999) Mapa Geológico de la Cordillera Occidental del Ecuador entre 0°-1°S. Quito-Ecuador: BGS & CODIGEM.

Hughes, R. A. and Pilatasig, L. F. (2002) Cretaceous and Tertiary terrane accretion in the Cordillera Occidental of the Andes of Ecuador, *Tectonophysics*, 345(1–4), pp. 29-48. doi: http://dx.doi.org/10.1016/S0040-1951(01)00205-0.

Hungerbühler, D. *et al.* (2002) Neogene stratigraphy and Andean geodynamics of southern Ecuador, *Earth-Science Reviews*, 57(1–2), pp. 75-124. doi: http://dx.doi.org/10.1016/S0012-8252(01)00071-X.

Hyndman, R. D. and Peacock, S. M. (2003) Serpentinization of the forearc mantle, *Earth and Planetary Science Letters*, 212(3), pp. 417-432. doi: https://doi.org/10.1016/S0012-821X(03)00263-2.

Jaillard, E. *et al.* (1995) Basin development in an accretionary, oceanic-floored fore-arc setting: southern coastal Ecuador during late Cretaceous-late Eocene time. doi: https://doi.org/10.1306/M62593C32.

Jaillard, E., Benitez, S. and Mascle, G. H. (1997) Palaeogene deformations of the forearc zone of south Ecuador in relation to the geodynamic evolution, *Bulletin De La Societe Geologique De France*, 168(4), pp. 403-403.

Jaillard, E. *et al.* (1999) Stratigraphy and evolution of the Cretaceous forearc Celica-Lancones basin of southwestern Ecuador, *Journal of South American Earth*

Sciences, 12(1), pp. 51-68. doi: https://doi.org/10.1016/S0895-9811(99)00006-1.

Jaillard, E. *et al.* (2002) Andean geodynamics: main issues and contributions from the 4th ISAG, Göttingen, *Tectonophysics*, 345(1–4), pp. 1-15. doi: http://dx.doi.org/10.1016/S0040-1951(01)00203-7.

Jaillard, E. *et al.* (2009) Accreted oceanic terranes in Ecuador; southern edge of the Caribbean Plate?, *Geological Society Special Publications*, 328, pp. 469-485. doi: http://dx.doi.org/10.1144/SP328.19.

Jarrard, R. D. (1986) Terrane Motion by Strike-Slip Faulting of Fore-Arc Slivers, *Geology*, 14(9), pp. 780-783. doi: https://doi.org/10.1130/0091-7613(1986)14%3C780:TMBSFO%3E2.0.CO;2.

John, T. *et al.* (2010) Subducted seamounts in an eclogite-facies ophiolite sequence: the Andean Raspas Complex, SW Ecuador, *Contributions to Mineralogy and Petrology*, 159(2), pp. 265-284. doi: http://dx.doi.org/10.1007/s00410-009-0427-0.

Kearey, P., Klepeis, K. A. and Vine, F. J. (2009) *Global tectonics*. Wiley-Blackwell, Chichester, United Kingdom.

Kellogg, J. N. *et al.* (1995) Tectonic development of Panama, Costa Rica, and the Colombian Andes: Constraints from Global Positioning System geodetic studies and gravity - Geologic and Tectonic Development of the Caribbean Plate Boundary in Southern Central America, in Mann, P. (ed.). Geological Society of America, pp. 0. doi: https://dx.doi.org/10.1130/SPE295-p75.

Kennan, L. and Pindell, J. L. (2009) Dextral shear, terrane accretion and basin formation in the Northern Andes: best explained by interaction with a Pacific-derived Caribbean Plate?, *Origin and Evolution of the Caribbean Plate*, 328, pp. 487-531. doi: https://doi.org/10.1144/SP328.20.

Kerr, A. C. *et al.* (1997) Cretaceous basaltic terranes in western Colombia: Elemental, chronological and Sr-Nd isotopic constraints on petrogenesis, *Journal of Petrology*, 38(6), pp. 677-702. doi: https://doi.org/10.1093/petroj/38.6.677.

Kerr, A. C. *et al.* (2002) The nature and provenance of accreted oceanic terranes in western Ecuador: geochemical and tectonic constraints, *Journal of the Geological Society*, 159, pp. 577-594. doi: https://doi.org/10.1144/0016-764901-151.

Kerr, A. C. (2005) La Isla de Gorgona, Colombia: A petrological enigma?, *Lithos*, 84(1–2), pp. 77-101. doi: http://dx.doi.org/10.1016/j.lithos.2005.02.006.

Kerr, A. C. and Tarney, J. (2005) Tectonic evolution of the Caribbean and northwestern South America: The case for accretion of two Late Cretaceous oceanic plateaus, *Geology*, 33(4), pp. 269-272. doi: https://doi.org/10.1130/G21109.1.

Kimura, G. (1986) Oblique Subduction and Collision - Fore-Arc Tectonics of the Kuril Arc, *Geology*, 14(5), pp. 404-407. Available at: <Go to ISI>://WOS:A1986C380700011.

Kimura, G. *et al.* (2014) Middle Miocene swift migration of the TTT triple junction and rapid crustal growth in southwest Japan: A review, *Tectonics*, 33(7), pp. 1219-1238. doi: https://doi.org/10.1002/2014TC003531.

Koch, C. D. *et al.* (2020) Structure of the Ecuadorian forearc from the joint inversion of receiver functions and ambient noise surface waves, *Geophysical Journal International*. doi: https://doi.org/10.1093/gji/ggaa237.

Kopp, H. and Kukowski, N. (2003) Backstop geometry and accretionary mechanics of the Sunda margin, *Tectonics*, 22(6). doi: https://doi.org/10.1029/2002TC001420.

Kopp, H. (2013) Invited review paper: The control of subduction zone structural complexity and geometry on margin segmentation and seismicity, *Tectonophysics*, 589, pp. 1-16. doi: http://dx.doi.org/10.1016/j.tecto.2012.12.037.

Lapierre, H. *et al.* (2000) Multiple plume events in the genesis of the peri-Caribbean Cretaceous oceanic plateau province, *Journal of Geophysical Research-Solid Earth*, 105(B4), pp. 8403-8421. doi: https://doi.org/10.1029/1998JB900091.

Lebrat, M. *et al.* (1985) Pre-Orogenic Volcanic Assemblages and Structure in the Western Cordillera of Ecuador between 1-Degrees-40s and 2-Degrees-20s, *Geologische Rundschau*, 74(2), pp. 343-351. doi: https://doi.org/10.1007/BF01824901.

Lebrat, M. *et al.* (1987) Geochemistry and Tectonic Setting of Pre-Collision Cretaceous and Paleogene Volcanic-Rocks of Ecuador, *Geological Society of America Bulletin*, 99(4), pp. 569-578. doi: https://doi.org/10.1130/0016-7606(1987)99%3C569:GATSOP%3E2.0.CO;2.

Lopez, E. (2009) *Evolution tectono-stratigraphique du double bassin avant-arc de la marge convergente Sud Colombienne - Nord Equatorienne pendant le Cénozoïque*, Université de Nice Sophia Antipolis. doi: 10.13140/RG.2.2.14321.12642.

Lucas, N. and Delgado, D. (2018) *Análisis tectono-estratigráfico de la Cuenca Borbón-Esmeraldas: Noroeste de Ecuador*, Escuela Superior Politécnica del Litoral.

Luzieux, L. *et al.* (2006) Origin and Cretaceous tectonic history of the coastal Ecuadorian forearc between 1 degrees N and 3 degrees S: Paleomagnetic, radiometric and fossil evidence, *Earth and Planetary Science Letters*, 249(3-4), pp. 400-414. doi: https://doi.org/10.1016/j.epsl.2006.07.008.

Luzieux, L. (2007) *Origin and late cretaceous-tertiary evolution of the Ecuadorian forearc*. doi: https://doi.org/10.3929/ethz-a-005348206.

Lynner, C. *et al.* (2019) Upper-plate structure in Ecuador coincident with the subduction of the Carnegie Ridge and the southern extent of large mega-thrust earthquakes, *Geophysical Journal International*, 220(3), pp. 1965-1977. doi: https://doi.org/10.1093/gji/ggz558.

MacDonald, W. D., Estrada, J. J. and Humberto, G. (1997) Paleoplate affiliations of volcanic accretionary terranes of the northern Andes, *Abstracts with Programs - Geological Society of America*, 29(6), pp. 45.

Malatesta, C. *et al.* (2013) Oblique subduction modelling indicates along-trench tectonic transport of sediments, *Nature Communications*, 4. doi: https://doi.org/10.1038/ncomms3456.

Mamberti, M. *et al.* (2003) Accreted fragments of the Late Cretaceous Caribbean-Colombian Plateau in Ecuador, *Lithos*, 66(3-4), pp. 173-199. doi: https://doi.org/10.1016/S0024-4937(02)00218-9.

Mamberti, M. *et al.* (2004) The Early Cretaceous San Juan Plutonic Suite, Ecuador: a magma chamber in an oceanic plateau?, *Canadian Journal of Earth Sciences*, 41(10), pp. 1237-1258. doi: https://doi.org/10.1139/e04-060.

Mankhemthong, N., Doser, D. I. and Pavlis, T. L. (2013) Interpretation of gravity and magnetic data and development of two-dimensional cross-sectional models for the Border Ranges fault system, south-central Alaska, *Geosphere*, 9(2), pp. 242-259. doi: https://doi.org/10.1130/GES00833.1.

Mann, P. (1997) Model for the formation of large, transtensional basins in zones of tectonic escape, *Geology*, 25(3), pp. 211-214. doi: https://doi.org/10.1130/0091-7613(1997)025%3C0211:MFTFOL%3E2.3.CO;2.

Mann, P. (2007) Global catalogue, classification and tectonic origins of restraining- and releasing bends on active and ancient strike-slip fault systems,

Geological Society, London, Special Publications, 290(1), pp. 13-142. doi: https://doi.org/10.1144/SP290.2.

Manzotti, P., Poujol, M. and Ballèvre, M. (2015) Detrital zircon geochronology in blueschist-facies meta-conglomerates from the Western Alps: implications for the late Carboniferous to early Permian palaeogeography, *International Journal of Earth Sciences*, 104(3), pp. 703-731. doi: 10.1007/s00531-014-1104-8.

Marcaillou, B. and Collot, J. Y. (2008) Chronostratigraphy and tectonic deformation of the North Ecuadorian-South Colombian offshore Manglares forearc basin, *Marine Geology*, 255(1-2), pp. 30-44. doi: http://dx.doi.org/10.1016/j.margeo.2008.07.003.

Mason, R. (1985) Ophiolites, *Geology Today*, 1(5), pp. 136-140. doi: https://doi.org/10.1111/j.1365-2451.1985.tb00315.x.

Mason, W. G. *et al.* (2010) Three-dimensional numerical models of the influence of a buoyant oceanic plateau on subduction zones, *Tectonophysics*, 483(1-2), pp. 71-79. doi: https://doi.org/10.1016/j.tecto.2009.08.021.

McCaffrey, R. (1992) Oblique Plate Convergence, Slip Vectors, and Fore-Arc Deformation, *Journal of Geophysical Research-Solid Earth*, 97(B6), pp. 8905-8915. doi: https://doi.org/10.1029/92JB00483.

McCourt, W. J. *et al.* (1999) Mapa Geológico de la Cordillera Occidental del Ecuador entre 1°-2°S. Quito-Ecuador: BGS & CODIGEM.

Melnick, D. and Echtler, H. P. (2006) Inversion of forearc basins in south-central Chile caused by rapid glacial age trench fill, *Geology*, 34(9), pp. 709-712. doi: https://doi.org/10.1130/G22440.1.

Michaud, F., Royer, J.-Y. and Witt, C. (2009) Influence of the subduction of the Carnegie volcanic ridge on Ecuadorian geology: Reality and fiction, in Suzanne Mahlburg Kay, V. A. R. and William, R. D. (ed.) *Backbone of the Americas: Shallow Subduction, Plateau Uplift, and Ridge and Terrane Collision.* Geological Society of America, pp. 217-228. doi: https://doi.org/10.1130/2009.1204(10).

Mitchell, C., Graham, S. A. and Suek, D. H. (2010) Subduction complex uplift and exhumation and its influence on Maastrichtian forearc stratigraphy in the Great Valley Basin, northern San Joaquin Valley, California, *GSA Bulletin*, 122(11-12), pp. 2063-2078. doi: https://doi.org/10.1130/B30180.1.

Mitouard, P., Kissel, C. and Laj, C. (1990) Postoligocene Rotations in Southern Ecuador and Northern Peru and the Formation of the Huancabamba

Deflection in the Andean Cordillera, *Earth and Planetary Science Letters*, 98(3-4), pp. 329-339. doi: https://doi.org/10.1016/0012-821X(90)90035-V.

Mix, A. C. *et al.* (2003) Leg 202 summary, *Proceedings of the Ocean Drilling Program, initial reports, Southeast Pacific paleoceanographic transects; covering Leg 202 of the cruises of the drilling vessel JOIDES Resolution; Valparaiso, Chile, to Balboa, Panama; sites 1232-1242, 29 March-30 May 2002*, 202, pp. 145. Available at: http://hdl.handle.net/10.2973/odp.proc.ir.202.101.2003.

Moore, G. F. *et al.* (2015) Evolution of tectono-sedimentary systems in the Kumano Basin, Nankai Trough forearc, *Marine and Petroleum Geology*, 67, pp. 604-616. doi: https://doi.org/10.1016/j.marpetgeo.2015.05.032.

Moreno, A. (1983) Estratigrafía detallada del Grupo Azúcar en los acantilados de Playas, *Escuela Superior Politécnica del Litoral*, pp. 182.

Moresi, L. *et al.* (2014) Dynamics of continental accretion, *Nature*, 508, pp. 245. doi: http://dx.doi.org/10.1038/nature13033.

Mourier, T. *et al.* (1988) An Accreted Continental Terrane in Northwestern Peru, *Earth and Planetary Science Letters*, 88(1-2), pp. 182-192. doi: https://doi.org/10.1016/0012-821X(88)90056-8.

Moxon, I. W. and Graham, S. A. (1987) History and controls of subsidence in the Late Cretaceous-Tertiary Great Valley forearc basin, California, *Geology*, 15(7), pp. 626-629. doi: https://doi.org/10.1130/0091-7613(1987)15%3C626:HACOSI%3E2.0.CO;2.

Nocquet, J. M. *et al.* (2014) Motion of continental slivers and creeping subduction in the northern Andes, *Nature Geoscience*, 7(8). doi: https://doi.org/10.1038/ngeo2099.

Noda, A. and TuZino, T. (2007) Characteristics of sediments and their dispersal systems along the shelf and slope of an active forearc margin, eastern Hokkaido, northern Japan, *Sedimentary Geology*, 201(3-4), pp. 341-364. doi: https://doi.org/10.1016/j.sedgeo.2007.07.002.

Noda, A. (2013) Strike-Slip Basin – Its Configuration and Sedimentary Facies, Mechanism of Sedimentary Basin Formation - Multidisciplinary Approach on Active Plate Margins. doi: 10.5772/56593.

Noda, A. (2016) Forearc basins: Types, geometries, and relationships to subduction zone dynamics, *Geological Society of America Bulletin*, 128(5-6), pp. 879-895. Available at: <Go to ISI>://WOS:000375212200012.

Okay, A. I. *et al.* (2000) Active faults and evolving strike-slip basins in the Marmara Sea, northwest Turkey: a multichannel seismic reflection study, *Tectonophysics*, 321(2), pp. 189-218. doi: https://doi.org/10.1016/S0040-1951(00)00046-9.

Ordoñez, M. (1995) Zona de radiolarios del Eoceno medio del grupo Ancon, Peninsula de Santa Elena, Ecuador, *Asociación Paleontológica Argentina*, (3).

Ordónez, M., Jiménez, N. and Suárez, J. (2006) *Micropaleontología ecuatoriana. datos bioestratigráficos y paleoecológicos de las cuencas: : Graben de Jambelí, Progreso, Manabí, Esmeraldas y Oriente; del levantamiento de la península de Santa Elena, y de las cordilleras Chongón Colonche, costera y Occidental*. Quito, Ecuador: Petroproducción y Centro de Investigaciones Geológicas de Guayaquil.

Pardo-Casas, F. and Molnar, P. (1987) Relative motion of the Nazca (Farallon) and South American Plates since Late Cretaceous time, *Tectonics*, 6(3), pp. 233-248. doi: http://dx.doi.org/10.1029/TC006i003p00233.

Pedoja, K. *et al.* (2014) Coastal staircase sequences reflecting sea-level oscillations and tectonic uplift during the Quaternary and Neogene, *Earth-Science Reviews*, 132, pp. 13-38. doi: https://doi.org/10.1016/j.earscirev.2014.01.007.

Petterson, M. G. (2010) A Review of the geology and tectonics of the Kohistan island arc, north Pakistan, *Geological Society, London, Special Publications*, 338(1), pp. 287-327. doi: 10.1144/sp338.14.

Philippon, M. and Corti, G. (2016) Obliquity along plate boundaries, *Tectonophysics*, 693, pp. 171-182. doi: https://doi.org/10.1016/j.tecto.2016.05.033.

Pinet, N. and Cobbold, P. R. (1992) Experimental Insights into the Partitioning of Motion within Zones of Oblique Subduction, *Tectonophysics*, 206(3-4), pp. 371-388. doi: https://doi.org/10.1016/0040-1951(92)90388-M.

Platt, J. P. (1993) Mechanics of Oblique Convergence, *Journal of Geophysical Research-Solid Earth*, 98(B9), pp. 16239-16256. doi: Doi 10.1029/93jb00888.

Rangin, C. *et al.* (2001) *Marine Atlas of the Sea of Marmara (Turkey)*. Plouzané, France: Ifremer. Available at: https://archimer.ifremer.fr/doc/00279/39006/.

Regalla, C. *et al.* (2013) Active forearc shortening in Tohoku, Japan: Constraints on fault geometry from erosion rates and fluvial longitudinal profiles,

Geomorphology, 195, pp. 84-98. doi: https://doi.org/10.1016/j.geomorph.2013.04.029.

Reyes, P. (2013) Relief Evolution along the Active Margins: Study of the Plio-Quaternary Deformation in the Coastal Cordillera of Ecuador, *Université de Nice-Sophia Antipolis – UFR Sciences*, PhD Thesis.

Reynard, B. (2013) Serpentine in active subduction zones, *Lithos*, 178, pp. 171-185. doi: https://doi.org/10.1016/j.lithos.2012.10.012.

Reynaud, C. *et al.* (1999) Oceanic plateau and island arcs of southwestern Ecuador: their place in the geodynamic evolution of northwestern South America, *Tectonophysics*, 307(3-4), pp. 235-254. doi: https://doi.org/10.1016/S0040-1951(99)00099-2.

Reynaud, J.-Y. *et al.* (2018) Tide-dominated deltas in active margin basins: Insights from the Guayas estuary, Gulf of Guayaquil, Ecuador, *Marine Geology*, 403, pp. 165-178. doi: https://doi.org/10.1016/j.margeo.2018.06.002.

Richards, J. P. (2009) Postsubduction porphyry Cu-Au and epithermal Au deposits: Products of remelting of subduction-modified lithosphere, *Geology*, 37(3), pp. 247-250. doi: https://doi.org/10.1130/G25451A.1.

Richards, J. P. (2011) Magmatic to hydrothermal metal fluxes in convergent and collided margins, *Ore Geology Reviews*, 40(1), pp. 1-26. doi: https://doi.org/10.1016/j.oregeorev.2011.05.006.

Roperch, P. *et al.* (1987) Rotated Oceanic Blocks in Western Ecuador, *Geophysical Research Letters*, 14(5), pp. 558-561. doi: https://doi.org/10.1029/GL014i005p00558.

Saad, A. H. (1969) Magnetic properties of ultramafic rocks from Red Mountain, California, *Geophysics*, 34(6), pp. 974-987. doi: https://doi.org/10.1190/1.1440067.

Sage, F., Collot, J. Y. and Ranero, C. R. (2006) Interplate patchiness and subduction-erosion mechanisms: Evidence from depth-migrated seismic images at the central Ecuador convergent margin, *Geology*, 34(12), pp. 997-1000. doi: https://doi.org/10.1130/G22790A.1.

Sanchez, J. *et al.* (2006) Puesta en evidencia de granitoides triásicos en los Amotapes–Tahuín: deflexión de Huancabamba, *XIII Congreso Peruano deGeologia*, pp. 312-315.

Sanclemente, E. (2014) *Seismic imaging of the structure of the central Ecuador convergent margin : relationship with the inter-seismic coupling variations.*, Université Nice Sophia Antipolis.

Sandwell, D. T. *et al.* (2014) New global marine gravity model from CryoSat-2 and Jason-1 reveals buried tectonic structure, *Science*, 346(6205), pp. 65-67.

Schoene, B. (2014) 4.10 - U–Th–Pb Geochronology, in Holland, H. D. and Turekian, K. K. (ed.) *Treatise on Geochemistry (Second Edition)*. Oxford: Elsevier, pp. 341-378. doi: https://doi.org/10.1016/B978-0-08-095975-7.00310-7.

Scholl, D. W. *et al.* (1980) Sedimentary Masses and Concepts About Tectonic Processes at Underthrust Ocean Margins, *Geology*, 8(12), pp. 564-568. doi: https://doi.org/10.1130/0091-7613(1980)8%3C564:SMACAT%3E2.0.CO;2.

Scholl, D. W. and von Huene, R. (2009) Implications of estimated magmatic additions and recycling losses at the subduction zones of accretionary (non-collisional) and collisional (suturing) orogens, *Geological Society, London, Special Publications*, 318(1), pp. 105-125. doi: https://doi.org/10.1144/SP318.4.

Schutte, P., Chiaradia, M. and Beate, B. (2010) Geodynamic controls on Tertiary arc magmatism in Ecuador: Constraints from U-Pb zircon geochronology of Oligocene-Miocene intrusions and regional age distribution trends, *Tectonophysics*, 489(1-4), pp. 159-176. doi: https://doi.org/10.1016/j.tecto.2010.04.015.

Seeber, L. *et al.* (2010) Continental Transform Basins: Why Are They Asymmetric?, *Eos, Transactions American Geophysical Union*, 91(4), pp. 29-30. doi: https://doi.org/10.1029/2010EO040001.

Seely, D. R. (1979) The evolution of structural highs bordering major forearc basins, *Memoir - American Association of Petroleum Geologists*, (29), pp. 245-260. doi: https://doi.org/10.1306/M29405C17.

Seno, T. (2005) Variation of downdip limit of the seismogenic zone near the Japanese islands: implications for the serpentinization mechanism of the forearc mantle wedge, *Earth and Planetary Science Letters*, 231(3), pp. 249-262. doi: https://doi.org/10.1016/j.epsl.2004.12.027.

Shemenda, A. I. (1993) Subduction of the lithosphere and back arc dynamics: Insights from physical modeling, *Journal of Geophysical Research: Solid Earth*, 98(B9), pp. 16167-16185. doi: https://doi.org/10.1029/93JB01094.

Shepherd, G. L. and Moberly, R. (1981) Coastal Structure of the Continental-Margin, Northwest Peru and Southwest Ecuador, *Geological Society of America Memoirs*, 154, pp. 351-391. doi: https://doi.org/10.1130/MEM154-p351.

Spadea, P. and Espinosa, A. (1996) Petrology and chemistry of late Cretaceous volcanic rocks from the southernmost segment of the Western Cordillera of Colombia (South America), *Journal of South American Earth Sciences*, 9(1), pp. 79-90. doi: http://dx.doi.org/10.1016/0895-9811(96)00029-6.

Spikings, R. *et al.* (2010) Syn- and post-accretionary cooling history of the Ecuadorian Andes constrained by their in-situ and detrital thermochronometric record, *Journal of South American Earth Sciences*, 30(3), pp. 121-133. doi: https://doi.org/10.1016/j.jsames.2010.04.002.

Spikings, R. *et al.* (2015) The geological history of northwestern South America: from Pangaea to the early collision of the Caribbean Large Igneous Province (290–75 Ma), *Gondwana Research*, 27(1), pp. 95-139. doi: http://dx.doi.org/10.1016/j.gr.2014.06.004.

Spikings, R. A. *et al.* (2005) Thermochronology of allochthonous terranes in Ecuador: Unravelling the accretionary and post-accretionary history of the Northern Andes, *Tectonophysics*, 399(1–4), pp. 195-220. doi: http://dx.doi.org/10.1016/j.tecto.2004.12.023.

Stéphane, B. *et al.* (2018) Reappraisal of the Tectonic Style of the Talara-Tumbes Forearc Basin: Regional Insights for Hydrocarbon Exploration *Petroleum Basins and Hydrocarbon Potential of the Andes of Peru and Bolivia.* The American Association of Petroleum Geologists. doi: https://doi.org/10.1306/13622126M1173772.

Stern, R. J. (2004) Subduction initiation: spontaneous and induced, *Earth and Planetary Science Letters*, 226(3-4), pp. 275-292. doi: https://doi.org/10.1016/j.epsl.2004.08.007.

Stern, R. J. *et al.* (2012) To understand subduction initiation, study forearc crust: To understand forearc crust, study ophiolites, *Lithosphere*, 4(6), pp. 469-483. doi: https://doi.org/10.1130/L183.1.

Sylvester, A. G. (1988) Strike-Slip Faults, *Geological Society of America Bulletin*, 100(11), pp. 1666-1703. doi: https://doi.org/10.1130/0016-7606(1988)100%3C1666:SSF%3E2.3.CO;2.

Takano, O., Itoh, Y. and Kusumoto, S. (2013) Variation in forearc basin configuration and basin-filling depositional systems as a function of trench slope break development and strike-slip movement: examples from the

Cenozoic Ishikari–Sanriku–Oki and Tokai-oki–Kumano-nada forearc basins, Japan, *Mechanism of Sedimentary Basin Formation - Multidisciplinary Approach on Active Plate Margins, InTech*, pp. 3-25.

Talavera, C. *et al.* (2012) Ediacaran to Lower Ordovician age for rocks ascribed to the Schist–Graywacke Complex (Iberian Massif, Spain): Evidence from detrital zircon SHRIMP U–Pb geochronology, *Gondwana Research*, 22(3), pp. 928-942. doi: https://doi.org/10.1016/j.gr.2012.03.008.

Tamay, J. *et al.* (2018) Gravity and magnetic anomalies of ecuadorian margin: Implications in the deep structure of the subduction of Nazca Plate and Andes Cordillera, *Journal of South American Earth Sciences*, 85, pp. 68-80. doi: https://doi.org/10.1016/j.jsames.2018.04.020.

Tetreault, J. L. and Buiter, S. J. H. (2014) Future accreted terranes: a compilation of island arcs, oceanic plateaus, submarine ridges, seamounts, and continental fragments, *Solid Earth*, 5(2), pp. 1243-1275. doi: https://doi.org/10.5194/se-5-1243-2014.

Teyssier, C., Tikoff, B. and Markley, M. (1995) Oblique Plate Motion and Continental Tectonics, *Geology*, 23(5), pp. 447-450. doi: https://doi.org/10.1130/0091-7613(1995)023%3C0447:OPMACT%3E2.3.CO;2.

Toft, P. B., Arkani-Hamed, J. and Haggerty, S. E. (1990) The effects of serpentinization on density and magnetic susceptibility: a petrophysical model, *Physics of the Earth and Planetary Interiors*, 65(1), pp. 137-157. doi: https://doi.org/10.1016/0031-9201(90)90082-9.

Ueda, K., Gerya, T. and Sobolev, S. V. (2008) Subduction initiation by thermal–chemical plumes: Numerical studies, *Physics of the Earth and Planetary Interiors*, 171(1), pp. 296-312. doi: https://doi.org/10.1016/j.pepi.2008.06.032.

Vallejo, C. *et al.* (2006) The early interaction between the Caribbean plateau and the NW South American Plate, *Terra Nova*, 18(4), pp. 264-269. doi: https://doi.org/10.1111/j.1365-3121.2006.00688.x.

Vallejo, C. (2007) *Evolution of the Western Cordillera in the Andes of Ecuador (Late Cretaceous-Paleogene)*. Eidgenoessische Technische Hochschule Zuerich, Zurich, Switzerland. doi: http://dx.doi.org/10.3929/ethz-a-005416411.

Vallejo, C. *et al.* (2009) Mode and timing of terrane accretion in the forearc of the Andes in Ecuador, *Geological Society of America Memoirs*, 204, pp. 197-216. doi: https://doi.org/10.1130/2009.1204(09).

Vallejo, C. *et al.* (2016) Geology of El Domo deposit in central Ecuador: a VMS formed on top of an accreted margin, *Mineralium Deposita*, 51(3), pp. 389-409. doi: https://doi.org/10.1007/s00126-015-0616-x.

Vallejo, C. *et al.* (2019) Chapter 8 - Late cretaceous to miocene stratigraphy and provenance of the coastal forearc and Western Cordillera of Ecuador: Evidence for accretion of a single oceanic plateau fragment, in Horton, B. K. and Folguera, A. (ed.) *Andean Tectonics.* Elsevier, pp. 209-236. doi: https://doi.org/10.1016/B978-0-12-816009-1.00010-1.

Van Melle, J. *et al.* (2008) Pre-collision evolution of the Pinon oceanic terrane of SW Ecuador: stratigraphy and geochemistry of the "Calentura Formation", *Bulletin De La Societe Geologique De France*, 179(5), pp. 433-443. doi: https://doi.org/10.2113/gssgfbull.179.5.433.

Vauchez, A., Tommasi, A. and Barruol, G. (1998) Rheological heterogeneity, mechanical anisotropy and deformation of the continental lithosphere, *Tectonophysics*, 296(1), pp. 61-86. doi: https://doi.org/10.1016/S0040-1951(98)00137-1.

Venkat-Ramani, M. and Tikoff, B. (2002) Physical models of transtensional folding, *Geology*, 30(6), pp. 523-526. doi: https://doi.org/10.1130/0091-7613(2002)030<0523:PMOTF>2.0.CO;2.

Vogt, K. and Gerya, T. V. (2014) From oceanic plateaus to allochthonous terranes: Numerical modelling, *Gondwana Research*, 25(2), pp. 494-508. doi: https://doi.org/10.1016/j.gr.2012.11.002.

Von Huene, R. and Scholl, D. W. (1991) Observations at Convergent Margins Concerning Sediment Subduction, Subduction Erosion, and the Growth of Continental-Crust, *Reviews of Geophysics*, 29(3), pp. 279-316. doi: https://doi.org/10.1029/91RG00969.

Wakabayashi, J. and Dilek, Y. (2003) What constitutes 'emplacement' of an ophiolite?: Mechanisms and relationship to subduction initiation and formation of metamorphic soles, *Geological Society, London, Special Publications*, 218(1), pp. 427-447. doi: https://doi.org/10.1144/GSL.SP.2003.218.01.22.

Wallace, L. M. *et al.* (2005) Rapid microplate rotations and backarc rifting at the transition between collision and subduction, *Geology*, 33(11), pp. 857-860. doi: https://doi.org/10.1130/G21834.1.

Wallace, L. M., Ellis, S. and Mann, P. (2009) Collisional model for rapid fore-arc block rotations, arc curvature, and episodic back-arc rifting in subduction

settings, *Geochemistry Geophysics Geosystems*, 10. doi: https://doi.org/10.1029/2008GC002220.

Whattam, S. A. and Stern, R. J. (2015) Late Cretaceous plume-induced subduction initiation along the southern margin of the Caribbean and NW South America: The first documented example with implications for the onset of plate tectonics, *Gondwana Research*, 27(1), pp. 38-63. doi: https://doi.org/10.1016/j.gr.2014.07.011.

Winkler, W. *et al.* (2005) The Chota basin and its significance for the inception and tectonic setting of the inter-Andean depression in Ecuador, *Journal of South American Earth Sciences*, 19(1), pp. 5-19. doi: https://doi.org/10.1016/j.jsames.2004.06.006.

Winter, L. S. *et al.* (2010) Volcanic Stratigraphy and Geochronology of the Cretaceous Lancones Basin, Northwestern Peru: Position and Timing of Giant VMS Deposits, *Economic Geology*, 105(4), pp. 713-742. doi: https://doi.org/10.2113/gsecongeo.105.4.713.

Witt, C. *et al.* (2006) Development of the Gulf of Guayaquil (Ecuador) during the Quaternary as an effect of the North Andean block tectonic escape, *Tectonics*, 25(3). doi: https://doi.org/10.1029/2004TC001723.

Witt, C. and Bourgois, J. (2010) Forearc basin formation in the tectonic wake of a collision-driven, coastwise migrating crustal block: The example of the North Andean block and the extensional Gulf of Guayaquil-Tumbes Basin (Ecuador-Peru border area), *Geological Society of America Bulletin*, 122(1-2), pp. 89-108. doi: https://doi.org/10.1130/B26386.1.

Witt, C. *et al.* (2017) Tracking ancient magmatism and Cenozoic topographic growth within the Northern Andes forearc: Constraints from detrital U-Pb zircon ages, *Geological Society of America Bulletin*. doi: https://doi.org/10.1130/B31530.1.

Witt, C. *et al.* (2018) An U-Pb zircon chronology based correlation for forearc sediments through the Ecuadorian - Peruvian border, *Réunion des Sciences de la Terre*, *Lille-France*, *22-26 October*.

Witt, C. *et al.* (2019a) *Evolution of the Northern Andes Cenozoic magmatic arc as recorded in the forearc detrital record*. Unpublished paper presented at 8th International Symposium on Andean Geodynamics (ISAG). Quito-Ecuador.

Witt, C. *et al.* (2019b) From accretion to forearc basin initiation: The case of SW Ecuador, Northern Andes, *Sedimentary Geology*, 379, pp. 138-157. doi: https://doi.org/10.1016/j.sedgeo.2018.11.009.

Woodcock, N. H. (1986) The Role of Strike-Slip-Fault Systems at Plate Boundaries, *Philosophical Transactions of the Royal Society a-Mathematical Physical and Engineering Sciences*, 317(1539), pp. 13-29. doi: https://doi.org/10.1098/rsta.1986.0021.

Xie, X. and Heller, P. L. (2009) Plate tectonics and basin subsidence history, *GSA Bulletin*, 121(1-2), pp. 55-64. doi: https://doi.org/10.1130/B26398.1.

Yepes, H. *et al.* (2016) A new view for the geodynamics of Ecuador: Implication in seismogenic source definition and seismic hazard assessment, *Tectonics*, 35(5), pp. 1249-1279. doi: https://doi.org/10.1002/2015TC003941.